

Clemson University

TigerPrints

All Dissertations

Dissertations

August 2017

Synthesis and Structure-Property Relationship of Phosphonium Polymers

Xiaoyan Yang

Clemson University, xiaoyay@g.clemson.edu

Follow this and additional works at: https://tigerprints.clemson.edu/all_dissertations

Recommended Citation

Yang, Xiaoyan, "Synthesis and Structure-Property Relationship of Phosphonium Polymers" (2017). *All Dissertations*. 2541.

https://tigerprints.clemson.edu/all_dissertations/2541

This Dissertation is brought to you for free and open access by the Dissertations at TigerPrints. It has been accepted for inclusion in All Dissertations by an authorized administrator of TigerPrints. For more information, please contact kokeefe@clemson.edu.

SYNTHESIS AND STRUCTURE-PROPERTY RELATIONSHIP OF PHOSPHONIUM
POLYMERS

A Dissertation
Presented to
the Graduate School of
Clemson University

In Partial Fulfillment
of the Requirements for the Degree
Doctor of Philosophy
Chemistry

by
Xiaoyan Yang
August 2017

Accepted by:
Rhett C. Smith, Committee Chair
Stephen E. Creager
George Chumanov
Daniel C. Whitehead

ABSTRACT*

In Chapter 1, recent advances in thermally stable polymers and polyelectrolytes are reviewed, with an emphasis on elucidating the extent to which structural variations influence thermal stability. Specific polymers such as polybenzimidazoles, polyimides and phosphonium polyelectrolytes (PELs) were selected to illustrate how properties can be tuned through modification of side chain, main chain and functional group composition. Recent development on PPELs are a particular emphasis in this chapter, and this serves as an introduction to the state-of-the-art prior to work conducted in the current dissertation.

The work presented in Chapters 2 and 3 is centered on structure-property relationship studies employing PELs that were prepared via condensation polymerization. The properties of PELs were evaluated in an effort to assess the influence of both side chain and main chain composition. The influence of side chain was examined by comparing properties of a series of PELs having hydrophobic octyloxy side chains to those of structural analogues lacking the side chains. The influence exerted by backbone flexibility/length of spacer between charges was revealed by comparing properties of two series of polymers with a variable number of methylene units between phosphonium charge-bearing sites. Side chain composition and spacing between phosphonium units lead to noteworthy influence on thermal stability, glass transition and crystallinity. The molecular structure of PELs also correlates with trends in film morphology and critical

* Portions of this abstract are reproduced in part from chapters being developed for submissions to a journal for publication.

surface energy of PEL dip-cast films. Sensitivity of morphology to humidity or water in the casting solvent was observed. The relationship between side chain and spacer on bactericidal activity against *Staphylococcus aureus* and *Escherichia coli* was assessed. Supramolecular assembly of films via layer-by-layer deposition of PELs alternating with anionic polythiophene derivative layers was also undertaken. The linearity of film growth, amount of material deposited in each bilayer, polycation:polyanion ratio and film roughness all show noteworthy trends that depend on both the presence/absence of side chains and on spacing between ionic centers.

Chapters 4 and 5 detail work on a series of phosphonium-containing covalent organic frameworks (COFs) (**P1-P4**) prepared via copolymerization of 1,4-diacetylbenzene and bis(4-acetylphenyl)diphenylphosphonium bromide in various ratios. The influence of COF composition on thermal stability, alkaline stability, char yield, water uptake, specific surface area, and CO₂ affinity was assessed in this work. The phosphonium COFs show good thermal stability with $T_{d,5\%}$ up to 435 °C. Increasing the phosphonium content (50%) leads to concomitantly better alkaline stability upon challenging the material in 6 M NaOH(aq) at 65 °C for 120 h. The specific surface areas estimated by BET for the materials are in the range of 3-63 m²/g. Decreasing phosphonium content leads to larger specific areas due to a more open-structure solid. **P3**, in which 33% of monomers comprise a phosphonium moiety, exhibited the highest CO₂ affinity.

DEDICATION

I would like to dedicate my dissertation to my parents and husband who always believe in me and encourage me when I had a hard time. Thanks to my friends, you always cheer me up and give me comfort.

ACKNOWLEDGMENTS

Firstly, I would like to thank Dr. Smith for taking me as a graduate student and giving me guidance timely help all the time. With your support, I could finish the work successfully and smoothly in a short period of time.

I would like to thank Dr. Chumanov, Dr. Creager and Dr. Whitehead for being my committee members and taking the time to support my Ph.D. study.

I really appreciate the collaboration with Dr. Chumanov on AFM. With the help of you and your graduate students, I learned a lot on AFM and had so many nice figures to publish.

I would also like to thank Dr. Creager for the valuable advice on surface area measurement and offering help on the instrument so that I could have high quality data to publish.

Finally, I would like to express my appreciation on the chemistry department for offering the nice research environment for me to study here.

TABLE OF CONTENTS

	Page
TITLE PAGE	i
ABSTRACT	ii
DEDICATION	iv
ACKNOWLEDGMENTS	v
LIST OF ABBERRIATIONS	viii
LIST OF TABLES	x
LIST OF FIGURES	xii
LIST OF SCHEMES	xiv
LIST OF CHARTS	xv
CHAPTER	
I. RECENT DEVELOPMENTS IN THERMALLY STABLE POLYMERS AND PHOSPHONIUM POLYELECTROLYTES.....	1
Introduction.....	1
Polybenzimidazoles	2
Polyimides	9
Copolymer.....	22
Phosphonium Polyelectrolytes.....	36
References.....	43
II. INFLUENCE OF SPACER LENGTH AND RIGIDITY ON PROPERTIES OF PHOSPHONIUM POLYMERS AND ON THEIR SUPRAMOLECULAR ASSEMBLY WITH A CONJUGATED POLYELECTROLYTE.....	51
Introduction.....	51
Experimental	55
Results and Discussion	60

Table of Contents (Continued)

	Page
Conclusions.....	69
References.....	69
Appendices.....	73
III. INFLUENCE OF STRUCTURE ON PHOSPHONIUM POLYMER PROPERTIES, SUPRAMOLECULAR ASSEMBLY AND BACTERICIDAL ACTIVITY	96
Introduction.....	96
Experimental.....	101
Results and Discussion	108
Conclusions.....	127
References.....	128
Appendices.....	134
IV. A NEW ROUTE TO PHOSPHONIUM POLYMER NETWORK SOLIDS VIA CYCLOTRIMERIZATION.....	164
Introduction.....	164
Experimental.....	166
Results and Discussion	169
Conclusions.....	177
References.....	177
Appendices.....	181
V. STRUCTURE-PROPERTY RELATIONSHIPS OF PHOSPHONIUM POLYMER FRAMEWORKS: THERMAL STABILITY, CHEMICAL STABILITY AND SURFACE AREA	191
Introduction.....	191
Experimental.....	194
Results and Discussion	196
Conclusions.....	205
References.....	207
Appendices.....	211

LIST OF ABBREVIATIONS

PBIs	polybenzimidazoles
sPBI	sulfonated polybenzimidazoles
PIs	polyimides
PEIs	poly(ether imide)s
PESIs	poly(ester imide)s
PAIs	poly(amide-imide)s
PELs	phosphonium polyelectrolytes
TGA	thermogravimetric analysis
DSC	differential scanning calorimetry
DMA	dynamic mechanical analysis
GPC	gel permeation chromatography
IDT	initial decomposition temperature
$T_{d, 5\%}$	5% decomposition temperature
$T_{d, 10\%}$	10% decomposition temperature
T_g	glass transition temperature
CTE	coefficient of thermal expansion
GPC	gel permeaion chromatography
DMF	<i>N, N</i> -dimethylformamide
DMAc	<i>N, N</i> -dimethylacetamide
DMSO	dimethyl sulfoxide
TPA	triarylamine

LbL	layer-by-layer
THF	tetrahydrofuran
NMP	<i>N</i> -methyl-2-pyrrolidone
M_n	number average molar mass
M_w	weight average molar mass
NMR	nuclear magnetic resonance
AFM	atomic-force microscopy
TEM	transmission electron microscopy
SEM	scanning electron microscope
$CDCl_3$	deuterium chloroform
DCM	dichloromethane
ppm	parts per million
ACN	acetonitrile
UV-vis	ultra-violet visible
BET	Brunauer–Emmett–Teller
S_{BET}	specific surface area estimated by BET

LIST OF TABLES

Table	Page
1.1 Thermal properties of PBIs.....	4
1.2 Thermal properties of PBIs containing sulfonyl linkages.....	5
1.3 Thermal properties of PBIs containing 4-phenyl phthalazinone units.....	6
1.4 Thermal properties of sPBI.....	8
1.5 Thermal properties of PIs with oxadiazole groups	11
1.6 Thermal Properties of PIs with <i>tert</i> -butyl groups	12
1.7 Thermal Properties of PIs with triphenylmethane or diphenylmethane spacers.....	14
1.8 Thermal properties of PIs with triarylamine as linkers.....	16
1.9 Thermal properties of PIs bearing triphenylamine units as side groups.....	17
1.10 Thermal properties of PIs with fluorene groups	18
1.11 Thermal properties of PIs with benzocyclobutene units.....	20
1.12 Thermal properties of PIs with crosslinkable units.....	21
1.13 Thermal properties of PEIs with triphenylamine units.....	24
1.14 Thermal stability of PEI 74 before and after thermal curing	25
1.15 Comparison of thermal stability of PEIs containing 4,5- diazfluorene units and PEIs with fluorene units	27
1.16 Thermal stability of PEIs with anthraquinone units	28
1.17 Thermal stability of PEIs containing perfluorobiphenyl groups.....	29
1.18 Thermal properties of PESIs and PEIs.....	31

List of Tables (Continued)

Table	Page
1.19 Thermal stability of poly(benzoxazole-amide-imide) copolymers.....	33
1.20 Thermal properties of PAIs containing phosphorus	35
1.21 Thermal properties of benzimidazole-based copolyimides	36
1.22 Thermal properties of copolymers containing benzimidazole and benzoxazole units	37
1.23 Thermal properties of PELs with different alkyl groups	39
1.24 Comparison of thermal properties of R1 , LX and LO polymers	40
1.25 Thermal properties of tetraarylphosphonium polyelectrolytes with [NTf ₂] ⁻ as the counterion	41
1.26 Thermal properties of tetraarylphosphonium polyelectrolytes	42
2.1 Molecular weights and degrees of polymerization values	63
3.1 Molecular weights and degrees of polymerization for LO	107
3.2 Comparison of $T_{d,5\%}$ and T_g of R1 , LX and LO polymers	111
3.3 Influence of humidity and solvent polarity on pores observed in dip-cast films of LO polymers.	115
3.4 Critical surface energies and contact angles with water	117
3.5 Distances in optimized geometry from semi-empirical calculations at the AM1 level.	124
5.1 Absorbance of bands at 1591 and 1116 cm ⁻¹ for P1- P4	199
5.2 Thermal properties and elemental microanalysis (calculated assuming complete conversion and experimental results) of P1-P4	201
5.3 Specific surface area and water uptake for P1-P4	204

LIST OF FIGURES

Figure	Page
2.1	Absorption spectra (left) and A475 vs. numbers (right) of LX polymers layered with Pc12-100 65
2.2	Influence of spacer on the amount of Pc12-100 per 50 bilayers. 67
2.3	Influence of spacer on the root mean squared roughness of films as measured over a 5 μm \times 5 μm area 68
3.1	The distribution of pores as provided by AFM 2D-height images (5 \times 5 μm)..... 113
3.2	Influence of spacer on the amount of Pc12-100 per 50 bilayers. 118
3.3	UV-vis absorbance measurements of Pc12-100 accumulation in LbL-assembled films with LO (white) or LX (black) at 50 bilayers. 121
3.4	Newman projection (left) and line-bond view of a segment of LX2 or LO2 (A) and a segment of LX3 or LO3 (B) demonstrate expected conformations..... 122
3.5	Optimized geometries obtained from semi-empirical calculations at the AM1 level: SM2 with HT (A) and SM3 with HT (B). 123
3.6	Plots of $\log(\text{survivors})$ versus exposure time for LO and LX polymers against <i>E. coli</i> (A) and <i>S. aureus</i> (B)..... 126
4.1	IR spectra of M1 , P1 (powder), P1 (film) and <i>p</i> -toluene sulfonic acid. 170
4.2	TGA curves of P1 under N ₂ (solid line) and synthetic air (dashed line)..... 173
4.3	IR spectra of P1 (top, dashed line) and P1 after soak in 6 <i>M</i> NaOH(aq) for 24h at room temperature (middle, grey line) and 60 $^{\circ}\text{C}$ (bottom, black line) 174

List of Figures (Continued)

Figure	Page
4.4 Nitrogen sorption isotherms at 77 K (top) and CO ₂ sorption isotherms at 273 K (bottom) of P1 . Adsorption points are presented by filled squares and desorption by empty squares	176
5.1 IR spectra of Phosphonium-containing COFs (P1-P4) and starting materials M1 , M2 and <i>p</i> -toluene sulfonic acid.....	198
5.2 Scatter plot of absorbance ratio at 1116:1591 cm ⁻¹ to the phosphonium content for P1-P4	199
5.3 A) TGA curves of P1 (grey solid line), P2 (black dash line), P3 (grey dash line) and P4 (black solid line) for data collected under N ₂ , B) Relationship between char yield and phosphonium content in COFs.....	200
5.4 Changes in the ratio of absorbance at 1116 cm ⁻¹ to the absorbance at 1591 cm ⁻¹ when soaking P2 (square), P3 (diamond) and P4 (triangle) in 6 M NaOH(aq) for 120 hours at room temperature (A) or 60 °C(B).....	202
5.5 Specific surface area and water uptake for P1-P4	204
5.6 Nitrogen sorption isotherms at 77 K (A) and CO ₂ sorption isotherms at 273 K (B) of P1 (circle), P2 (square), P3 (diamond) and P4 (triangle).....	206

LIST OF SCHEMES

Scheme	Page
1.1 Synthetic route of sPBI	8
1.2 Structures of PIs having pendent pyrazole rings with amino and cyano groups.	14
1.3 Structures of acetylene-terminated PI 57	20
2.1 Synthesis of LX polymers with different spacers 'X'	61
3.1 Synthesis of LO polymers with different lengths of alkylene spacers 'X' between phosphonium centers.....	107
4.1 Examples of polyelectrolytes (A) and a network solid having tetrahedral vertices (B).....	164
4.2 P–C coupling route to $[\text{Ar}_2\text{PPh}_2]^+$ salts from HPPh ₂	171
4.3 Synthetic route to prepare M1	171
4.4 Synthetic route to prepare P1	171
5.1 Examples of COFs	192
5.2 Synthetic route of polymer network PX (X=1, 2, 3 and 4) From cyclotrimerization of M1 and M2 in a molar ratio of 0:1 (P1), 1:1 (P2), 1:2 (P3) and 1:4(P4)	197

LIST OF CHARTS

Chart		Page
2.1	Anionic polyelectrolytes that have been used in layer-by-layer assembly with phosphonium polymers.....	51
2.2	Some phosphonium-bearing polymers	54
3.1	Examples of phosphonium polyelectrolytes (PELs).....	97
3.2	Anionic polyelectrolytes that have been used in layer-by-layer assembly with phosphonium polymers.....	100
3.3	Structure of P3BHT and M3	110

CHAPTER ONE

RECENT DEVELOPMENTS IN THERMALLY STABLE POLYMERS AND PHOSPHONIUM POLYELECTROLYTES[†]

1.1 Introduction

Recent advancements in the development of thermally-stable polymers and polyelectrolytes is one motivation for researchers due to the growing interest in replacing inorganic materials with tunable and more affordably-processed organic polymers. Thermally stable polymers are generally defined as those exhibit less than 5% weigh loss when heated up to 300 °C in air or 500 °C in inert atmospheres and possess high glass transition temperature($T_g > 200$ °C),^{1,2} while maintaining their structural integrity.

One early interest in thermally stable polymers was their application in military and aerospace contexts.³⁻⁵ Later on, thermally stable polymers found possible applications in adhesives, coatings, composite matrices, fibers, films, foams, membranes and moldings.⁶ It is estimated that the worldwide market for high temperature polymers was valued at \$4360 million in 2000,² and is on an upward trajectory. According to the US industry study with forecasts for 2017 and 2012, the US demand for high temperature plastics is expected to expand by 5.8% per year and reach \$3.1 billion by 2017.⁷ More recently, polyelectrolytes possessing high thermal stability became another hot topic. The ionic groups endow polyelectrolytes with better solubility in common protic solvents such as water, making them environmental friendly and readily-processable materials.

[†] This chapter is currently in development for submission as a review article

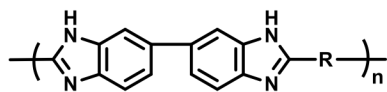
Moreover, ionic groups afford the possibility for ion exchange as a route to diversify the optical, thermal and redox profile of such materials.^{8,9}

There have been previous reviews discussion progress on thermally stable polymers up to 1991.¹⁰ Some of the review covered a wide range of polymers while other reviews focused only two or three subclasses of thermally robust polymer (e.g. poly (arylene ether)s) and aromatic polyimides containing trifluoromethyl groups.^{11,12} Readers are referred to these accounts for data appearing before 1991. This brief review will focus specifically on structure-property relationships, especially on how chemical structure can be addressed at the synthetic level to affect desired thermal properties in recent years. Polybenzimidazoles and polyimides are two well-known classes of thermally stable polymers which are the main focuses in this paper. The structure and thermal properties of these polymers were summarized and the relationship of functional groups with thermal properties will be discussed below. The most recent review about polybenzimidazoles was about their applications in fuel cell and published in 2009¹³ while a general review was published in 1997.¹⁴ Some publications about polybenzimidazoles after 2008 will be discussed. Two recent reviews about polyimides and their applications in membrane were published in 2012 and 2013,^{12,15} so papers after 2013 will be included in the following discussion. Phosphonium polyelectrolytes have received growing attention in recent years and papers related to phosphonium polyelectrolytes with improved thermal stability in recent five years will be discussed here.

1.2 Polybenzimidazoles

Polybenzimidazoles (PBIs) comprise one class of high-temperature polymers. Some PBIs can exhibit less than 10% weight loss after heating to 500 °C in air or to 700 °C in an inert atmosphere.¹⁶ The most common industrial route to fully aromatic PBIs, via polycondensation of aromatic tetraamines with aromatic dicarboxylic acids, was initially disclosed in 1961.¹⁷ Subsequent studies on high molecular weight PBIs with high performance such as good thermal stability, physical toughness at elevated temperatures, etc., became an ever-expanding area.^{3,5,18-34} Aromatic PBIs exhibit high glass transition temperatures, flame retardance and resistance to acids. As a result, they are promising candidate for ion exchange membranes^{25,27,33-35} and gas separation membranes.^{22,30,32,35} Despite these advantages, PBIs has low solubility in common organic solvents which limit their processability.¹⁷ Commercial PBIs, for example, Celazole[®], has good gas transport properties but limited solubility.^{31,36} Therefore, one of recent development in PBIs is focusing on deigning functional monomers for PBIs to improve their processability without sacrificing thermal stability and mechanical strength.³⁷⁻⁴¹ By varying the dicarboxylic acid-derived repeat unit linker, Kharul's group studied the effect of different functional groups on thermal properties of PBIs (Table 1.1, **1-7**).⁴¹ PBIs **1**, **3**, **4** and **7** showed good solubility in NMP (*N*-methyl-2-pyrrolidone), DMAc (*N,N*-dimethylacetamide), DMF (*N,N*-dimethylformamide) and DMSO (dimethyl sulfoxide) at room temperature at the concentration of 1% w/v. Although **1** and **2** share a phenylene spacer in common, the substitution pattern at this spacer has a significant difference in their solubility and thermal properties. Among all the PBIs in table 1.1, **2** exhibited the highest initial decomposition temperature (IDT = 600 °C) and char yield after heating to

Table 1.1: Thermal properties of PBIs.



PBIs ^c	R	IDT ^a (°C)	Char Yield ^b (%)
1		600	67
2		620	82
3		525	65
4		400	56
5		440	55
6		600	78
7		535	61

^a Initial decomposition temperature under N₂ with the heating rate of 10 °C/min.

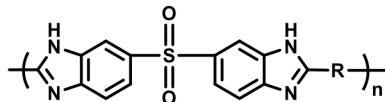
^b Residue weight% at 900 °C under N₂.

^c Data from reference 41.

900 °C. This result indicated the high thermal stability of *para*-phenylene over *meta*-phenylene spacers. PBI 4 had the lowest IDT at 400 °C, attributable to the breakage of

the C–Br bond.⁴² PBI **6** had comparable IDT and char yield to **2** indicating good thermal

Table 1.2: Thermal properties of PBIs containing sulfonyl linkages.



PBIs ^c	R	$T_{dN,5\%}$ ^a (°C)	T_g ^b (°C)
8		485	428
9		499	480
10		503	447

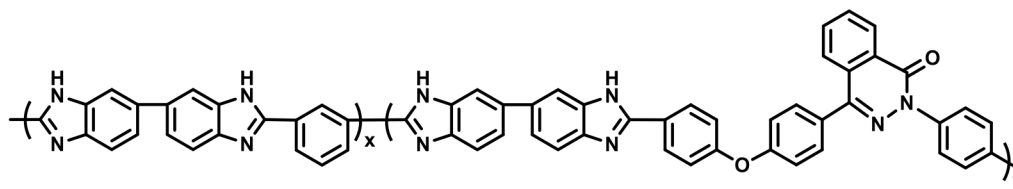
^a Determined by TGA at a heating rate of 10 °C/min under N₂.

^b Determined by DMA (Dynamic Mechanical Analysis) at a heat rate of 2 °C /min in a frequency of 1 Hz under N₂.

^c Data from reference 31.

stability of pyridine group. PBIs **4** and **7** had better gas selectivity $\alpha_{(H_2/O_2)}$ compared to the analogue PBIs **1-7**. Riffle's group prepared a series of PBIs bearing sulfone linkage between the two diaminophenyl groups (Table 1.2, **8-10**). The introduction of sulfonyl linkages in the PBI backbones was expected to reduce the chain packing efficiency and improve the gas transport properties of the PBIs.³¹ PBIs **8-10** were soluble in NMP, DMAc and DMSO in the concentration of 50 mg/mL under room temperature except that **9** was only soluble in NMP under refluxing temperature. The glass transition temperature (T_g) of PBIs **8-10** were in the range of 428-480 °C and the 5% decomposition temperature

Table 1.3: Thermal properties of PBIs containing 4-phenyl phthalazinone units.



PBIs ^d	x:y	$T_{dN,5\%}$ ^a (°C)	T_g ^b (°C)	Char yield ^c (%)
11	0:100	535	402	66
12	20:80	516	398	73
13	40:60	537	400	66
14	60:40	534	404	69
15	80:20	594	408	80

^a Determined by TGA at a heating rate of 20 °C/min under N₂.

^b Determined by DSC at a heat rate of 10 °C /min in a frequency of 10 Hz under N₂.

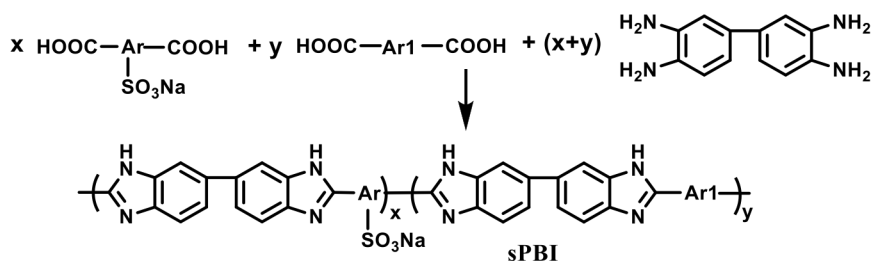
^c Residue weight% at 800 °C under N₂.

^d Data from reference 43.

under N₂ ($T_{dN,5\%}$) of them were from 485 to 503 °C. The $T_{dN,5\%}$ seems to be dependent on the substituted position of the functional groups. PBI **9** with *para* substituted benzene ring has higher $T_{dN,5\%}$ than that of **8** containing *meta* substituted benzene ring. Similar result was also found in **1** and **2** in Table 1.1. Introducing bulky group is another method to improve polymer processability by lowering the propensity for tight interchain packing. Jian's group reported a series of PBIs bearing 4-phenylphthalazinone moiety and the effect of 4-phenylphthalazinone moiety on the solubility and thermal properties were studied (Table 1.3, **11-15**).⁴³ PBIs **13-15** are soluble in NMP, DMAc, DMF, DMSO and H₂SO₄ in the concentration of 10 mg/mL under room temperature. PBIs **11** and **12** are

only partially soluble in DMSO and DMF but fully soluble in *m*-cresol while the other PBIs are insoluble. The authors attributed the improved solubility to the 4-phenyl phthalazinone group and flexible aryl ether spacer. PBIs **11-15** exhibited good thermal stability, with $T_{\text{dN},5\%}$ in the range of 516-594 °C. The $T_{\text{dN},5\%}$ of **11-15** were higher than those of the PBIs discussed before (**8-10**) indicating that the introduction of 4-phenyl phthalazinone help to improve thermal stability. The T_g of **11-15** were from 398 to 408 °C and the char yields of **11-15** were relatively high, ranging from 66 to 80% resulted from the high aromatic content. This work indicated that bulky groups like 4-phenyl phthalazinone group could improve the processability of PBIs while maintain good thermal properties, making them attractive in high temperature applications.

A large portion of recent development in modified PBIs centered on the application in ion-exchange membranes. A good reviews in this area was published in 2013,²² so a summary focused on structure-property relationships is provided here. Sulfonated polybenzimidazoles (sPBIs) have received increasing attention in fuel cell applications due to their high operating temperature (>100 °C), overcoming a drawback of current Nafion proton exchange membrane fuel cells.^{38,39,44} There are two methods to prepare sPBIs: 1) sulfonation of the PBI backbone by post-synthetic functionalization;^{17,45,46} 2) copolymerization of a sulfonated aromatic diacid with an aromatic tetraamine (Scheme 1.1) or sulfonated tetraamine with aromatic diacid.^{24,47} Among the three methods, the third one leads to the lowest incidence of side reactions while providing controllable degree of sulfonation in the ultimate sPBI. Varieties of structurally well-defined sPBI were thus synthesized and studied for their potential



Scheme 1.1: Synthetic route of sPBI.

Table 1.4: Thermal properties of sPBIs.

sPBI ^c	x:y	$T_{dN,5\%}$ ^a (°C)	T_g ^b (°C)	Char yield ^c (%)
16	0	517	322	73.8
17	1: 4	535	251	78.3
18	2: 3	547	215	81.2
19	3: 2	554	197	80.8
20	7: 3	561	196	78.5
17H^d	1: 4	438	NA	60.3
18H^d	2: 3	438	NA	71.8
19H^d	3: 2	451	NA	72.5
20H^d	7: 3	422	NA	65.6

^a Determined by TGA at a heating rate of 20 °C/min under N₂.

^b Determined by DMA at a heat rate of 10 °C /min in a frequency of 10 Hz under N₂.

^c Residue weight% at 750 °C under N₂.

^d Acid form of sPBI.

^e Data from reference 39.

applications in proton-exchange membranes.^{23,24,34,48-50} In order to explore the

relationship between degree of sulfonation degree and sPBI properties, Yan's research group prepared a series of sPBI copolymers and evaluated their thermal properties (Table 1.4).³⁹ Analysis of $T_{dN,5\%}$, T_g and char yields at 750 °C for sPBIs in free acid or sodium salts revealed that the $T_{dN,5\%}$ of the sodium form sPBIs **16-20** increased with increasing sulfonation degree. The sodium-form sPBI were shown to be more thermally stable than the corresponding free acidic forms. The authors attributed the good thermal stabilities to the sulfonic groups attached to the deactivated positions in the sPBI chains. The T_g of **16-20** were greatly affected by the sulfonic groups which T_g decreased as the sulfonation degree increased. Similar results were also reported in other sPBI.³⁸ All the sPBIs had high T_g (299-312 °C) due to ionic cross-linking as well as the rigid polymer backbones. It is interesting to note that the sPBI with higher IECs tend to have higher T_g due to the larger cross-linking densities.

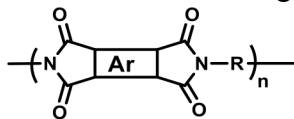
1.3 Polyimides

Aromatic polyimides (PIs) were first produced in 1908⁶ and since then they have attracted growing attention because of their excellent thermal and chemical stability, high mechanical properties and good electrical properties. PIs are promising as components of electronics, electrochromic devices, separation technologies, adhesives and coatings.^{6,51} Despite their attributes and wide applications, PIs have suffered from low solubility in common organic solvents, making them difficult to process. The low solubility results from strong inter-chain interactions in these densely packing polymers. By introducing bulky side groups, asymmetric units, flexible linkers and fluorinated groups to disrupt the

strong inter chain interaction, the solubility of PIs could be improved at the expense of decreased thermal stability and mechanical strength.⁵² Three commercially available PIs, Ultem[®], Kapton[®] and Upilex[®] have been reported since then and they often acted as standard to be compared with newly developed PIs. The glass transition temperature for Ultem[®] and Kapton[®] are 215 and 400°C respectively.⁵³ While Ultem[®] is soluble in organic solvents, Kapton[®] is a thermoset polymer. In order to balance these properties, a lot of work has been devoted to design novel PIs with increased solubility and enhanced performance.^{6,52,54-56} By atomistic molecular dynamics (MD) simulations, Sudharsan, et al. demonstrated that it was possible to increase the T_g of PIs by 80 °C by simple chemical substitution without affecting mechanical properties.⁵³ Some excellent reviews on the field of designing new monomers for polyimides have been published in 2012¹² and 2013,⁵⁷ and readers interested in this area are directed to these excellent resources for work earlier than 2013. Papers reported advances in organosoluble PIs published after 2013 will be discussed here. Recent developments in PIs are mainly focused on introducing functional groups into PIs for special photophysical or electrochemical properties to enhance processability and maintain thermal stability and mechanical strength. Another trend in modified PIs is mixing nanoparticles or inorganic particles with polymers to make composite films.⁵⁴⁻⁵⁶ Maasoomah, et al. found that the strong chemical bonding between SiC nanoparticles and polymer matrix lead to higher T_g , T_d and tensile strength.⁵⁴ The photoluminescence intensity is also dependent on the content of SiC nanoparticles.

Functional groups could be introduced either in the back bone of PIs or as pendant

Table 1.5: Thermal properties of PIs with oxadiazole groups.



PIs ^c	Ar	R	$T_{dN,5\%}$ ^a (°C)	T_g ^b (°C)
21			440	NA
22			462	318
23			505	231

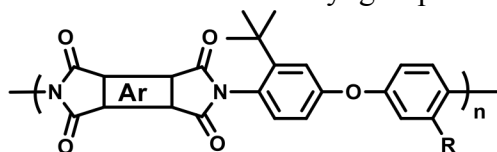
^a Determined by TGA with the heating rate of 10 °C/min under N₂.

^b Determined by DSC under N₂ atmosphere with the heating rate of 20 °C/min.

^c Data from reference 6.

substituents by different monomers. Marzena, et al. found that introducing oxadiazole moieties in PIs backbone could create donor–acceptor (D–A) system that was desirable for organic optoelectronic and electronic applications (Table 1.5, **21-23**).⁶ The T_g of **22** and **23** are 231 and 318°C, respectively. The $T_{dN,5\%}$ of the three PIs were from 440 to 505 °C. PIs **21** and **22** were partially soluble in NMP and DMSO after heating at 180 °C for 30 min. PI **23** exhibited good solubility in NMP and DMSO at room temperature which is probably due to ether linkages. Char yields of **21-23** were 55%, 66% and 43% after heating to 800 °C, respectively indicating the introduction of ether linkages could possibly decrease the char yields. It was found that carbonyl group in **22** had the highest T_g which was probably due to the rigidity of carbonyl group.

Table 1.6: Thermal properties of PIs with *tert*-butyl groups.



PIs ^c	Ar	R	$T_{dN,5\%}$ ^a (°C)	T_g ^b (°C)
24		H	525	337
25			500	341
26		H	512	279
27			510	299
28		H	502	293
29			500	303
30		H	507	217
31			512	262

^a Determined by TGA under N₂ with the heating rate of 10 °C/min.

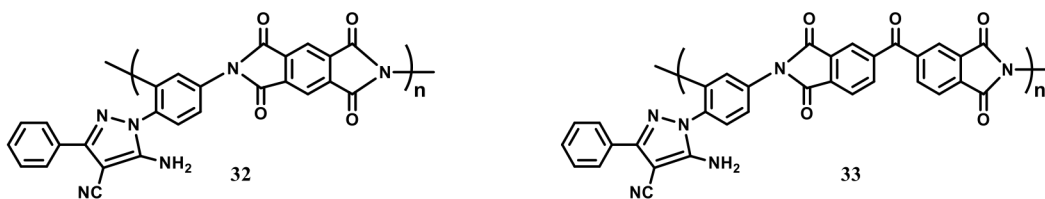
^b Determined by DSC under N₂ with the heating rate of 10 °C/min.

^c Data from reference 58

Incorporating bulky pendent groups into PIs is another method to increase the solubility. For example, Lang, et al reported that PIs with *tert*-butyl units as bulky pendant groups exhibited excellent solubility, high T_g and good transparency in film

(Table 1.6, **24-31**).⁵⁸ The authors found that *tert*-butyl groups could improve T_g of polyimides by up to 79 °C. They were soluble in common organic solvents such as NMP, DMAc, THF (tetrahydrofuran) and CH₃Cl. PIs with two *tert*-butyl pendant groups have higher T_g and better solubility than PIs with only one *tert*-butyl group. It is obvious that, the more flexible the linker between imide groups, the lower of the glass transition temperature. The elongation at break of **30** and **31**, which have the most flexible linkers, was above 60%.

More bulky pendent groups were studied by other research groups. Kim, et al reported two PIs (**32** and **33** in scheme 1.2) having pendent pyrazole rings with amino and cyano groups having enhanced solubility in NMP and DMSO compared those PIs incorporating pyrazole rings in the main chain(Scheme 1.2).⁵⁹ The $T_{dN,5\%}$ for **32** and **33** are 465 and 481 °C, respectively, indicating good thermal stability. The relative low molecular weight PIs **32** and **33** yielded brittle films because of the bulky pendent pyrazole groups. Augilar-Lugo, et al synthesized two kinds of PIs **34-36** and PIs **37-39** with triphenylmethane or diphenylmethane spacers and compared their applications in gas selectivity (Table 1.7).⁶⁰ The $T_{dN,5\%}$ of **34-39** were in the range 490–544 °C and the T_g of them were from 262 to 301 °C. PIs **37-39** with triphenylmethane groups tend to have higher $T_{dN,5\%}$ which is probably due to the high thermal stability of phenyl group. Flexible linkers such as ether group and carbonyl group tend to lower the glass transition temperature due to the decrease in rigidity of the polymer backbone. Among the six modified PIs, **39** with trifluoromethyl (CF₃) substituents showed higher gas permeability coefficient for CO₂ (23.73 Barrer) and the best ideal selectivity for the gas pair CO₂/CH₄



Scheme 1.2: Structures of PIs having pendent pyrazole rings with amino and cyano groups.

Table 1.7: Thermal properties of PIs with triphenylmethane or diphenylmethane spacers.

PIs ^c	Ar	R	$T_{dN,5\%}$ ^a (°C)	T_g ^b (°C)
34		H	513	262
35		H	511	276
36		H	490	301
37			544	269
38			510	278
39			500	293

^a Determined by TGA under N₂ atmosphere with the heating rate of 5 °C/min.

^b Determined by TMA under N₂ atmosphere with the heating rate of 5 °C/min.

^c Data from reference 60.

($\alpha = 28.93$).

Another modification of PIs is introducing triarylamine (TPA) units to endow electrochromic properties to PIs. TPA units can be either in the main chain or as the side groups of PIs. Hsiao's group found that introduction of triphenylamine units could enhance the solubility of PIs as well as bring electrochromic properties.^{52,61-63} The reaction went smoothly in DMAc at room temperature and the inherent viscosities of poly(amic acid) precursors are from 0.72-1.20 dL g⁻¹ and they could form tough films (Table 1.8, **40-45**).⁶¹ PIs **40-45** with triarylamine groups in the main chain are partially soluble in common organic solvents such as NMP, DMAc and DMF in the concentration of 10 mg/mL. The T_g of **40-45** were in the range of 290-313 °C. PIs **40-45** were thermally stable up to 480 °C, comparable to the previous-discussed PIs with di- or triphenylmethane in the polymer backbone (**34-39**). The char yields of the PIs series were from 66% to 73% which was probably due to the high aromatic content. The introduction of 4-morpholinyl substituent on the triarylamine units resulted in lower oxidation onset potentials indicating their potential in optoelectronics applications. In order to increase the solubility, this research team designed another series of PIs with triphenylamine as side groups (Table 1.9, **46-51**).⁵⁹ The polymerization of dianhydride and diamine monomers with TPA only yielded oligomers. Then the authors tried copolymerization with two diamine monomers with 1:1 ratio. The copolymerized PIs displayed excellent thermal stability with T_g in the range of 284-309 °C which was similar to the PIs with triarylamine in the backbone (**40-45**). These PIs exhibited no significant weight loss up to 450 °C under N₂ (Table 1.9). The introduction of electron-donating aliphatic units into

Table 1.8: Thermal properties of PIs with triarylamine as linkers.

PIs ^d	Ar	$T_{dN,5\%}$ ^a (°C)	T_g ^b (°C)	Char Yield ^c (%)
40		487	NA	70
41		502	306	73
42		510	292	71
43		497	290	70
44		499	313	66
45		484	296	72

^a Determined by TGA with the heating rate of 20 °C/min.

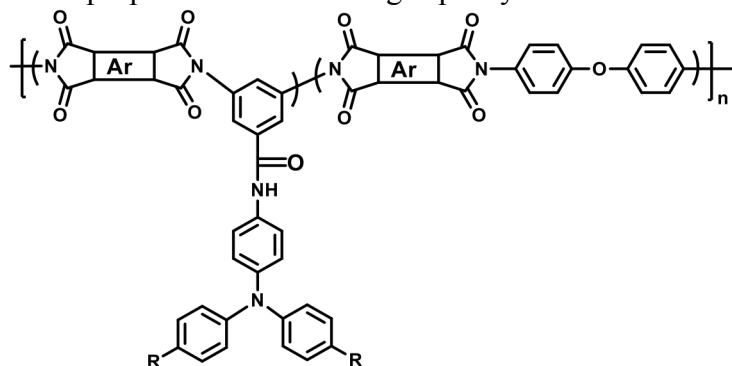
^b The sample were heated from 50 to 400 °C at a scan rate of 30 °C min⁻¹ followed by rapid cooling to 50 °C at -200 °C min⁻¹ in N₂. The midpoint temperature of baseline shift on the subsequent DSC trace (from 50 to 400 °C at heating rate 30 °C min⁻¹) was de fined as T_g .

^c Residual weight % at 800 °C under nitrogen.

^d Data from reference 61.

TPA groups lead to a small decrease of $T_{dN,10\%}$ (10% decomposition temperature under

Table 1.9: Thermal properties of PIs bearing triphenylamine units as side groups.



PIs ^c	Ar	R	$T_{dN,10\%}$ ^a (°C)	T_g ^b (°C)
46		H	510	302
47		H	552	296
48			490	309
49			542	298
50			469	284
51			531	287

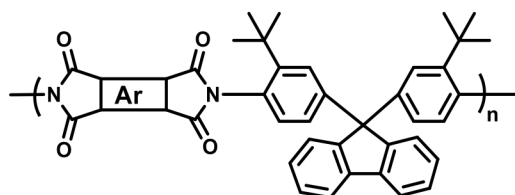
^a Determined by TGA with the heating rate of 20 °C/min.

^b Midpoint temperature of the baseline shift on the second DSC heating trace under N₂ atmosphere with the heating rate of 20 °C/min.

^c Data from reference 59.

N₂) which indicated less stability of *tert*-butyl and methoxy groups. All the PIs except **46**

Table 1.10: Thermal properties of PIs with fluorene groups.



PIs ^d	Ar	$T_{dN,5\%}$ ^a (°C)	T_g ^b (°C)	CTE ^c (ppm/°C)
52		532	NA	62
53		535	381	50
54		539	343	60
55		526	356	59
56		526	343	46

^a Determined by TGA under N₂ in the heat rate of 20 °C/min.

^b Determined by DSC under N₂ in the heat rate of 20 °C/min.

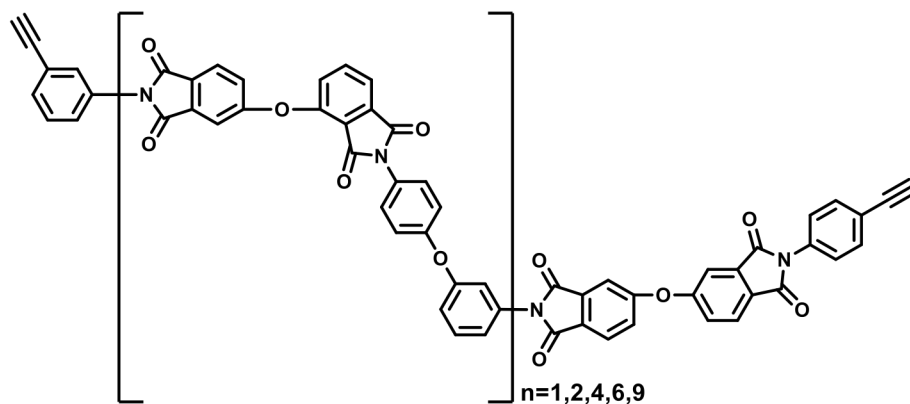
^c Determined by TMA under N₂ in the heat rate of 10 °C/min.

^d Data from reference 64

exhibited good solubility (10 mg/mL) in NMP, DMAc, DMF, THF and DMSO at room temperature which was an improvement compared to the PIs with triarylamine in the backbone. Except **48**, other PIs could be soluble in m-cresol when heated to 100 °C at the concentration of 10 mg/mL. These modified PIs were readily to form smooth pale yellow

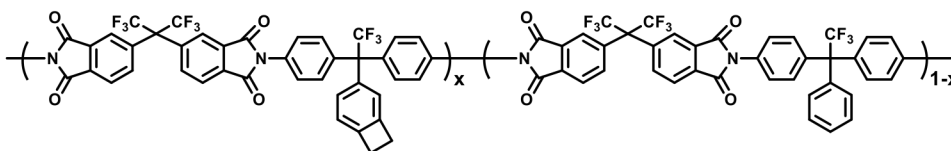
films by solvent casting. Other research groups have also reported PIs with bulky group in the polymer backbone. As discussed before, *tert*-butyl groups are widely used to increase the processability and transparency of PIs. Fluorene unit, known as a bulky group, is widely used in modification of PIs. Yi, et al tried to combine the two functional groups and incorporated them to the main chain of PIs to make tough and transparent films (Table 1.10, **52-56**).⁶⁴ The films exhibited lower cut-off wavelengths of UV-vis absorption than that of Kapton[®] film. All the PIs except **52** that had benzene as the spacer between two imide groups offered excellent solubility in CHCl₃, THF, DMF, NMP, DMAc, DMSO and m-cresol. The T_g of **53-56** were in the range of 343-381 °C, higher than all the previous discussed PIs series. The improved T_g was due to the rigidity of fluorene unit introduced to the polymer backbone. The thermal stability was not affected by the bulky fluorene groups and the PIs series were thermally stable up to 500 °C. The bulky units led to relatively higher coefficients of thermal expansion (CTE) of PIs which was probably because the decreased chain packing density and increased free volume.⁶⁴

Another advance in high-performance PIs is designing thermoplastic PIs containing crosslinkable moieties (e.g., nitrile, phthalonitrile and ethynyl units) as terminal or pendant groups.⁶⁵⁻⁶⁹ Crosslinked PIs were reported to have high thermal stability and mechanical strength and the processability and solubility of these polyimides could also be improved. It was reported that after thermal cure, the T_g of acetylene-terminated **57** could increase by 144 °C (structure in scheme 1.3).⁶⁷ Fang's research group synthesized a series of PIs with different content of thermo-polymerizable benzocyclobutene units (Table 1.11, **58-62**).⁶⁶ PIs **58-62** could undergo a ring-opening



Scheme 1.3: Structure of acetylene-terminated PI **57**

Table 1.11: Thermal properties of PIs with benzocyclobutene units



PIs ^d	x (mol%)	$T_{dN,5\%}$ ^a (°C)	T_g ^b (°C)	Tensile Strength ^c (MPa)
58	0	534	329	71.1
59	5	532	335	91.8
60	10	531	346	99.1
61	20	528	368	88.2
62	40	522	>400	74.3

^a Determined by TGA under N₂ in the heat rate of 10 °C/min.

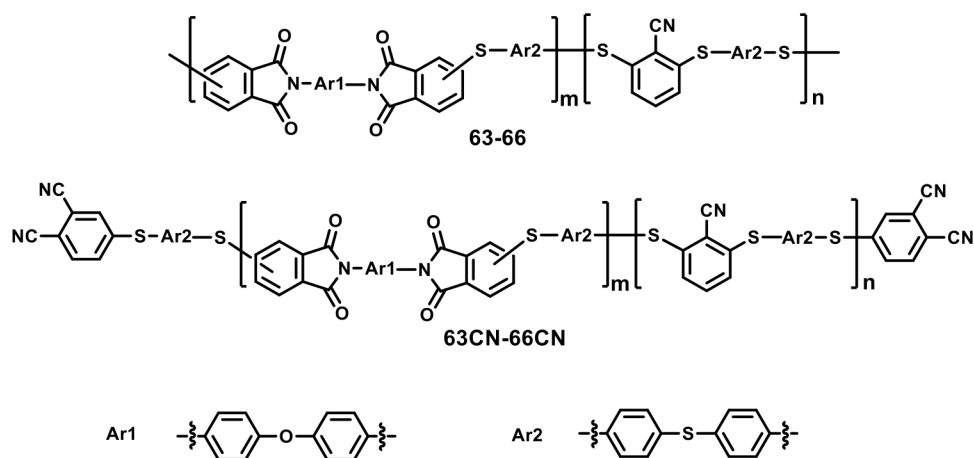
^b Determined by DSC under N₂ in the heat rate of 20 °C/min.

^c Determined by DMA under N₂ in the heat rate of 5 °C/min.

^d Data from reference 66.

reaction under high temperature (>200 °C) and tend to form poly(o-xylylene). These PIs

Table 1.12: Thermal properties of PIs with crosslinkable units.



Polymer ^e	m:n	$T_{dN,5\%}$ ^a (°C)	T_g ^b (°C)	Char Yield ^c (%)
63	10:0	494	213	52.5
64	9:1	496 (511) ^d	205 (231)	53.5
65	8:2	506 (508)	202 (248)	53.0
66	7:3	509	191	48.5
63CN	10:0	486 (512)	211 (ND)	51.9
64CN	9:1	495 (509)	205 (ND)	51.6
65CN	8:2	471 (506)	203 (ND)	50.9
66CN	7:3	494 (502)	195(ND)	52.3

^a Determined by TGA under N₂ in the heat rate of 10 °C/min.

^b Determined by DSC under N₂ in the heat rate of 20 °C/min.

^c Determined under N₂ at 800 °C.

^d Values in parentheses are from PIs after crosslinking.

^e Data from reference 65.

demonstrated good solubility in common organic solvents and high T_g .⁶⁶ The $T_{dN,5\%}$ of

58-62 were in the range of 522-534 °C indicating good thermal stability. The thermal and mechanical properties could be tuned by changing the content of crosslinkable groups (benzocyclobutene). When the content of benzocyclobutene units reached to 40 mol%, no T_g is observed when heated up to 400 °C. They also found that the tensile strength of **59** and **60** with 5-10 mol% benzocyclobutene moieties could increase by up to 39% compared to **58**. In order to access the improved performance brought by crosslinkable units, Mushtaq, et al synthesized two series of PIs and their thermal and mechanical properties were compared (Table 1.12, **63CN-66CN** and **63-66**).⁶⁵ Before thermal crosslinking, **63-66** and **63CN-66CN** were soluble in NMP, DMAc, DMF, DMSO, THF and CHCl₃ in the concentration of 20 mg/mL at room temperature which was an improvement compared the aforementioned modified PIs series. The author proposed that flexible ether and thioether linkers, isomeric asymmetrical units and pendant nitrile and phthalonitrile groups were the three possible reasons for improved solubility. After crosslinked, both series were insoluble in all the solvents tested before. **63-66** and **63CN-66CN** had similar T_g (~200 °C). As the content of pendant nitrile group increase, $T_{dN,5\%}$ slightly increased in both series (Table 1.12). After thermal cured at 360 °C for 6 h, there was a larger increase in $T_{dN,5\%}$ of **63CN-66CN** than that of **63-66**. No obvious T_g observed for **63CN-66CN** when heated up to 450 °C while the T_g of **63-66** increased up to 46 °C (e.g., **65**). All the thermal results indicated that **63CN-66CN** with phthalonitrile groups exhibited better crosslinking ability of than PI series with nitrile groups.⁶⁵

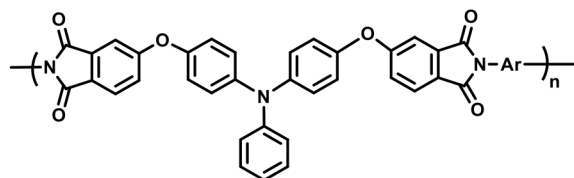
1.4 Copolymer

Copolymerization is one common method to combine the attributes of different polymers and improve the performance of thermally stable polymers. Some good reviews on this topic were published in 1997, 1998 and 2003.^{2,14,70} For example, poly (arylene ethers) and polysulfone are commonly used to copolymerize with other polymers to produce thermally and chemically stable products. A series of copolymer bearing polyimides in the backbone and the effect of substituents on their thermal properties will be discussed below.

1.4.1 Poly (ether imide)s and Poly(ester-imide)s

Poly(ether imide)s (PEIs) is one kind of thermally stable polymer which exhibited better solubility than PIs without sacrificing other properties such as thermal stability.⁷¹ In previous discussion Hsiao's research group synthesized a series of PIs with triarylamine groups as pendant groups or in the polymer backbone.^{52,59,63,69} PIs with triarylamine groups in the main chain have high T_g (up to 313 °C) and good thermal stability but are partially soluble in organic solvents.⁶³ An alternative way is to introduce triarylamine groups as pendent groups while oligomers with low molecular weight was achieved.⁵⁹ In order to make flexible films with high coloration efficiency and high redox stability, they tried to copolymerize PIs with polyether to make poly (ether-imide)s with triphenylamine in the back bone (Table 1.13, **67-73**).⁷² No significant weight loss were observed for **67-73** when heated to 500 °C under N₂ or air and their T_g were in the range of 211-299 °C. As it was discussed before, more rigidity of spacer led to higher T_g (e.g., **71**). By comparing PEIs **67-73** in Table 1.13 and PIs **40-45** bearing triphenylamine groups in the backbone in Table 1.8, it was found that PEIs **67-73** have relatively lower

Table 1.13: Thermal properties of PEIs with triphenylamine units.



PEIs ^d	Ar	$T_{dN,5\%}$ ^a (°C)	T_g ^b (°C)	Char Yield (%)
67		505	239	61
68		536	227	58
69		513	211	60
70		572	227	66
71		571	299	66
72		527	252	65
73		536	260	60

^a Determined by TGA under N₂ in the heat rate of 20 °C/min.

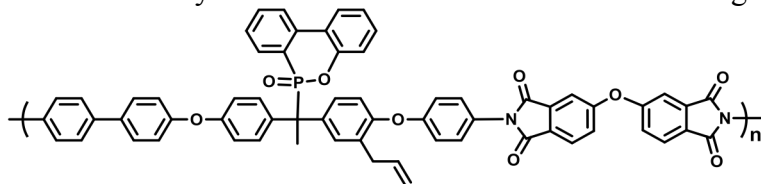
^b Determined by DSC under N₂ in the heat rate of 20 °C/min.

^c Residual weight at 800 °C under N₂.

^d Data from reference 72.

T_g , which was probably due to the flexible ether linkers.⁷³ After chemical imidization,

Table 1.14: Thermal stability of PEI **74** before and after thermal curing.



PEIs ^f	$T_{dN,5\%}$ ^a (°C)	T_g ^b (°C)	Char Yield ^c (%)	CTE ^d (ppm/°C)
74	443(447) ^e	253 (307)	54(60)	52(29)

^a Determined by TGA under N₂ in the heat rate of 20 °C/min,

^b Determined by DMA under N₂ in the heat rate of 5 °C/min.

^c Residual weight at 800 °C under N₂.

^d Coefficient of thermal expansion in the range of 50–150 °C.

^e Values in parentheses are the from polymer after thermal curing.

^f Data from reference 74

PEIs **68-72** exhibited good solubility in NMP, DMAc, DMF and CHCl₃ in the concentration of 10 mg/mL under room temperature. The authors reported that the PEIs films have reversible electrochemical oxidation and strong color changes which was promising in anodically coloring materials.

Thermo-curable PEIs is another advance recently. As it was discussed before, PIs terminated with crosslinkable groups displayed excellent thermal stability and mechanical strength. So some research groups have devoted to inventing thermo-curable PEIs. Lin's group have reported thermosetting PEIs containing allyl groups (Table 1.14, **74**).⁷⁴ After thermal curing, the T_g of **74** increase from 253 to 307 °C. The $T_{dN,5\%}$ did not increase a lot which was probably due to the breakage of P-C bond. The char yield of **74** after thermal curing increased by 6%. The coefficient of thermal expansion (CTE) of **74**

after thermal curing decreased a lot, from 52 to 29 ppm/°C, which indicated that thermal crosslinking could help to decrease CTE.

Incorporating bulky groups such as fluorene units were discussed before and the modified PIs displayed outstanding thermal stability (Table 1.10, T_g in the range of 343-381 °C).⁶⁴ Herein, Li's group synthesized a series of PEIs with 4,5-diazafluorene and trifluoromethyl groups (Table 1.15, **75-79**).⁷⁵ The number-average molecular weights (M_n) of **75-79** were in the range of 13,000-18,000 measured by GPC (gel permeation chromatography) using polystyrene as standards and the inherent viscosities (η_{inh}) were from 0.63 to 0.83 dL/g in the concentration of 0.5 g dL⁻¹ in DMAc at 30 °C. The PEIs films of **77-79** after thermal imidization were still soluble in NMP, DMAc, DMF, DMSO, m-cresol and pyridine in the concentration of 5 mg/mL. This was an improvement compared to the PIs with bulky groups (e.g., fluorene units) discussed before, which most of the PIs films after thermal imidization were insoluble in organic solvents.^{61,64,75} The author attributed the improved solubility to the bipyridine moiety in the 4,5-diazafluorene group. To access the effect of 4,5-diazafluorene on thermal stability of **77-79**, the author compared the properties of **77-79** with their analogues incorporating fluorene units in the backbone (Table 1.15, **80-83**).⁷⁶ The T_g of **75-79** were in the range of 310 to 344 °C which was roughly 60 °C higher than their analogues **80-83**. The author attributed the rigidity of bipyridine moieties to the increase of T_g . Compared to the PIs **52-56** with fluorene units in Table 1.10, T_g of PEIs **75-79** were slightly lower which was probably resulted from the flexible ether linkage and trifluoromethyl groups. Among the PEIs **75-79**, **78** had the lowest T_g , indicating that the flexibility of phenyl ether linkage decreased

Table 1.15: Comparison of thermal stability of PEIs containing 4,5-diazafluorene units and PEIs with fluorene units.

PEIs	Ar	$T_{dN,5\%}^a$ (°C)	T_g^b (°C)	Char Yield ^c (°C)
75		535	344	64
76		532	336	63
77		530	321	66
78		543	310	66
79		525	331	61
80		NA	281	NA
81		NA	270	NA
82		NA	258	NA
83		NA	276	NA

^a Determined by TGA under N₂ in the heat rate of 20 °C/min.

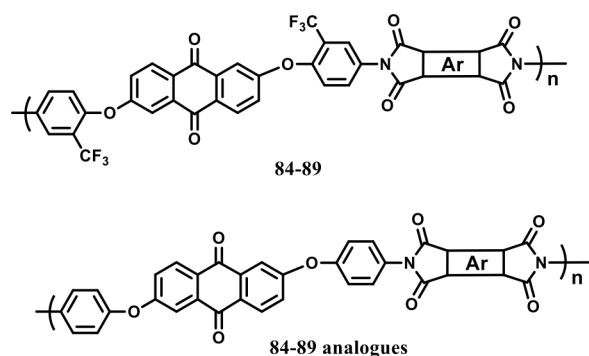
^b Determined by DSC under N₂ in the heat rate of 20 °C/min.

^c Residual weight% at 800 °C under N₂.

^d Data from reference 75 (**77-79**) and 76 (**80-83**).

T_g . The $T_{dN,5\%}$ of **75-79** were from 525 to 543 °C and **78** had the highest $T_{dN,5\%}$ which

Table 1.16: Thermal stability of PEIs with anthraquinone units.



PEIs ^c	Ar	$T_{dN,5\%}$ ^a (°C)	T_g ^b (°C)	Char Yield ^c (°C)
84		513(587) ^d	312(318)	54(64)
85		565(574)	289(295)	56(65)
86		545(564)	275(288)	53(63)
87		547(583)	263(270)	53(62)
88		451(525)	276(289)	50(58)
89		536(565)	281(285)	51(56)

^a Determined by TGA under N₂ in the heat rate of 20 °C/min.

^b Determined by DSC under N₂ in the heat rate of 20 °C/min.

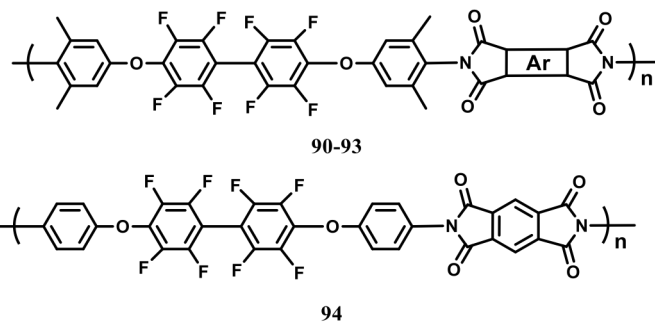
^c Residual weight% at 800 °C under N₂.

^d Values in parentheses are from their analogues.

^e Data from reference 77.

implied the good thermal stability brought by phenyl ether linkage. The char yields of **75-79** were in the range of 61%-66%, slightly higher than those PIs **52-56** with fluorene groups in the backbone.

Table 1.17: Thermal stability of PEIs containing perfluorobiphenyl groups.



PEIs ^d	Ar	$T_{dN,5\%}$ ^a (°C)	T_g ^b (°C)	Char Yield ^c (°C)
90		481	286	50
91		478	345	53
92		484	300	55
93		480	280	53
94	—	559	338	48

^a Determined by TGA under N₂ in the heat rate of 10 °C/min.

^b Determined by DSC under N₂ in the heat rate of 10 °C/min.

^c Residual weight% at 800 °C under N₂.

^d Data from reference 78

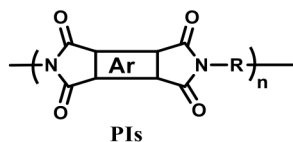
Fluorination is believed to be an effective and promising route to enhance the (electro)chemical, thermal and hydrolytical stability, mainly because of the higher bond strength of the C–F bond compared to the C–H bond.^{77,78} Other than the adventure in incorporating triarylamine units in to PEIs and PIs, Hsiao's group also studied aromatic fluorinated PEIs with anthraquinone moieties (Table 1.16, **84-89** and their analogues).⁷⁷ The T_g of **84-89** were in the range of 263–312 °C. Consistent to what discussed before,

PEI bearing phenyl ether spacer (**87**) had the lowest T_g . Except for **88**, no obvious weight loss was observed when heated up to 500 °C under N₂ for other PEIs. The relatively low $T_{dN,5\%}$ of **88** was probably resulted from the sulfonyl group between the phthalimide units. The author also compared **84-89** to their analogues without CF₃ pendent groups. As expected, PEIs with CF₃ units (**84-89**) exhibited better solubility than their analogues without CF₃ units. Introducing CF₃ pendent groups lead to slightly lower T_g . The $T_{dN,5\%}$ of **88** without CF₃ substituents increased by 74 °C indicating that the thermal stability could be decreased by introducing too many electron-withdrawing groups in the polymer main chain.

Yeo, et al reported a series of PEIs containing perfluorobiphenyl groups (Table 1.17, **90-93**).⁷⁸ The methyl groups at the *ortho* position were expected to improve the T_g of **90-93** as it hindered intermolecular packing. This hypothesis was confirmed by the slightly higher T_g of **91** than that of **94** without methyl groups. The T_g of **90-93** were from 280 to 345 °C and $T_{dN,5\%}$ of **90-93** were in the range of 478-484 °C which was lower than previous discussed PEIs **84-89**. It was found that **90** and **93** have similar T_g and $T_{dN,5\%}$, consistent with previous reported PIs **27** and **29** containing *tert*-butyl as pendent groups in Table 1.6 that also had similar T_g and $T_{dN,5\%}$.⁵⁸ The high fluorine content resulted from perfluorobiphenyl groups lead to low refractive indices making them promising in advanced optoelectronics.

Poly(ester imide)s (PESIs) were demonstrated to be an effective way to modify PIs and PESIs usually had high T_g and low water absorption which are attractive in electronic devices.^{79,80} In order to study the effect of electron affinities on the properties

Table 1.18: Thermal properties of PESIs and PEIs.



Polymer ^c	Ar	R	$T_{dN,5\%}^a$ (°C)	T_g^b (°C)
95			481	220
96			494	250
97			481	217
98			484	236
99			541	211
100			546	222

^a Determined by TGA under N₂ with the heating rate of 10 °C/min.

^b Determined by DSC under N₂ with the heating rate of 20 °C/min.

^c Data from reference 79.

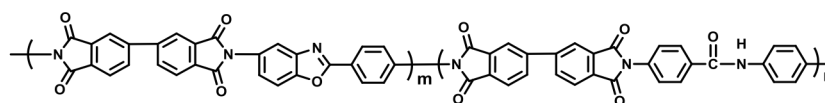
of PESIs, Fang's group reported two kinds of PESIs and PEIs as standards (Table 1.18, PESIs **95-98**, PEIs **99-100**).⁷⁹ PESIs **95-98** could form transparent and tough films and they were soluble in common organic solvents mentioned above in the concentration of 10 mg/mL at room temperature. The position of ester groups seems to have little effect on the solubility. The T_g of **95-100** were in the range of 211-250 °C and the PIs containing

CF₃ groups exhibited higher T_g compared to their analogues without CF₃ groups. The author attributed the increase in T_g to the increased chain rigidity and steric effect brought by *meta* substituted CF₃ groups. As expected, PESIs **95** and **96** with electron withdrawing groups closer to imide groups had higher T_g while PEIs bearing electron donating groups like phenyl ether had relatively lower T_g (PEIs **99** and **100**). And the variation in the position of ester linkage led to slightly difference in T_g . The $T_{dN,5\%}$ of these polymers were from 481 to 556 °C. PESIs **95-98** had lower $T_{dN,5\%}$ than that of PEIs **99** and **100** which was probably due to the decomposition of ester groups. The char yields of PESIs **95-98** were in the range of 46% to 50% which was slightly smaller than those of PEIs **99** and **100**, ranging from 52 to 54%.

1.4.2 Poly(amide-imide)s

Poly(amide-imide)s (PAIs) which have amide and cyclic imide groups on the polymer backbone is one method to increase the processability and keep relatively high thermal stability of PIs.⁸¹⁻⁸⁴ Gu's group reported a series of poly(benzoxazole-amide-imide) copolymers that are suitable for interlevel dielectrics in microelectronics and explored the effect of amide content on thermal stabilities (Table 1.19, **101-105**).⁸¹ The $T_{dN,5\%}$ of **101-105** were from 557 to 567 °C indicating good thermal stability. And the $T_{dN,5\%}$ increased as the amide content increase. PAIs **101-103** exhibited two T_g and the author assumed that the higher T_g was related to the amorphous chains located close to or at the ordered domains and the lower T_g results from amorphous domain.⁸¹ The increase in T_g of **101-104** corresponded to hydrogen-bonding interaction from amide groups. The char yields of **101-105** were in the range of 58-63% which decreased as the amide

Table 1.19: Thermal stability of poly(benzoxazole-amide-imide) copolymers.



PAIs ^d	m:n	$T_{dN,5\%}$ ^a (°C)	T_g ^b (°C)	Char Yield ^c (%)
101	100:0	582	304, 410	63
102	80:20	567	326, 364	63
103	60:40	562	322, 414	62
104	40:60	560	440	60
105	0:100	557	446	58

^a Determined by TGA under N₂ in the heat rate of 10 °C/min.

^b Determined by DMA at 1 Hz under N₂ in the heat rate of 10 °C/min.

^c Residual weight% at 800 °C under N₂.

^d Data from reference 81.

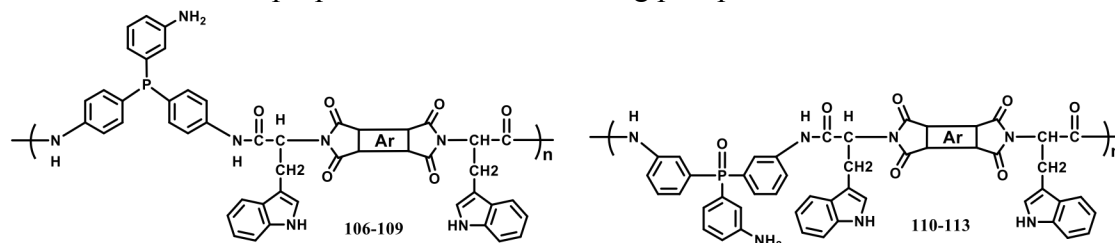
content increased. Narula's group reported two series of PAIs containing phosphorus and explored their application in flame retardant materials (Table 1.20, **106-113**).⁸³ The incorporation of organophosphorus groups (phosphine or phosphine oxide) and bulky pendent triphenylamine group were expected to endow the polymers with outstanding thermal oxidative stability, improved solubility in organic solvents and good adhesion to other compounds. Qualitative solubility test indicated that **106-113** exhibited excellent solubility in NMP, DMSO, DMAc, DMF, pyridine and H₂SO₄. The $T_{dN,10\%}$ of **106-113** were from 518 to 592 °C. Compared to **106-109**, there was smaller difference in $T_{dN,10\%}$ of **110-113** indicating that the thermal stability was dependent on the phosphine oxide groups. The char yields of **106-113** were in the range of 49-70% resulting from high

aromatic content. It was found that the T_g of **111** and **112** that containing phosphine oxide groups had slightly higher T_g than that of **107** and **108**.

1.4.3 Benzimidazole-imide Copolymers

PBIs and PIs are all high-performance polymers discussed before. Some publications have been reported to combine these two polymers to make desired materials for electronic devices which required linear coefficient of thermal expansion. Dang's groups reported a series of copolymer with different content of benzimidazole content and the effect of benzimidazole content on thermal properties were studied (Table 1.21, **114-119**).⁸⁵ The coefficients of thermal expansion (CTE) of copolymer were from 4.7 to 41.3 ppm/°C which was lower than common PIs. Compare to the PEIs discussed before, the copolymer exhibited higher T_g that is in the range of 282-331 °C. The $T_{dN,5\%}$ of **114-119** were in the range of 515-562 °C, comparable to PEIs discussed before. As the benzimidazole content increased, the T_g and $T_{dN,5\%}$ increased correspondingly. Their results indicated that incorporation of benzimidazole units to PIs could increase the T_g and decrease CTE without affecting other properties making these copolymers attractive in applications of microelectronics. Sun, et al. reported a series of copolyimide fibers containing benzimidazole and benzoxazole units in the polymer backbone (Table 1.22, **120-124**).⁸⁶ The introduction of benzoxazole moieties was believed to improve the mechanical properties.⁸⁷ So the effect of benzoxazole content on thermal and mechanical properties was studied in this paper. The $T_{dN,5\%}$ of **120-124** were from 563 to 570 °C, indicating good thermal stability. As the benzoxazole content increased, the thermal stability slightly decreased. **120** with only benzimidazole units exhibited the highest

Table 1.20: Thermal properties of PAIs containing phosphorus moieties.



PAIs	Ar	$T_{dN,10\%}^a$ (°C)	T_g^b (°C)	Char Yield ^c (°C)
106		518	228	52
107		592	253	63
108		555	226	65
109		531	224	49
110		565	226	70
111		567	265	66
112		569	251	61
113		558	211	65

^a Determined by TGA under N₂ atmosphere with the heating rate of 10 °C/min.

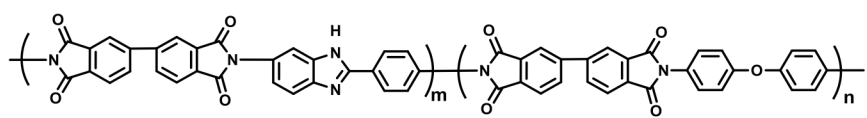
^b Determined by DSC under N₂ atmosphere with the heating rate of 10 °C/min.

^c Residual weight% at 800 °C under N₂.

^d Data from reference 83.

$T_{dN,5\%}$ which was probably due to the hydrogen-bonding intermolecular interactions brought by benzimidazole groups. The T_g of **121-123** decreased from 321 to 308 °C as

Table 1.21: Thermal properties of benzimidazole-based copolyimides.



Polymers ^d	m:n	$T_{dN,5\%}$ ^a (°C)	T_g ^b (°C)	CTE ^c (ppm/°C)
114	1:9	515	282	41.3
115	2:8	530	290	37.1
116	3:7	543	301	31.0
117	4:6	553	310	23.8
118	5:5	558	331	16.7
119	6:4	562	–	4.7

^a Determined by TGA under N₂ atmosphere with the heating rate of 5 °C/min.

^b Determined by DSC under N₂ atmosphere with the heating rate of 10 °C/min.

^c Coefficient of thermal expansion was measured under N₂ atmosphere with the heating rate of 5 °C/min..

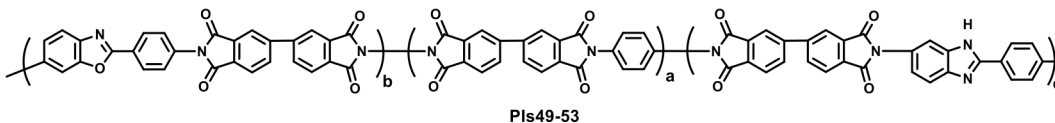
^d Data from reference 85.

the benzoxazole content increased. The optimum tensile strength was 2.26 GPa for **121** and the optimum initial modulus was 145.0 GPa for **123**. The author attributed the improved mechanical properties to the hydrogen-bonding intermolecular interactions from benzimidazole groups and high molecular orientation from benzoxazole moieties.

1.5 Phosphonium Polyelectrolytes

Polyelectrolytes have receiving growing interest due to their versatile properties such as solubility in protic solvents^{58,59,61} and ability to self-assemble as by via layer-by-layer (LbL) processes.^{62,63} Phosphonium salts have promise in biological,^{64,88} alkaline-exchange membrane,^{65,66} solar cell⁶⁷⁻⁶⁹ and electronics applications.⁸⁹ Cationic

Table 1.22: Thermal properties of copolymers containing benzimidazole and benzoxazole units.



Polymers ^c	b:c	$T_{dN,5\%}$ ^a (°C)	T_g ^b (°C)
120	0:4	570	–
121	1:3	567	321
122	1:1	565	318
123	3:1	564	308
124	4:0	563	–

^a Determined by TGA under N₂ with the heating rate of 10 °C/min.

^b Determined by DMA under N₂ with the heating rate of 5 °C/min and a load frequency of 1 Hz at the temperature from 50 to 450 °C.

^c Data from reference 86.

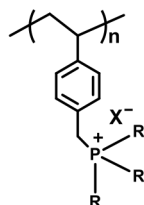
polyelectrolytes that incorporating phosphonium, ammonium and imidazolium groups in the main chain or side chain have been demonstrated to be excellent candidates for anti-bacterial application,^{72,88,90-94} gene delivery agent⁶⁴ and phase transfer catalyst.⁶⁸ As discussed in previous sections, polymers bearing phosphine or phosphine oxide groups exhibited improved thermal stability and flame retardancy.^{74,83} Some research articles have reported that PELs have better thermal stability compared to their ammonium analogues.⁸ Thermal stability is one of the important properties for the wide applications of cationic polymers. Tetraarylphosphonium salts in the form of [PAr₄]⁺[NTf₂]⁻ was

reported to be thermally stable up to 425 °C in the air for several days.⁹⁵ Phosphonium polyelectrolytes incorporating tetraarylphosphonium units were also demonstrated to be thermally stable up to 460 °C under N₂.

It is desired to study the structure-property relationship of cationic polyelectrolytes to design high-performance polyelectrolytes. Long's group studied the effect of counterions and alkyl substituents on the thermal properties of PELs (Table 1.23, **125-128**).⁸ They also compared the thermal stability of PELs with ammonium analogues and found that PELs exhibited improved thermal stability. As the alkyl chain length of R group increased from methyl to butyl, both $T_{dN,5\%}$ and T_g of **125-128** decreased. The author attributed the decreased T_g to the increased free volume brought by the longer alkyl chain. This hypothesis was again demonstrated by the results that PELs with bulkier counterions such as BF₄⁻ and NTf₂⁻ had lower T_g than PELs containing smaller counterions Cl⁻. They also found that ammonium analogues show similar T_g but significant lower $T_{d,5\%}$ which implied that the thermal stability was highly dependent on the cationic center. The instability of ammonium polyelectrolytes resulted from two possible degradation pathways: 1) Hoffman elimination; 2) reverse Menschutkin degradation.⁸ The thermal stability was also found to be dependent on the basicity of the counterions. PELs containing Cl⁻ have the lowest $T_{dN,5\%}$ and PELs containing NTf₂⁻ was the most thermal stable one and similar results also reported in another paper.⁹⁶ With this information, Long's group moved on to study the effect of charge density on thermal stability and the structure of **R1** was in the Table 1.24.⁹⁷ Similar research has also been carried out in Smith's group which they studied the influence of spacers and side chains on the thermal

properties of PELs. They reported two series of PELs that are **LX** and **LO** (Table 1.24).⁹⁸

Table 1.23: Thermal properties of PELs with different alkyl groups.



PELs ^c	R	$T_{dN,5\%}$ ^a			T_g ^b		
		Cl ⁻	BF ₄ ⁻	NTf ₂ ⁻	Cl ⁻	BF ₄ ⁻	NTf ₂ ⁻
125	methyl	421	437	465	284	230	91
126	ethyl	393	417	462	240	195	68
127	propyl	377	422	452	195	167	71
128	butyl	374	427	437	177	143	66

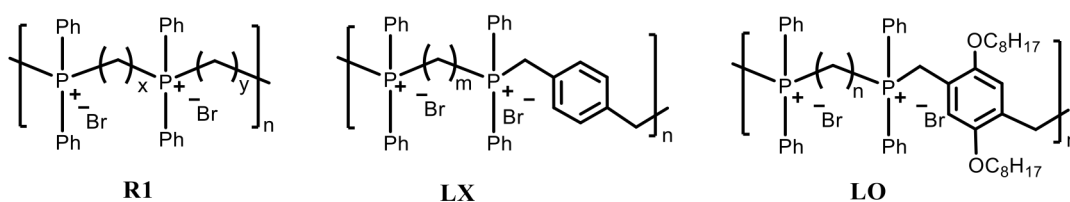
^a Determined by TGA under N₂ with the heating rate of 10 °C min⁻¹

^b Determined by DSC under N₂ with the heating rate of 10 °C min⁻¹

^c Data from reference 8.

The $T_{d,5\%}$ of **LX** is higher than that of **R1** with similar charge density, which indicates that the introduction of *para*-substituted xylol group could increase the thermal stability of PELs. **LO** series exhibited lower $T_{dN,5\%}$ resulting from the instability of octyloxy groups. The charge density could affect both $T_{dN,5\%}$ and T_g which PELs with four methylene groups between the two phosphonium charge sites have the best thermal stability. By comparing the T_g of **LO** and **R1** series, it was found that PELs bearing octyloxy as side groups have lower T_g which is probably due to the increased free volume brought by side chains.

Table 1.24: Comparison of thermal properties of **R1**, **LX** and **LO** polymers.



R1^e			LX^f			LO		
x, y	$T_{dN,5\%}^a$ (°C)	T_g^b (°C)	m	$T_{dN,5\%}^c$ (°C)	T_g^d (°C)	n	$T_{dN,5\%}^c$ (°C)	T_g^d (°C)
2, 12	300	148	2	312	NA	2	271	NA
--	--	--	3	362	NA	3	277	137
4, 4	339	172	4	364	NA	4	278	124
6, 4	329	154	5	355	200.7	5	275	118
6, 6	328	n.d.	8	356	NA	8	275	96

^a Determined by TGA with the heating rate of 10 °C min⁻¹ under N₂

^b Determined by DSC with the heating rate of 10 °C min⁻¹ under N₂

^c Determined by TGA with the heating rate of 20 °C min⁻¹ under N₂

^d Determined by DSC with the heating rate of 20 °C min⁻¹ under N₂

^e Data from reference 97

^f Data from reference 98

One of the important applications of PELs is ion-exchange membrane which requires excellent chemical resistance and thermal stability. It was found that PELs with α -H adjacent to phosphonium units could undergo nucleophilic substitution leading to P-C bond breakage or deprotonation to form phosphine oxide.⁹⁹ In order to improve the chemical and thermal stability, Smith group reported a simple synthetic route to tetraarylphosphonium polyelectrolytes in order to eliminate the α -H and possible reaction

Table 1.25: Thermal properties of tetraarylphosphonium polyelectrolytes with $[\text{NTf}_2]^-$ as the counterion.

PELs	R	$T_{\text{dN},5\%}^{\text{a}}$ ($^{\circ}\text{C}$)
129		403
130		440
131		460

^a Determined by TGA with the heating rate of $20\text{ }^{\circ}\text{C min}^{-1}$ under N_2

^b Data from reference 9.

pathways under nucleophile attack.^{9,99-101} The PELs **129-131** exhibited excellent thermal stability and chemical resistance (Table 1.25). As it discussed before, PELs with ditriflamide ($[\text{NTf}_2]^-$) as counterions had better thermal stability than PELs with halide counterions. PELs **129-131** were synthesized from bromide monomers and contain bromide as counterions and were underwent anion exchange for better thermal stability. PELs **129-131** exhibited $T_{\text{dN},5\%}$ higher than $400\text{ }^{\circ}\text{C}$ and **131** were stable in $6\text{ M NaOH}(aq)$ at $65\text{ }^{\circ}\text{C}$ for at least 24 h .⁹ This is a big improvement compared to previous mentioned

Table 1.25: Thermal properties of tetraarylphosphonium polyelectrolytes with [NTf₂]⁻ as the counterion.

PELs	R	$T_{dN,5\%}$ ^a (°C)
129		403
130		440
131		460

^a Determined by TGA with the heating rate of 20 °C min⁻¹ under N₂

^b Data from reference 9.

LX and **LO** polymers that have sp³ carbon connected to phosphonium charge centers. And the thermal stability was also greatly affected by the functional groups bonded to phosphonium units. PEL **131** had the highest $T_{d,5\%}$ which is 57 °C higher than that of **129**. To move one step further, Smith group reported another series of PELs maintaining good thermal stability without anion exchange (Table 1.26, **132-139**).¹⁰¹ Neutral polymers such as polyimides bearing these functional groups on the backbone were discussed before and they all exhibited $T_{dN,5\%}$ over 450 °C.^{61,72} The $T_{dN,5\%}$ for **132-139** were in the range of 355 to 441 °C. The author attributed to the lower stability of **138** to the strong electro-

withdrawing group sulfonyl attached tetraarylphosphonium units. This hypothesis was demonstrated by that **132** bearing electron-donating group on the polymer backbone had the highest $T_{dN,5\%}$. The author also found that the chemical stability was greatly dependent on whether an electro-withdrawing group was attached to the aryl ring.¹⁰¹

As a summary, this paper summarized the recent development in thermally stable polymers and polyelectrolytes. The effect of functional groups, charge density and counterions on thermal properties was discussed. The information is beneficial for those who are working on designing new materials with good thermal stability.

1.6 Reference

1. P. M. Hergenrother. *Recl. Trav. Chim. Pays-Bas-J. Roy. Neth. Chem. Soc.* **1991**, *110*, 481-491.
2. P. M. Hergenrother. *High Perform. Polym.* **2003**, *15*, 3-45.
3. R. T. Foster, C. S. Marvel. *J. Polym. Sci.* **1965**, *3*, 417-421.
4. H. Vogel, C. S. Marvel. *Journal of Polymer Science* **1961**, *50*, 511-539.
5. H. Vogel, C. S. Marvel. *J. Polym. Sci.* **1963**, *1*, 1531-1541.
6. C. E. Sroog. *Prog. Polym. Sci.* **1991**, *16*, 561-694.
7. Freedonia, US Industry Study with Forecasts for 2017 & 2022. High-Temperature Plastics **2013**.
8. S. T. Hemp, M. Q. Zhang, M. H. Allen, S. J. Cheng, R. B. Moore, T. E. Long. *Macromol. Chem. Phys.* **2013**, *214*, 2099-2107.
9. W. Wan, X. Yang, R. C. Smith. *Chem. Commun.* **2017**, *53*, 252-254.
10. M. A. Meador. *Annual Review of Materials Science* **1998**, *28*, 599-630.

11. M. G. Dhara, S. Banerjee. *Prog. Polym. Sci.* **2010**, *35*, 1022-1077.
12. D. J. Liaw, K. L. Wang, Y. C. Huang, K. R. Lee, J. Y. Lai, C. S. Ha. *Prog. Polym. Sci.* **2012**, *37*, 907-974.
13. Q. F. Li, J. O. Jensen, R. F. Savinell, N. J. Bjerrum. *Prog. Polym. Sci.* **2009**, *34*, 449-477.
14. T. S. Chung. *Journal of Macromolecular Science-Reviews in Macromolecular Chemistry and Physics* **1997**, *C37*, 277-301.
15. K. Vanherck, G. Koeckelberghs, I. F. J. Vankelecom. *Prog. Polym. Sci.* **2013**, *38*, 874-896.
16. D. I. Packham, J. D. Davies, H. M. Paisley. *Polymer* **1969**, *10*, 923-931.
17. P. Staiti, F. Lufrano, A. S. Arico, E. Passalacqua, V. Antonucci. *J. Membr. Sci.* **2001**, *188*, 71-78.
18. M. Ueda, M. Sato, A. Mochizuki. *Macromolecules* **1985**, *18*, 2723-2726.
19. M. A. Bingham, B. J. Hill. *J. Therm. Anal.* **1975**, *7*, 347-358.
20. D. R. Coffin, G. A. Serad, H. L. Hicks, R. T. Montgomery. *Text. Res. J.* **1982**, *52*, 466-472.
21. Q. F. Li, R. H. He, R. W. Berg, H. A. Hjuler, N. J. Bjerrum. *Solid State Ionics* **2004**, *168*, 177-185.
22. Q. F. Li, J. O. Jensen, R. F. Savinell, N. J. Bjerrum. *Prog. Polym. Sci.* **2009**, *34*, 449-477.
23. J. A. Mader, B. C. Benicewicz. *Macromolecules* **2010**, *43*, 6706-6715.
24. J. Jouanneau, R. Mercier, L. Gonon, G. Gebel. *Macromolecules* **2007**, *40*, 983-990.

25. L. Xiao, H. Zhang, T. Jana, E. Scanlon, R. Chen, E. W. Choe, L. S. Ramanathan, S. Yu, B. C. Benicewicz. *Fuel Cells* **2005**, *5*, 287-295.
26. J. A. Asensio, S. Borros, P. Gomez-Romero. *Electrochem. Commun.* **2003**, *5*, 967-972.
27. J. P. Ni, M. S. Hu, D. Liu, H. X. Xie, X. Z. Xiang, L. Wang. *Journal of Materials Chemistry C* **2016**, *4*, 4814-4821.
28. R. S. Bhavsar, S. C. Kumbharkar, U. K. Kharul. *J. Membr. Sci.* **2014**, *470*, 494-503.
29. J. C. Chen, P. Y. Chen, Y. C. Liu, K. H. Chen. *J. Membr. Sci.* **2016**, *513*, 270-279.
30. B. Zhang, G. Y. Li, J. Yan, Z. G. Wang. *Journal of Physical Chemistry C* **2015**, *119*, 13080-13087.
31. H. Borjigin, K. A. Stevens, R. Liu, J. D. Moon, A. T. Shaver, S. Swinnea, B. D. Freeman, J. S. Riffle, J. E. McGrath. *Polymer* **2015**, *71*, 135-142.
32. J. C. Chen, P. Y. Chen, S. W. Lee, G. L. Liou, C. J. Chen, Y. H. Lan, K. H. Chen. *React. Funct. Polym.* **2016**, *108*, 122-129.
33. L. C. Jheng, S. L. C. Hsu, B. Y. Lin, Y. L. Hsu. *J. Membr. Sci.* **2014**, *460*, 160-170.
34. C. Liu, X. P. Li, S. H. Zhang, Z. Li, Y. Cao, X. G. Jian. *Solid State Ionics* **2014**, *261*, 67-73.
35. D. C. Villa, S. Angioni, S. Dal Barco, P. Mustarelli, E. Quartarone. *Adv. Energy Mater.* **2014**, *4*.
36. K. A. Berchtold, R. P. Singh, J. S. Young, K. W. Dudeck. *J. Membr. Sci.* **2012**, *415*, 265-270.
37. H. J. Xu, K. C. Chen, X. X. Guo, J. H. Fang, J. Yin. *Polymer* **2007**, *48*, 5556-5564.

38. L. Sheng, H. J. Xu, X. X. Guo, J. H. Fang, L. A. Fang, J. Yin. *J. Power Sources* **2011**, *196*, 3039-3047.
39. S. B. Qing, W. Huang, D. Y. Yan. *Eur. Polym. J.* **2005**, *41*, 1589-1595.
40. K. J. Scariah, V. N. Krishnamurthy, K. V. C. Rao, M. Srinivasan. *J. Polym. Sci. Pol. Chem.* **1987**, *25*, 2675-2687.
41. S. C. Kumbharkar, M. N. Islam, R. A. Potrekar, U. K. Kharul. *Polymer* **2009**, *50*, 1403-1413.
42. M. Szwarc, B. N. Ghosh, A. H. Sehon. *J. Chem. Phys.* **1950**, *18*, 1142-1149.
43. C. Liu, X. P. Li, J. Xu, X. G. Jian. *Eur. Polym. J.* **2011**, *47*, 1852-1860.
44. A. Sannigrahi, S. Ghosh, J. Lalnuntluanga, T. Jana. *Journal of Applied Polymer Science* **2009**, *111*, 2194-2203.
45. M. B. Gieselman, J. R. Reynolds. *Macromolecules* **1992**, *25*, 4832-4834.
46. J. M. Bae, I. Honma, M. Murata, T. Yamamoto, M. Rikukawa, N. Ogata. *Solid State Ionics* **2002**, *147*, 189-194.
47. J. A. Asensio, S. Borros, P. Gomez-Romero. *J. Polym. Sci. Pol. Chem.* **2002**, *40*, 3703-3710.
48. G. Wang, G. Y. Xiao, D. Y. Yan. *J. Membr. Sci.* **2011**, *369*, 388-396.
49. M. P. Kulkarni, T. J. Peckham, O. D. Thomas, S. Holdcroft. *J. Polym. Sci. Pol. Chem.* **2013**, *51*, 3654-3666.
50. O. D. Thomas, T. J. Peckham, U. Thanganathan, Y. S. Yang, S. Holdcroft. *J. Polym. Sci. Pol. Chem.* **2010**, *48*, 3640-3650.

51. M. Grucela-Zajac, M. Filapek, L. Skorka, K. Bijak, K. Smolarek, S. Mackowski, E. Schab-Balcerzak. *Synth. Met.* **2014**, *188*, 161-174.
52. S. H. Hsiao, W. J. Guo, T. H. Tsai, Y. T. Chiu. *Journal of Polymer Research* **2014**, *21*.
53. M. Bazzar, M. Ghaemy. *Compos. Sci. Technol.* **2013**, *86*, 101-108.
54. S. Pandiyan, P. V. Parandekar, O. Prakash, T. K. Tsotsis, N. N. Nair, S. Basu. *Chem. Phys. Lett.* **2014**, *593*, 24-27.
55. S. K. Kim, X. Y. Wang, S. Ando, X. G. Wang. *Eur. Polym. J.* **2015**, *64*, 206-214.
56. G. L. Wu, J. L. Li, K. K. Wang, Y. Q. Wang, C. Pan, A. L. Feng. *J. Mater. Sci. - Mater. Electron.* **2017**, *28*, 6544-6551.
57. P. Thiruvassagam. *Des. Monomers Polym.* **2013**, *16*, 197-221.
58. L. Yi, C. Y. Li, W. Huang, D. Y. Yan. *Polymer* **2015**, *80*, 67-75.
59. S. D. Kim, S. Lee, H. S. Lee, S. Y. Kim, I. S. Chung. *Des. Monomers Polym.* **2016**, *19*, 227-235.
60. C. Aguilar-Lugo, J. L. Santiago-Garcia, M. I. Loria-Bastarrachea, D. Guzman-Lucero, L. Alexandrova, M. Aguilar-Vega. *J. Polym. Res.* **2016**, *23*.
61. S. H. Hsiao, Y. H. Hsiao, Y. R. Kung. *J. Electroanal. Chem.* **2016**, *764*, 31-37.
62. H. M. Wang, S. H. Hsiao. *Journal of Materials Chemistry C* **2014**, *2*, 1553-1564.
63. S. H. Hsiao, Y. T. Chou. *Polymer* **2014**, *55*, 2411-2421.
64. L. Yi, C. Y. Li, W. Huang, D. Y. Yan. *J. Polym. Sci. Pol. Chem.* **2016**, *54*, 976-984.
65. N. Mushtaq, G. F. Chen, L. R. Sidra, Y. Liu, X. Z. Fang. *Polym. Chem.* **2016**, *7*, 7427-7435.

66. Y. J. Luo, J. Sun, J. J. Wang, K. K. Jin, F. K. He, Q. Fang. *Macromol. Chem. Phys.* **2016**, *217*, 856-862.
67. P. Yu, Y. Wang, J. R. Yu, J. Zhu, Z. M. Hu. *Journal of Applied Polymer Science* **2015**, *132*.
68. P. Yu, Y. Wang, J. R. Yu, J. Zhu, Z. M. Hu. *Polym. Adv. Technol.* **2017**, *28*, 222-232.
69. C. H. Zhang, G. D. Su, H. Chen, Y. Sun, H. R. Song, L. L. Tong. *Journal of Applied Polymer Science* **2015**, *132*, 41303-41307.
70. E. W. Neuse. *Adv. Polym. Sci.* **1982**, *47*, 1-42.
71. C. P. Yang, Y. Y. Su, Y. C. Chen. *Eur. Polym. J.* **2006**, *42*, 721-732.
72. S. H. Hsiao, P. C. Chang, H. M. Wang, Y. R. Kung, T. M. Lee. *J. Polym. Sci. Pol. Chem.* **2014**, *52*, 825-838.
73. P. M. Hergenrother, B. J. Jensen, S. J. Havens. *Polymer* **1988**, *29*, 358-369.
74. C. H. Lin, S. L. Chang, Y. R. Wang, C. K. Hsu, T. Y. Juang. *J. Polym. Sci. Pol. Chem.* **2013**, *51*, 1734-1741.
75. H. Li, S. J. Zhang, C. L. Gong, Y. Liang, Z. G. Qi, Y. F. Li. *Polym. Int.* **2015**, *64*, 352-360.
76. Z. L. Wu, B. C. Han, C. H. Zhang, D. Y. Zhu, L. X. Gao, M. X. Ding, Z. H. Yang. *Polymer* **2012**, *53*, 5706-5716.
77. S. H. Hsiao, J. Y. Lin. *Journal of Fluorine Chemistry* **2015**, *178*, 115-130.
78. H. Yeo, M. Goh, B. C. Ku, N. H. You. *Polymer* **2015**, *76*, 280-286.
79. Y. Zhou, G. F. Chen, W. Wang, L. H. Wei, Q. J. Zhang, L. P. Song, X. Z. Fang. *RSC Adv.* **2015**, *5*, 79207-79215.

80. M. Hasegawa, A. Tominaga. *Macromol. Mater. Eng.* **2011**, *296*, 1002-1017.
81. Y. B. Zhuang, Y. Gu. *J. Polym. Res.* **2013**, *20*.
82. S. H. Hsiao, N. E. Liu, Y. R. Kung. *J. Polym. Res.* **2015**, *22*.
83. S. Agrawal, A. K. Narula. *Polym. Bull.* **2013**, *70*, 3241-3260.
84. S. H. Hsiao, W. J. Guo, T. H. Tsai, Y. T. Chiu. *J. Polym. Res.* **2014**, *21*.
85. S. UrRehman, G. L. Song, H. Jia, H. W. Zhou, X. G. Zhao, G. D. Dang, C. H. Chen. *Journal of Applied Polymer Science* **2013**, *129*, 2561-2570.
86. M. Sun, J. J. Chang, G. F. Tian, H. Q. Niu, D. Z. Wu. *J. Mater. Sci.* **2016**, *51*, 2830-2840.
87. Y. B. Zhuang, X. Y. Liu, Y. Gu. *Polym. Chem.* **2012**, *3*, 1517-1525.
88. A. Kanazawa, T. Ikeda, T. Endo. *Journal of Applied Polymer Science* **1994**, *54*, 1305-1310.
89. H. Ghassemi, D. J. Riley, M. Curtis, E. Bonaplata, J. E. McGrath. *Appl. Organomet. Chem.* **1998**, *12*, 781-785.
90. A. Kanazawa, T. Ikeda, T. Endo. *J. Polym. Sci. Pol. Chem.* **1993**, *31*, 3031-3038.
91. A. Kanazawa, T. Ikeda, T. Endo. *J. Polym. Sci. Pol. Chem.* **1993**, *31*, 1441-1447.
92. A. Kanazawa, T. Ikeda, T. Endo. *J. Polym. Sci. Pol. Chem.* **1993**, *31*, 1467-1472.
93. A. Kanazawa, T. Ikeda, T. Endo. *Journal of Applied Polymer Science* **1994**, *53*, 1245-1249.
94. A. Kanazawa, T. Ikeda, T. Endo. *J. Polym. Sci. Pol. Chem.* **1994**, *32*, 1997-2001.
95. C. G. Cassity, A. Mirjafari, N. Mobarrez, K. J. Strickland, R. A. O'Brien, J. H. Davis, Jr. *Chem. Commun.* **2013**, *49*, 7590-7592.

96. A. I. Abdulahad, C. Jangu, S. T. Hemp, T. E. Long. *Macromol. Symp.* **2014**, *342*, 56-66.
97. S. T. Hemp, M. S. Zhang, M. Tamami, T. E. Long. *Polym. Chem.* **2013**, *4*, 3582-3590.
98. X. Yang, C. A. Conrad, W. Wan, M. S. Bedford, L. Hu, G. Chumanov, R. C. Smith. *J. Mater. Chem. C* **2015**, *3*, 4537-4544.
99. M. S. Bedford, X. Yang, K. M. Jolly, R. L. Binnicker, S. B. Cramer, C. E. Keen, C. J. Mairena, A. P. Patel, M. T. Rivenbark, Y. Galabura, I. Luzinov, R. C. Smith. *Polym. Chem.* **2015**, *6*, 900-908.
100. X. Yang, Y. Wen, G. Chumanov, R. C. Smith. *J. Polym. Sci., Part A: Polym. Chem.* **2017**, *55*, 1620-1625.
101. W. Wan, X. Y. Yang, R. C. Smith. *J. Polym. Sci., Part A: Polym. Chem.* **2017**, *55*, 1984-1990.

CHAPTER TWO

INFLUENCE OF SPACER LENGTH AND RIGIDITY ON PROPERTIES OF PHOSPHONIUM POLYMERS AND ON THEIR SUPRAMOLECULAR ASSEMBLY WITH A CONJUGATED POLYELECTROLYTE[‡]

2.1 Introduction

Polymers featuring ionic functionalities, referred to as polyelectrolytes, ionenes or ionomers, represent a rapidly-growing research area. Some of the reasons for such widespread interest in ionic polymers include the fact that many are water-processable and exhibit better water solubility for biological applications, their composite films have high surface energies, and they can supramolecularly assembly with other materials via ion-ion or ion-dipole interactions.

One notable yet still underexplored area of polyelectrolyte research is in the area of chromophore-derivatized or conjugated polyelectrolytes (i.e., Chart 2.1). These

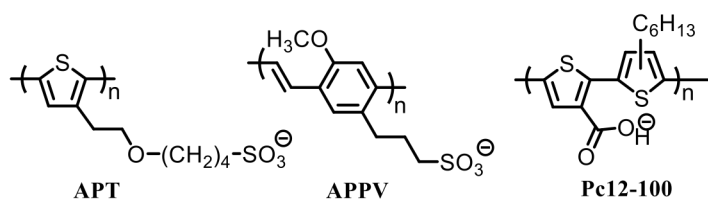


Chart 2.1: Anionic polyelectrolytes that have been used in layer-by-layer assembly with phosphonium polymers

[‡]Adapted from X. Yang, C. A. Conrad, W. Wan, M. S. Bedford, L. Hu, G. Chumanov, R. C. Smith. *J. Mater. Chem. C* **2015**, 3, 4537-4544, with permission.

materials can exploit the desirable properties of polyelectrolytes for use in organic electronics and photonics. As an example, layers comprised of a mixture of anionic polyelectrolyte poly(styrenesulfonate) (PSS) with the conjugated polymer poly(3,4-ethylenedioxythiophene) (PEDOT) are ubiquitous in organic electronics. Several research teams including Buriak,¹⁻⁵ Reynolds and Schanze,⁶⁻⁸ and Bazan,⁹ to name a few, have explored polyelectrolytes as components of organic photovoltaic cells and related devices. Notable improvements in device operation and interfacial effects⁴ can result from the incorporation of ionic polymers in place of neutral polymers.

One attractive charge-bearing unit for incorporation into polymers is the phosphonium moiety. Phosphonium salts can exhibit very good chemical stability under both acidic and basic conditions and can have remarkable thermal stability.¹⁰ Phosphonium-bearing polyelectrolytes have been reported that feature the phosphonium moieties either in the polymer main chain (e.g., **R1**,¹¹ **R2**,¹² **EGT1**,¹³ **SLK1**,¹⁴ **FLoct** and **FLone**,¹⁵ and **CAC1** in Chart 2.2)¹⁶ or as sidechain components (e.g., **R3**¹⁷) and have shown particular promise as antibacterial coatings or as components of alkaline fuel cells. Surprisingly, there are very few examples of phosphonium polyelectrolytes that feature chromophores or π -conjugated segments in the polymer backbone. In fact, it appears that Baumgartner's polymer **R1** (Chart 2.2) is the only reported fully conjugated polyelectrolyte bearing a phosphonium moiety in the polymer chain.

The Smith group's work in the area of polyelectrolytes has primarily been on polymers that, like **R1**¹¹, feature both chromophores and phosphonium moieties in the polymer main chain. Such chromophore-derivatized polyelectrolytes were targeted as

components of optically-active films that could be employed as elements of organic electronics or other photonic applications. One drawback is the synthetic pathways requiring >10 steps for monomer synthesis to produce polymers such as **R1**, **EGT1**,¹³ and **SLK1**¹⁴ would likely make them too expensive for practical application. It was therefore of interest to pursue phosphonium ionomers that, like **R2**,¹² could be prepared from commercial monomers. We thus recently reported on the preparation of chromophore-derivatized **FLoct** and **FLone** from commercially-available monomers.¹⁵ The monomers employed for those polymers were still relatively expensive, however, and the absorbance of films of these polymers was in the blue to UV region of the spectrum. More affordable commercially-available monomers 1,2-bis(diphenylphosphino)ethane, 1,1'-bis(diphenylphosphino)ferrocene, and 1,4-bis(diphenylphosphino)benzene were used to prepare **CAC1a-b**(Chart 2.2)¹⁶ with the aim of using them to prepare films with absorption farther into the visible region of the spectrum. Although **CAC1a-b** do not themselves exhibit absorption in the visible region of the spectrum, they can still be used in the layer-by-layer assembly of films in which the alternate layers are comprised of commercially-available anionic conjugated polyelectrolytes such as polythiophene derivative **APT** and poly(*p*-phenylene vinylene) derivative **APPV** (Chart 2.1). The investigation of the layer-by-layer assembly process involving **CAC1** revealed that polymers having flexible linkers, as are present in **CAC1a**, exhibit significantly better substrate coverage and linearity of film growth as compared to more rigid materials such as **CAC1b**.

The early findings from studies on the materials shown in Chart 2.2 and the existing literature on well-defined anionic¹⁸⁻²⁰ and cationic^{21,22} polyelectrolytes drew our interest in further investigating the structure-property relationships that depend on the spacer flexibility and distance between charges along the polymer backbone in phosphonium polymers. Herein we describe the preparation of seven new phosphonium polymers and investigate how the spacer identity influences properties such as crystallinity, thermal stability, film morphology, the supramolecular layer-by-layer film growth process with anionic polythiophene derivative **Pc12-100** (Chart 2.1), and the composition of LbL films.

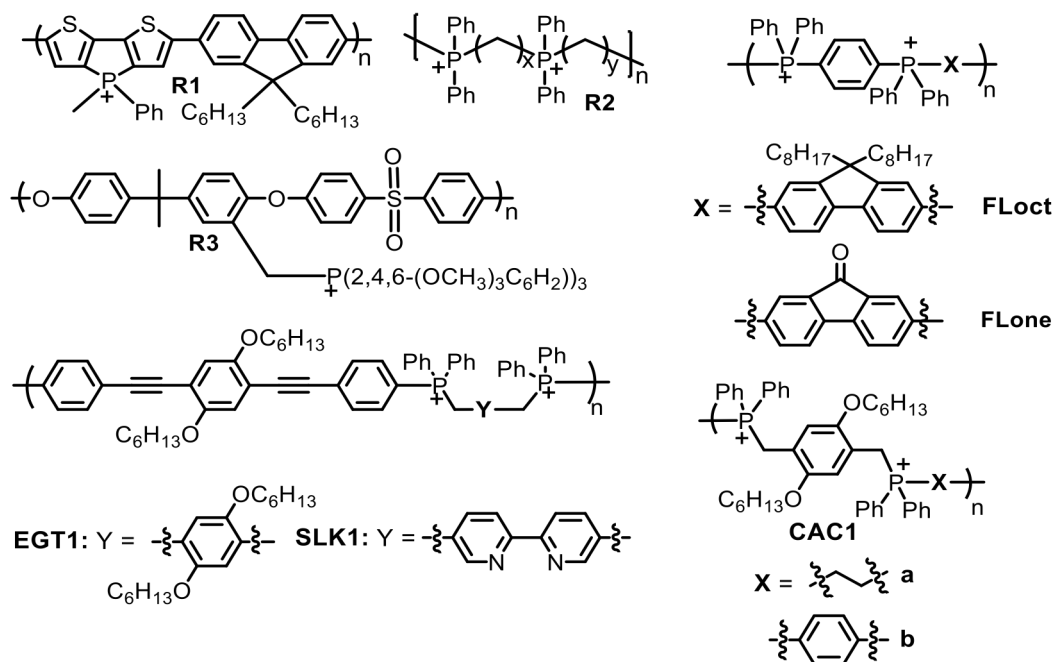


Chart 2.2: Some phosphonium-bearing polymers.

2.2 Experimental

2.2.1 General Considerations.

All air-sensitive reactions were performed in an MBraun UNILab glovebox under nitrogen. Anhydrous solvents were dried and degassed using an MBraun solvent purifier. Monomers **M1** were obtained from Sigma-Aldrich or Strem Chemical. Glass slides were purchased from Fisher Scientific. Other chemicals were used without further purification after purchased. All the NMR spectra were collected on a Joel ECX-300 MHz spectrometer operating at 300 and 121.4 MHz for ^1H and ^{31}P , respectively. Thermogravimetric analysis (TGA) was performed on TA Instruments Q5000 TGA from 25 °C to 600 °C with a heating rate of 20 °C min⁻¹. Differential scanning calorimetry (DSC) was performed on TA Instruments Q1000 DSC with a heat/cool/heat cycle at 20 °C min⁻¹ for heating and 10 °C min⁻¹ for cooling, and report T_g data for the second scan.

2.2.2 Layer-by-layer technique.

The procedure is similar with that published in our previous work.²³ A glass microscope slide was cleaned by soaking in concentrated nitric acid, then sequential rinsing with deionized water and tetrahydrofuran. The slide was visually inspected for scuffs or scratches. Solutions of **LX** and **Pc12-100** (5×10^{-4} M) were prepared in 50:50 ACN:H₂O and 2:1 THF:water (pH of water adjusted to 9 with NaOH), respectively. For each film preparation, the slide was first dipped in the **LX** solution then briefly shaken to remove excess solution droplets. The process was then repeated using the **Pc12-100** solution. The spectrum of the slide was immediately collected using a Cary 50 UV-vis

spectrometer with a scanning range of 275 to 800 nm. This procedure was repeated until the desired number of bilayers was obtained.

2.2.3 Atomic Force Microscopy (AFM).

All AFM experiment were conducted using an AIST SmartSPMTM 1000 in semicontact mode within a $1\ \mu\text{m} \times 1\ \mu\text{m}$ or $5\ \mu\text{m} \times 5\ \mu\text{m}$ sample area using an aluminium tip (spring constant = 5 N/m, 160 kHz resonance frequency). Images were processed by AIST-NT and WSxM 5.0 Develop 7.0 software.²⁴

2.2.4 Synthesis of **LX1** (X = CH₂).

Monomers α,α' -dibromo-*p*-xylene (132 mg, 0.500 mmol) and bis(diphenylphosphino)methane (192 mg, 0.500 mmol) were placed in a heavy-walled glass pressure tube with *N,N*-dimethylformamide (DMF, 10 mL) under nitrogen. The tube was sealed with an O-ring equipped Teflon screw cap. The tube was then heated to 90 °C for 24 h. After cooling the reaction vessel to room temperature it was opened to air and 10 mL of diethyl ether was added. This yielded a white cloudy suspension that was collected by vacuum filtration. The crude product was then rinsed with 10 mL of diethyl ether ($\times 3$) and then dried in a vacuum oven for 48 h. The desired product was isolated as a white powder (0.332 g, 100%). ¹H NMR (300 MHz, (CD₃)₂SO) δ : 8.45-7.15 (br m, 20H), 7.12-6.14 (br m, 4H), 6.03-3.70 (br m, 4H), 2.59-2.52 (br m, 2H); ³¹P{¹H} NMR (121.4 MHz, (CD₃)₂SO) δ : 25.4-19.3 (main polymer peak) and 27.6 (end groups). Anal. Calcd. for monomer formula C₃₃H₃₄Br₂P₂O₂ (ignoring end groups): C, 57.91; H, 5.01; Found: C, 58.55; H, 5.34%.

2.2.5 Synthesis of **LX2** (X = (CH₂)₂).

This synthesis followed the same procedure as described for **LX1**, but using as monomers α,α' -dibromo-*p*-xylene (80 mg, 0.20 mmol) and 1,2-bis(diphenylphosphino)ethane (49 mg, 0.20 mmol). The product was isolated as a white powder (40 mg, 33%). ^1H NMR (300 MHz, $(\text{CD}_3)_2\text{SO}$) δ : 8.5-7.4 (br m, 20H), 7.3-6.3 (br m, 4H), 5.3-4.1 (br m, 4H), 3.6-3.0 (br d, 4H); $^{31}\text{P}\{^1\text{H}\}$ NMR (121.4 MHz, $(\text{CD}_3)_2\text{SO}$) δ : 28.6 (main polymer peak) and 32.8 (end groups). Anal. Calcd. for monomer formula $\text{C}_{34}\text{H}_{32}\text{Br}_2\text{P}_2$ (ignoring end groups): C, 58.47; H, 5.20; Found: C, 59.27; H, 4.94%.

2.2.6 Synthesis of **LX3** (X = $(\text{CH}_2)_3$)

This synthesis followed the same procedure as described for **LX1**, but using as monomers α,α' -dibromo-*p*-xylene (132 mg, 0.500 mmol) and 1,3-bis(diphenylphosphino)propane (206 mg, 0.500 mmol). The product was isolated as a white powder (0.314 g, 92.9%). ^1H NMR (300 MHz, $(\text{CD}_3)_2\text{SO}$) δ : 8.1-7.6 (br m, 20H), 6.6-7.0 (br m, 4H), 5.1-4.6 (br m, 4H), 3.7-3.5 (br m, 4H), 1.8-1.6 (br d, 2H); $^{31}\text{P}\{^1\text{H}\}$ NMR (121.4 MHz, $(\text{CD}_3)_2\text{SO}$) δ : 25.4 (main polymer peak) and 26.4 (end groups); Anal. Calcd. for monomer formula $\text{C}_{35}\text{H}_{34}\text{Br}_2\text{P}_2$ (ignoring end groups): C, 59.01; H, 5.38; Found: C, 59.76; H, 5.49%.

2.2.7 Synthesis of **LX4** (X = $(\text{CH}_2)_4$)

This synthesis followed the same procedure as described for **LX1**, but using as monomers α,α' -dibromo-*p*-xylene (132 mg, 0.500 mmol) and 1,4-bis(diphenylphosphino)butane (213 mg, 0.500 mmol). The product was isolated as a white powder (0.321 g, 93.0%). ^1H NMR (300 MHz, $(\text{CD}_3)_2\text{SO}$) δ : 7.9-7.6 (br m, 20H), 7.8-7.7 (br m, 4H), 4.8-4.7 (br m, 4H), 3.1-2.9 (br m, 4H), 1.6-1.5 (br m, 4H); $^{31}\text{P}\{^1\text{H}\}$

NMR (121.4 MHz, (CD₃)₂SO) δ : 27.8 (main polymer peak) and 26.3(end groups). Anal. Calcd. for monomer formula C₃₆H₃₆Br₂P₂ (ignoring end groups): C, 59.52; H, 5.55; Found: C, 60.88; H, 5.50%.

2.2.8 Synthesis of **LX5** (X = (CH₂)₅)

This synthesis followed the same procedure as described for **LX1**, but using as monomers α,α' -dibromo-*p*-xylene (132 mg, 0.500 mmol) and 1,5-bis(diphenylphosphino)pentane (220 mg, 0.500 mmol) The product was isolated as a white powder (0.349 g, 99.1%). ¹H NMR (300 MHz, (CD₃)₂SO) δ : 8.10-7.45 (br m, 20H), 7.31-6.57 (br m, 4H), 4.98-4.40 (br m, 4H), 3.00-2.68 (br m, 4H), 1.61-1.17 (br m, 6H); ³¹P{¹H} NMR (121.4 MHz, (CD₃)₂SO) δ : 30.3-28.1 (main polymer peak); Anal. Calcd. for monomer formula C₃₇H₄₂Br₂P₂O₂ (ignoring end groups): C, 60.01; H, 5.72; Found: C, 60.62; H, 5.95%.

2.2.9 Synthesis of **LX8** (X = (CH₂)₈)

This synthesis followed the same procedure as described for **LX1**, but using as monomers α,α' -dibromo-*p*-xylene(132 mg, 0.500 mmol) and 1,8-bis(diphenylphosphino)octane (241 mg, 0.500 mmol) The product was isolated as a white powder (0.359 g, 96.2%). ¹H NMR (300 MHz, (CD₃)₂SO) δ : 8.15-7.50 (br m, 20H), 7.12-6.65 (br m, 4H), 4.92-4.56 (br m, 4H), 3.01-2.65 (br m, 4H), 1.66-0.90 (br m, 12H); ³¹P{¹H} NMR (121.4 MHz, (CD₃)₂SO) δ : 30.8-26.0 (main polymer peak); Anal. Calcd. for monomer formula C₄₀H₄₈Br₂P₂O₂ (ignoring end groups): C, 61.39; H, 6.18; Found: C, 63.07; H, 6.03%.

2.2.10 Synthesis of **LXPh** (X = C₆H₅)

This synthesis followed the same procedure as described for **LX1**, but using as monomers α,α' -dibromo-*p*-xylene (132 mg, 0.500 mmol) and 1,4-bis(diphenylphosphino)benzene (223 mg, 0.500 mmol). The product was isolated as a white powder (0.336 g, 94.6%). ^1H NMR (300 MHz, $(\text{CD}_3)_2\text{SO}$) δ : 8.38-7.49 (br m, 24H), 7.09-6.67 (br m, 4H), 5.53-5.10 (br m, 4H); $^{31}\text{P}\{^1\text{H}\}$ NMR (121.4 MHz, $(\text{CD}_3)_2\text{SO}$) δ : 27.3-25.9 (main polymer peak); Anal. Calcd. for monomer formula $\text{C}_{38}\text{H}_{36}\text{Br}_2\text{P}_2\text{O}_2$ (ignoring end groups): C, 61.14; H, 4.86; Found: C, 60.36; H, 5.04%.

2.2.11 Synthesis of Poly[(dodecyl-3-thiophenecarboxylate-2,5-diyl)-alt-(3-hexylthiophene-2,5-diyl)] (**Pc12**)

Preparation followed a literature procedure for the synthesis,²⁵ with a modified isolation procedure. To a 35 mL pressure tube in drybox under an atmosphere of nitrogen were added dodecyl 2,5-dibromo-3-thiophenecarboxylate (1.1 g, 2.0 mmol), 2,5-bis(trimethylstannyl)-3-hexylthiophene (1.0 g, 2.4 mmol), copper(I) bromide (0.015 g, 0.10 mmol) and anhydrous potassium fluoride (0.12 g, 2.0 mmol) in a solvent mixture comprised of 12.5 mL of anhydrous THF and 12 mL of anhydrous DMF. Tetrakis(triphenylphosphine)palladium(0) (0.58 g, 0.50 mmol) was then added into the mixture. The mixture was stirred at 105–110 °C for 24 h. After cooling to room temperature, the tube was opened and 200 mL of methanol was added. The crude product precipitated and was separated via centrifugation. The supernatant was decanted away to leave a red pellet. The crude polymer pellet was shaken with 5 mL of THF to form a fine suspension. The polymer was collected by centrifugation and the pellet was then dried in a vacuum oven to yield the red product (0.49 g, 53%). ^1H NMR (300 MHz, CDCl_3): δ

(ppm): 7.00-7.50 (m, 2H), 4.15-4.35 (br. d, 2H), 2.45-2.85 (br. d, 2H), 1.10-1.80 (m, 28H), 0.80-0.95 (br. d, 6H).

2.2.12 Hydrolysis of Pc12 to give Pc12-100

To a solution of **Pc12** (50 mg, 0.011 mmol) in 30 mL of THF was added 10 mL of 20 wt.% NaOH(aq). The solution was then heated to reflux and stirred for 48 h under nitrogen. After cooling to room temperature the solution was made acidic (pH ~2) by careful addition of 3 M hydrochloride acid. The product was extracted from the aqueous fraction by use of dichloromethane/THF (3:1). The organic fraction was collected and all volatiles removed under reduced pressure. The product was washed with methanol ($\times 3$) and *n*-hexane ($\times 3$) then dried in a vacuum oven to yield the dark red solid (31 mg, 96%). ^1H NMR (300 MHz, THF- d^8): δ (ppm): 7.07-7.68 (m, 2H), 2.36-2.92 (br. m, 2H), 1.16-1.52 (m, 8H), 0.78-0.95 (s, 3H).

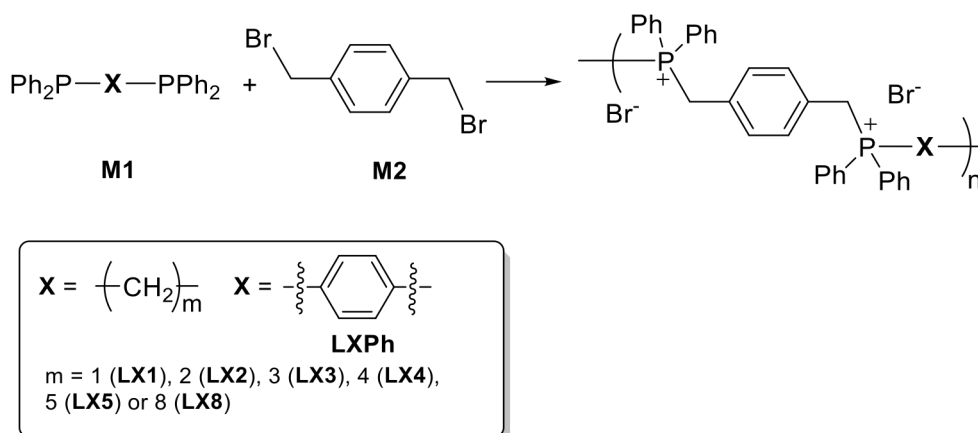
2.3 Results and Discussion

2.3.1 Design and Synthesis

The selection of spacers (X in Scheme 2.1) between phosphonium units for the current study was made on the basis of two criteria. First, it was desirable for the diphosphine monomers (**M1**) to be commercially available for practical application of materials. Second, it was necessary to sample a range of flexibility and distance between phosphonium units. On the basis of these criteria, we selected the diphosphine monomers shown in Scheme 1. The comonomer **M2** was selected because it is an affordable commercial reagent, and it provides the same spacing between phosphonium units as

present in **CAC1** (Chart 2.1), which had previously shown outstanding layer-by-layer assembly with anionic polythiophene derivative **APT** (Chart 2.2). It was also anticipated that the rigid nature of the *p*-xylene chain component provided by **M2** would help prevent the formation of cyclic oligomers of the type that were observed in preparation of **R2**,¹² which has only flexible methylene units in spacers between phosphonium sites.

The polymerization of **M1** and **M2** (Scheme 2.1) proceeded readily upon heating at 90 °C under an atmosphere of dry nitrogen in DMF solution for 24 hours. Isolation was also straightforward and involved simple precipitation and rinsing with diethyl ether followed by drying in a vacuum oven to yield **LX1-8** and **LXPh** as white powders. The polymer composition was characterized by a combination of ¹H and ³¹P NMR spectrometry (spectra are provided in the Appendix 2A) and elemental microanalysis. The microanalysis data show excellent correlation of experimental and theoretical values considering the polydisperse nature of the materials and the presence of end groups that are not accounted for in the theoretical repeat unit formula. The solids are only sparingly



Scheme 2.1: Synthesis of **LX** polymers with different spacers ‘X’.

soluble in acetonitrile, but have reasonable solubility in dimethylsulfoxide and are fully soluble in a water/acetonitrile mixture.

One challenging aspect of ionic polymers is that they are not easily analysed for molecular weight distribution by standard gel permeation chromatography (GPC) techniques. This is a result of their affinity to column media, although some researchers have reported success using formic acid in the mobile phase.²⁶ NMR end group analysis has therefore become the preferred method for obtaining reliable number average molecular weights (M_n) for phosphonium polyelectrolytes, which generally show a degree of polymerization of 14-25.¹³⁻¹⁶ On the basis of NMR end group analysis we were able to obtain the M_n values and corresponding degrees of polymerization (n) provided in Table 2.1. Low intensities of end group resonances precluded successful determination of molecular weights for **LX1**, **LX2** and **LXPh**. All of the phosphonium polyelectrolytes prepared in the analogous manner to **LX** polymers have exhibited values of n between 16 and 21. On the basis of this data, the degrees of polymerization of **LX1**, **LX2** and **LXPh** can be estimated to be not less than 19.

2.3.2 Thermal properties and structural characterization

Thermogravimetric analysis (TGA) was used to probe the thermal stability of the **LX** polymers. The TGA raw data are provided in the Appendix 2B and the data are summarized in Table 2.2. Thermal stability increased with distance between phosphonium cations for **LX1-LX3**. Lower stability for shorter spacer lengths is attributable to the destabilizing Coulombic repulsion imposed by proximal phosphonium moieties. Once the phosphonium units are far enough apart to alleviate this

destabilization, all of the methylene-spaced polymers **LX3-8** have about the same T_d (355-362 °C), which is somewhat higher than that observed for **R2**¹² (Chart 2, T_d = 300-339 °C depending on spacers) or **CAC1**¹⁶ (Chart 2, T_d = 264 °C).

Table 2.1: Molecular weights and degrees of polymerization values

Polymer	M_n (Da)	n
LX1	9,700	14
LX2	11,900	17
LX3	≥13,500	≥19
LX4	≥13,800	≥19
LX5	≥14,100	≥19
LX8	≥14,900	≥19
LXPh	11,400	15

The X-ray powder diffraction (patterns provided in the Appendix 2B) shows that all the polymers are semicrystalline. It is therefore not surprising that broad melting peaks (endothermic) exist in differential scanning calorimetry (DSC) traces (see Appendix 2B) when data are collected in the range from -150 to 0 °C. The crystallization peaks are also broad in the cooling curve at the top of each trace. It is of interest to find that **LX5** has a T_g at 200 °C (Table 2.1), which is unique among the series. It was initially puzzling to observe a T_g for only one member of the series, even after rerunning the analysis. The Long group, however, has also observed that some members of a phosphonium polymer series differing only by the alkyl spacer do not exhibit a T_g ¹² while others do. This observation is presumably due to subtle influences exerted by structure on crystalline domains in the solid state.

2.3.3 Layer-by-layer assembly of LX polymers with polyelectrolytes

Phosphonium polyelectrolytes have been found to form supramolecular structures via layer-by-layer (LbL) assembly with anionic conjugated polymers in previous work.²³ In the current study it is of interest to explore the LbL assembly of **LX** polymers with an anionic polythiophene (**Pc12-100**, Chart 2.1) and to assess how morphology and film composition are influenced by the spacer between charged units. The LbL process involved first coating a prepared glass substrate with a monolayer of the cationic **LX** polymer solution, followed by exposure to a solution of anionic **Pc12-100** to create a bilayer of the cationic and anionic polyelectrolytes. Recursive alternate exposure to cationic and anionic polyelectrolyte solutions results in controlled film growth.

In order to monitor the film growth process, a UV-vis absorption spectrum of the film was acquired after every two bilayers. Figure 2.1 provides plots of absorbance at 475 nm (the absorption maximum attributable to absorbance by **Pc12-100**) versus number of bilayers for the LbL process for each of the seven polymers in the **LX** series. The absorption increase is quite linear for flexible alkyl spacers, but LbL film growth appears to become less linear with the more rigid 1,4-phenylene spacer in **LXPh**, consistent with the previous study on phosphonium LbL film growth.¹⁶ It is also noteworthy that the polymers with methylene spacers show better linearity of film growth when spacers have an odd number of methylene units (**LX1**, **LX3**, **LX5**) compared to polymers having an even numbers of methylene units in their spacers (**LX2**, **LX4**, **LX8**).

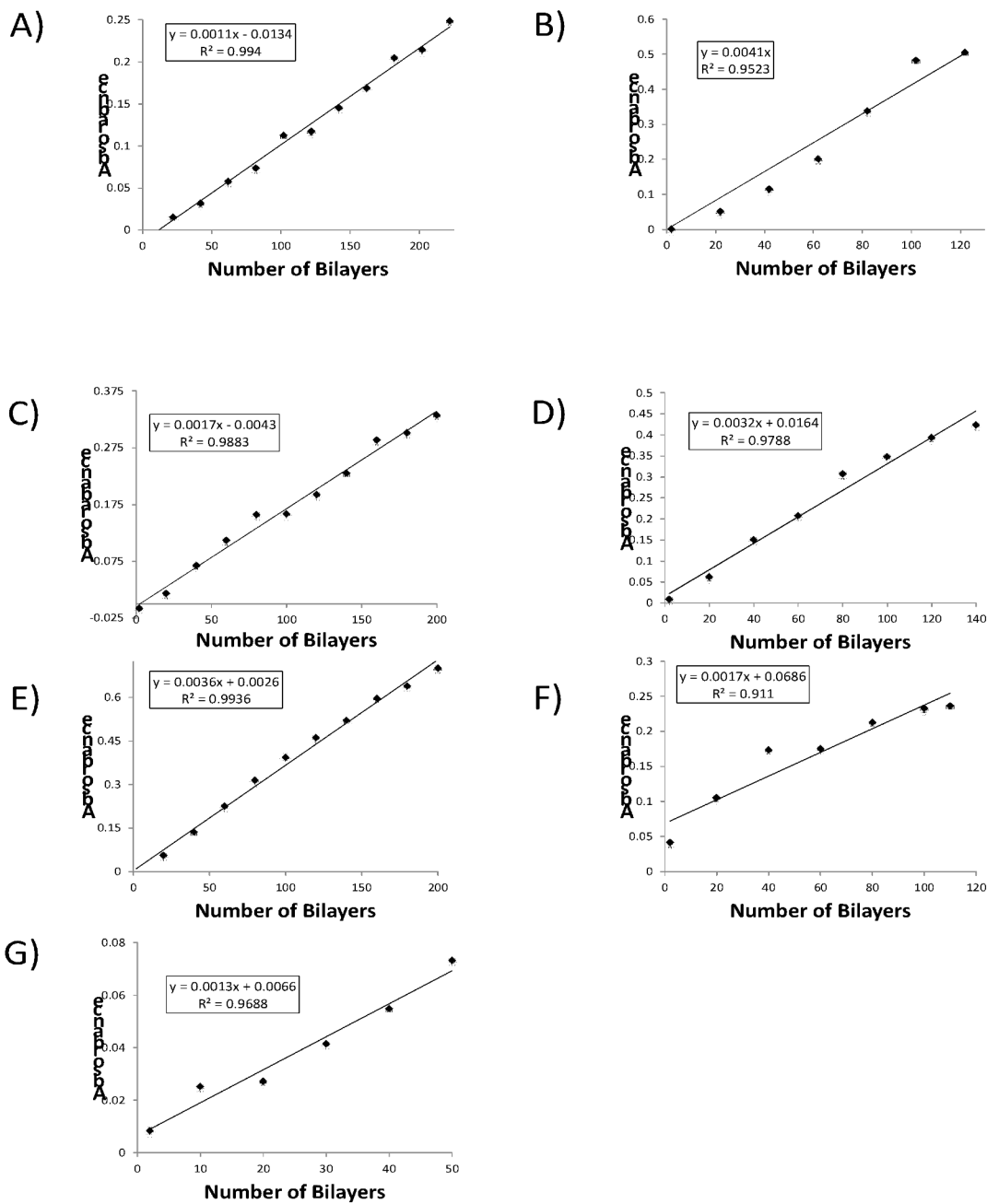
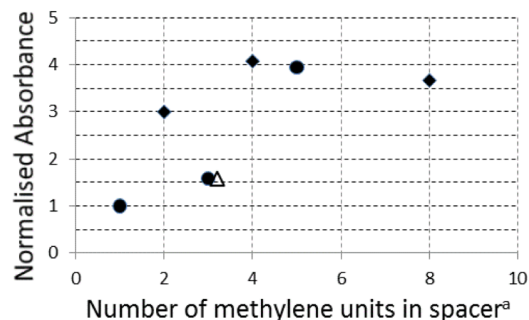


Figure 2.1: Absorption spectra (left) and A475 vs. numbers (right) of LX polymers layered with Pc12-100: LX1/Pc12-100 (A), LX2/Pc12-100 (B), LX3/Pc12-100 (C), LX4/Pc12-100 (D), LX5/Pc12-100 (E), LX8/Pc12-100 (F) and LXPh/Pc12-100 (G).

Another important structure-property relationship is how the spacer identity influences the amount of polymer that is deposited in each bilayer. In order to assess this relationship, we plotted the normalized absorbance of a 50 bilayer film versus the number of methylene units in the spacer (Figure 2.2, wherein absorbance of a 50 bilayer film of **LX1** is set to unity). Several trends emerge from these data. First, materials with an odd number of methylene spacers (represented by circles in Figure 2.2) generally deposit less material per bilayer than do the polymers with an even number of methylene spacers (represented by diamonds in Figure 2.2). Similar “even-odd” effects on film formation processes have been noted previously.^{71, 72}

Whether the spacer is composed of an even or odd number of methylene units, however, the amount of material deposited increases as the length of the spacer increases. This observation can be attributed to the fact that the Coulombic repulsion between chains decreases as the space between cationic sites increases. This property allows for surface coverage of more chains per unit area as the spacer length increases. The same trend was observed in a previous study in which the charge per unit length of a phosphonium polyelectrolyte could be tuned by binding of cationic Zn^{2+} ions.¹⁴ At some point, when the spacer becomes flexible enough, the surface coverage is maximized and the amount of material deposited seems to level off at about four times as much as was deposited for **LX1**.

Interestingly, the more rigid polymer **LXPh** (triangular marker in Figure 2.2) has almost exactly the same amount of material deposition per bilayer as does **LX3**. The distance between charged sites in **LXPh** is about the same as in the most favorable



^aThe triangular data marker corresponds to **LXPPh**, in which the spacer is not composed of methylene units. This marker is placed near that of **LX3**, the methylene-spacer polymer with which **LXPPh** properties most closely correspond.

Figure 2.2: Influence of spacer on the amount of **Pc12-100** per 50 bilayers. The polymers having an even number of methylene units in their spacers (circles) are distinguished from those with an even number (diamonds). The corresponding data marker for **LXPPh** is given as a triangle.

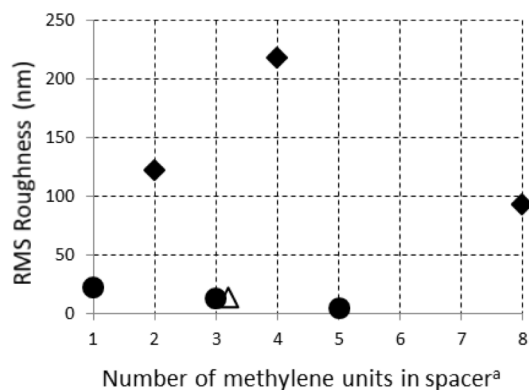
conformation of **LX3**, suggesting that the amount of material deposited depends more on the distance between charges sites than on the flexibility of the spacer, providing additional evidence for the dominance of Coulombic factors in dictating film composition.

2.3.4 Morphology of layer-by-layer assembled films

Atomic force microscopy was performed to explore the effect of varying spacers on LbL film morphology of polymers with **Pc12-100**. The representative $1 \times 1 \mu\text{m}$ and $5 \times 5 \mu\text{m}$ images of all the LbL films (Appendix 2C) were collected at several locations and one for each **LX** polymer. The freshly cleaned glass slide consists of small grain

particles with size around 2 nm. After the LbL assembly procedure, the features differ significantly from the clean substrate in all cases, providing more evidence for successfully surface modification suggested by the absorption data in Figure 2.1. The general trend that emerges upon comparison of the AFM images with the linearity of film growth (Figure 2.1) is that linear film growth is associated with formation of more uniformly-sized particles in the film.

An interesting trend was also observed between the identity of the spacer and the root-mean-squared (RMS) roughness of the films (Figure 2.3). The RMS roughness



^aThe triangular data marker corresponds to **LXPh**, in which the spacer is not composed of methylene units. This marker is placed near that of **LX3**, the methylene-spacer polymer with which **LXPh** properties most closely correspond.

Figure 2.3: Influence of spacer on the root mean squared roughness of films as measured over a 5 μm \times 5 μm area. The polymers having an even number of methylene units in their spacers (circles) are distinguished from those with an even number (diamonds). The corresponding data marker for **LXPh** is given as a triangle.

values for films of polymers with odd numbers of methylene units in their spacers (**LX1**, **LX3**, **LX5**, circle data markers in Figure 2.3) are significantly lower than the values for polymers with even numbers of methylene units in their spacers (**LX2**, **LX4**, **LX8**, diamond data markers in Figure 2.3). **LXPh** (triangular data marker in Figure 2.3) again mirrors the properties of **LX3**, suggesting that the distance between ionic units dominates the morphological outcome.

It is noteworthy that the smoother films are the same as those that were produced by a more linear film growth process and which contain a smaller amount of material deposited per bilayer. All the data in the current study point to a film growth process dictated by two primary factors: 1) interchain and intrachain Coulombic repulsion between like-charged polyelectrolytes dictates initial surface coverage; and 2) conformational accessibility of cation-anion matching, which improves for flexible materials.

2.4 Conclusions

Spacer length and rigidity were proven to have significant influence on the properties of phosphonium polyelectrolytes, such as thermal stabilities, crystallinity and LbL supramolecular assembly. A dependence of film composition, film growth and surface roughness on spacer length and on whether the spacer had an odd or even number of methylene spacers was revealed. Further work to unveil the effect of spacer in polyelectrolytes with precisely-placed ionic units is currently underway.

2.5 Reference

1. Q. Chen, B. J. Worfolk, T. C. Hauger, U. Al-Atar, K. D. Harris, J. M. Buriak. *ACS ACS Appl. Mater. Interfacs.* **2011**, *3*, 3962-3970.
2. W. Li, B. J. Worfolk, P. Li, T. C. Hauger, K. D. Harris, J. M. Buriak. *J. Mater. Chem.* **2012**, *22*, 11354-11363.
3. S. A. McClure, B. J. Worfolk, D. A. Rider, R. T. Tucker, J. A. M. Fordyce, M. D. Fleischauer, K. D. Harris, M. J. Brett, J. M. Buriak. *ACS Appl. Mater. Interfacs.* **2010**, *2*, 219-229.
4. D. A. Rider, B. J. Worfolk, K. D. Harris, A. Lalany, K. Shahbazi, M. D. Fleischauer, M. J. Brett, J. M. Buriak. *Adv. Funct. Mater.* **2010**, *20*, 2404-2415.
5. B. J. Worfolk, T. C. Hauger, K. D. Harris, D. A. Rider, J. A. M. Fordyce, S. Beaupre, M. Leclerc, J. M. Buriak. *Advanced Energy Materials* **2012**, *2*, 361-368.
6. M. B. Ramey, J. A. Hiller, M. F. Rubner, C. Tan, K. S. Schanze, J. R. Reynolds. *Macromolecules* **2005**, *38*, 234-243.
7. P. Taranekar, Q. Qiao, H. Jiang, I. Ghiviriga, K. S. Schanze, J. R. Reynolds. *J. Am. Chem. Soc.* **2007**, *129*, 8958-8959.
8. X. Zhao, M. R. Pinto, L. M. Hardison, J. Mwaura, J. Mueller, H. Jiang, D. Witker, V. D. Kleiman, J. R. Reynolds, K. S. Schanze. *Macromolecules* **2006**, *39*, 6355-6366.
9. Y. Jin, G. C. Bazan, A. J. Heeger, J. Y. Kim, K. Lee. *Appl. Phys. Lett.* **2008**, *93*, 346-349.
10. C. G. Cassity, A. Mirjafari, N. Mobarrez, K. J. Strickland, R. A. O'Brien, J. H. Davis. *Chem Commun* **2013**, *49*, 7590-7592.
11. S. Durben, Y. Dienes, T. Baumgartner. *Org. Lett.* **2006**, *8*, 5893-5896.

12. S. T. Hemp, M. S. Zhang, M. Tamami, T. E. Long. *Polym. Chem.* **2013**, *4*, 3582-3590.
13. E. G. Tennyson, S. He, N. C. Osti, D. Perahia, R. C. Smith. *J. Mater. Chem.* **2010**, *20*, 7984–7989.
14. S. L. Kristufek, T. R. Maltais, E. G. Tennyson, N. C. Osti, D. Perahia, A. G. Tennyson, R. C. Smith. *Polym. Chem.* **2013**, *4*, 5387-5394.
15. M. S. Bedford, X. Yang, K. M. Jolly, R. L. Binnicker, S. B. Cramer, C. E. Keen, C. J. Mairena, A. P. Patel, M. T. Rivenbark, Y. Galabura, I. Luzinov, R. C. Smith. *Polym. Chem.* **2015**, *6*, 900 - 908.
16. C. A. Conrad, M. S. Bedford, A. A. Buelte, Y. Galabura, I. Luzinov, R. C. Smith. *Polym Int* **2015**, Submitted for publication.
17. S. Gu, R. Cai, T. Luo, Z. Chen, M. Sun, Y. Liu, G. He, Y. Yan. *Angew. Chem., Int. Ed.* **2009**, *48*, 6499-6502, S6499/6491-S6499/6494.
18. C. F. Buitrago, K. L. Opper, K. B. Wagener, K. I. Winey. *ACS Macro Lett.* **2012**, *1*, 71-74.
19. T. W. Baughman, C. D. Chan, K. I. Winey, K. B. Wagener. *Macromolecules* **2007**, *40*, 6564-6571.
20. C. F. Buitrago, J. E. Jenkins, K. L. Opper, B. S. Aitken, K. B. Wagener, T. M. Alam, K. I. Winey. *Macromolecules* **2013**, *46*, 9003-9012.
21. B. S. Aitken, C. F. Buitrago, J. D. Heffley, M. Lee, H. W. Gibson, K. I. Winey, K. B. Wagener. *Macromolecules* **2012**, *45*, 681-687.

22. C. F. Buitrago, T. M. Alam, K. L. Opper, B. S. Aitken, K. B. Wagener, K. I. Winey. *Macromolecules* **2013**, *46*, 8995-9002.
23. E. G. Tennyson, S. He, N. C. Osti, D. Perahia, R. C. Smith. *J. Mater. Chem.* **2010**, *20*, 7984-7989.
24. I. Horcas, R. Fernandez, J. M. Gomez-Rodriguez, J. Colchero, J. Gomez-Herrero, A. M. Baro. *Rev. Sci. Instrum.* **2007**, *78*.
25. C. Y. Zhou, L. T. Yam, L. N. Zhang, X.D.Ai, T. X. Li, C. A. Dai. *J. Macromol. Sci. A* **2012**, *49*, 293–297.
26. A. G. Tennyson, J. W. Kamplain, C. W. Bielawski. *Chem. Commun.* **2009**, 2124-2126.

APPENDICES

Appendix 2A

NMR spectra

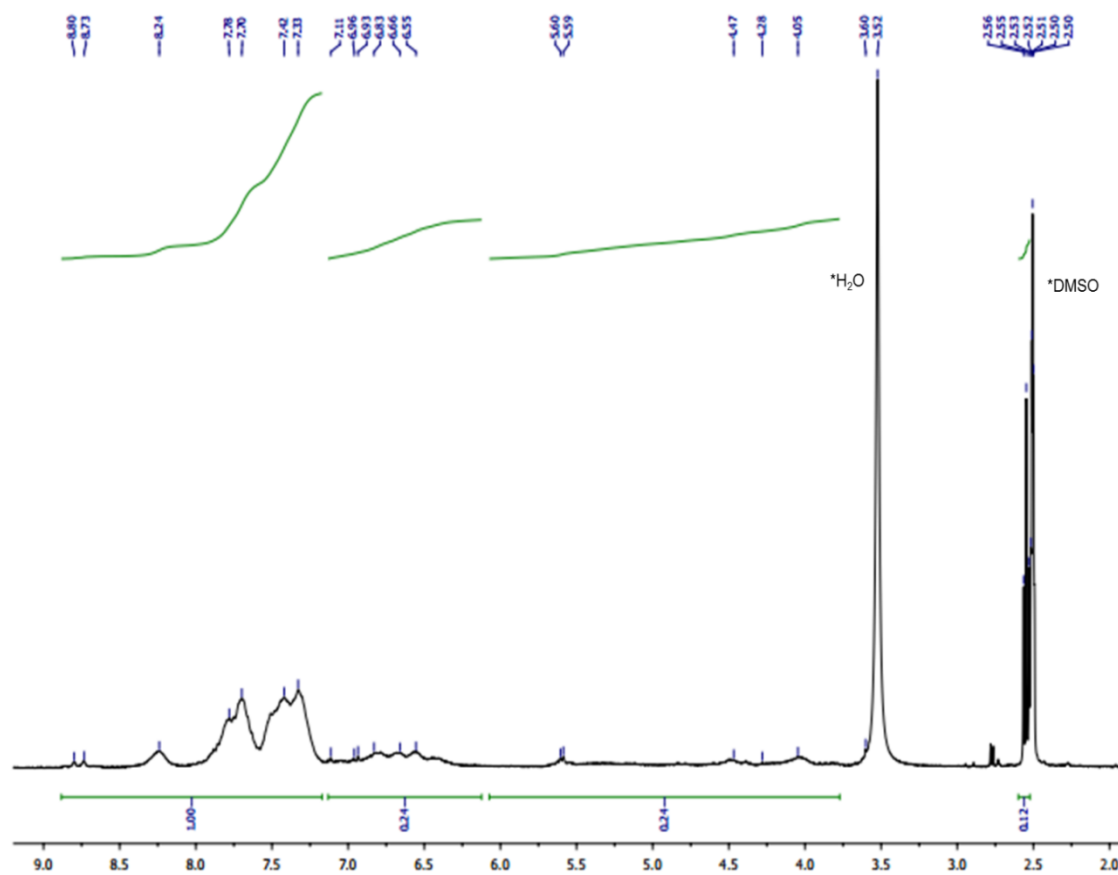


Figure 2A.1: Proton NMR spectrum of **LX1** ($(\text{CD}_3)_2\text{SO}$, 300 MHz). Peak marked with an asterisk correspond to solvent signals.

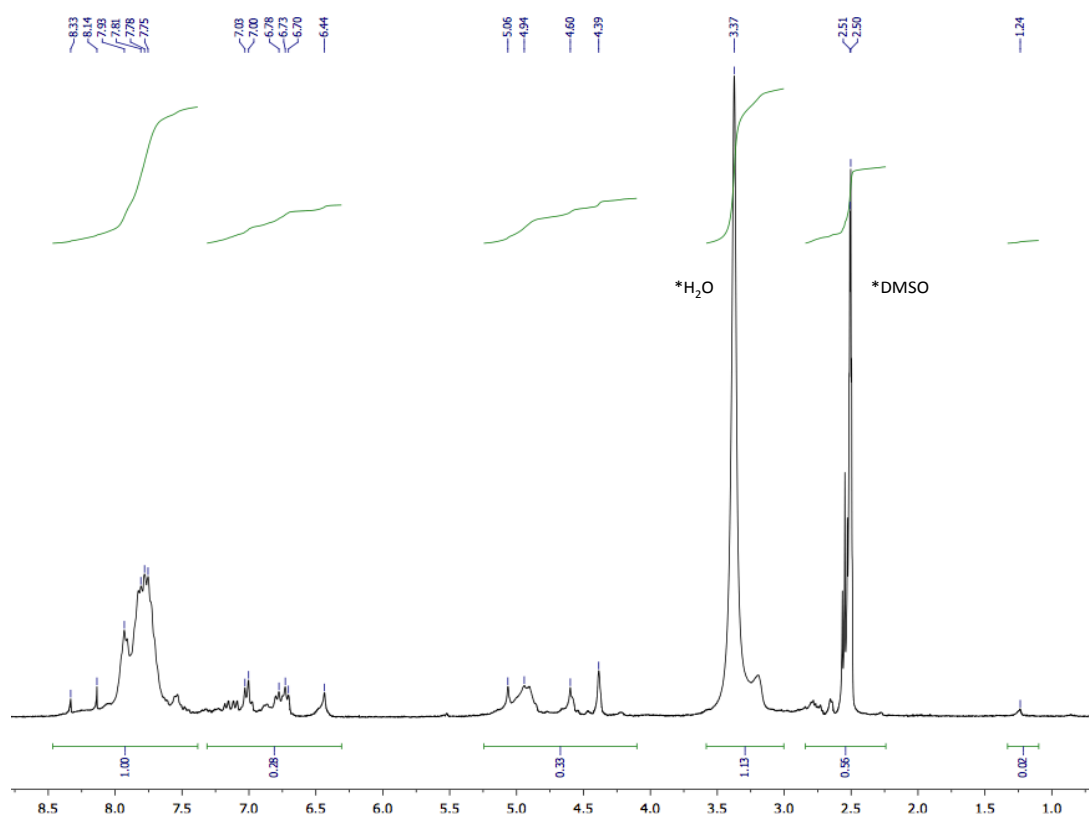


Figure 2 A.2: Proton NMR spectrum of **LX2** ((CD₃)₂SO, 300 MHz). Peak marked with an asterisk correspond to solvent signals.

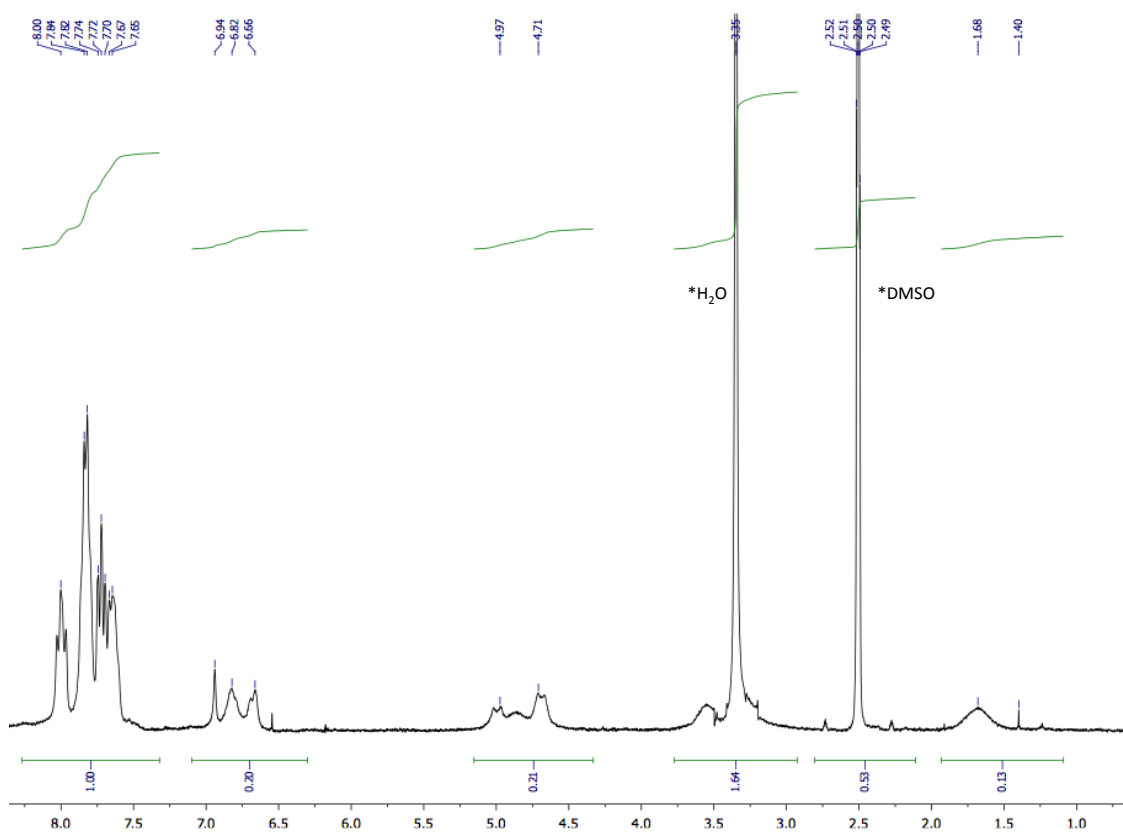


Figure 2 A.3 Proton NMR spectrum of **LX3** ($(\text{CD}_3)_2\text{SO}$, 300 MHz). Peak marked with an asterisk correspond to solvent signals.

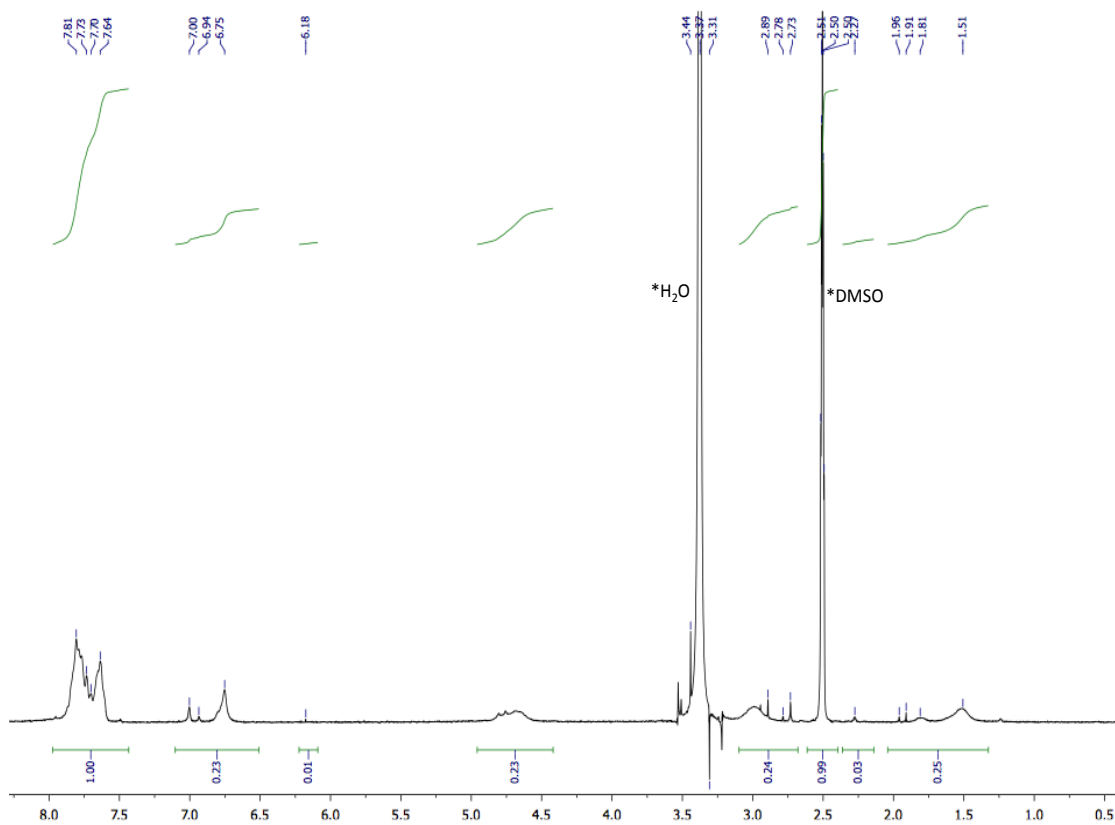


Figure 2 A.4: Proton NMR spectrum of **LX4** ((CD₃)₂SO, 300 MHz). Peak marked with an asterisk correspond to solvent signals.

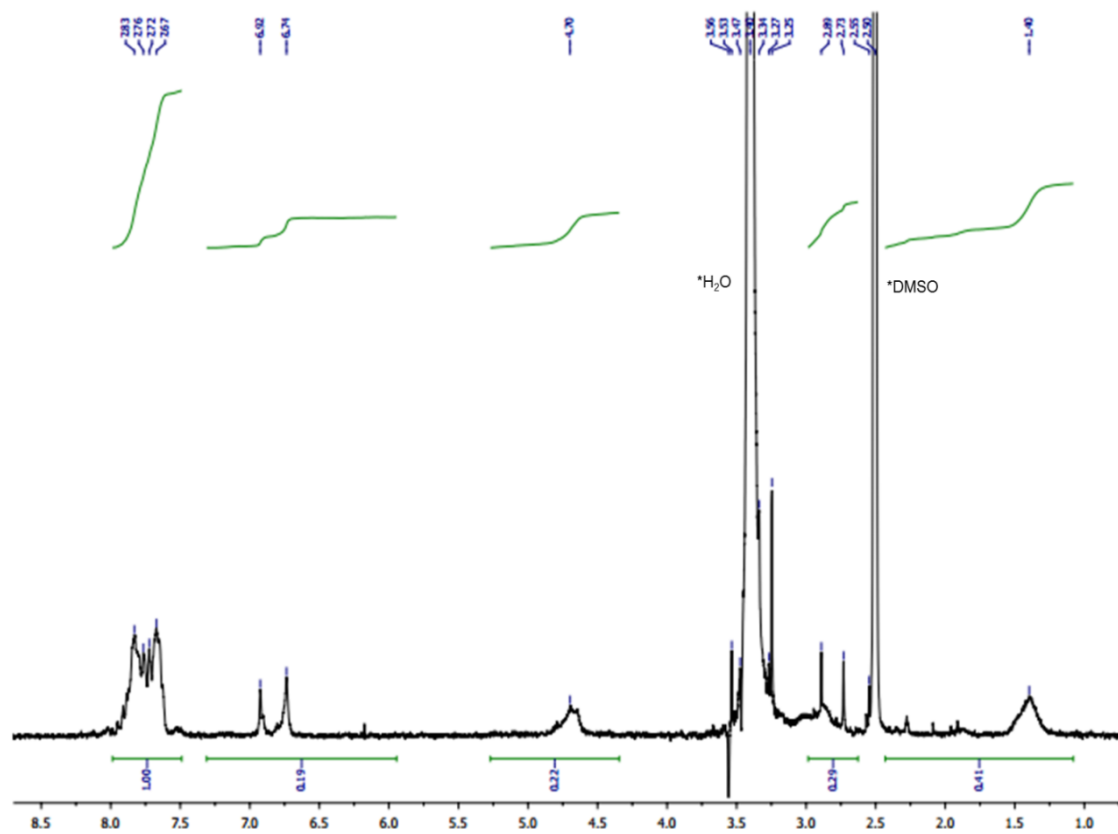


Figure 2 A.5: Proton NMR spectrum of **LX5** ($(\text{CD}_3)_2\text{SO}$, 300 MHz). Peak marked with an asterisk correspond to solvent signals.

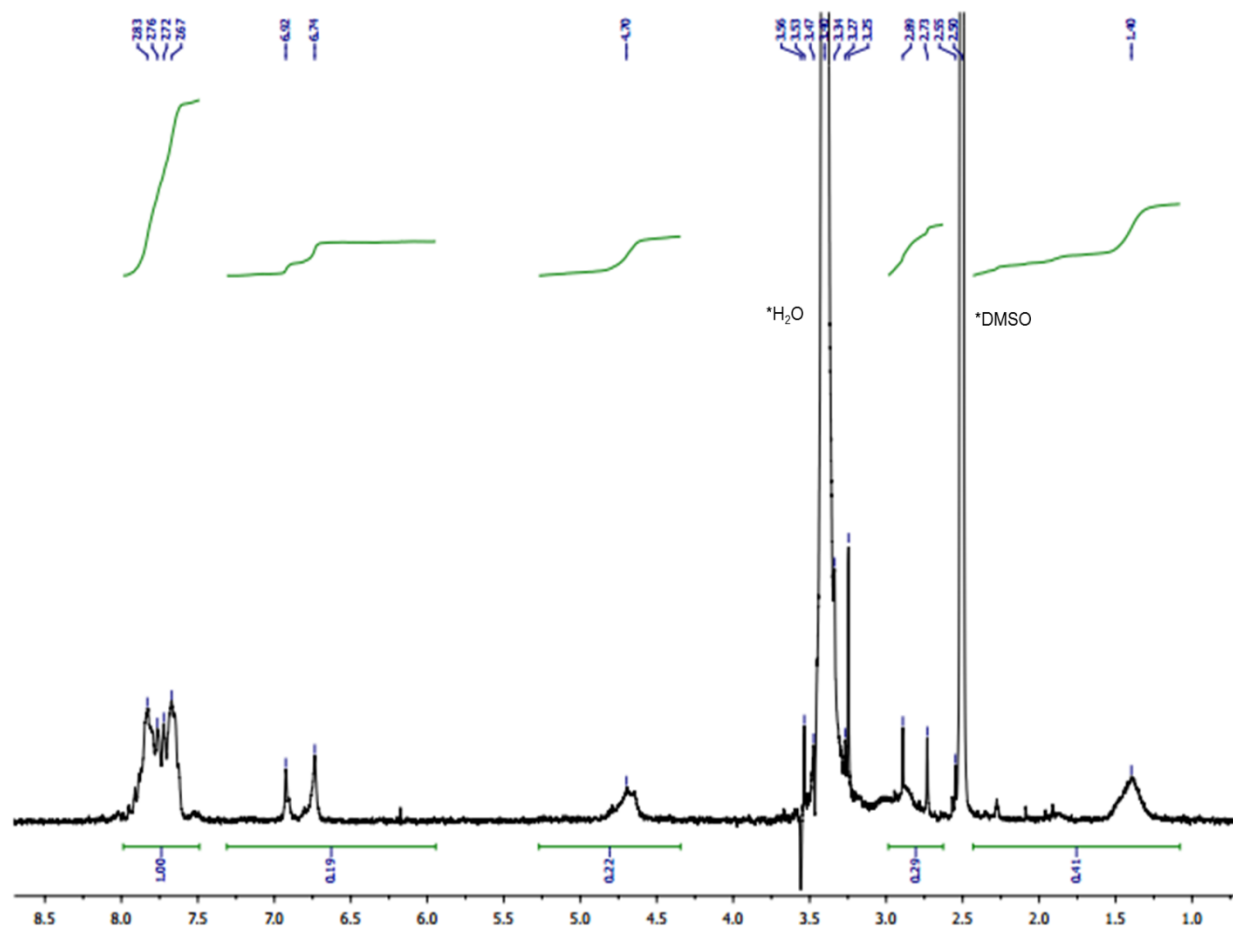


Figure 2 A.5: Proton NMR spectrum of **LX5** ($(\text{CD}_3)_2\text{SO}$, 300 MHz). Peak marked with an asterisk correspond to solvent signals.

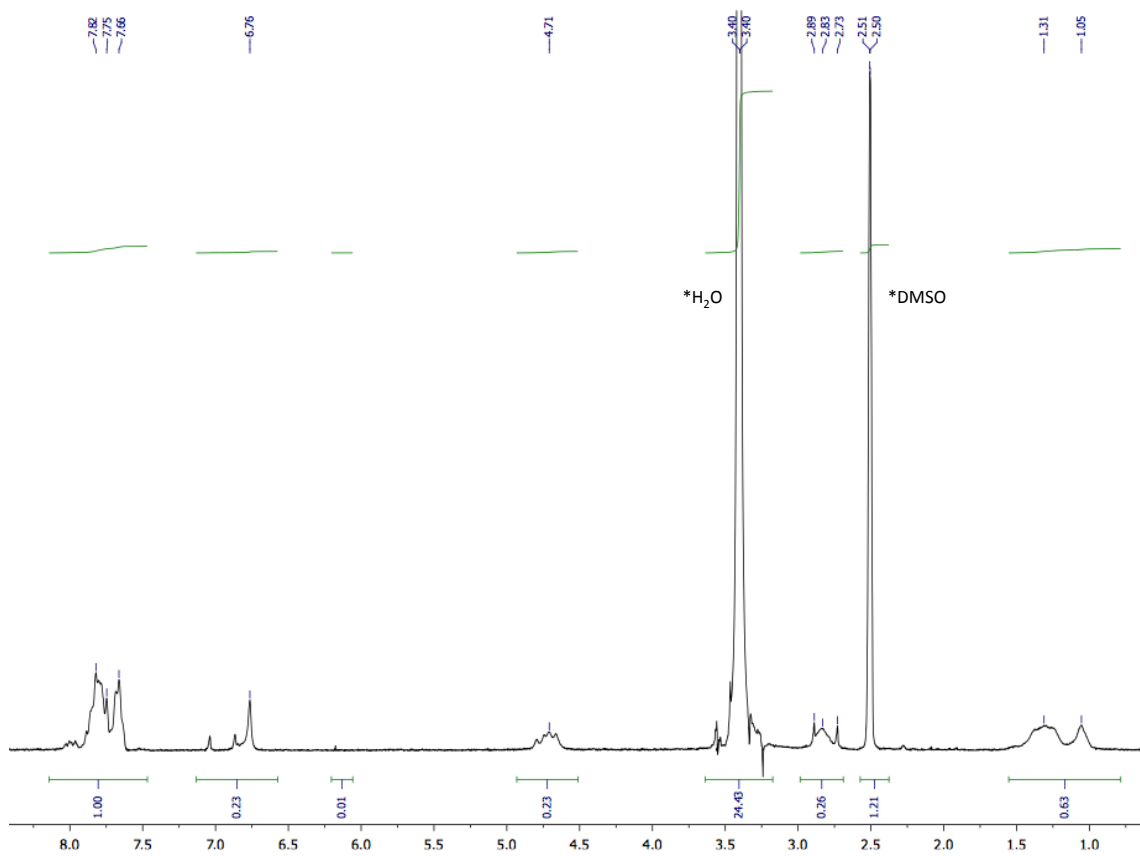


Figure 2 A.6: Proton NMR spectrum of **LX8** ((CD₃)₂SO, 300 MHz). Peak marked with an asterisk correspond to solvent signals.

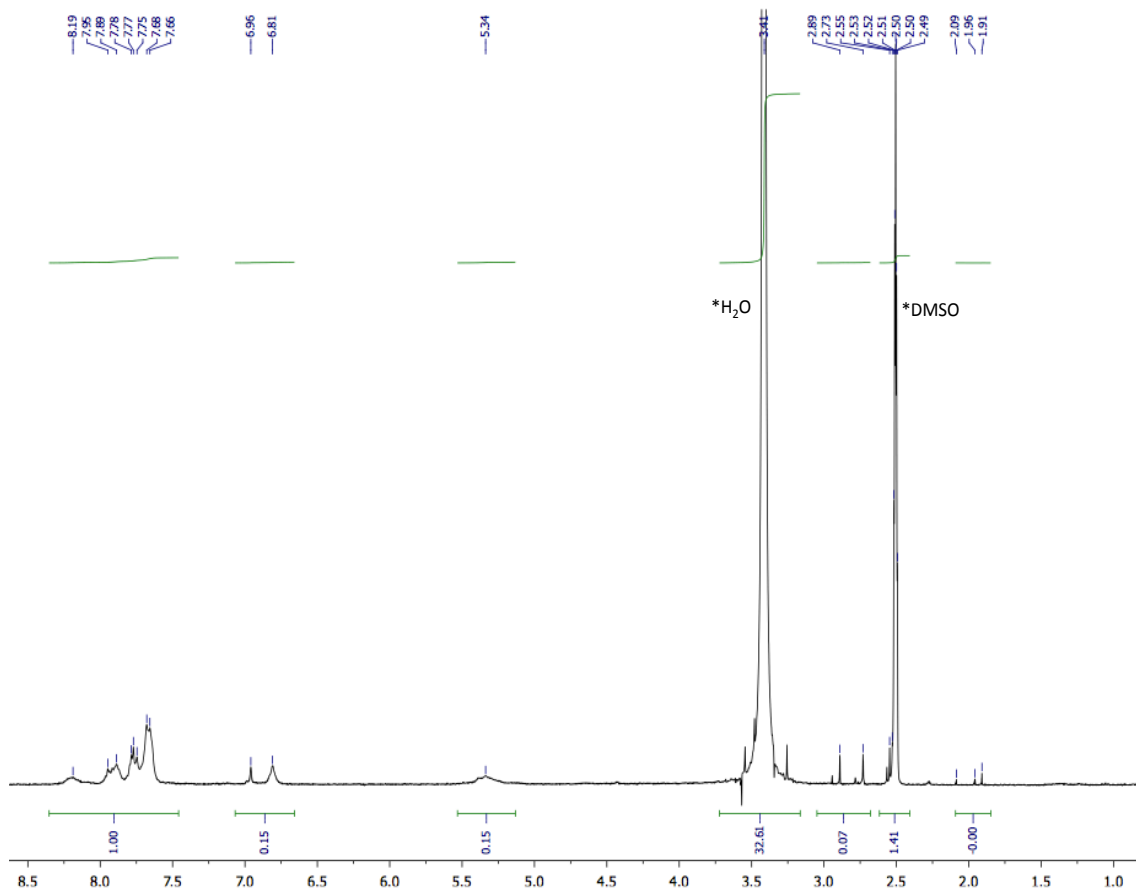


Figure 2 A.7: Proton NMR spectrum of **LXPb** ((CD₃)₂SO, 300 MHz). Peak marked with an asterisk correspond to solvent signals.

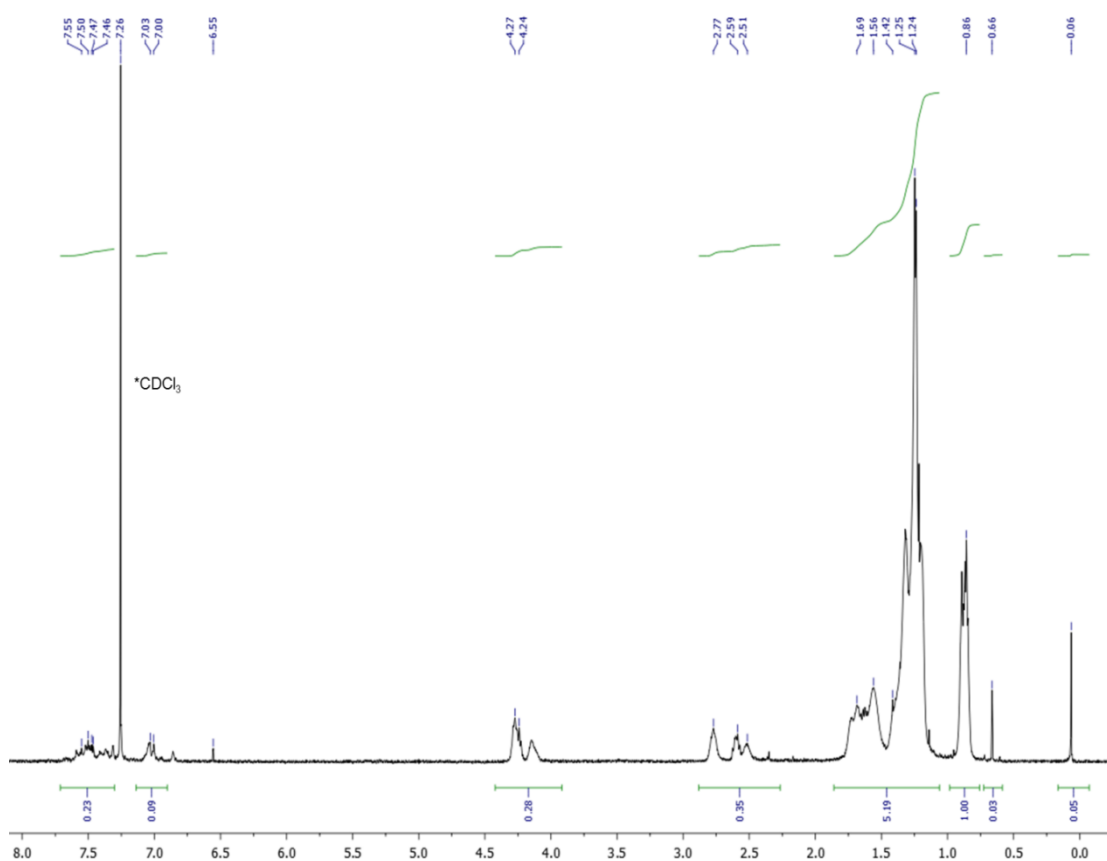


Figure 2 A.8: Proton NMR spectrum of **Pc12** (CDCl₃, 300 MHz). Peak marked with an asterisk correspond to solvent signals.

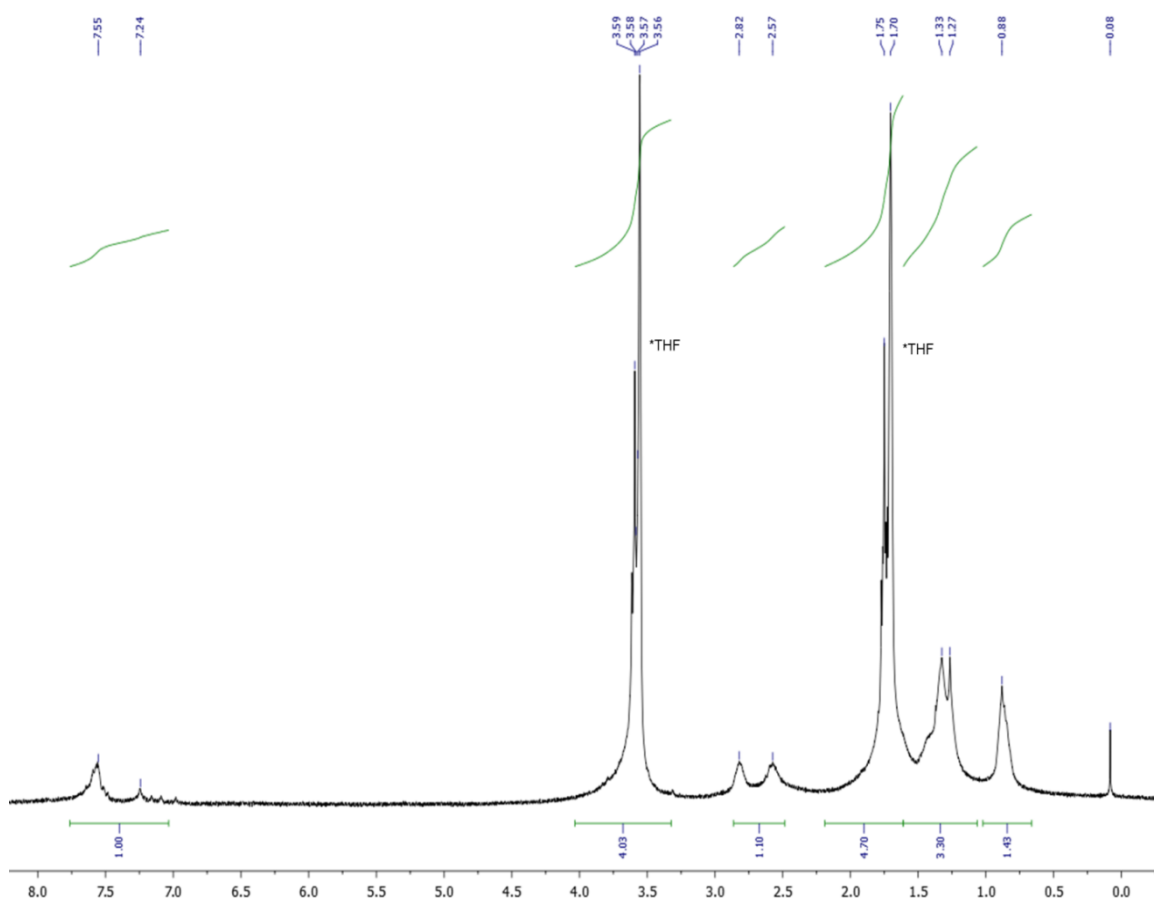


Figure 2 A.9: Proton NMR spectrum of **Pc12-100** (THF-d⁸, 300 MHz). Peak marked with an asterisk correspond to solvent signals.

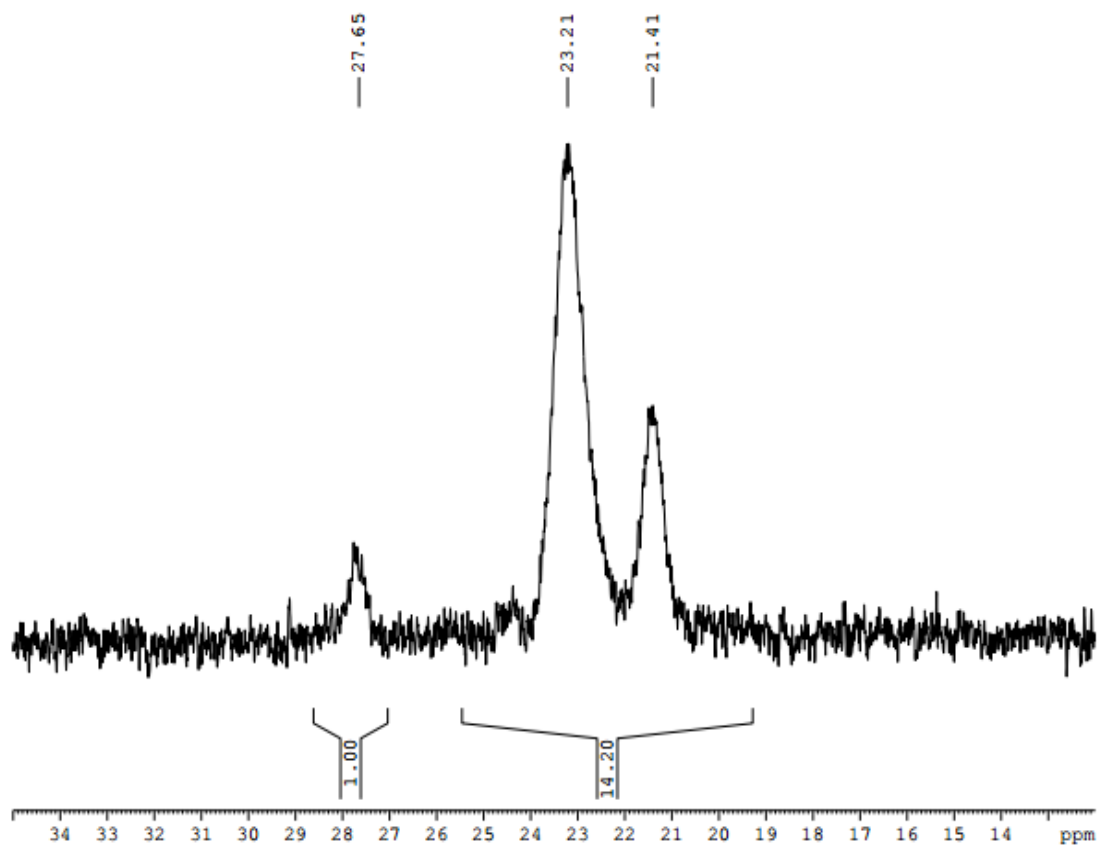


Figure 2 A.10: Phosphorous-31 NMR of compound **LX1** ($(\text{CD}_3)_2\text{SO}$, 121 MHz)

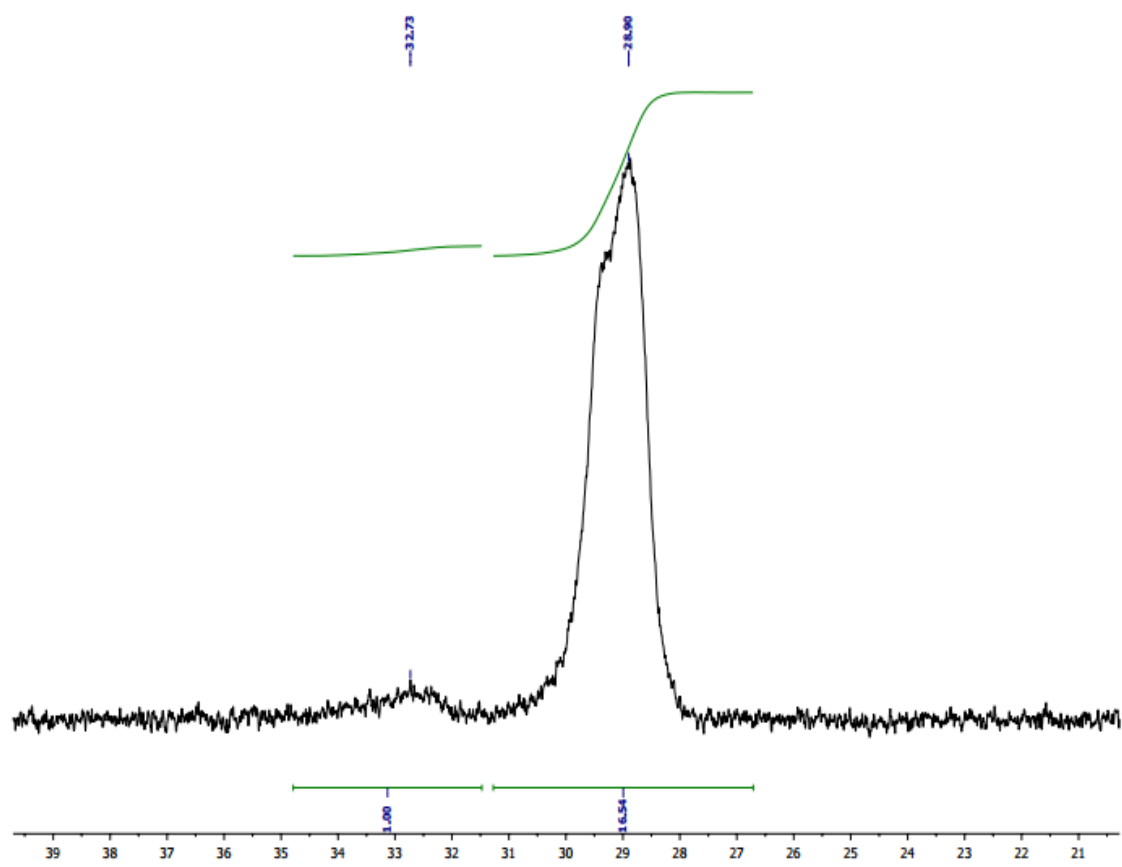


Figure 2 A.11: Phosphorous-31 NMR of compound LX2 ($(\text{CD}_3)_2\text{SO}$, 121 MHz)

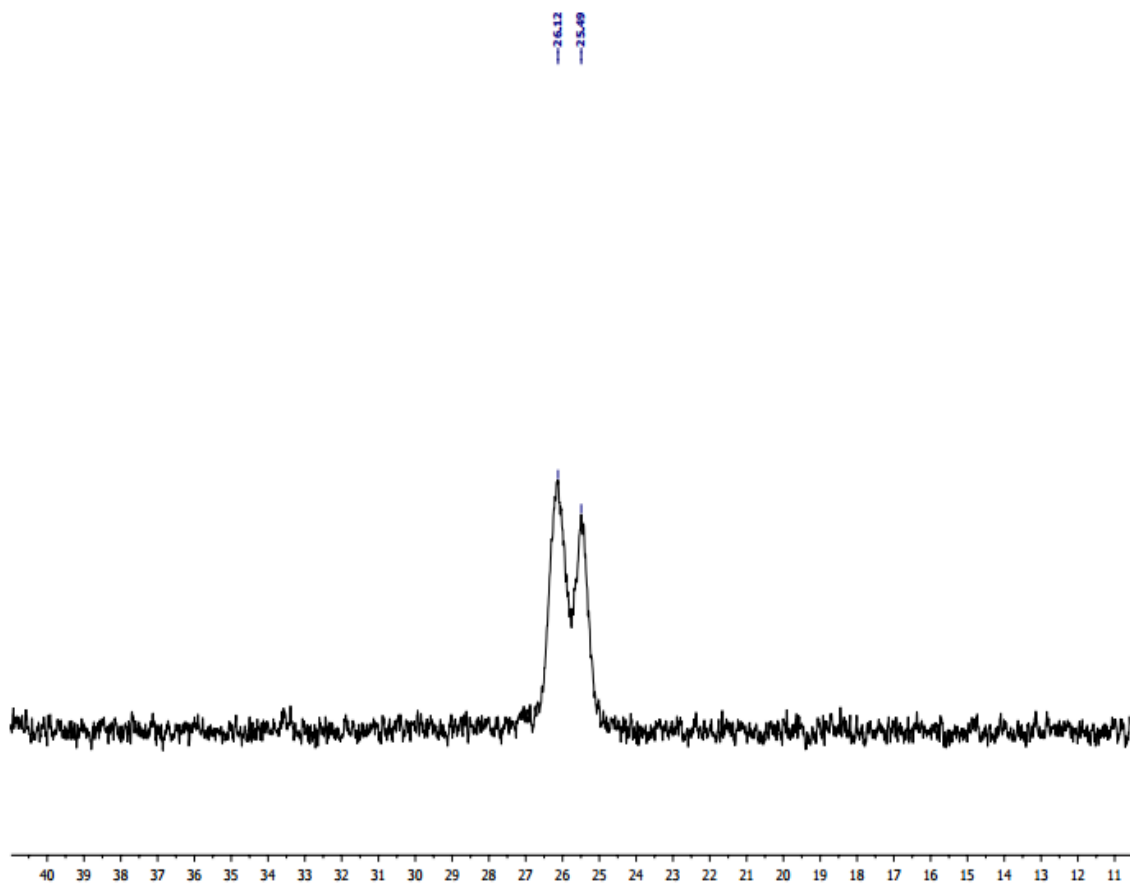


Figure 2 A.12: Phosphorous-31 NMR of compound **LX3** ($(\text{CD}_3)_2\text{SO}$, 121 MHz)

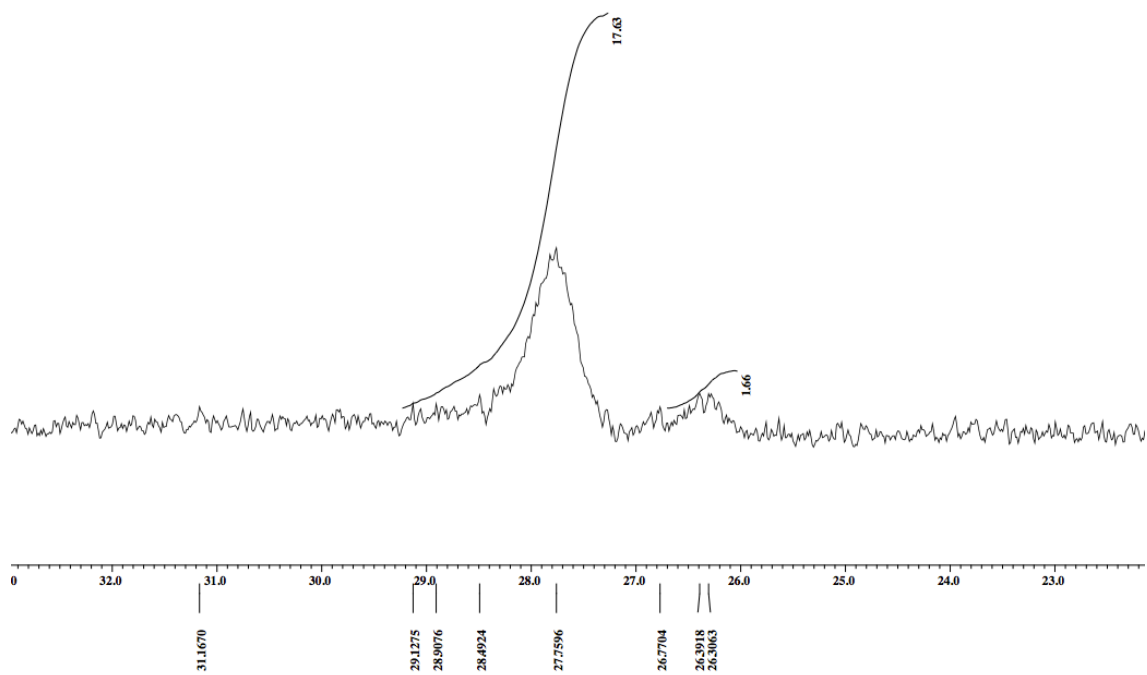


Figure 2 A.13: Phosphorous-31 NMR of compound **LX4** ($(\text{CD}_3)_2\text{SO}$, 121 MHz)

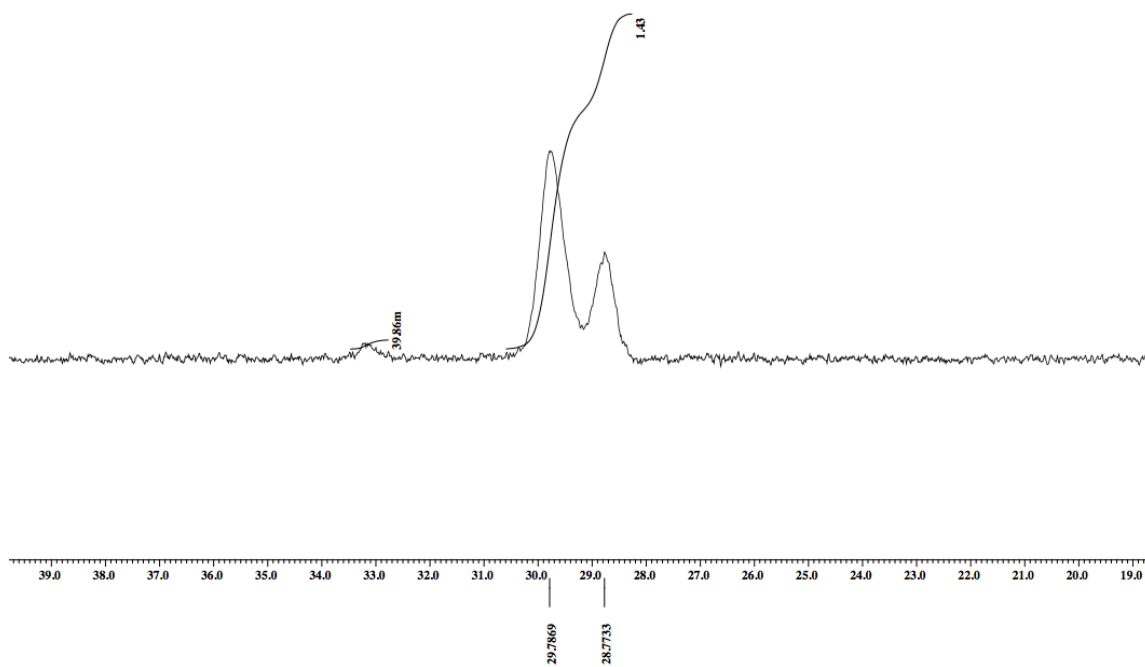


Figure 2 A.14: Phosphorous-31 NMR of compound **LX5** ($(\text{CD}_3)_2\text{SO}$, 121 MHz)

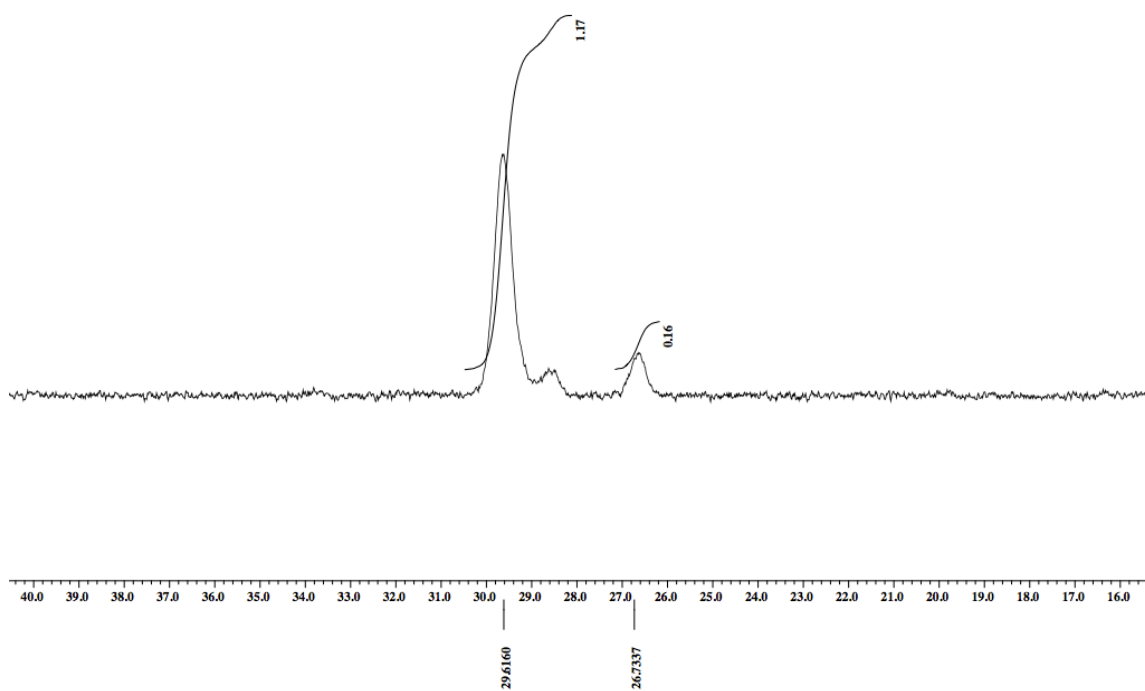


Figure 2 A.15: Phosphorous-31 NMR of compound **LX8** ($(\text{CD}_3)_2\text{SO}$, 121 MHz)

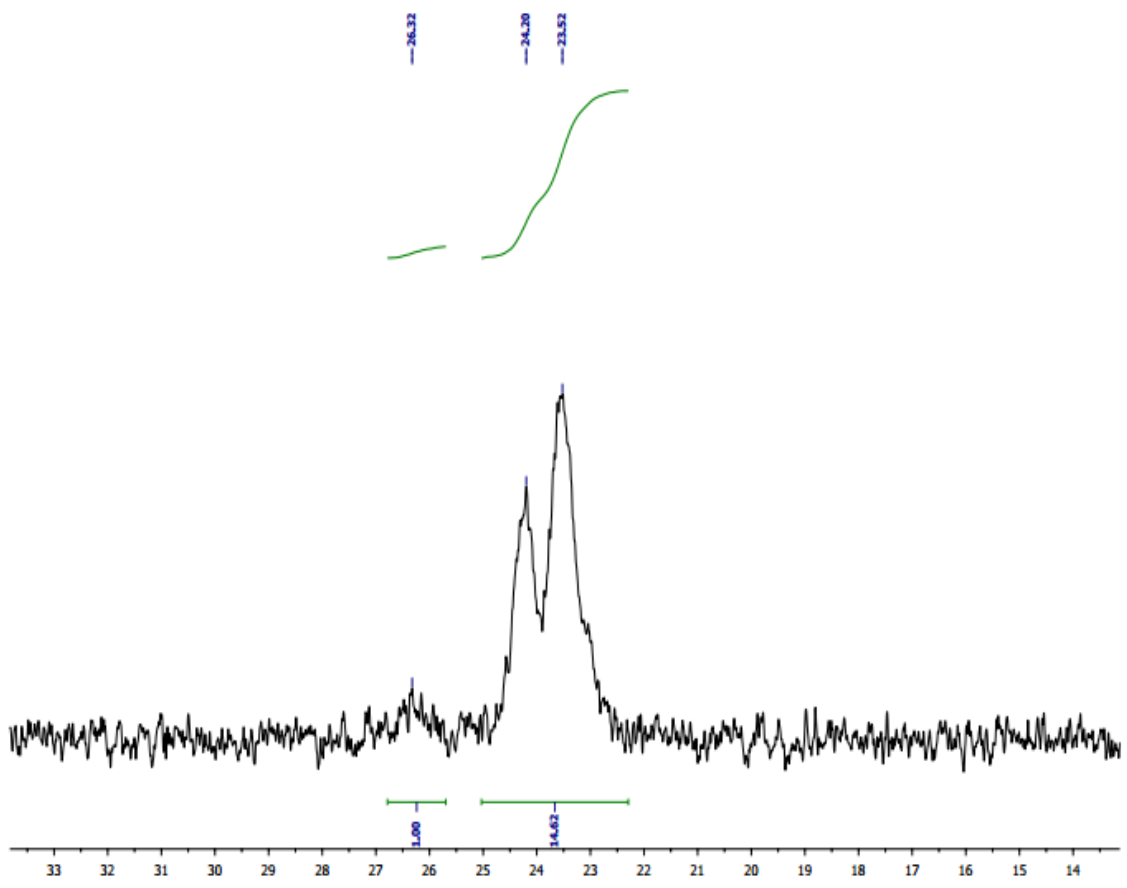


Figure 2 A.16: Phosphorous-31 NMR of compound **LXPh** ($(\text{CD}_3)_2\text{SO}$, 121 MHz)

Appendix 2B

X-ray powder diffraction, TGA and DSC Traces

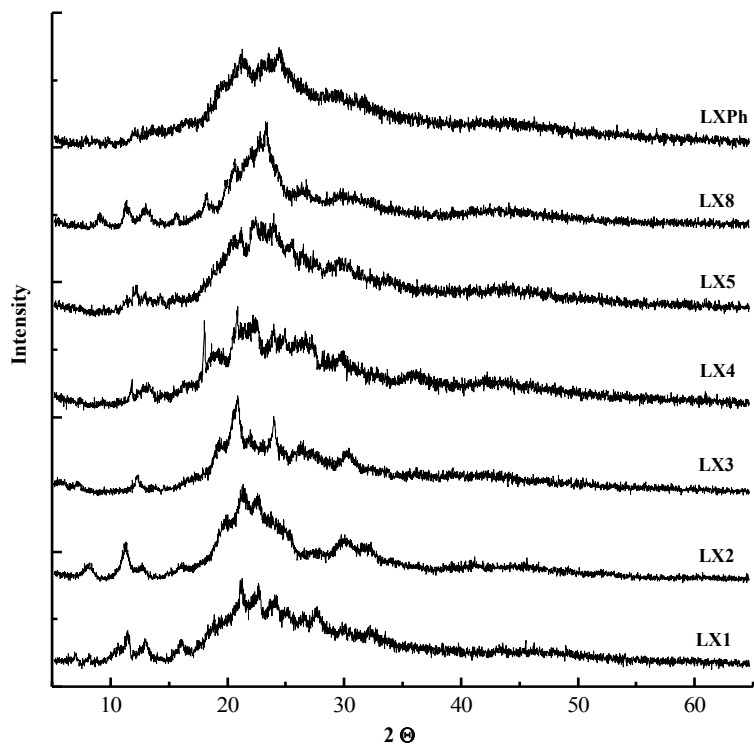


Figure 2 B.1: X-ray Powder Diffraction of polymers.

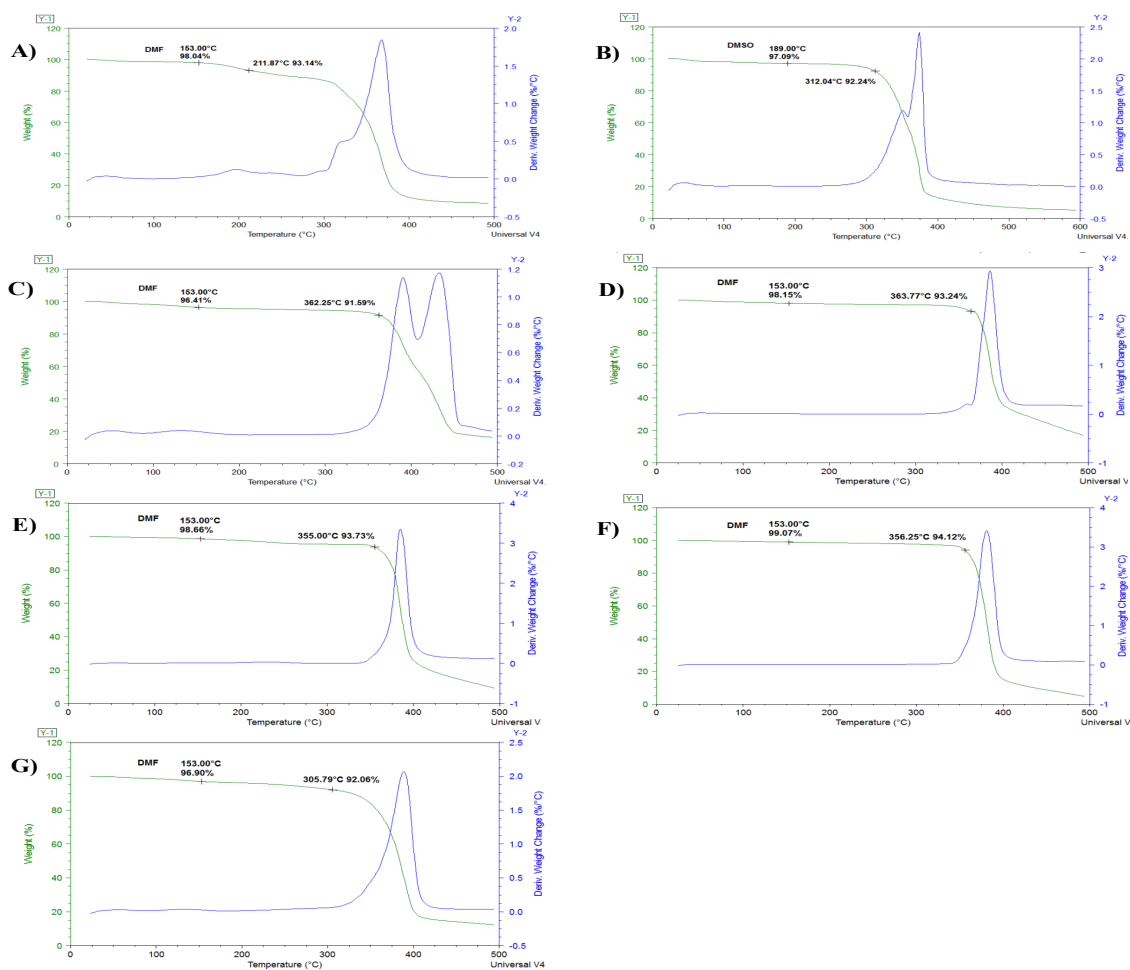


Figure 2 B.2: TGA of LX polymers: LX1 (A), LX2 (B), LX3 (C), LX4 (D), LX5 (E), LX8 (F) and LXPh (G).

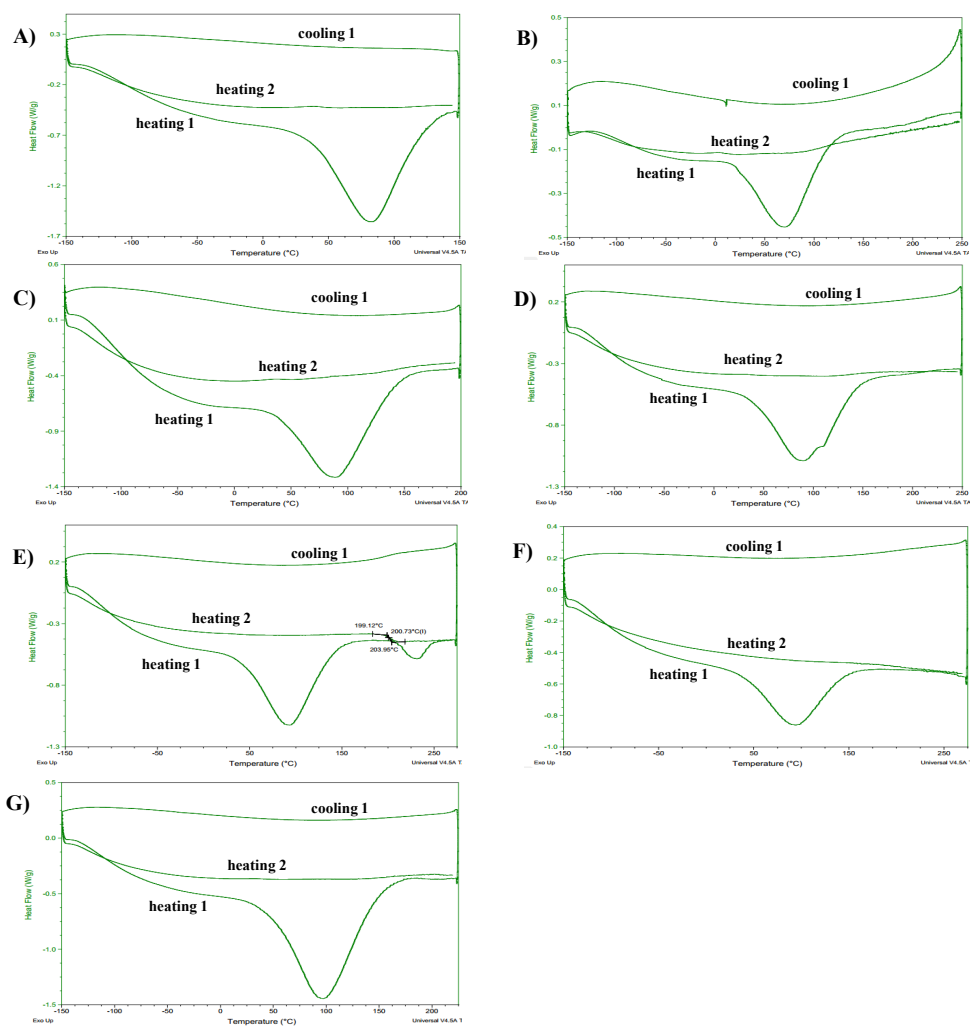


Figure 2 B.3: DSC of LX polymers: LX1 (A), LX2 (B), LX3 (C), LX4 (D), LX5 (E), LX8 (F) and LXPh (G).

Appendix 2C

AFM images

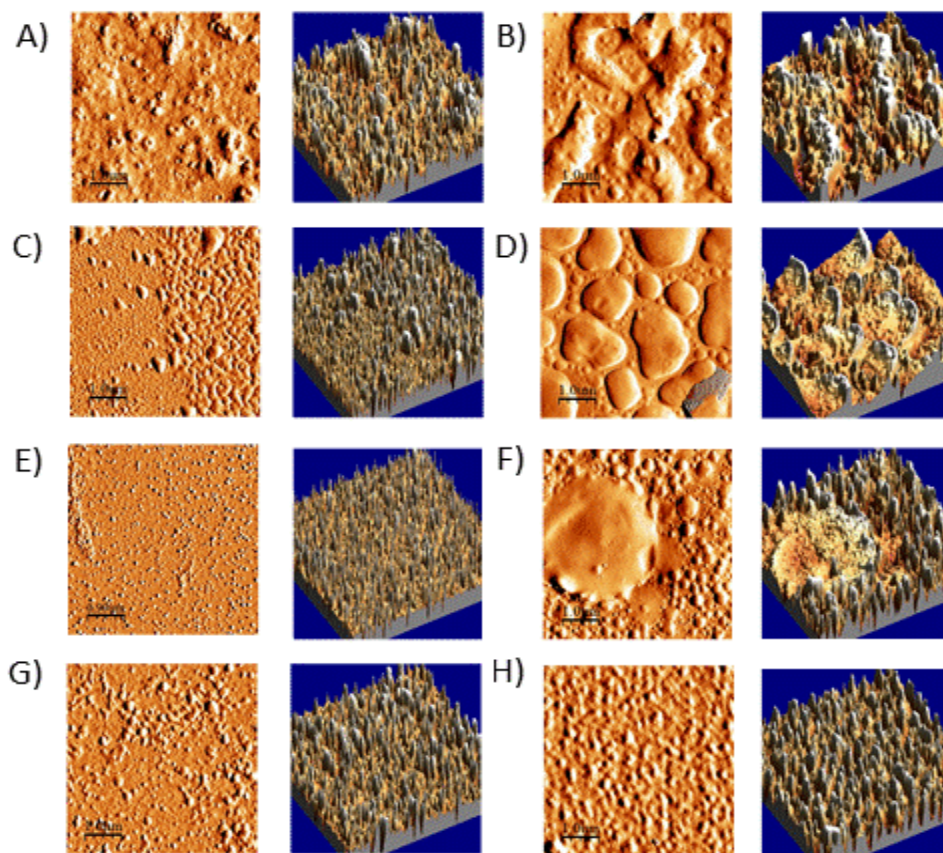


Figure 2 C.1: AFM ($5 \times 5 \mu\text{m}$) 2D height images and 3D images of LbL films of LX with Pc12-100: LX1/Pc12-100 (A), LX2/Pc12-100 (B), LX3/Pc12-100 (C), LX4/Pc12-100 (D), LX5/Pc12-100 (E), LX8/Pc12-100 (F) and LXPh/Pc12-100 (G) and clean glass slide (H).

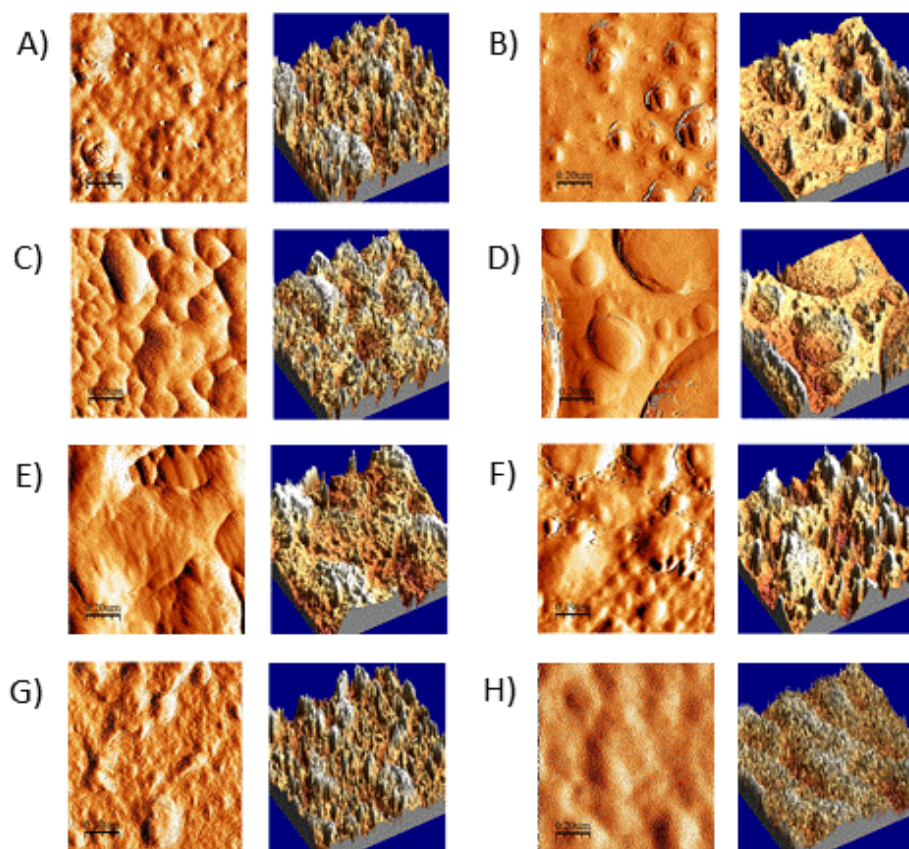


Figure 2 C.2: AFM ($1 \times 1 \mu\text{m}$) 2D height images and 3D images of LbL films of LX with Pc12-100: LX1/Pc12-100 (A), LX2/Pc12-100 (B), LX3/Pc12-100 (C), LX4/Pc12-100 (D), LX5/Pc12-100 (E), LX8/Pc12-100 (F) and LXPh/Pc12-100 (G) and clean glass slide (H)

CHAPTER THREE[§]

INFLUENCE OF STRUCTURE ON PHOSPHONIUM POLYMER PROPERTIES, SUPRAMOLECULAR ASSEMBLY AND BACTERICIDAL ACTIVITY[#]

3.1 Introduction

The intriguing physical properties of polyelectrolytes (alternatively called ionomers or ionic polymers) have led to their adaptation in an ever-expanding cadre of applications in recent years. Many polyelectrolytes can be processed from aqueous solution, making them attractive from an environmental and economic standpoint as well as rendering them suitable for biological applications.¹ Fluorescent sensors comprised by conjugated polyelectrolytes, for example can be used for detection of charged biomolecules (e.g., protein²⁻⁴ and DNA⁵⁻⁸) at low concentrations in biological milieu. The electrostatic interaction and supramolecular self-assembly endowed by ionic functionalities provides exciting opportunities for hierarchical assembly of films for optoelectronic^{9,10} and electrochemical¹¹⁻¹³ devices as well.

Existing work on cationic polyelectrolytes most commonly has featured ammonium,¹⁴ pyridinium,^{15,16} imidazolium,^{17,18} guanidinium¹⁹ or phosphonium groups,²⁰ each of which may be in the main chain or in side chain components. The Smith group's research on these materials has concentrated on properties and applications of phosphonium polyelectrolytes (PELs), some examples of which are displayed in Chart 3.1. Compared to ammonium salts, phosphonium

[§] This chapter is being developed for submission to a journal for publication.

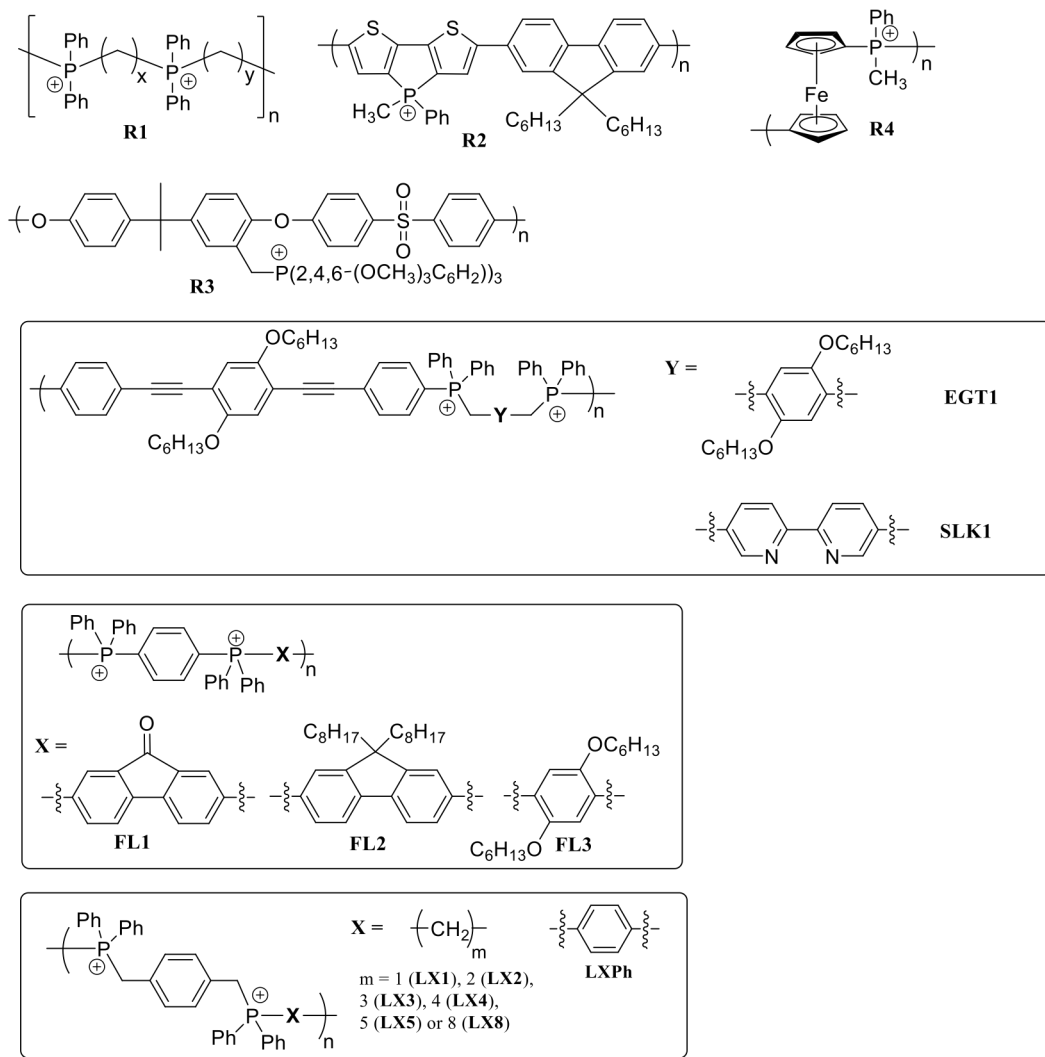


Chart 3.1: Examples of phosphonium polyelectrolytes (PELs).

salts often exhibit better thermal and chemical stability, making these particular species especially attractive in terms of performance under such duress over longer operational lifetimes. As an example of the thermal stability attainable, **R4**²¹ synthesized in Manners' group is thermally stable up to 400 °C, and small molecular phosphonium salts represent the most thermally robust ionic liquids

known.²² An example in which chemical stability is paramount is in an alkaline fuel cell, where the membrane must tolerate extended heating at temperatures up to 80 °C in the presence of aqueous hydroxide. The PEL **R3**²³ has proven stable enough for test devices under such conditions, and recent advances in the preparation of tetraarylphosphonium polymers²⁴ suggest that more advances are on the horizon in this area as structural elements leading to improved stability are identified. PELs also offer advantages in medicinal contexts. For example, PELs exhibit higher bactericidal activity²⁵ and higher efficiency/lower toxicity to human cells in gene delivery²⁶ versus ammonium analogues.

PELs incorporating chromophore-derivatized or conjugated moieties in the polymer main chain have been surprisingly scarce to date. This is especially surprising in light of the obvious applications (i.e., fluorescent sensors or optoelectronic films) in which these robust materials could find utility. The few examples of chromophore-derivatized PELs include **R2**,²⁷ **EGT1**,²⁸ **SLK1**²⁹ and **FL1-2** (Chart 1).²⁴ All of these polymers exhibit significant absorption and photoluminescence in the UV-visible region of the spectrum, and some exhibit significant solvatochromic effects in response to changing polarity of their environment, making them possible elements of stimuli-responsive systems.^{30,31}

Ionic units endow polyelectrolytes with the ability to form strong ion-ion and ion-dipole interactions with surfaces and other molecules, and are consequently excellent candidates as components of supramolecularly-assembled structures. The

layer-by-layer (LbL) deposition of alternating monolayers of two or more components is a remarkably facile process to attain ordered thin polymer films of precisely-controlled thickness and composition.³²⁻³⁴ LbL assembly of PELs has recently been demonstrated on various substrates that are employed in opto/electronic applications (e.g. ITO, glass, silicon wafer and mica).^{35,36} Controlled LbL assembly of PELs with anionic polymers such as **PAA**, **APT**, **APPV** (Chart 3.2) has thus been employed to yield visible-absorbing ordered films.²⁹ An interesting example of how the LbL assembly of PELs can be tailored is offered by **SLK1**. **SLK1** is composed of phosphonium moieties and metal-ligating 2,2'-bipyridyl (bipy) units in the polymer backbone. When there is no metal bound to the bipy unit, the charge per repeat unit is +2, whereas coordination of a divalent metal ion (i.e., Zn^{2+}) doubles this to +4 per repeat unit. The ability to tune charge density by metal ion coordination is accompanied by commensurate changes in the polyanion:PEL ratio in LbL-assembled films of these materials, and thus the relative absorptivity at wavelengths associated with each component.²⁹ The insights provided by these studies on **SLK1** led to additional studies³⁷ into the influence that inter-ion spacing and density of charged sites along the PEL backbone have on film growth and morphological properties of LbL-assembled films. These studies aimed to reveal the structure-property relationships that govern material bulk properties analogous to such studies that have significantly advanced understanding of these effects in classic polymer systems such as polyethylene derivatives.³⁸⁻⁴²

A detailed study on the **LX** series (Chart 3.1) confirmed that the spacer flexibility and distance between phosphonium charge bearing units have significant effect on the properties of the PEL and LbL films with polyanions.⁴³ The study on the **LX** series differed from previous LbL assembly of PELs in that **Pc12-100** (Chart 3.2) was employed in place of the anionic polythiophene derivative **APT** that had been used in prior studies. In **APT**, the distance between anionic sites is not rigidly enforced because the anionic functional group interfaces with the polythiophene backbone via a long flexible side chain. As a result, the dependence of supramolecular assembly properties on inter-cation distance and inter-cation spacer flexibility may be washed out to some degree. In contrast, **Pc12-100** features well-defined inter-anion spacing because the carboxylate units are attached directly to the rigid backbone. As anticipated, the influence of inter-cation spacer was more apparent in the study involving LbL deposition of the PELs with **Pc12-100**.

Although significant strides have been made in understanding backbone effects on PEL properties,^{37,43,44} the role of side chains has not been systematically

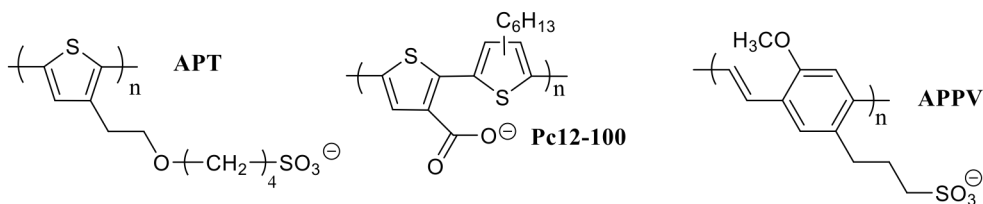


Chart 3.2: Anionic polyelectrolytes that have been used in layer-by-layer assembly with phosphonium polymers.

addressed. Herein, we described polymers **LO** (Scheme 3.1), which are structural analogues of the **LX** series (Chart 3.1), but in which the phenylene units in **LX** have been replaced with 2,5-dioctyloxyphenylene units. The effects of side chains on thermal stability, glass transitions, crystallinity, film morphology, critical surface energy and supramolecular-assembly of these PELs were examined and compared with those of previously-studied structural analogues with the aim of sharpening the understanding of PEL structure-property relationships.

3.2 Experimental

3.2.1 General Considerations

All air-sensitive reactions were performed in an MBraun UNILab glovebox under nitrogen. Anhydrous solvents were dried and degassed using an MBraun solvent purifier. Anionic polythiophene derivative **Pc12-100** and **LX** series polymers were prepared as previously reported.⁴³ Monomers **M1** were obtained from Sigma-Aldrich or Strem Chemical. Glass slides were purchased from Fisher Scientific. Other chemicals were used without further purification after purchased. All the NMR spectra were collected on a Joel ECX-300 MHz spectrometer operating at 300 and 121.4 MHz for ¹H and ³¹P, respectively. Thermogravimetric analysis (TGA) was performed on TA Instruments Q5000 TGA from 25 °C to 600 °C with a heating rate of 20 °C min⁻¹. Differential scanning calorimetry (DSC) was performed on TA Instruments Q1000 DSC with a heat/cool/heat cycle at 20 °C min⁻¹ for heating and 10 °C min⁻¹ for cooling, and report *T_g* data for the second scan.

3.2.2 Dip-cast technique

Glass substrates were cut from Fisherfinest[®] Premium microscope slides, cleaned in piranha solution, rinsed with deionized water, then ethanol, blown with N₂, and dried for 12 h in a 140 °C oven. Films were prepared by dip-casting (Mayer Feintechnik, model D-3400) from a 5 mg/mL solution with a linear rate of 6 mm/s.

3.2.3 Layer-by-layer technique

The procedure is similar with that published in our previous work.²⁸ Glass microscope slides were cleaned by concentrated nitric acid, rinsed with deionized water, and then with tetrahydrofuran (THF). The slide was visually inspected for scuffs or scratches. Solutions of **LO** and **Pc12-100** (5×10^{-4} M) were prepared in CH₃CN/H₂O (4:1) and THF/water (2:1). The pH of water used to prepare **Pc12-100** solution was adjusted to 9 with NaOH to deprotonate carboxylic acid side chains. The slide was first dipped into the **LO** solution then briefly shaken to remove any excess solution droplets. The process was then repeated using the **Pc12-100** solution. The spectrum of the film was immediately collected using a Cary 50 UV-vis spectrometer with a scanning range of 275 to 800 nm. This procedure was repeated until the desired number of bilayers was obtained.

3.2.4 Atomic Force Microscopy (AFM)

All the AFM experiments were performed with an AIST SmartSPM[™] 1000 instrument in semi-contact mode within $1 \times 1 \mu\text{m}$ and $5 \times 5 \mu\text{m}$ sample areas using an aluminium tip (spring constant = 5 N/m, 160 kHz resonance frequency). Images were processed by AIST-NT and WSxM 5.0 Develop 7.0 software (www.wsxmsolutions.com).⁴⁵

3.2.5 Contact Angle Measurements

Glass substrates were prepared as previously described for dip-cast technique. Each substrate was placed in an individual vial and dried for 12 h in a 140 °C oven. The vials were removed and sealed under N₂. Substrates were exposed to ambient atmosphere for less than 30 s before dip-casting from solutions of 5 mg/mL CHCl₃ (**LO** series) or CH₃CN/H₂O (4:1) (**LX** series) using a Mayer Feinttechnik, D-3400 instrument with a linear rate of 6 mm/s. Samples were placed under vacuum for 12 h, then sealed under N₂. Before placement of the test drop for contact angle measurement, substrates were exposed to ambient atmosphere for less than 30 s. A 2.0 mm diameter Luer needle was used to place the test drop with a maximum variation in volume from 1.5 – 4.5 μL. The drop rested for 60 s before contact angle was measured with a Krüss DSA 10 Mk2 goniometer. Test drops were placed for 16.7%, 5.0%, 1.6%, and 0% mol/mol aqueous acetic acid solutions with surface tensions of 40.3, 51.2, 61.7 and 72.0 mN/m, respectively, at 25 °C. Four measurements were taken to generate each data point and a Zisman plot was produced for cosine contact angle versus surface tension of the test liquid. The critical surface energy was calculated for the intercept of line, cosine $\theta = 1$.

3.2.6 Bactericidal Activity Studies

Tryptic Soy Agar (TSA) plates were made as needed. An overnight was started one day (approximately 18 hours) prior to the assay with Tryptic Soy Broth (TSB) and one bacterial colony from an *E. coli* or *S. aureus* plate at 37 °C. On the day of the assay, 19 mL of the overnight were placed in 50 mL Falcon tubes, one for the control and one for each of the polymers tested. A dilution series was carried out in TSB to 10⁻⁷ to

determine the starting colony concentration. Plates were placed in an incubator overnight at 37 °C. The starting absorbance was taken at 600 nm. This was labelled as “start time data.” The fresh solutions of polymer in methanol (1 mg/mL) were filtered through 0.1 µm PTFE syringe filters prior to use. **LX2** was sparingly soluble in methanol, ethanol, DMSO, and Polysorbate 80, but had the best solubility in methanol and was added without filtration. A 2 mL aliquot of a given polymer solution was added to the cultures in the Falcon tubes, and the time of addition noted as “time 0”. Cultures were incubated at 37 °C. The procedure (dilution series plating and absorbance reading) was repeated for times of 0, 30, 60, 90, and 120 min. After 24 h, plates were removed from the incubator and visible colonies were counted. Plate counts were used to determine polymer efficacy against the bacteria in comparison to the control in which methanol was added without any dissolved polymer.

3.2.7 Synthesis of **LO2** (n = 2)

Monomers 2,5-bis(bromomethyl)-1,4-bis(octyloxy)benzene (234 mg, 0.450 mmol) and 1,2-bis(diphenylphosphino)-ethane (199 mg, 0.500 mmol) were placed in a heavy-walled glass pressure tube with anhydrous *N, N*-dimethylformamide (DMF, 3 mL) under nitrogen. The tube was sealed with an O-ring-equipped Teflon screw cap. The tube was then heated to 90 °C with stirring for 15 h. After cooling the reaction vessel to room temperature, it was opened to air. Then 10 mL of diethyl ether was added yielding a white cloudy suspension from which the crude white solid was collected by vacuum filtration. The crude product was then rinsed with 50 mL of diethyl ether (×3) while stirring and dried in a vacuum oven for 48 h. The desired product was a white powder

(358 mg, 86.7%). ^1H NMR (300 MHz, CDCl_3) δ : 8.71-7.29 (br m, 20H), 7.08-6.38 (br m, 2H), 5.48-4.40 (br m, 4H), 4.01-3.12 (br m, 4H), 3.11-0.52 (br m, 34H); $^{31}\text{P}\{^1\text{H}\}$ NMR (121.4 MHz, CDCl_3) δ : 29.5-27.0 (main polymer peak) and 33.3 (end groups). Anal. Calcd. for monomer formula $\text{C}_{50}\text{H}_{66}\text{Br}_2\text{P}_2\text{O}_3$ (ignoring end groups): C, 64.10; H, 7.10; Found: C, 64.90; H, 7.12%.

3.2.8 Synthesis of **LO3** (n = 3)

The synthesis of **LO3** involves same procedures as discussed for **LO2**. The monomers were 2,5-bis(bromomethyl)-1,4-bis(octyloxy)benzene (234 mg, 0.450 mmol) and 1,3-bis(diphenylphosphino)propane (206 mg, 0.500 mmol). The product was white powder (261 mg, 62.1%). ^1H NMR (300 MHz, CDCl_3) δ : 8.49-7.31 (br m, 20H), 7.08-6.51 (br m, 2H), 5.60-4.30 (br m, 4H), 4.25-3.26 (br m, 6H), 3.25-0.52 (br m, 34H); $^{31}\text{P}\{^1\text{H}\}$ NMR (121.4 MHz, CDCl_3) δ : 25.6 (main polymer peak) and 33.2 (end groups). Anal. Calcd. for monomer formula $\text{C}_{51}\text{H}_{68}\text{Br}_2\text{P}_2\text{O}_3$ (ignoring end groups): C, 64.42; H, 7.21; Found: C, 64.43; H, 7.23%.

3.2.9 Synthesis of **LO4** (n = 4)

The synthesis of **LO4** involves same procedures as discussed for **LO2**. The monomers were 2,5-bis(bromomethyl)-1,4-bis(octyloxy)benzene (234 mg, 0.450 mmol) and 1,4-bis(diphenylphosphino)butane (213 mg, 0.500 mmol). The product was a white powder (384 mg, 90.1%). ^1H NMR (300 MHz, CDCl_3) δ : 8.70-7.31 (br m, 20H), 6.90-6.30 (br m, 2H), 5.60-4.30 (br m, 4H), 4.23-3.10 (br m, 8H), 2.95-0.62 (br m, 34H); $^{31}\text{P}\{^1\text{H}\}$ NMR (121.4 MHz, CDCl_3) δ : 26.7 (main polymer peak) and 33.1 (end groups).

Anal. Calcd. for monomer formula $C_{52}H_{70}Br_2P_2O_3$ (ignoring end groups): C, 64.73; H, 7.31; Found: C, 64.69; H, 7.38%.

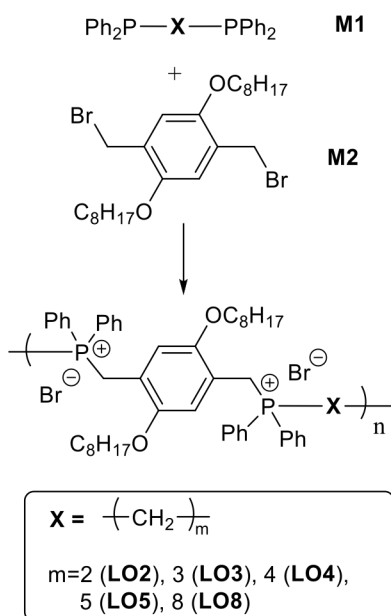
3.2.10 Synthesis of **LO5** (n = 5)

The synthesis of **LO5** involves same procedures as discussed for **LO2**. The monomers were 2,5-bis(bromomethyl)-1,4-bis(octyloxy)benzene (234 mg, 0.450 mmol) and 1,5-bis(diphenylphosphino)pentane (220 mg, 0.500 mmol). The product was a white powder (302 mg, 69.9%). 1H NMR (300 MHz, $CDCl_3$) δ : 8.30-7.38 (br m, 20H), 7.10-6.30 (br m, 2H), 5.40-4.52 (br m, 4H), 4.45-2.10 (br m, 10H), 1.75-0.62 (br m, 34H); $^{31}P\{^1H\}$ NMR (121.4 MHz, $CDCl_3$) δ : 28.0-23.5 (main polymer peak) and 33.0 (end groups). Anal. Calcd. for monomer formula $C_{53}H_{72}Br_2P_2O_3$ (ignoring end groups): C, 65.03; H, 7.41; Found: C, 64.47; H, 7.36%.

3.2.11 Synthesis of **LO8** (n = 8)

The synthesis of **LO5** involves same procedures as discussed for **LO2**. The monomers were 2,5-bis(bromomethyl)-1,4-bis(octyloxy)benzene (234 mg, 0.450 mmol) and 1,8-bis(diphenylphosphino)octane (241 mg, 0.500 mmol). The product was a white powder (338 mg, 74.9%). 1H NMR (300 MHz, $CDCl_3$) δ : 8.70-7.30 (br m, 20H), 7.10-6.28 (br m, 2H), 5.45-4.60 (br m, 4H), 4.49-1.60 (br m, 16H), 1.55-0.70 (br m, 34H); $^{31}P\{^1H\}$ NMR (121.4 MHz, $CDCl_3$) δ : 28.2-25.2 (main polymer peak) and 33.3 (end groups). Anal. Calcd. for monomer formula $C_{56}H_{78}Br_2P_2O_3$ (ignoring end groups): C, 65.88; H, 7.70; Found: C, 65.83; H, 7.76%.

3.2.12 Synthesis of 1,4-bis(octyloxy)-2,5-xylenebis(triphenyl phosphonium bromide)(**M3**)



Scheme 3.1: Synthesis of **LO** polymers with different lengths of alkylene spacers ‘X’ between phosphonium centers.

Table 3.1: Molecular weights and degrees of polymerization for **LO**

Polymer	M_n (Da)	n
LO2	11 900	12
LO3	18 700	19
LO4	11 400	11
LO5	17 300	17
LO8	11 000	10

Triphenylphosphine (101 mg, 0.385 mmol) and 2,5-bis(bromomethyl)-1,4-bis(octyloxy)benzene (99 mg, 0.190 mmol) were placed in a round bottom flask with 10 mL toluene. The reaction was refluxed at 90 °C for 20 h. After cooling, toluene was removed under reduced pressure yielding a white solid. 20 mL of diethyl ether was added to the flask and it was refluxed for 0.5 h. The product was washed by 40 mL of diethyl ether and separated by vacuum filtration. A white powder was obtained after vacuum

drying for 48 h (74 mg, 37%). ^1H NMR (300 MHz, CDCl_3) δ : 0.75-0.99 (t, 6H), 1.00-1.45 (m, 24H), 2.80-3.12 (t, 4H), 5.26-5.40 (d, 4H, $^4J_{\text{HH}} = 12$ Hz), 6.75 (s, 2H), 7.57-7.77 (m, 30H). $^{31}\text{P}\{^1\text{H}\}$ NMR (121.4 MHz, CDCl_3) δ : 21.6.

3.3 Results and Discussion

3.3.1 Design and Synthesis

The aim of the current work was to assess the extent to which flexible hydrophobic side chains influence the properties of PELs, PEL films and PEL supramolecular assembly into layer-by-layer (LbL) films with polyanions. The series of PELs (**LO2-8**, Scheme 3.1) was selected for this study on the basis of several considerations. Firstly, octyloxy side chains are anticipated to increase the solubility of the polymers in organic solvent and thus to improve processability. Secondly, side chains are well known to lower the glass transition temperature and decrease crystallinity, and the interplay of these established trends with the influence of inter-cation spacer had not been examined for PELs. On the basis of prior studies on PELs,^{37,43} the improved solubility was also expected to lead to better film growth linearity for LbL self-assembly films and smoother/more uniform films. Finally, the **LO** backbone is identical to that of the **LX** polymer series, allowing direct comparison of data for the two series in the effort to derive more general structure-property correlations.

The synthesis of **LO** polymers was carried out as shown in Scheme 1. Monomer **M2** was readily prepared by the reported route,⁴⁶ and monomers **M1** were commercially available. Polymerization of **M1** with **M2** to yield **LO** polymers proceeded well under the same conditions that proved successful for **LX**, via reaction in DMF at 90 °C under N_2

for 15 h. As expected, the **LO** products were found to be much more soluble in organic solvents than the **LX** polymers, so the workup and isolation steps required precipitation and washing with diethyl ether several times followed by drying in a vacuum oven. The polymers were initially characterized by elemental analysis and ^1H and ^{31}P NMR spectrometry (all spectra are provided in the Appendix 3A). The molecular weights and degrees of polymerization are summarized in Table 3.1. The degrees of polymerization were determined from NMR end group analysis^{24,28,29,37,47} and range from 10 to 19, similar to those reported for **EGT1**,²⁸ **SLK1**,²⁹ and **LX**⁴³ polymers that were prepared by the same step-growth polymerization route.

3.3.2 Crystallinity and thermal properties

The presence of conformationally-flexible octyloxy side chains in **LO** polymers would be expected to make them considerably more amorphous than the analogous **LX** polymers. This anticipation was borne out by X-ray powder diffraction patterns (see Appendix 3C). In contrast to semicrystalline **LX** polymers, all of the **LO** polymers except **LO2** are amorphous. The proximity of charged sites in **LO2** maximizes the potential for cooperative Coulombic interaction with bromide counteranions and likely drives formation of some crystalline domains in **LO2**. The largest d -spacing of 15.49 Å observed in **LO2** is 3.96 Å greater than the largest d -spacing of 11.53 Å for **LX2**. The increase in interchain spacing in the crystalline regions of **LO2** versus that in **LX2** is attributable to the additional space required to accommodate the octyloxy side chains of **LO2**. A similar increase in d -spacing (4.19 Å) was reported when phenylene units were replaced with 2,5-dioctyloxyphenylene units in a poly(*p*-phenylene vinylene) oligomer.⁴⁸

It was also of interest to compare thermal stabilities of **LO** to the previously-reported **LX** and **R1** series (Chart 3.1). Data for the three series of PELs are summarized in Table 2. In contrast to the **LX** polymers, all of the **LO** polymers have about the same decomposition temperature (defined here as the temperature at which 5% weight loss occurs upon heating under nitrogen; TGA traces are provided in the Appendix 3C) at ~ 270 °C. This T_d is notably lower than those for **LX** and **R1** polymers and is consistent with decomposition via loss of the octyloxy groups. To further reinforce this supposition, we prepared small molecule model compound **M3** (Chart 3.3) and found that it has a T_d , 5% of 261 °C with loss of its octyloxy side chains.

DSC analyses (traces are provided in the Appendix 3C) reveal an inverse relationship between T_g and the length of the alkylene spacers (Table 3.2). As the spacer length increases from three to eight methylene units, chain flexibility increases with concomitantly lower T_g . A similarly predictable trend in T_g is noted in the **R1** series. Only

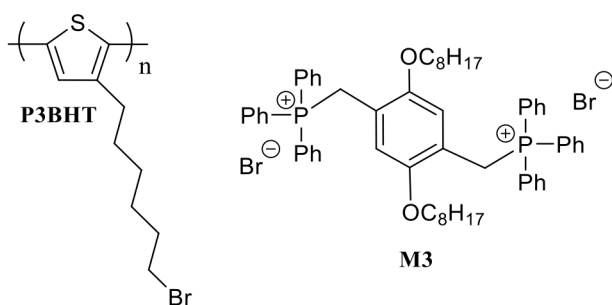


Chart 3.3: Structure of **P3BHT** and **M3**.

polymer **LO2** did not exhibit a glass transition between -150 and 200 °C. In the first heating, a record of irreversible thermal history, **LO2-8** were also found to exhibit segmental motion or an increase in free volume in a broad temperature range beginning

Table 3.2: Comparison of $T_{d,5\%}$ and T_g of **R1**, **LX** and **LO** polymers.

R1		LX		LO						
R1		LX		LO						
x, y	$T_{d,5\%}^a$ (°C)	T_g^a (°C)	m	$T_{d,5\%}^b$ (°C)	T_g^c (°C)	Largest d - spacing (Å)	n	$T_{d,5\%}^b$ (°C)	T_g^c (°C)	Largest d - spacing (Å)
2, 12	300	148	2	312	NA	11.53	2	271	NA	15.49
--	--	--	3	362	NA	7.26	3	277	137	NA
4, 4	339	172	4	364	NA	7.54	4	278	124	NA
6, 4	329	154	5	355	200.7	7.35	5	275	118	NA
6, 6	328	n.d.	8	356	NA	10.08	8	275	96	NA

^a Data from reference 44: TA DSC Q1000, 10 °C min⁻¹, TA TGA Q50, 10 °C min⁻¹.

^b TA TGA Q5000 20 °C min⁻¹. ^c TA DSC Q1000, 20 °C min⁻¹.

around 50 °C, analogous to the familiar alkyl side motion at ~ 56 °C observed, for example, in **P3BHT** (Chart 3.3).⁴⁹

3.3.3 Influence of Spacer, Solvent and Humidity on Thin Film Morphology

Although prior studies had reported on the properties of LbL-assembled films of **LX** and other PELs with polyanions, there have been no systematic studies on how structure might influence neat PEL film properties. Dip-cast films of **LO** or **LX** polymers were thus prepared for the current study. Initial visual analysis of AFM images revealed that some of the films featured pores of relatively uniform size, whereas other films were

smooth and essentially featureless (AFM images for 1×1 and 5×5 μm areas are provided in the Appendix 3D). Further investigation revealed that the number of pores per unit area, pore diameter and pore depth are all influenced by the absence or presence of water at various stages of film preparation and storage. Different effects were noted depending on whether the film was cast from a water-containing solvent, was exposed to ambient humidity as it dried, or was exposed to ambient humidity after the film had been previously dried in the absence of water. The AFM 2D-height images of **LO2** in $\text{CH}_3\text{CN}/\text{CHCl}_3$ (1:1) and CHCl_3 with different post-cast handling methods are provided in Figure 3.1, and film parameters are summarized in Table 3.3.

A film of **LO2** cast from water-free CHCl_3 and dried in a desiccator featured the greatest pore depth and diameter of all the films. The pores in these films had an average diameter of 223 ± 74 nm and average depth of 47 ± 8 nm, with 15 pores/ μm^2 . After aging this film in the presence of ambient humidity (approximately 25% relative humidity) for 18 d, the average pore diameter and depth had diminished to 214 ± 58 (not statistically significant) and 29 ± 6 nm, respectively, with 12 pores/ μm^2 . The decrease in pore depth can be attributed to swelling as water is absorbed into the polar polymer film. When a film of **LO2** was cast under the same conditions and allowed to dry in the presence of ambient humidity for only 8 d, the pore diameter and depth are both significantly smaller, at only 116 ± 21 and 12 ± 3 nm, respectively, leading to a decrease in total pore volume to 11% of that observed in the desiccator-dried film. The effect on films allowed to dry in the presence of humidity versus the effect on films dried in the absence of humidity can be explained by the greater mobility of polar segments, plasticized by water, leading to

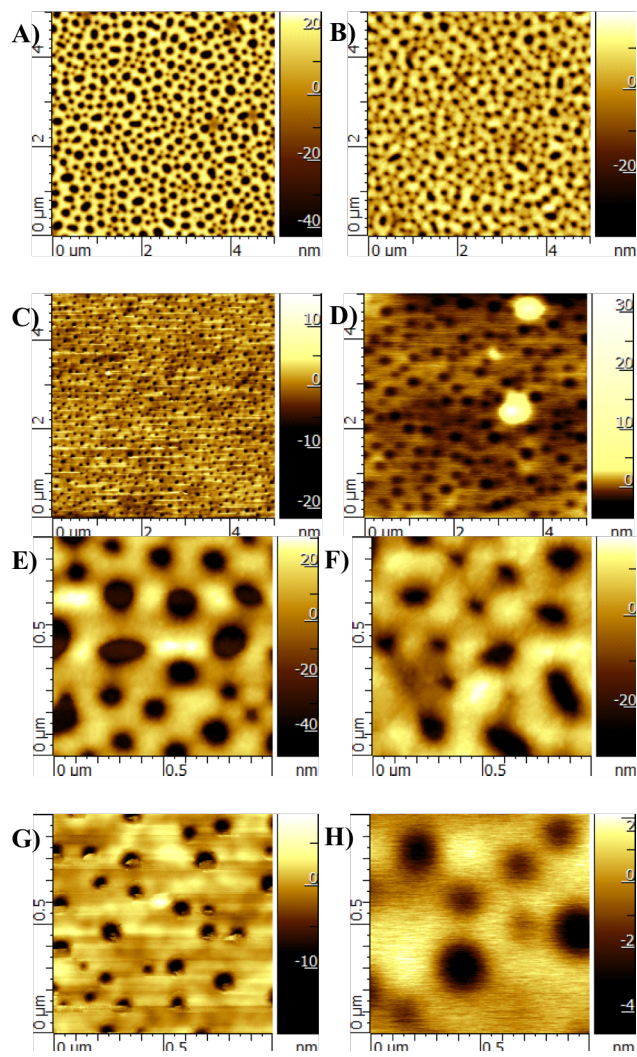


Figure 3.1: The distribution of pores as provided by AFM 2D-height images ($5 \times 5 \mu\text{m}$) of **LO2** films cast from CHCl_3 , dried in a desiccator (A) and later stored in ambient conditions for 18 d (B); cast from CHCl_3 and dried in ambient conditions (C), and cast from $\text{CHCl}_3/\text{CH}_3\text{CN}$ (1:1) then dried in a desiccator (D). A closer view ($1 \times 1 \mu\text{m}$ images) reveals the relative size of pores of **LO2** films cast from CHCl_3 and dried in a desiccator (E) and later stored in ambient conditions for 18 d (F); cast from CHCl_3 and dried in ambient conditions (G), and cast from $\text{CHCl}_3/\text{CH}_3\text{CN}$ (1:1) then dried in a desiccator (H).

water from the air, and phosphonium-containing polymers have even been incorporated as active films in humidity sensors.⁵⁰⁻⁵²

The length of backbone alkylene spacer also influences pore dimensions and frequency. For films cast from CHCl_3 and dried in ambient humidity, pores are observed for **LO2-4** but not for **LO5** and **LO8**. The pore diameter and depth decrease as the length of the spacer increases from **LO2** to **LO4**. Specifically, the pore diameter decreased from 116 ± 21 for **LO2** to 80 ± 14 nm for **LO4**, and pore depth diminished from 12 ± 3 for **LO2** to 3 ± 1 nm for **LO4**, leading to over two orders of magnitude drop in total pore volume.

The propensity of polymers having both hydrophobic and hydrophilic domains to form dimples/holes/pores is well-known and has been attributed to nanoscale phase separation of polar and nonpolar domains of the polymers due to their differential solubility in the casting solvents.^{53,54} Some polycations that show behavior similar to that exhibited by **LO** polymers are poly(methyl methacrylate) or poly(styrene) modified with K^+ -complexed dibenzo-18-crown-6 moieties.⁵⁵ AFM analysis of films of these polycations revealed pores of about 300 nm in diameter with a depth of about 50 nm, on the same order of magnitude as those observed for **LO** polycations. The more polar and more rigid crown ether-modified polycations also showed greater propensity to form pores than did more flexible analogues, again in line with the trend observed for the **LO** series. The diminished chain mobility and thus lower solubility of ionic segments in the more rigid polymers leads to formation of homogeneous domains. This process is thought to arise from diminishing entropy concomitant with solvent evaporation until complete

surface coverage is no longer energetically favored, resulting in formation of the pores.^{53,54,56}

The influence of humidity on pore size in polymers having both hydrophilic (here phosphonium) and hydrophobic moieties (here methylene spacer chains and octyloxy side chains) is also a well-known phenomenon. A recent example is provided by the borinic acid-derivatized block copolymers reported by the Jakle group.⁵⁷ When these polymers are cast from THF with small amounts of water present (up to 3% by volume),

Table 3.3: Influence of humidity and solvent polarity on pores observed in dip-cast films of **LO** polymers.

Polymer (casting solvent)	Post-cast handling	Pore Diameter (nm)	Pore Depth (nm)	Pores per μm^2	Total Pore volume ($\times 10^5 \text{ nm}^3$)
LO2 (CHCl_3)	Desiccator	223 \pm 74	47 \pm 8	15	280
LO2 (CHCl_3)	Desiccator then 18 d ambient	214 \pm 58	29 \pm 6	12	120
LO2 (CHCl_3)	Ambient (8 d)	116 \pm 21	12 \pm 3	23	29
LO3 (CHCl_3)	Ambient (8 d)	99 \pm 19	6 \pm 1	14	6.5
LO4 (CHCl_3)	Ambient (8 d)	80 \pm 14	3 \pm 1	16	2.4
LO5 (CHCl_3)	Ambient (8 d)	NA	NA	NA	0
LO8 (CHCl_3)	Ambient (8 d)	NA	NA	NA	0
LO2 (1:1 $\text{CH}_3\text{CN}/\text{CHCl}_3$)	desiccator	279 \pm 77	4 \pm 2	6	44
LO2 (2:1 CH_3CN $/\text{CHCl}_3$)	desiccator	NA	NA	NA	0

the pore size increased as the amount of water increased. This observation was attributed to the formation of water droplets as the more volatile THF evaporated more quickly in the course of film formation. In the current case, we observe the opposite trend, pore size decreasing with increased water exposure or water in casting solvent, and we attribute concomitantly shrinking pore size to a simple effect of polymer swelling and variable ratio of hydrophobic to hydrophilic domain sizes. None of the films cast from solvents containing water ($\text{CH}_3\text{CN}/\text{H}_2\text{O}$, up to 4:1) exhibited pores. These included all of the **LX** films, because **LX** polymers are only soluble in very polar solvent mixtures and the 4:1 $\text{CH}_3\text{CN}/\text{H}_2\text{O}$ was the only suitable solvent found for all members of both **LX** and **LO** series to allow direct comparison.

LO2 was selected for further investigation into the influence of environmental and solvent effects on pore formation/dimensions. Having already shown that the presence of water in the casting solvent suppresses pore formation, water-free $\text{CH}_3\text{CN}/\text{CHCl}_3$ (1:1 and 2:1) were used as casting solvents to assess whether water is required specifically to prevent pore formation or if simply increasing the polarity of the solvents would induce a similar effect.

The film of **LO2** cast from the more polar 1:1 $\text{CH}_3\text{CN}/\text{CHCl}_3$ (1:1) featured many fewer pores than did the film cast from CHCl_3 , only 6 pores per μm^2 . The pores that form were similar in diameter (279 ± 77 nm) but far more shallow (4 ± 2 nm) than those in the film cast from CHCl_3 . Increasing the polarity of the casting solvent even further to the $\text{CH}_3\text{CN}/\text{CHCl}_3$ (2:1) system effectively suppressed pore formation as was the case for films cast from $\text{CH}_3\text{CN}/\text{H}_2\text{O}$ (4:1). In the current case, the influence of solvent on pore

formation/dimensions seems to be related to the ability of the casting solvent to effectively solubilize both the very polar phosphonium salt moieties and the very nonpolar alkyl side chains of the polymers. When the solvent system is chosen to effectively dissolve both components, smooth films result. If a solvent is chosen that effectively solubilizes only the nonpolar alkyl chains, for example chloroform in which even small molecule phosphonium salts lacking alkyl side chains are poorly soluble, then polymers will form pores as the phosphonium moieties are pushed into the pores.

The influence of casting solvent on pore formation/size also clearly affects the root-mean-square roughness (R_{rms}) for the thin films (Figure 3.2). When cast from CHCl_3 , **LO3** has a higher R_{rms} (~12 nm) while the R_{rms} values for the other films are below 6 nm. Large bumps on the surface of **LO3** lead to increasing roughness, similar to what was observed previously in **LX** films previously. The R_{rms} values for **LO2**, **LO3** and **LO4** films cast from $\text{CHCl}_3/\text{CH}_3\text{CN}$ (1:1) are around 2 nm, increasing significantly for **LO5** and **LO8** in which longer hydrophobic chains between phosphonium sites lead to larger features of aggregated chains. In contrast, films of all the **LO** series have R_{rms} around 6 nm when films are cast from $\text{CH}_3\text{CN}/\text{H}_2\text{O}$ (4:1), a solvent that adequately solubilizes both the hydrophobic and hydrophilic domains.

3.3.3 Critical Surface Energy of Dip-Cast Films

In a previous study, the critical surface energy (γ_c) of tetraarylphosphonium polyelectrolytes (**FL1-3**, Chart 3.1) was reported to range from 58.2-72.8 mJ/m^2 .²⁴ This range extends to the γ_c of PEDOT:PSS (70 mJ/m^2),⁵⁸ a polymer mixture that finds broad utility in organic optoelectronic devices. Given the importance of interface effects in

organic electronic devices, the influence of backbone and side chain structure on γ_c was investigated for the **LX** and **LO** polymers. Critical surface energy is readily estimated by

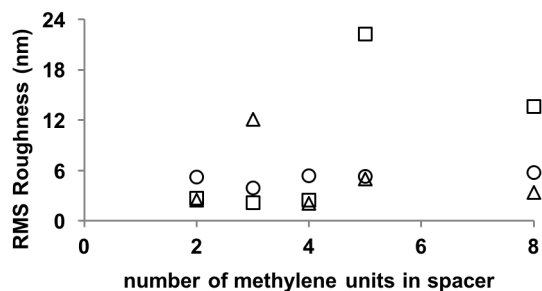


Figure 3.2. Root mean squared roughness of **LO** films cast from CHCl_3 (triangle), $\text{CHCl}_3/\text{CH}_3\text{CN}$ (1:1) (square) and $\text{CH}_3\text{CN}/\text{H}_2\text{O}$ (4:1) (circle) as measured over a $5 \times 5 \mu\text{m}$ area.

Table 3.4: Critical surface energies and contact angles with water.

Polymer	Dry film		After 7 days in ambient humidity
	$\theta_{c,w}$ (°)	γ_c (mJ/m ²)	γ_c (mJ/m ²)
LO2	46.6	38.2	39.5
LO3	47.8	38.0	38.4
LO4	44.4	37.7	39.4
LO5	40.1	35.5	38.1
LO8	41.7	35.0	38.9
LX2	9.0	73.6	ND
LX3	17.4	72.9	ND
LX4	9.4	73.3	ND
LX5	11.7	72.8	ND
LX8	19.7	71.8	ND

measuring contact angles (θ_c) for a series of test liquids and analysing them via the Zisman plot method (Zisman plots provided in the Appendix 3D).⁵⁹ The γ_c and the contact angles between water and dip-cast films ($\theta_{c,w}$) of **LO2-8** and **LX2-8** are provided in Table 3.4.

Each of the γ_c values in Table 3.4 represents the average of at least four individual measurements (each of which is itself an average of 5 drops per test liquid) that yielded results with a standard deviation of not more than 0.04 in $\cos(\theta_c)$. Initially, films were rigorously excluded from exposure to humidity so that absorption of humidity from the air (*vide supra*) would not influence the measurements. The γ_c values for films of the very polar **LX** polymers (72.0-73.6 mJ/m²) are in a range similar to PEDOT:PSS and **FL1-3**. Not surprisingly, the presence of hydrophobic side chains in the **LO** polymers led to significantly lower γ_c values (35.0-38.2 mJ/m²). As a point of comparison, the γ_c values for **LO** polymers, despite their ionic main chains, are in the range of common polymers such as polystyrene ($\gamma_c = 34$ mJ/m²),⁶⁰ poly(methyl methacrylate) ($\gamma_c = 37.5$ mJ/m²)⁶¹ and polyethylene terephthalate ($\gamma_c = 39$ mJ/m²).⁶² The γ_c values for **LX** films are relatively uniform across the series, with no clear dependence on the nature of the spacer between the phosphonium units. The γ_c values for the **LO** polymer films show a small but statistically significant decrease in γ_c as the length of the spacer between phosphonium sites increases. This would be expected as the hydrophobic segment increases, and a similar relationship between γ_c and length of alkylene spacer is noted for polyamides such as nylon 6 ($\gamma_c = 43.9$ mJ/m²)⁶³ versus nylon 12 ($\gamma_c = 37.1$ mJ/m²).⁶⁴

The aforementioned humidity-induced swelling of pores in **LO** films observed by AFM led us to examine the influence on γ_c after exposing films to ambient humidity. If films absorb water from the atmosphere, the γ_c would be expected to increase from smaller contact angles due to pre-wetting. As anticipated, large increases in γ_c of up to 4.9 mJ/m^2 were observed. The difference is greater than what was exerted by the change in spacer length from two to eight methylene units across the series. The observations herein regarding the marked influence of humidity on morphology and critical surface energy of PEL films should serve as a cautionary note regarding the importance of film preparation and handling prior to measurements, especially for polar and ionic materials.

3.3.4 Layer-by-layer assembly of **LO** polymers with polyelectrolytes

The LbL assembly of **LO** polymers with **Pc12-100** following the same procedure used for the **LX** polymers⁴³ was undertaken to assess the influence of spacer on the LbL process and films. Film growth was monitored by UV-vis spectroscopy, and Figure 3.3 provides absorbance for 50-bilayer films made by LbL assembly of **LO** and **LX** polymers with **Pc12-100**. In contrast to the trends observed for LbL deposition of **LX** polymers, the linearity of film growth, amount of material deposited and the roughness of films were all independent of the spacer length when **LO** polymers were employed (plots of film growth versus bilayer number are provided in the Appendix 3C). This observation may suggest that octyloxy side chains counteract the difference of absorbance between odd and even number of methylene units in spacers of **LO** during LbL assembly with **Pc12-100**.

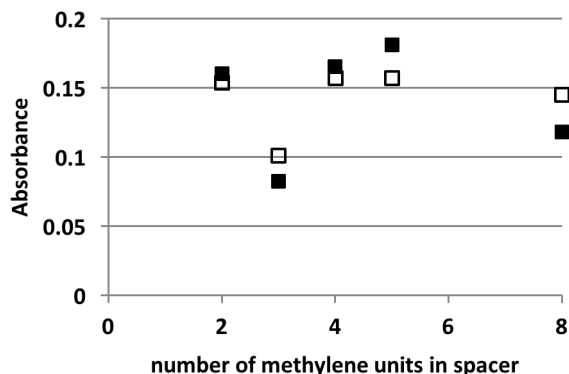


Figure 3.3: UV-vis absorbance measurements of **Pc12-100** accumulation in LbL-assembled films with **LO** (white) or **LX** (black) at 50 bilayers.

The plot of absorbance versus the number of methylene units between the phosphonium sites for each LbL film (Figure 3.3) reveals relatively uniform absorbance for films comprised of 50 bilayers with the exception of the polymer with three methylene units in its spacer for both **LX** and **LO** series. It was hypothesized that this behavior might be related to two influencing factors: 1) thermally-accessible polymer backbone conformation and 2) the extent to which the interior spacing (d_{PP}) of the PEL matches that of the **Pc12-100** (d_{OO}).

As a result of the sterically-encumbered BnPh_2P -substituent flanking each side of the ethylene spacer in **LO2/LX2**, one would expect the conformation about this spacer to be confined to a narrow range about the energy minimum of the *anti*-conformation about the *C1-C2* bond (Figure 3.4A). In this conformation, the two phosphonium units are pointed in opposing directions about the linker. In contrast, the odd number of methylene units between phosphonium sites in **LO3/LX3** should lead to a lowest-energy conformation in which the two phosphonium units are directed in the same direction off

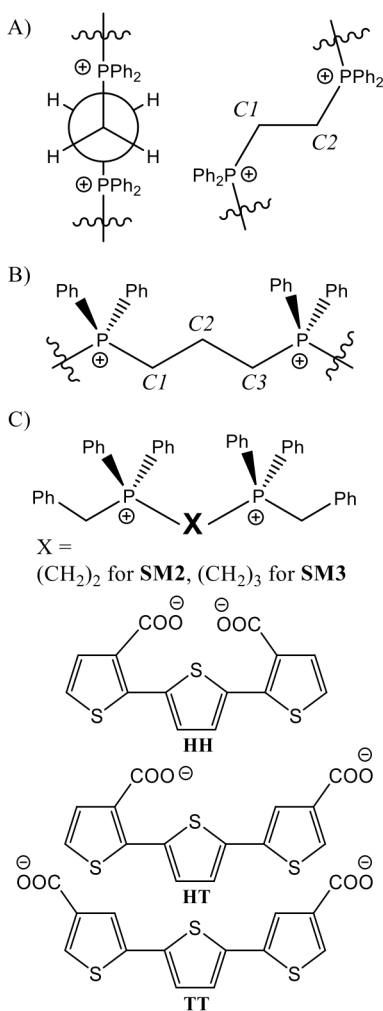


Figure 3.4: Newman projection (left) and line-bond view of a segment of **LX2** or **LO2** (A) and a segment of **LX3** or **LO3** (B) demonstrate expected conformations. Structures for model compounds SM2, SM3, HH, HT and TT used in semi-empirical calculations are provided in (C).

of the backbone resulting from *anti*-conformations about both *C1-C2* and *C2-C3* bonds (Figure 3.4B). Semi-empirical calculations at the AM1 level support the lowest-energy conformations as expected for small molecular models $\text{BnPh}_2\text{P-C}_2\text{H}_4\text{-PPh}_2\text{Bn}$ (**SM2**, a

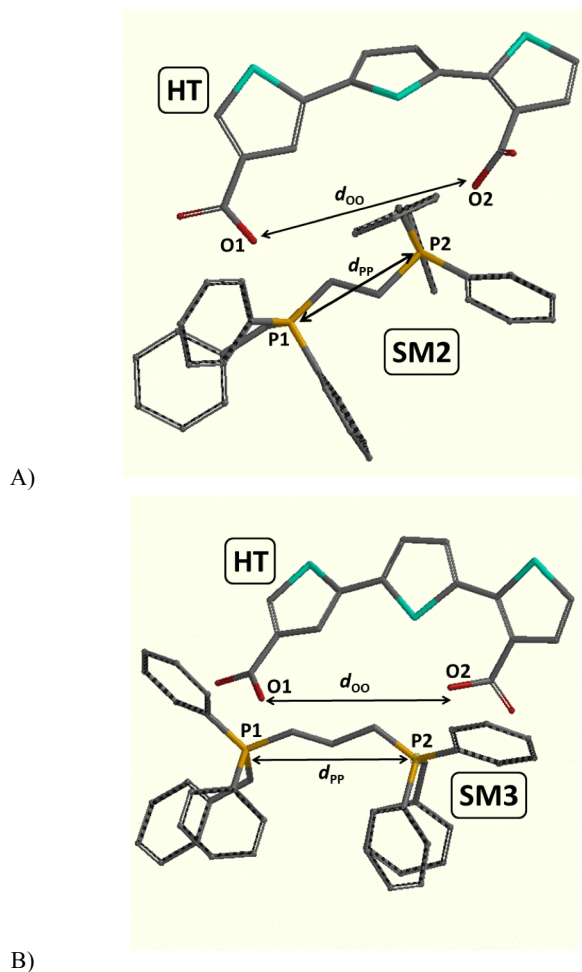


Figure 3.5: Optimized geometries obtained from semi-empirical calculations at the AM1 level: SM2 with HT (A) and SM3 with HT (B).

model for **LO2/LX2**) and $\text{BnPh}_2\text{P}-\text{C}_3\text{H}_6-\text{PPh}_2\text{Bn}$ (**SM3**, a model for **LO2/LX2**, Figure 3.4C).

In order to better understand the extent to which the spacer length might influence the accessibility of anion-cation matching between **LO/LX** and **Pc12-100**, the structure of **Pc12-100** must also be considered in more detail. There are three structural subunits in **Pc12-100** that are possible on the basis of the synthetic route used to prepare the polymer.

These subunits result from either head-to-head (leading to subunit **HH**), head-to-tail (leading to subunit **HT**, the one most prevalent) or tail-to-tail (leading to subunit **TT**) coupling of the monomers, and lead to three different possible anion-anion distances along the backbone (Figure 3.4C). Semi-empirical (AM1) calculations were undertaken to assess the interaction of **SM2** and **SM3** with models for each of the possible structural subunits **HT** and **TT**. **SM2** and **SM3** were initially placed in their energy-minimized geometries in the vicinity of the requisite oligothiophene, but no constraints were applied for calculations of the interactions. Representative optimized geometries are provided in Figure 3.5 and the values for d_{PP} , d_{OO} and the difference between these interanion spacings (Δ_{OP}) are summarized in Table 3.5.

From the data in Table 3.5, it is clear that there is a considerably better match of d_{PP} to d_{OO} for **SM3** than for **SM2** and the oligothiophene carboxylates in the calculated geometries. Since the **HT** geometry predominates in **Pc12-100**, the interaction between **HT** and the phosphonium models provide the best approximation for most of the sites in the LbL films. The geometries for **SM2/HT** (Figure 3.5A) and **SM3/HT** (Figure 3.5B) emphasize the improved interaction possible for **SM3**. In **SM2/HT**, not only is there a poor match in distances but there is also apparent steric deflection between *O2* and one of the phenyl groups on *P2* that leads to a deflection of the carboxylate away from the phosphonium site in **SM2**, leading to a longer d_{OO} of 6.369 Å in **SM2/HT** versus that of 5.880 Å in **SM3/HT**.

Taken together, the absorption data and calculated interactions suggest that the optimal anion-cation spacing between **Pc12-100** (approximated by **HT**) and **LX3/LO3**

(approximated by **SM3**) results in maximum intrinsic ion pairing and thus requires a smaller amount of **Pc12-100** to achieve charge balance in the LbL films. Polymer rigidity and mismatched inter-ion distance along polymer backbones has also been observed to influence self-assembly and coacervate formation of, for example, chitosan (persistence length = 6.5 nm and inter-ion distance ~0.6 nm) with hyaluronic acid (persistence length = 4.0 nm and inter-ion distance ~1.3 nm) in which charges are twice as far apart.⁶⁵⁻⁶⁷ When charge matching is not possible due to this mismatch in inter-ion spacing, extrinsic sites occupied by non-polyelectrolyte-bound counterions are necessarily present so that one polymer is present in excess on a molar basis.^{68,69} The findings in the current study emphasize the potential to co-deposit rigid polyelectrolytes with variable interion distances as an additional avenue to control the polycation:polyanion ratio in LbL-assembled films.

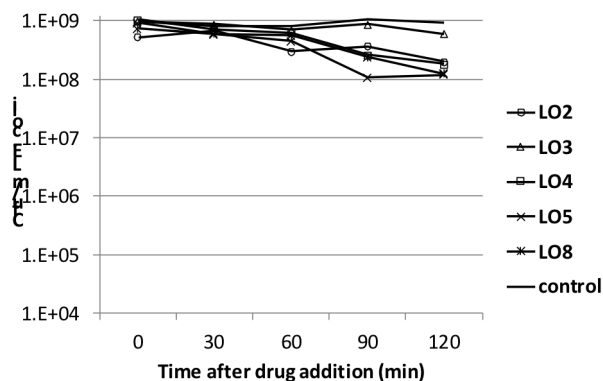
Table 3.5: Distances in optimized geometry from semi-empirical calculations at the AM1 level.

Pairing	Distances (Å)		
	d_{PP}	d_{OO}	Δ_{OP}
SM2/HH	4.111	5.828	1.717
SM2/HT	4.151	6.369	2.218
SM2/TT	4.149	6.485	2.336
SM3/HH	5.224	6.094	0.870
SM3/HT	5.248	5.880	0.632
SM3/TT	5.056	6.727	1.671

3.3.5 Antimicrobial Properties

Ammonium and phosphonium salts are well-established antimicrobial agents, and phosphonium polymers specifically were studied in some detail as agents against both Gram-positive and Gram-negative bacteria.⁷⁰⁻⁷⁹ The proposed mechanism of bacterial death is one in which the polycation aggregates around the negatively-charged bacterial cell envelope concomitant with penetration of hydrophobic polymer backbone or side chain components into the cell wall, whereby phospholipid packing is disrupted, leading to membrane failure and cell death. In the current work, **LO2**, **LO3**, **LO4**, **LO5**, **LO8**,

A)



B)

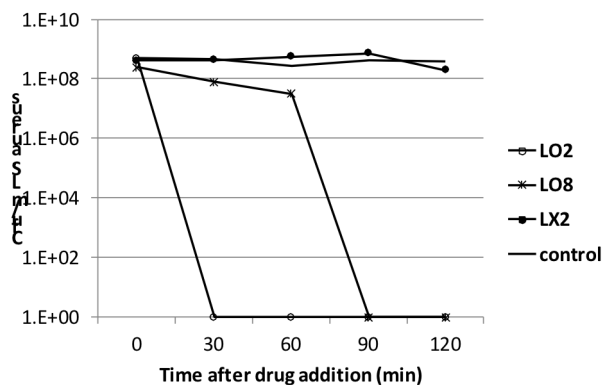


Figure 3.6: Plots of $\log(\text{survivors})$ versus exposure time for **LO** and **LX** polymers against *E. coli* (A) and *S. aureus* (B).

and **LX2** were tested against *Staphylococcus aureus* and *Escherichia coli* via a dilution plating assay (data are summarized in Figure 3.6). None of the polymers screened showed high potency against Gram-negative *E. coli* (Figure 3.6A). This observation is similar to the earlier studies and consistent with the membrane-disruption mechanism because Gram-negative bacteria like *E. coli* have more complex membrane structures that resist penetration more than do those of Gram-positive bacteria. The **LO** polymers were more effective against *S. aureus* than was **LX2**, attributable to involvement of the hydrophobic octyloxy sidechains in **LO** polymers, absent in **LX2**, with bacterial cell walls. **LO2** showed the highest and **LO8** the lowest antimicrobial ability against *S. aureus* of all polymers tested. These data suggest that the greater density of cationic sites in **LO2** is more influential than is the presence of the additional hydrophobicity endowed by the (CH₂)₈ backbone of **LO8**. The failure of **LX2** against *S. aureus*, however, still confirms that while high cation density is required, it is not a sufficient structural motif for high antimicrobial activity.

3.4 Conclusions

Nonpolar side chains reduce the thermal stability, crystallinity and glass transition temperatures of phosphonium polyelectrolytes. The presence of both ionic groups and hydrophobic segments/sidechains can facilitate domain segregation, which in turn drive film morphology and critical surface energy. The amount of material deposited in each layer of LbL self-assembled films of the phosphonium polymers with anionic polyelectrolytes was found to depend not only on flexibility of the backbone, but also on the inter-ion distance match between polyelectrolytes. The

antimicrobial activity of the phosphonium polymers can also be related to structure, with hydrophobic sidechains and high cation density improving activity. Future work will build on the structure-property relationships elucidated by this work in an effort to rationally control surface morphologies, critical surface energies and self-assembly processes involving phosphonium polyelectrolytes.

3.5 References

1. H. Jiang, P. Taranekar, J. R. Reynolds, K. S. Schanze. *Angew. Chem.-Int. Edit.* **2009**, *48*, 4300-4316.
2. S. J. Dwight, B. S. Gaylord, J. W. Hong, G. C. Bazan. *J. Am. Chem. Soc.* **2004**, *126*, 16850-16859.
3. C. H. Fan, K. W. Plaxco, A. J. Heeger. *J. Am. Chem. Soc.* **2002**, *124*, 5642-5643.
4. I. B. Kim, U. H. F. Bunz. *J. Am. Chem. Soc.* **2006**, *128*, 2818-2819.
5. K. Lee, L. K. Povlich, J. Kim. *Adv. Funct. Mater.* **2007**, *17*, 2580-2587.
6. F. D. Feng, F. He, L. L. An, S. Wang, Y. H. Li, D. B. Zhu. *Adv. Mater.* **2008**, *20*, 2959-2964.
7. Y. Liu, K. Ogawa, K. S. Schanze. *J. Photochem. Photobiol. C-Photochem. Rev.* **2009**, *10*, 173-190.
8. F. Xia, X. L. Zuo, R. Q. Yang, Y. Xiao, D. Kang, A. Vallee-Belisle, X. Gong, J. D. Yuen, B. B. Y. Hsu, A. J. Heeger, K. W. Plaxco. *Proceedings of the National Academy of Sciences of the United States of America* **2010**, *107*, 10837-10841.
9. C. V. Hoven, A. Garcia, G. C. Bazan, T. Q. Nguyen. *Adv. Mater.* **2008**, *20*, 3793-3810.
10. A. Duarte, K. Y. Pu, B. Liu, G. C. Bazan. *Chem. Mater.* **2011**, *23*, 501-515.

11. X. Zhang, F. Shi, X. Yu, H. Liu, Y. Fu, Z. Q. Wang, L. Jiang, X. Y. Li. *J. Am. Chem. Soc.* **2004**, *126*, 3064-3065.
12. M. Hamed, A. Herland, R. H. Karlsson, O. Inganäs. *Nano Letters* **2008**, *8*, 1736-1740.
13. J. L. Lutkenhaus, P. T. Hammond. *Soft Matter* **2007**, *3*, 804-816.
14. T. J. Clark, N. J. Robertson, H. A. Kostalik, E. B. Lobkovsky, P. F. Mutolo, H. D. Abruna, G. W. Coates. *J. Am. Chem. Soc.* **2009**, *131*, 12888-+.
15. V. Sambhy, B. R. Peterson, A. Sen. *Angew Chem Int Edit* **2008**, *47*, 1250-1254.
16. D. Izuhara, T. M. Swager. *J. Am. Chem. Soc.* **2009**, *131*, 17724-17725.
17. X. Chen, S. Kang, M. J. Kim, J. Kim, Y. S. Kim, H. Kim, B. Chi, S. J. Kim, J. Y. Lee, J. Yoon. *Angew Chem Int Edit* **2010**, *49*, 1422-1425.
18. D. W. Kim, D. Y. Chi. *Angew Chem Int Edit* **2004**, *43*, 483-485.
19. J. H. Wang, S. H. Li, S. B. Zhang. *Macromolecules* **2010**, *43*, 3890-3896.
20. K. J. T. Noonan, K. M. Hugar, H. A. Kostalik, E. B. Lobkovsky, H. D. Abruna, G. W. Coates. *J. Am. Chem. Soc.* **2012**, *134*, 18161-18164.
21. T. J. Peckham, A. J. Lough, I. Manners. *Organometallics* **1999**, *18*, 1030-1040.
22. C. G. Cassity, A. Mirjafari, N. Mobarrez, K. J. Strickland, R. A. O'Brien, J. H. Davis. *Chem. Commun. (Cambridge, U. K.)* **2013**, *49*, 7590-7592.
23. S. Gu, R. Cai, T. Luo, Z. Chen, M. Sun, Y. Liu, G. He, Y. Yan. *Angew. Chem.-Int. Edit.* **2009**, *48*, 6499-6502.

24. M. S. Bedford, X. Yang, K. M. Jolly, R. L. Binnicker, S. B. Cramer, C. E. Keen, C. J. Mairena, A. P. Patel, M. T. Rivenbark, Y. Galabura, I. Luzinov, R. C. Smith. *Polym. Chem.* **2015**, *6*, 900-908.
25. A. Kanazawa, T. Ikeda, T. Endo. *J. Polym. Sci., Part A: Polym. Chem.* **1993**, *31*, 335-343.
26. C. Ornelas-Megiatto, P. R. Wich, J. M. J. Frechet. *J. Am. Chem. Soc.* **2012**, *134*, 1902-1905.
27. S. Durben, Y. Dienes, T. Baumgartner. *Org. Lett* **2006**, *8*, 5893-5896.
28. E. G. Tennyson, S. He, N. C. Osti, D. Perahia, R. C. Smith. *J. Mater. Chem.* **2010**, *20*, 7984-7989.
29. S. L. Kristufek, T. R. Maltais, E. G. Tennyson, N. C. Osti, D. Perahia, A. G. Tennyson, R. C. Smith. *Polym. Chem.* **2013**, *4*, 5387-5394.
30. C. J. Chua, Y. Ren, M. Stolar, S. Xing, T. Linder, T. Baumgartner. *Eur. J. Inorg. Chem.* **2014**, *2014*, 1767-1774.
31. A. S. Ionkin, B. M. Fish, Z. R. Li, L. Liang, M. E. Lewittes, L. K. Cheng, C. Westphal, J. G. Pepin, F. Gao. *Solar Energy Materials and Solar Cells* **2014**, *124*, 39-47.
32. J. A. Jaber, J. B. Schlenoff. *Curr. Opin. Colloid Interface Sci.* **2006**, *11*, 324-329.
33. P. Schaaf, J. B. Schlenoff. *Langmuir* **2009**, *25*, 14007-14010.
34. G. Decher. *Science* **1997**, *277*, 1232-1237.
35. M. Cui, W. S. Ng, X. Wang, P. Darmawan, P. S. Lee. *Adv. Funct. Mater.* **2015**, *25*, 401-408.

36. H. L. Li, S. P. Pang, S. Wu, X. L. Feng, K. Mullen, C. Bubeck. *J. Am. Chem. Soc.* **2011**, *133*, 9423-9429.
37. C. A. Conrad, M. S. Bedford, A. A. Buel, Y. Galabura, I. Luzinov, R. C. Smith. *Polym. Int* **2015**, *64*, 1381-1388.
38. C. F. Buitrago, K. L. Opper, K. B. Wagener, K. I. Winey. *ACS Macro Lett.* **2012**, *1*, 71-74.
39. B. S. Aitken, C. F. Buitrago, J. D. Heffley, M. Lee, H. W. Gibson, K. I. Winey, K. B. Wagener. *Macromolecules* **2012**, *45*, 681-687.
40. T. W. Baughman, C. D. Chan, K. I. Winey, K. B. Wagener. *Macromolecules* **2007**, *40*, 6564-6571.
41. C. F. Buitrago, T. M. Alam, K. L. Opper, B. S. Aitken, K. B. Wagener, K. I. Winey. *Macromolecules* **2013**, *46*, 8995-9002.
42. C. F. Buitrago, J. E. Jenkins, K. L. Opper, B. S. Aitken, K. B. Wagener, T. M. Alam, K. I. Winey. *Macromolecules* **2013**, *46*, 9003-9012.
43. X. Yang, C. A. Conrad, W. Wan, M. S. Bedford, L. Hu, G. Chumanov, R. C. Smith. *J. Mater. Chem. C* **2015**, *3*, 4537-4544.
44. S. T. Hemp, M. S. Zhang, M. Tamami, T. E. Long. *Polym. Chem.* **2013**, *4*, 3582-3590.
45. I. Horcas, R. Fernandez, J. M. Gomez-Rodriguez, J. Colchero, J. Gomez-Herrero, A. M. Baro. *Review of Scientific Instruments* **2007**, *78*.
46. M. Goel, K. Narasimha, M. Jayakannan. *Journal of Physical Chemistry B* **2015**, *119*, 5102-5112.

47. M. Hadadpour, J. Gwyther, I. Manners, P. J. Ragona. *Chem. Mat.* **2015**, *27*, 3430-3440.
48. R. E. Gill, A. Meetsma, G. Hadziioannou. *Adv. Mater* **1996**, *8*, 212-214.
49. D. A. Rider, B. J. Worfolk, K. D. Harris, A. Lalany, K. Shahbazi, M. D. Fleischauer, M. J. Brett, J. M. Buriak. *Adv. Funct. Mater.* **2010**, *20*, 2404-2415.
50. C.-W. Lee, O. Kim, M.-S. Gong. *J. Appl. Polym. Sci.* **2003**, *89*, 1062-1070.
51. C.-W. Lee, M.-s. Gong. *Macromol. Res.* **2003**, *11*, 322-327.
52. C.-W. Lee, H.-W. Rhee, M.-S. Gong. *Synt. Met.* **1999**, *106*, 177-182.
53. H. Elbs, K. Fukunaga, R. Stadler, G. Sauer, R. Magerle, G. Krausch. *Macromolecules* **1999**, *32*, 1204-1211.
54. S. Walheim, M. Böltau, J. Mlynek, G. Krausch, U. Steiner. *Macromolecules* **1997**, *30*, 4995-5003.
55. X. S. Feng, L. F. Yan, J. Wen, C. Y. Pan. *Polymer* **2002**, *43*, 3131-3137.
56. J. P. Gao, P. Zhang, J. Fu, B. Y. Li, Y. C. Han, X. Yu, C. Y. Pan. *Polymer* **2007**, *48*, 2425-2433.
57. F. Cheng, W. M. Wan, Y. Zhou, X. L. Sun, E. M. Bonder, F. Jakle. *Polym. Chem.* **2015**, *6*, 4650-4656.
58. M. Petrosino, A. Rubino. *Synt. Met.* **2011**, *161*, 2714-2717.
59. W. A. Zisman. *Industrial and Engineering Chemistry* **1963**, *55*, 18-38.
60. T. P. Yin, S. Wu. *J. Polym. Sci., Part C: Polym. Symp.* **1971**, *No. 34*, 265-271.
61. C. J. Van Oss, R. J. Good, M. K. Chaudhury. *J. Colloid Interface Sci.* **1986**, *111*, 378-390.

62. C. J. Van Oss, M. K. Chaudhury, R. J. Good. *Sep. Sci. Technol.* **1989**, *24*, 15-30.
63. E. J. McNally, In Contact Angle, Wettability and Adhesion; Mittal, K. L., Ed.:
Utrecht, The Netherlands, **1993**, pp 575-584.
64. H. W. Fox, W. A. Zisman. *J. Colloid Sci.* **1952**, *7*, 109-121.
65. Y. Liu, M. Kong, X. J. Cheng, Q. Q. Wang, L. M. Jiang, X. G. Chen. *Carbohydr. Polym.* **2013**, *94*, 309-316.
66. H.-D. Lu, H.-Q. Zhao, K. Wang, L.-L. Lv. *Int. J. Pharm.* **2011**, *420*, 358-365.
67. F. X. Liu, L. R. Liu, X. M. Li, Q. Q. Zhang. *J. Mater. Sci. Mater. Med.* **2007**, *18*,
2215-2224.
68. H. M. Fares, Y. E. Ghoussoub, R. L. Surmaitis, J. B. Schlenoff. *Langmuir* **2015**, *31*,
5787-5795.
69. H. W. Jomaa, J. B. Schlenoff. *Macromolecules* **2005**, *38*, 8473-8480.
70. A. Kanazawa, T. Ikeda, T. Endo. *J. Polym. Sci., A* **1993**, *31*, 3031-3038.
71. A. Kanazawa, T. Ikeda, T. Endo. *J. Polym. Sci., A* **1993**, *31*, 3003-3011.
72. A. Kanazawa, T. Ikeda, T. Endo. *J. Polym. Sci., A* **1993**, *31*, 1441-1447.
73. A. Kanazawa, T. Ikeda, T. Endo. *J. Polym. Sci., A* **1993**, *31*, 1467-1472.
74. A. Kanazawa, T. Ikeda, T. Endo. *J. Polym. Sci., A* **1993**, *31*, 335-343.
75. A. Kanazawa, T. Ikeda, T. Endo. *J. Appl. Polym. Sci* **1994**, *54*, 1305-1310.
76. A. Kanazawa, T. Ikeda, T. Endo. *J. Appl. Polym. Sci* **1994**, *53*, 1245-1249.
77. A. Kanazawa, T. Ikeda, T. Endo. *J. Appl. Polym. Sci* **1994**, *53*, 1237-1244.
78. A. Kanazawa, T. Ikeda, T. Endo. *J. Appl. Polym. Sci.* **1994**, *52*, 641-647.
79. A. Kanazawa, T. Ikeda, T. Endo. *J. Polym. Sci., A* **1994**, *32*, 1997-2001.

APPENDICES

Appendix 3A

NMR spectra

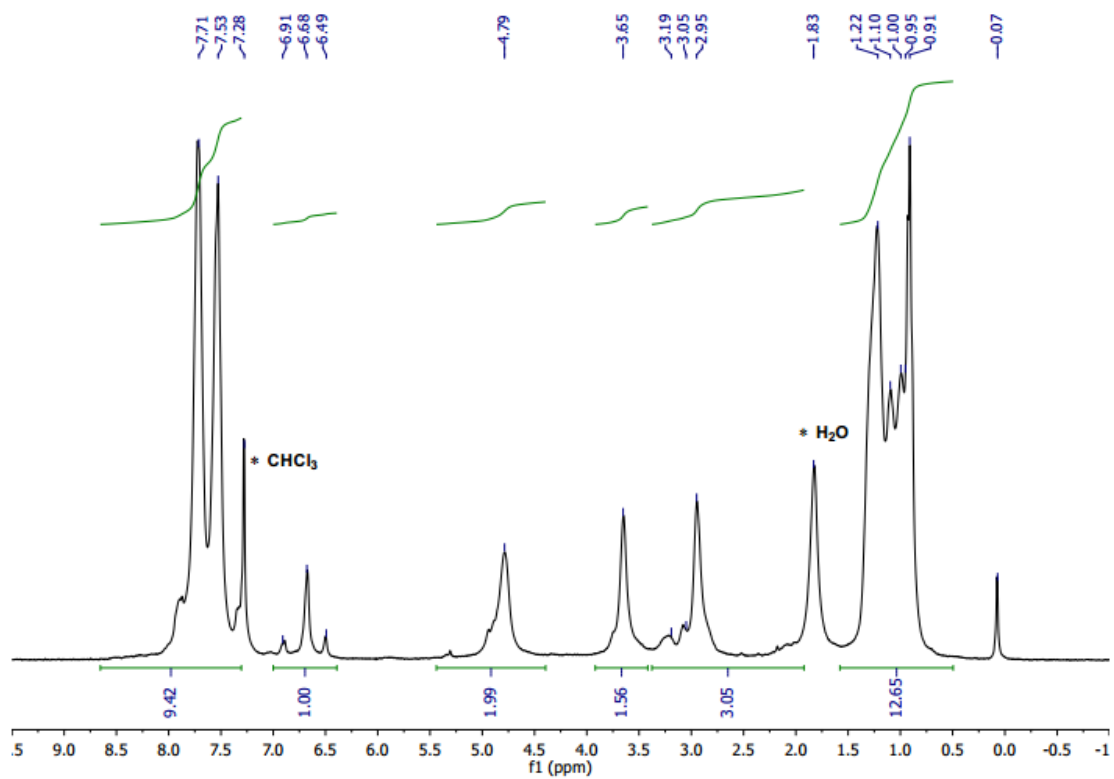


Figure 3 A.1: Proton NMR spectrum of **LO2**. Each peak marked with an asterisk correspond to a solvent signal.

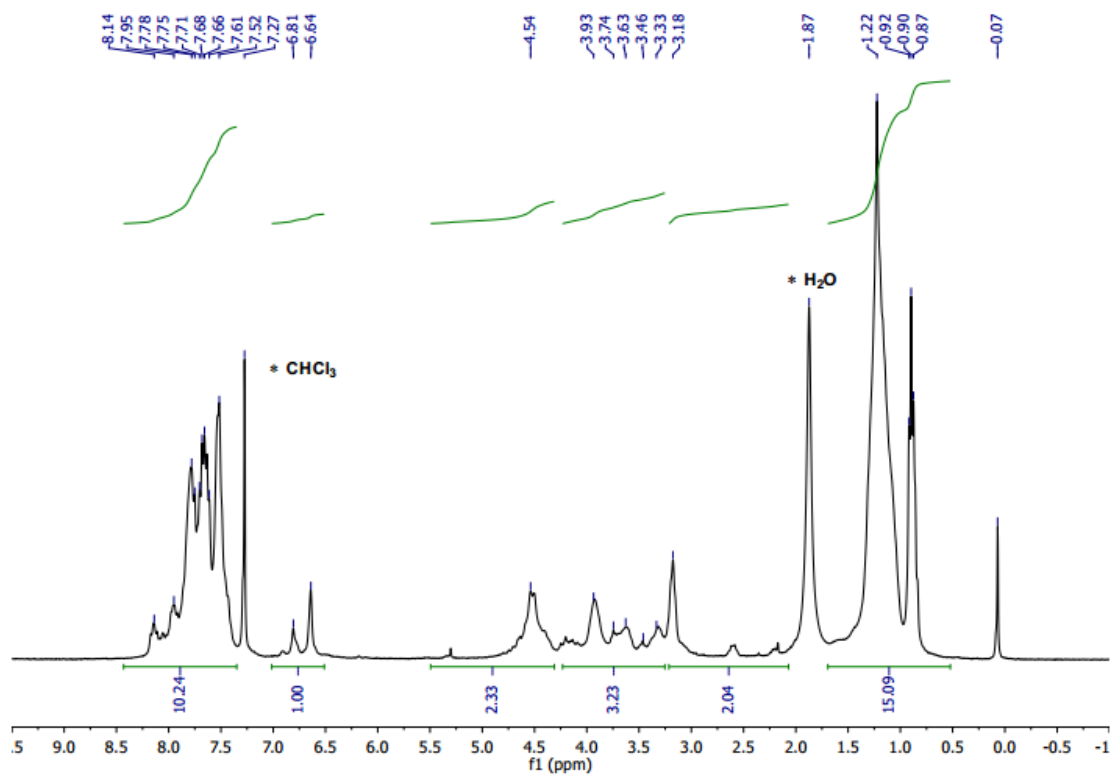


Figure 3 A.2 Proton NMR spectrum of **LO3**. Peak marked with an asterisk correspond to solvent signals.

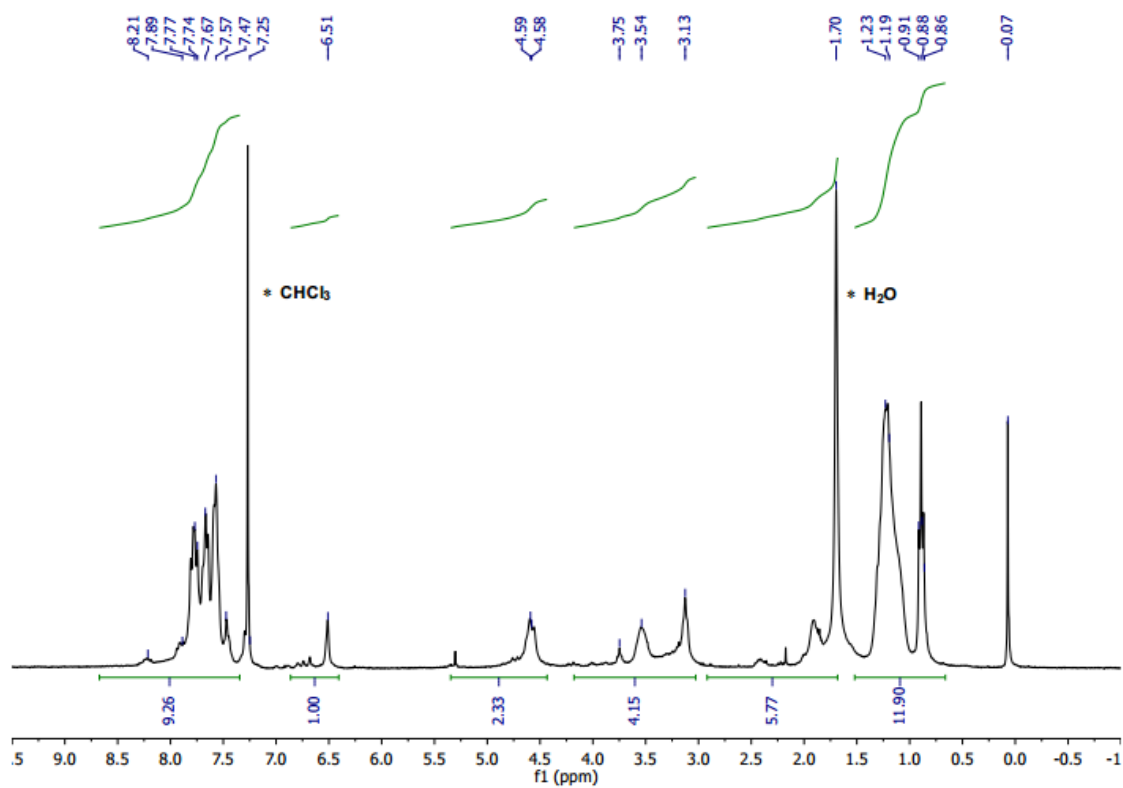


Figure 3 A.3: Proton NMR spectrum of **LO4**. Peak marked with an asterisk correspond to solvent signals.

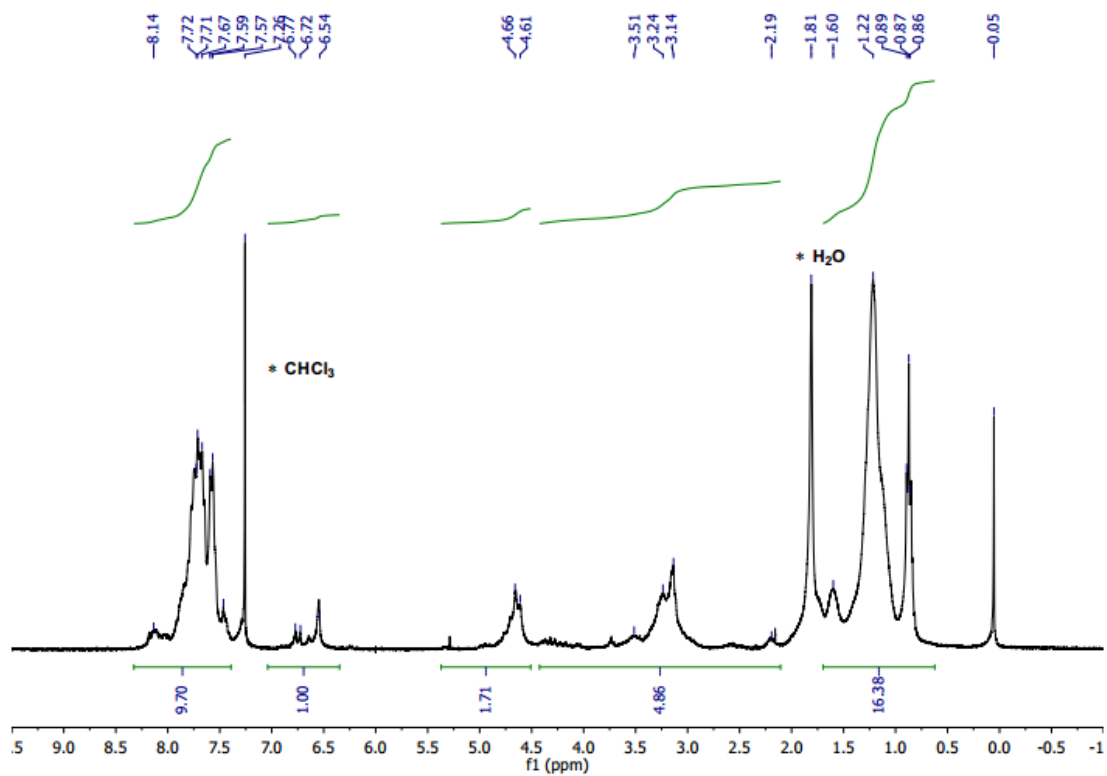


Figure 3 A.4 Proton NMR spectrum of **LO5**. Peak marked with an asterisk correspond to solvent signals.

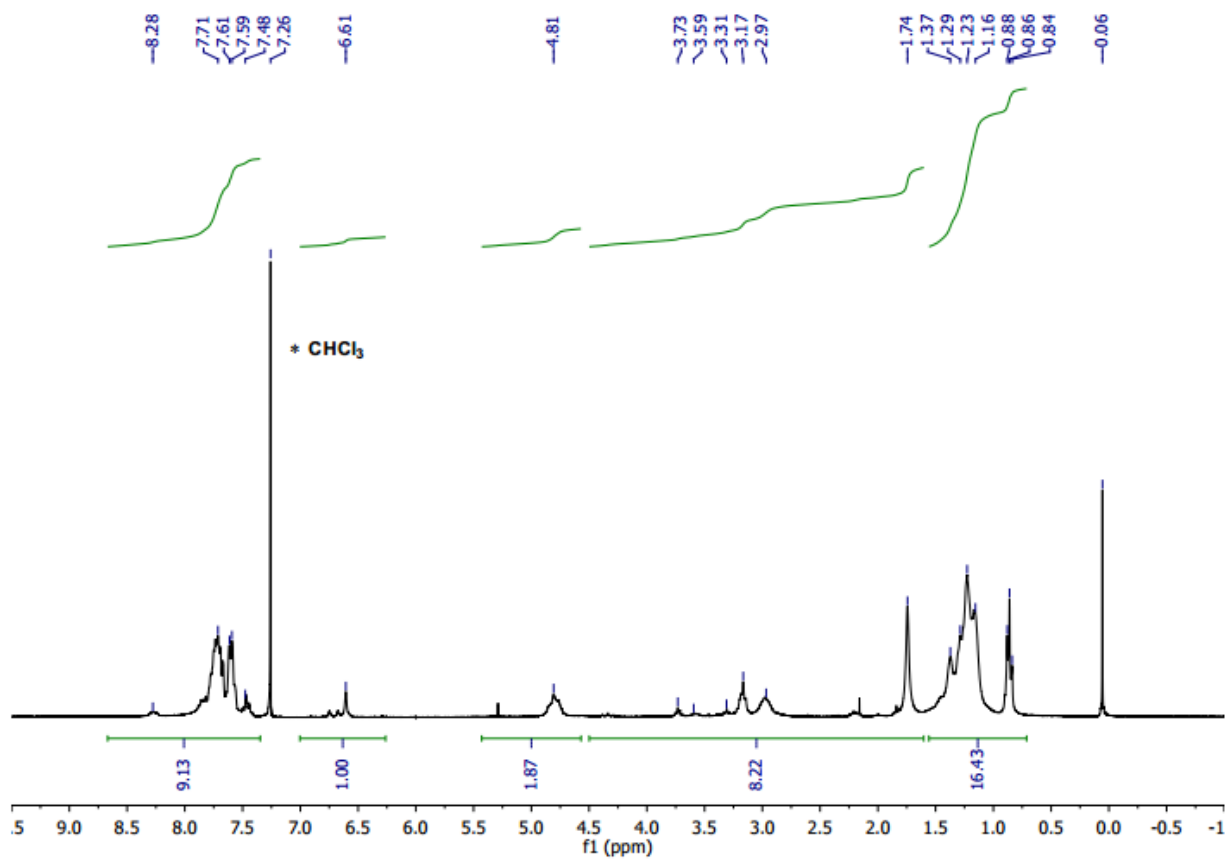


Figure 3 A.5: Proton NMR spectrum of **LO8**. Peak marked with an asterisk correspond to solvent signals.

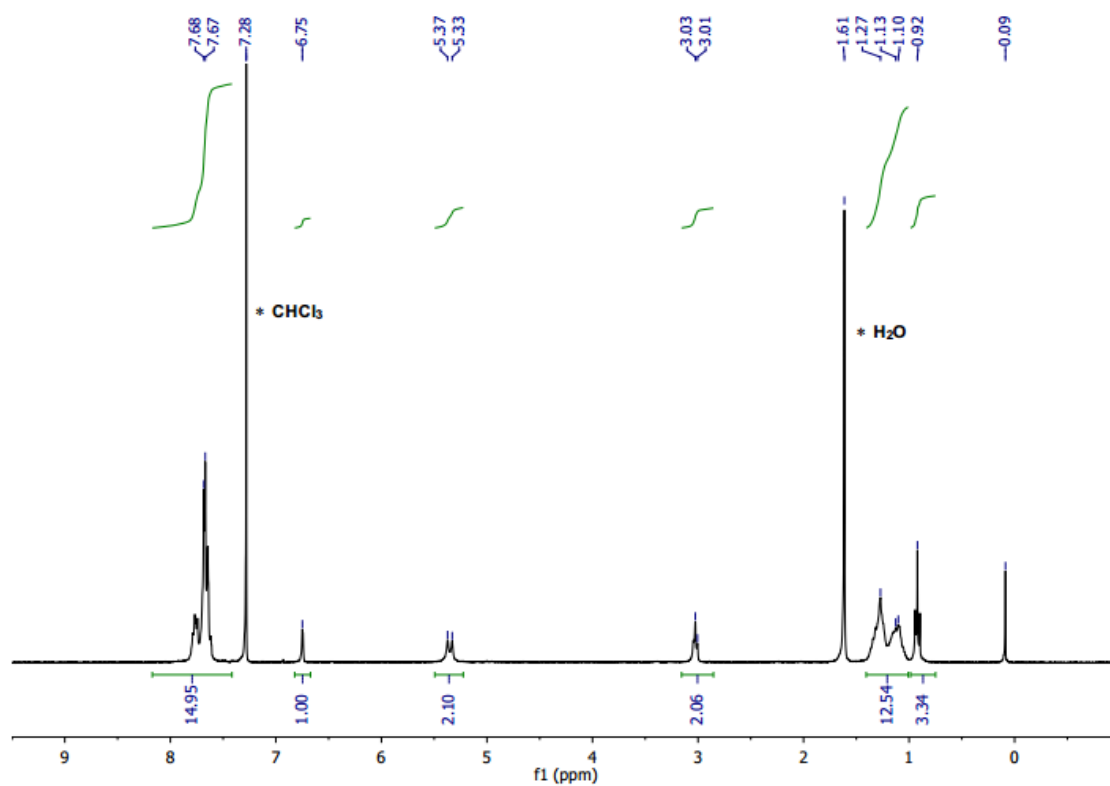


Figure 3 A.6: Proton NMR spectrum of 1,4-bis(octyloxy)-2,5-xylenebis(triphenylphosphonium bromide). Peak marked with an asterisk correspond to solvent signals.

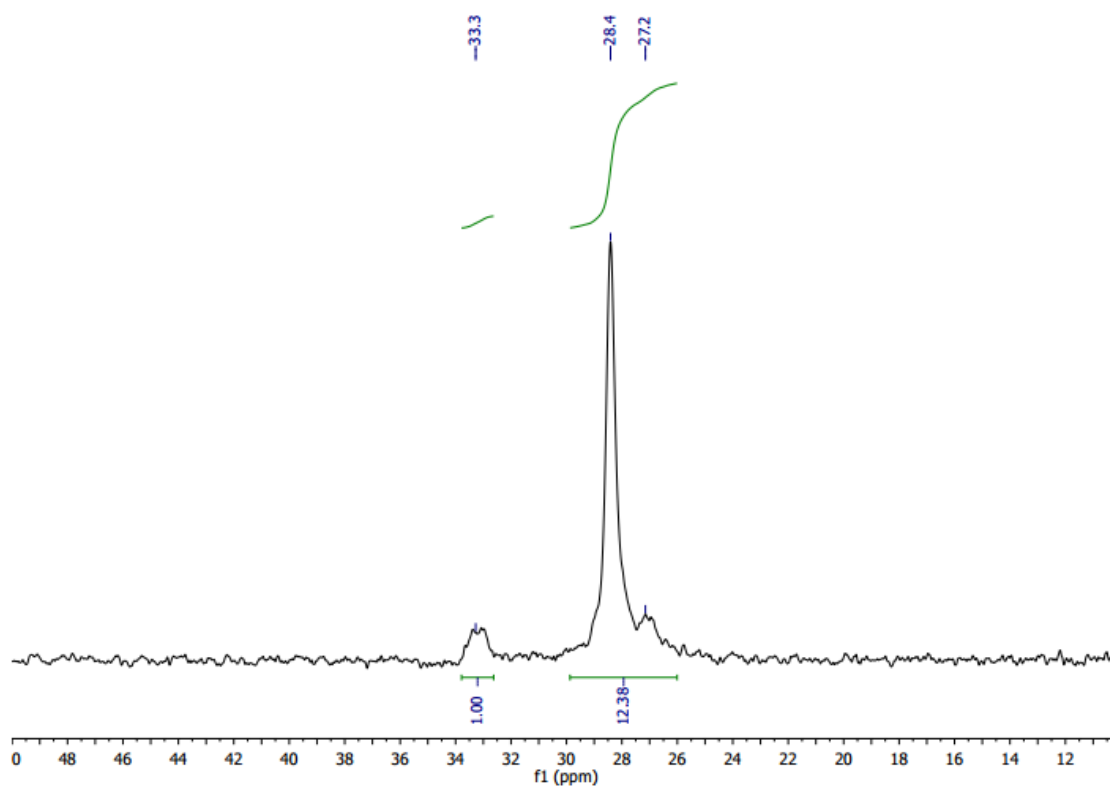


Figure 3 A.7: Phosphorus-31 NMR of compound **LO2** (CDCl_3 , 121 MHz).

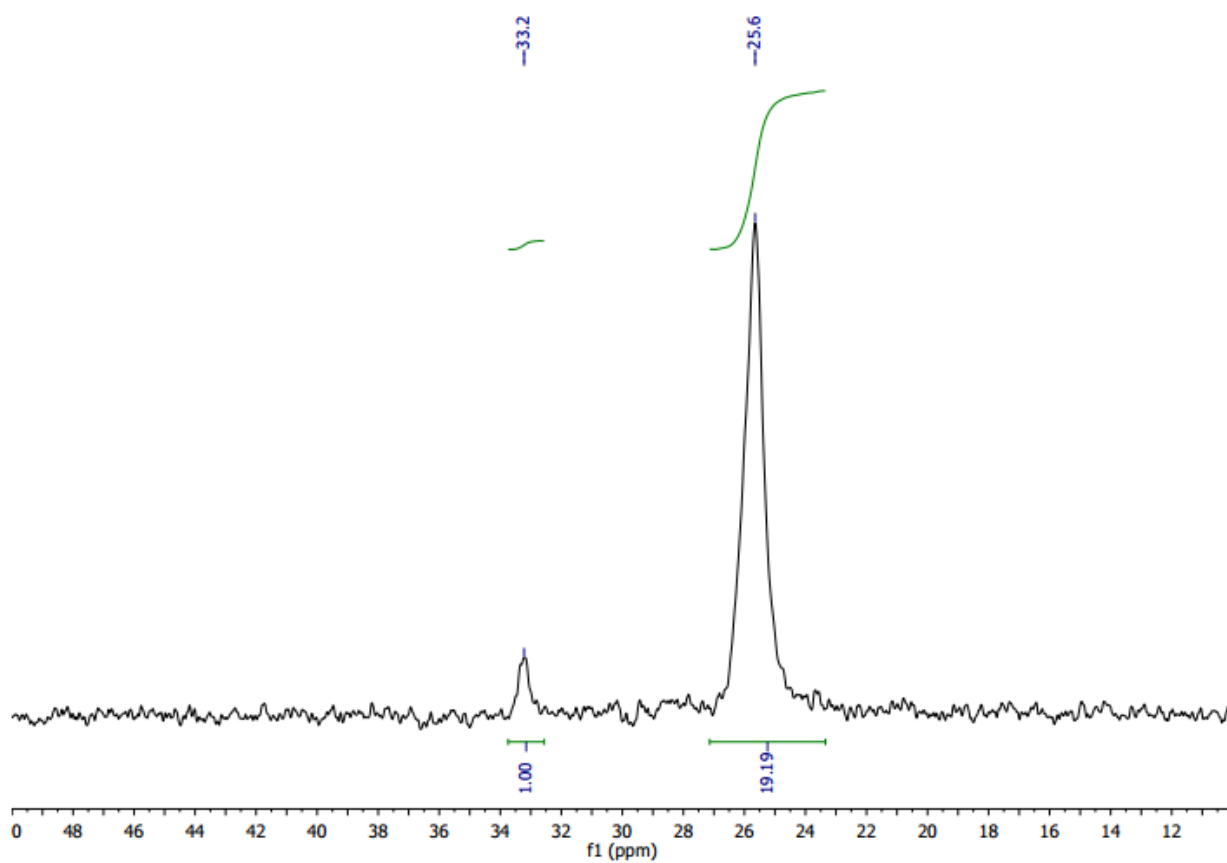


Figure 3 A.8: Phosphorus-31 NMR of compound **LO3** (CDCl₃, 121 MHz).

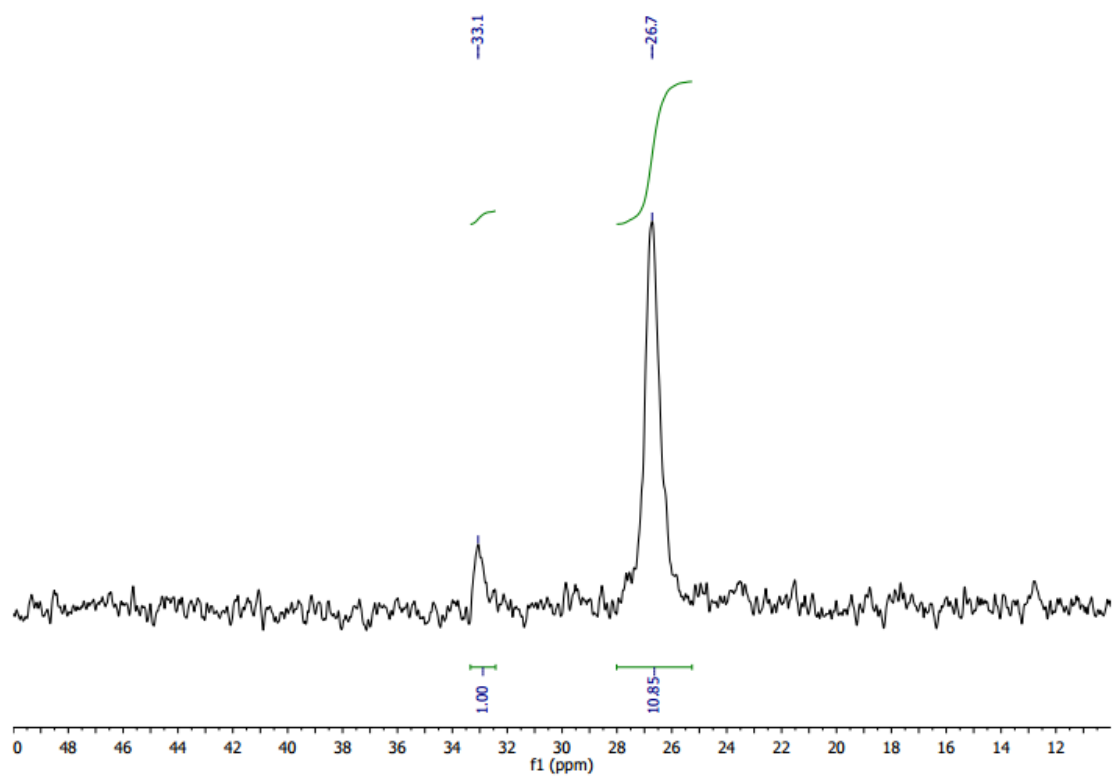


Figure 3 A.9: Phosphorus-31 NMR of compound **LO4** (CDCl₃, 121 MHz).

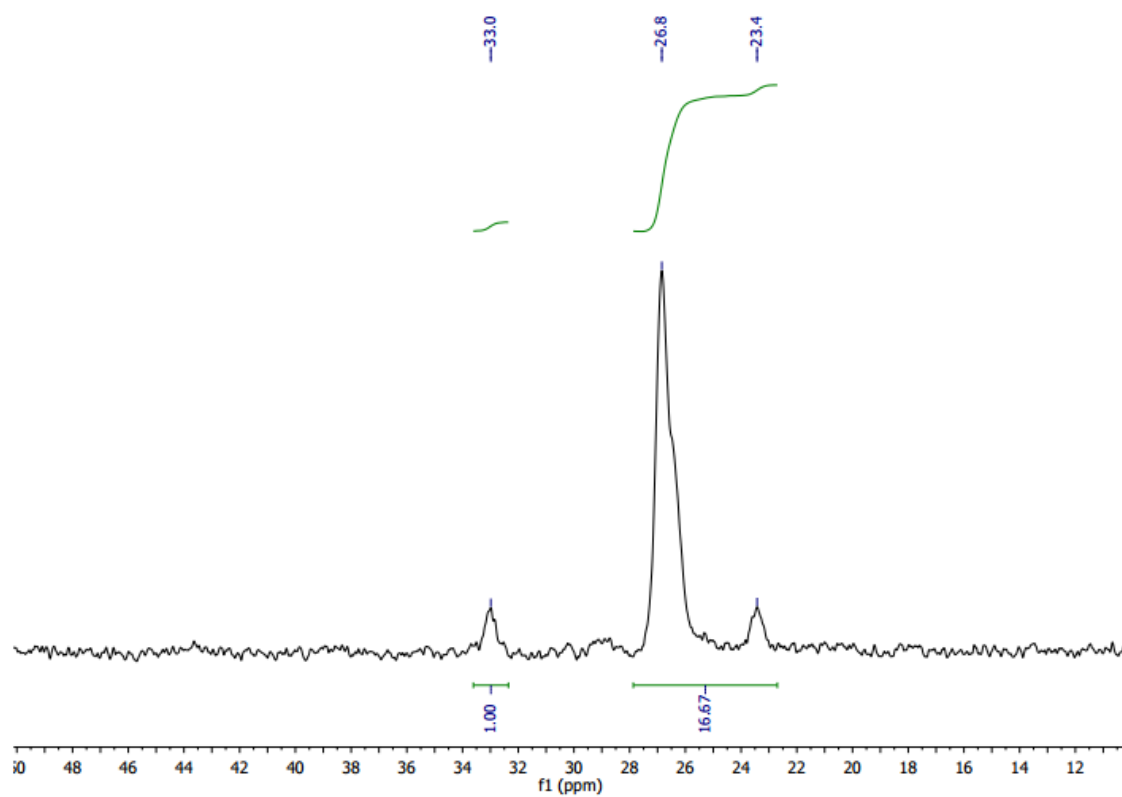


Figure 3 A.10: Phosphorus-31 NMR of compound **LO5** (CDCl_3 , 121 MHz).

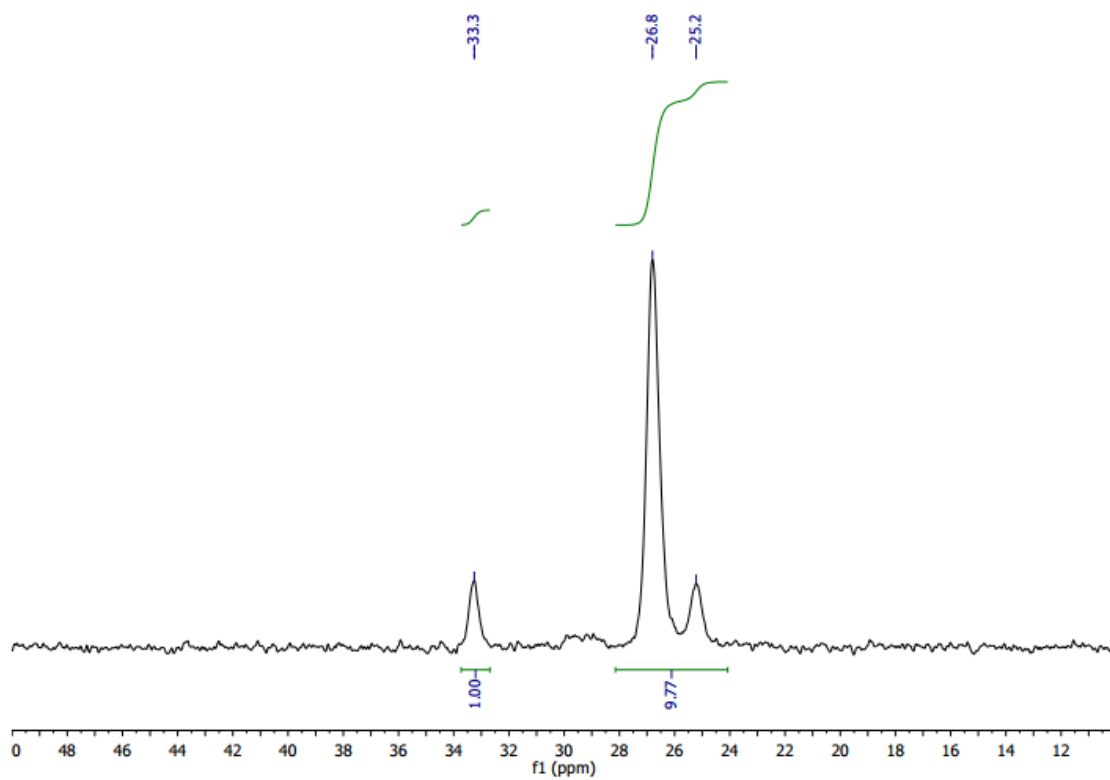


Figure 3 A.11: Phosphorus-31 NMR of compound **LO8** (CDCl_3 , 121 MHz).

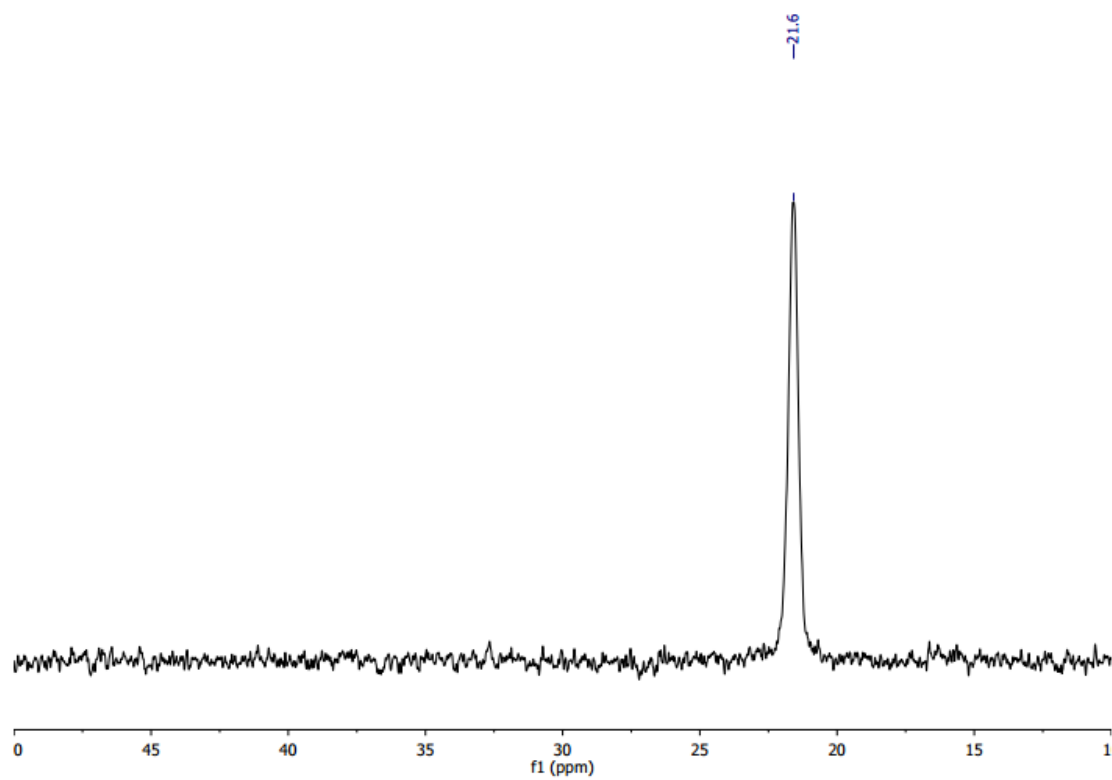


Figure 3 A.12: Phosphorus-31 NMR of **M3**(CDCl₃, 121 MHz)

Appendix 3B

Layer-by-layer linear plot

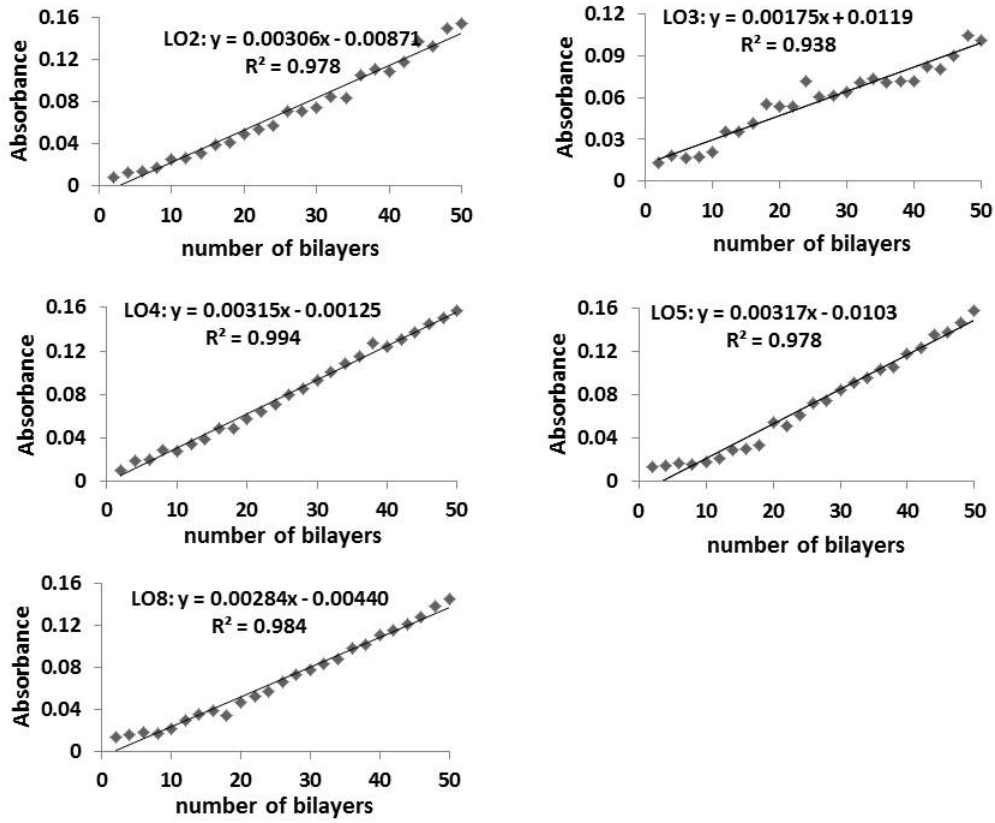


Figure 3 B.1 linear plots of film growth versus bilayer number of LO with **Pc2-100**

Appendix 3C

X-ray powder diffraction, TGA and DSC Traces

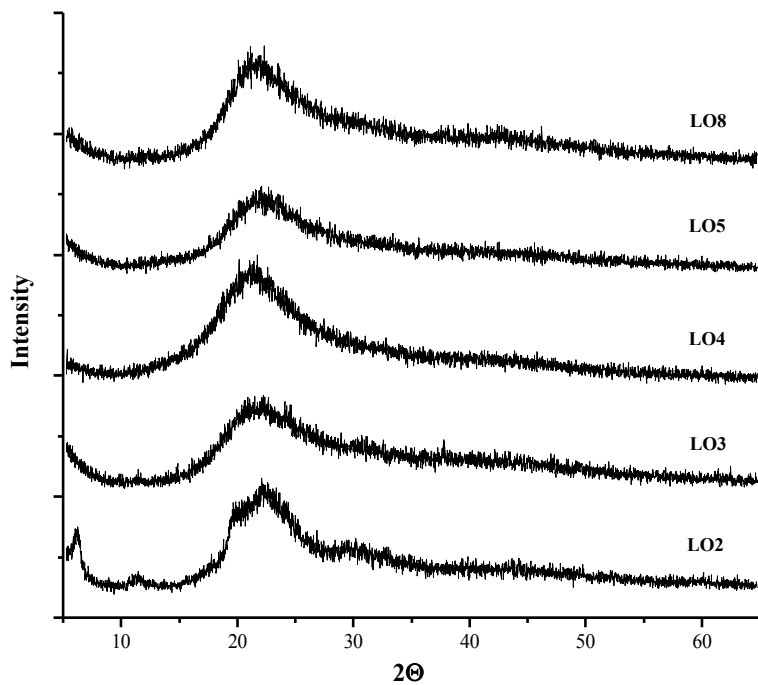


Figure 3 C.1: X-ray powder diffraction of **LO**.

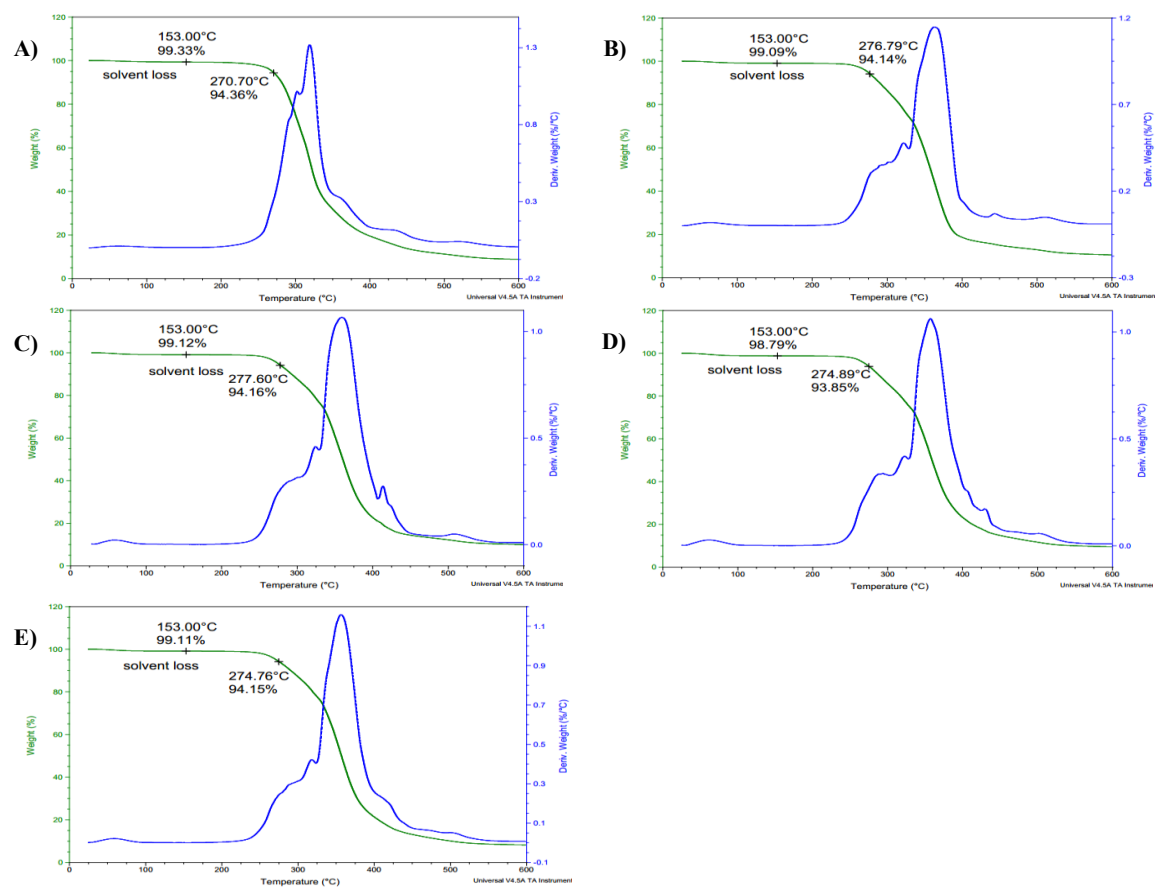


Figure 3 C.2: TGA traces of LO polymers: LO2 (A), LO3 (B), LO4 (C), LO5 (D) and LO8 (E).

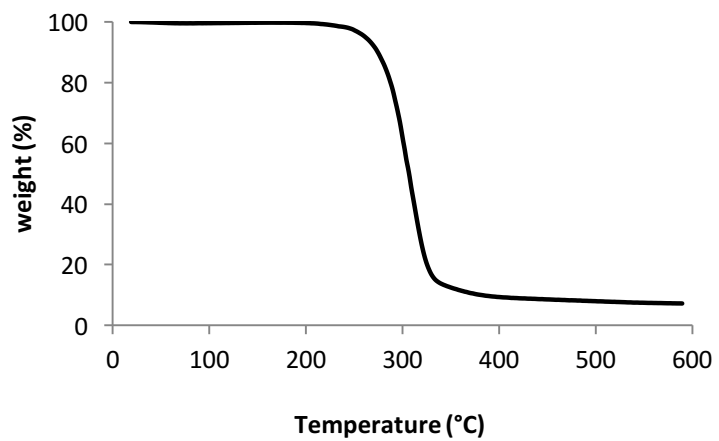


Figure 3 C.3: TGA trace of **M3**

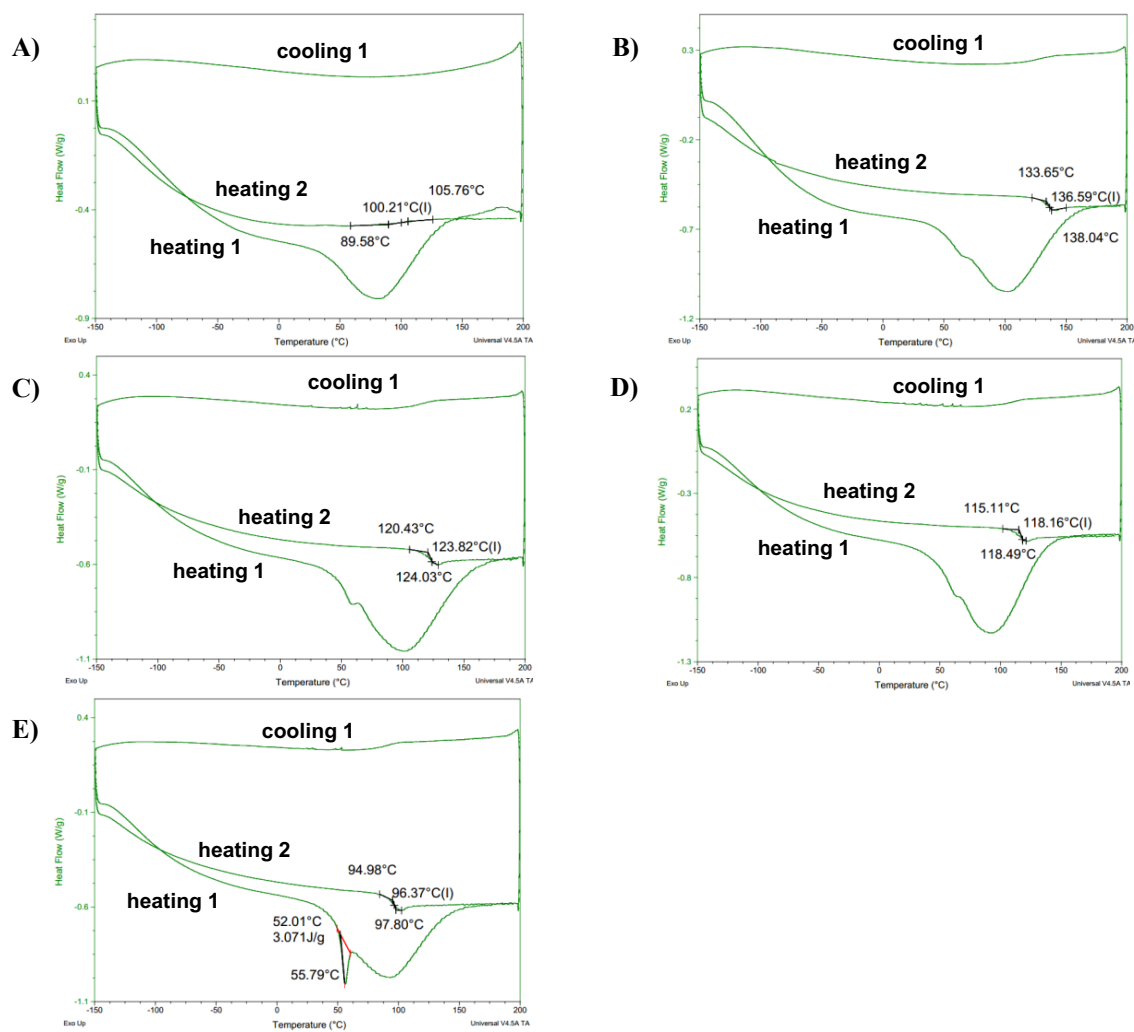


Figure 3 C.4: DSC traces of LO polymers: LO2 (A), LO3 (B), LO4 (C), LO5 (D) and LO8 (E).

Appendix 3D

AFM and microscope images

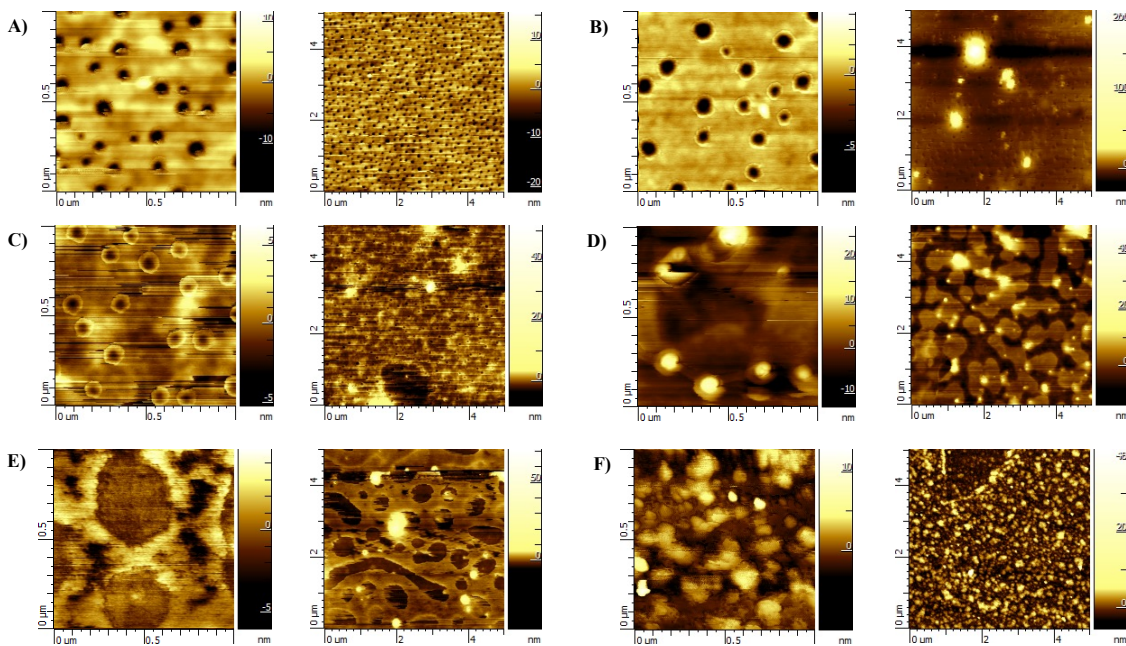


Figure 3 D.1: AFM 2D-height images of $1 \times 1 \mu\text{m}$ (left column) and $5 \times 5 \mu\text{m}$ (right column) of **LO** polymers cast from CHCl_3 and dried in ambient conditions: **LO2** (A), **LO3** (B), **LO4** (C), **LO5** (D), **LO8** (E) and blank (F).

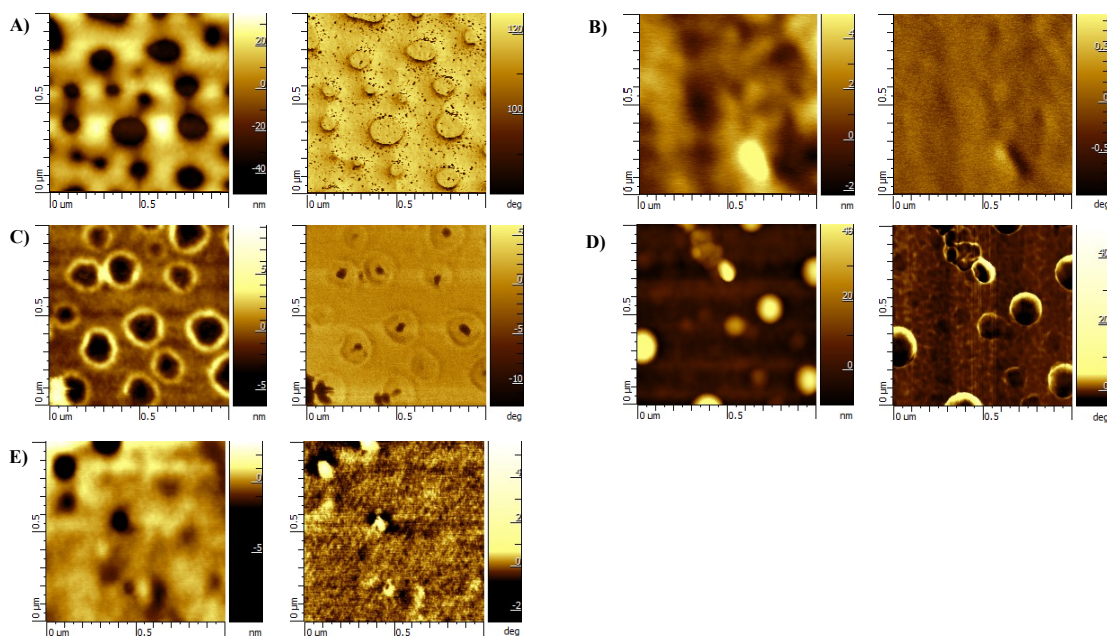


Figure 3 D.2: $1 \times 1 \mu\text{m}$ AFM 2D-height (left column) and phase (right column) images of LO polymers cast from $\text{CH}_3\text{CN}/\text{CHCl}_3$ (1:1): LO2 (A), LO3 (B), LO4 (C), LO5 (D) and LO8 (E).

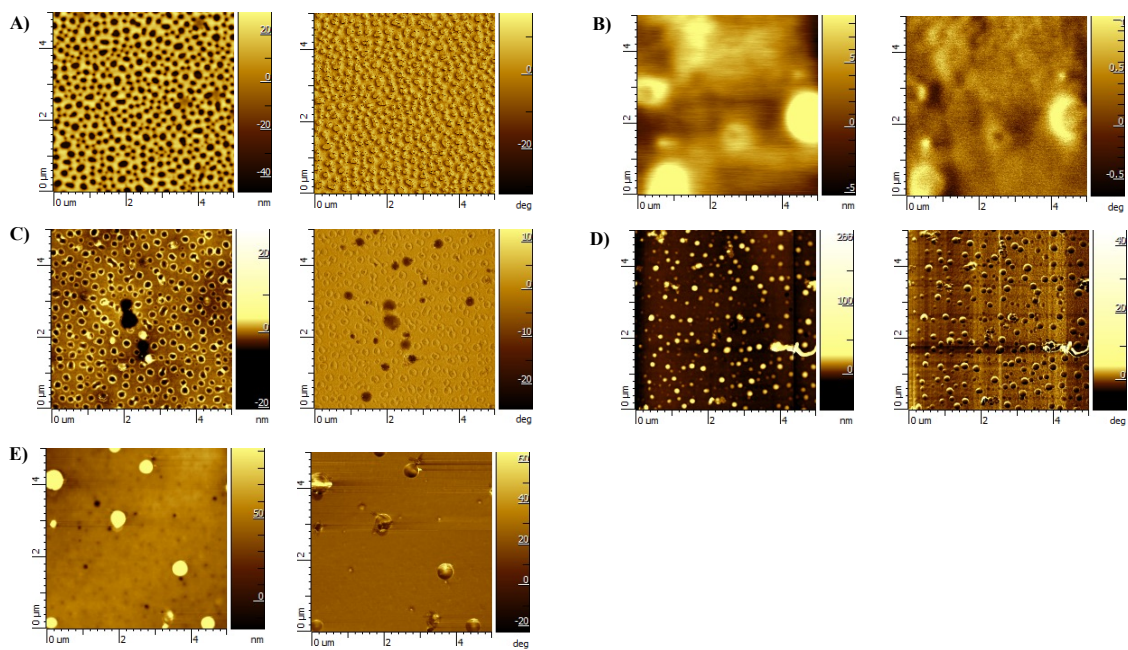


Figure 3 D.3: $5 \times 5 \mu\text{m}$ AFM 2D-height (left column) and phase (right column) images of LO polymers cast from $\text{CH}_3\text{CN}/\text{CHCl}_3$ (1:1): LO2 (A), LO3 (B), LO4 (C), LO5 (D) and LO8 (E).

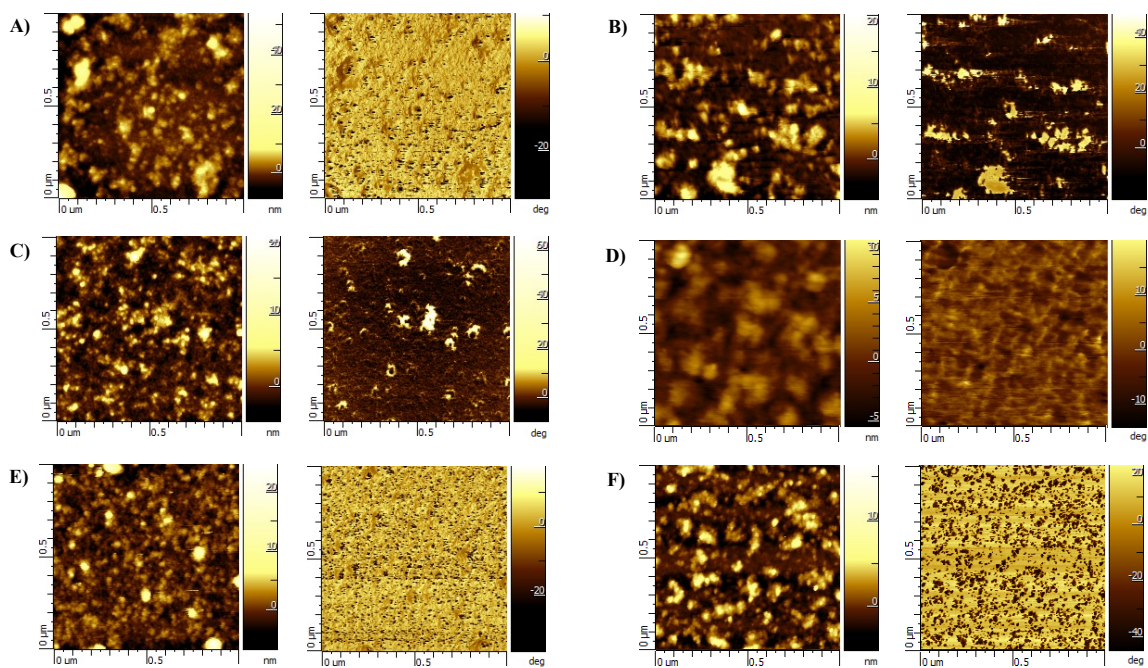


Figure 3 D.4: $1 \times 1 \mu\text{m}$ AFM 2D-height (left column) and phase (right column) images of **LO** polymers cast from $\text{CH}_3\text{CN}/\text{H}_2\text{O}$ (4:1): **LO2** (A), **LO3** (B), **LO4** (C), **LO5** (D), **LO8** (E) and blank (F).

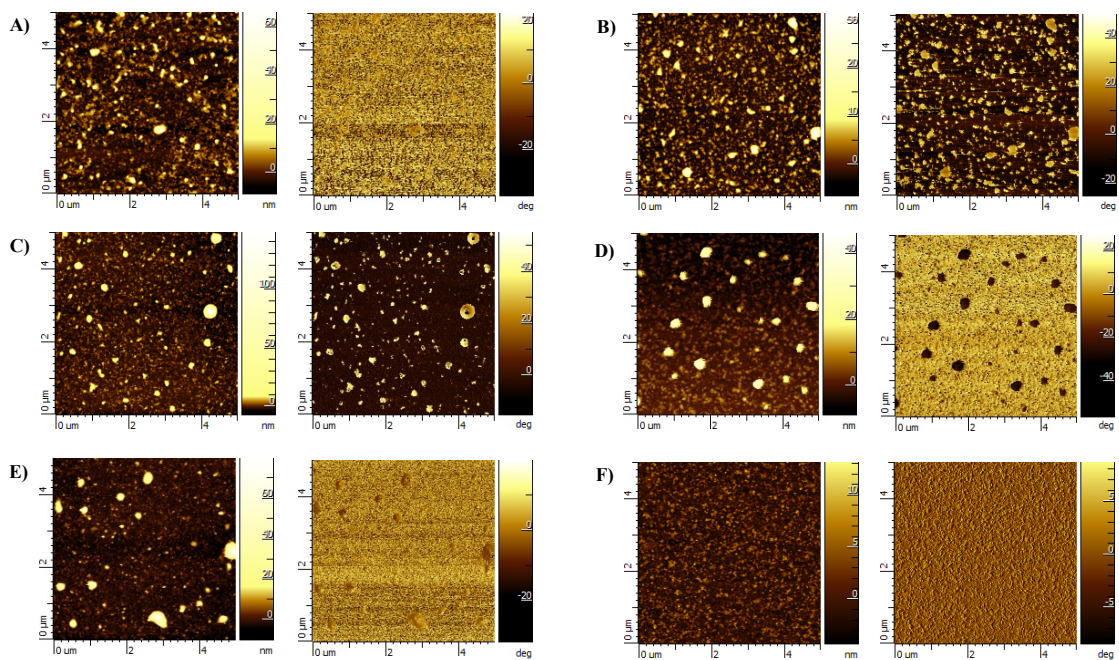


Figure 3 D.5: $5 \times 5 \mu\text{m}$ AFM 2D-height (left column) and phase (right column) images of LO polymers cast from $\text{CH}_3\text{CN}/\text{H}_2\text{O}$ (4:1): **LO2** (A), **LO3** (B), **LO4** (C), **LO5** (D), **LO8** (E) and blank (F).

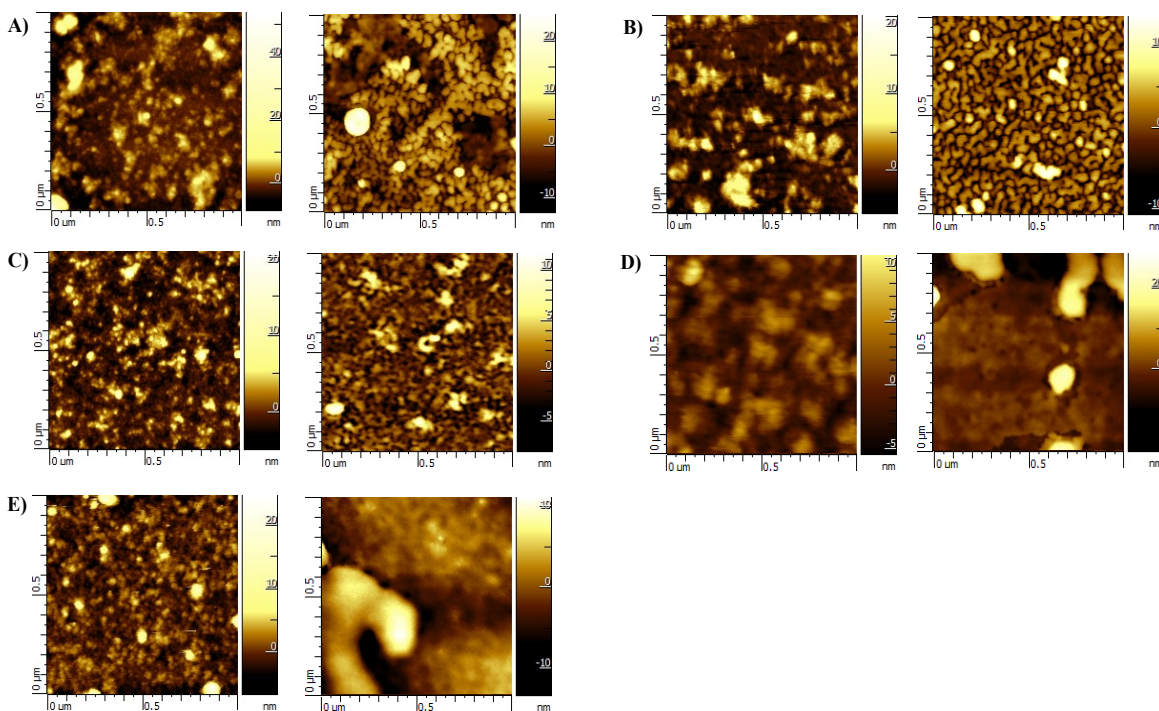


Figure 3 D.6: $1 \times 1 \mu\text{m}$ AFM 2D-height images of **LO** (left column) and **LX** (right column) cast from $\text{CH}_3\text{CN}/\text{H}_2\text{O}$ (4:1): **LO2** and **LX2** (A), **LO3** and **LX3** (B), **LO4** and **LX4** (C), **LO5** and **LX5** (D), **LO8** and **LX8** (E).

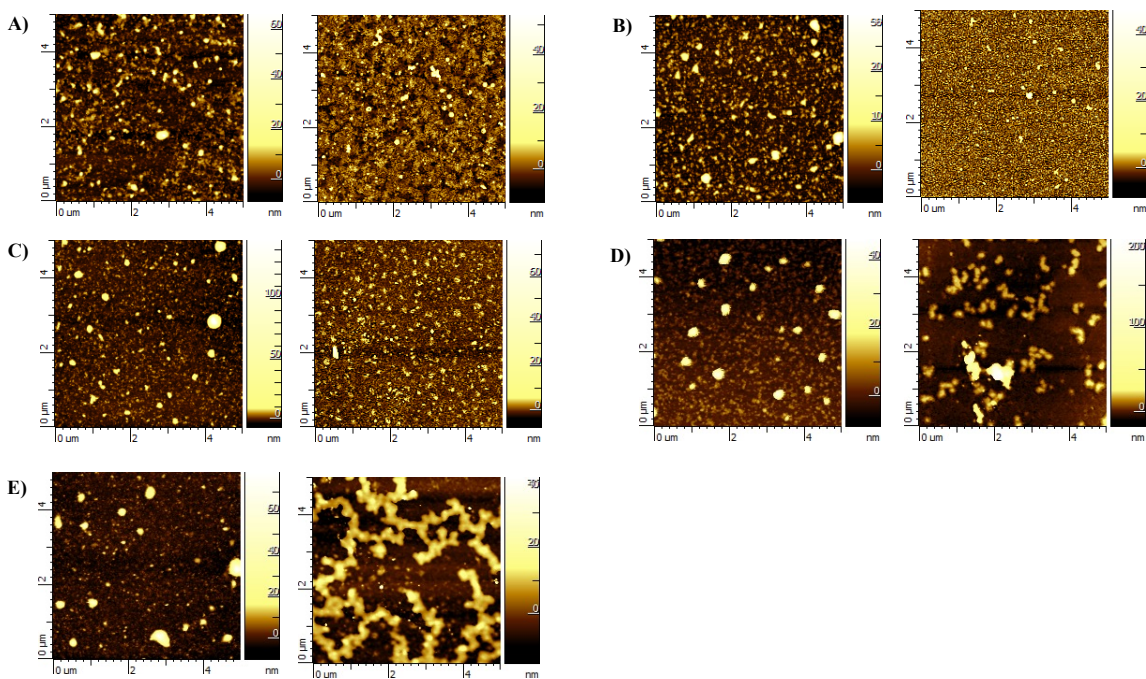


Figure 3 D.7: $5 \times 5 \mu\text{m}$ AFM 2D-height images of dip-cast films of **LO** (left column) and **LX** (right column) cast from $\text{CH}_3\text{CN}/\text{H}_2\text{O}(4:1)$: **LO2** and **LX2** (A), **LO3** and **LX3** (B), **LO4** and **LX4** (C), **LO5** and **LX5** (D), **LO8** and **LX8** (E).

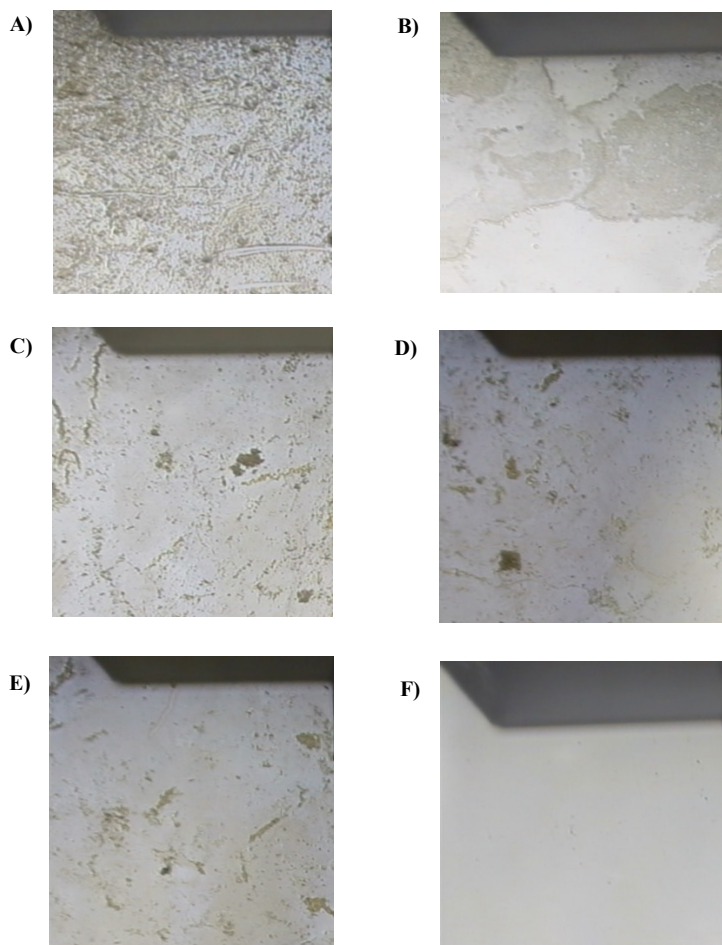


Figure 3 D.7: Optical microscopy images ($\sim\times 80$) of LbL films of **LO** with **Pc12-100**: **LO2** (A), **LO3** (B), **LO4** (C), **LO5**(D), **LO6** (E) and clean glass slide (F).

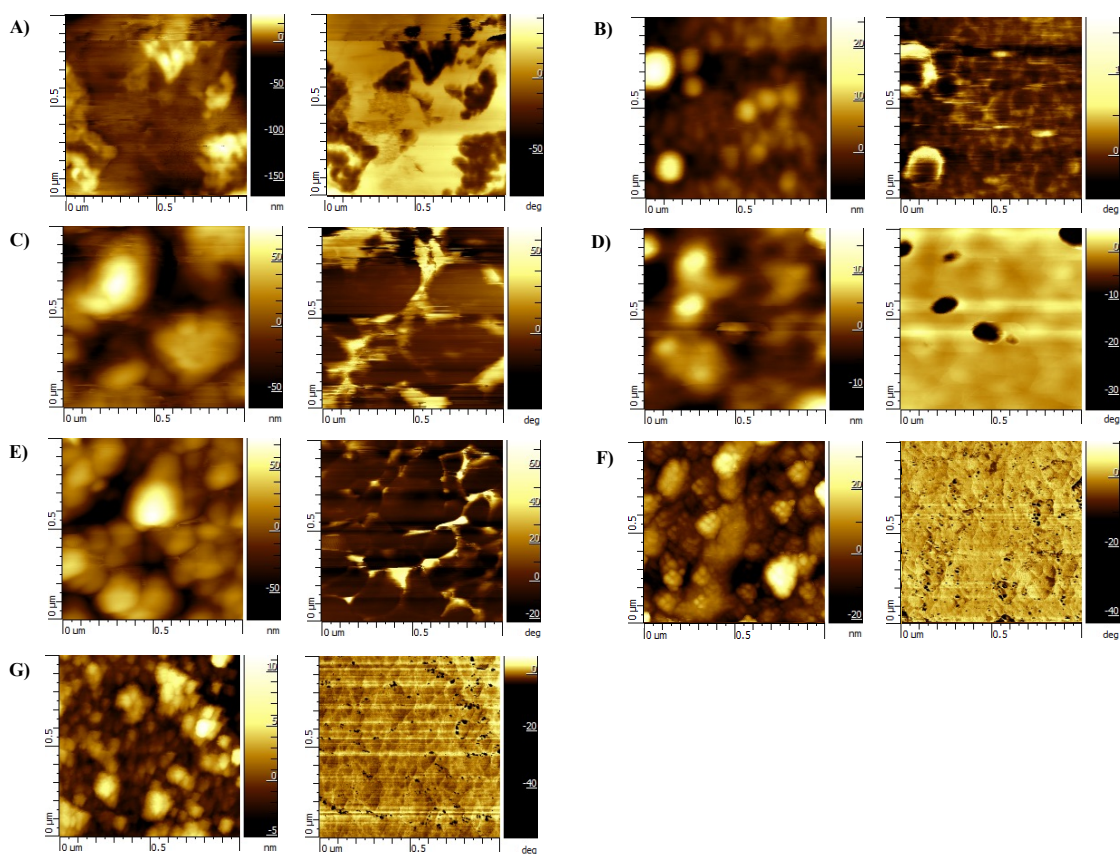


Figure 3 D.8: $1 \times 1 \mu\text{m}$ AFM 2D height images viewed from perpendicular to the film plane (left column) and phase images (right column) of LO layer-by-layer with **Pc12-100**: LO2 (A), LO3-white (B), LO3-dark (C), LO4 (D), LO5 (E), LO8 (F) and clean glass slide (G). LO3-dark corresponds to the large island displayed in the optical image in Figure S25 B.

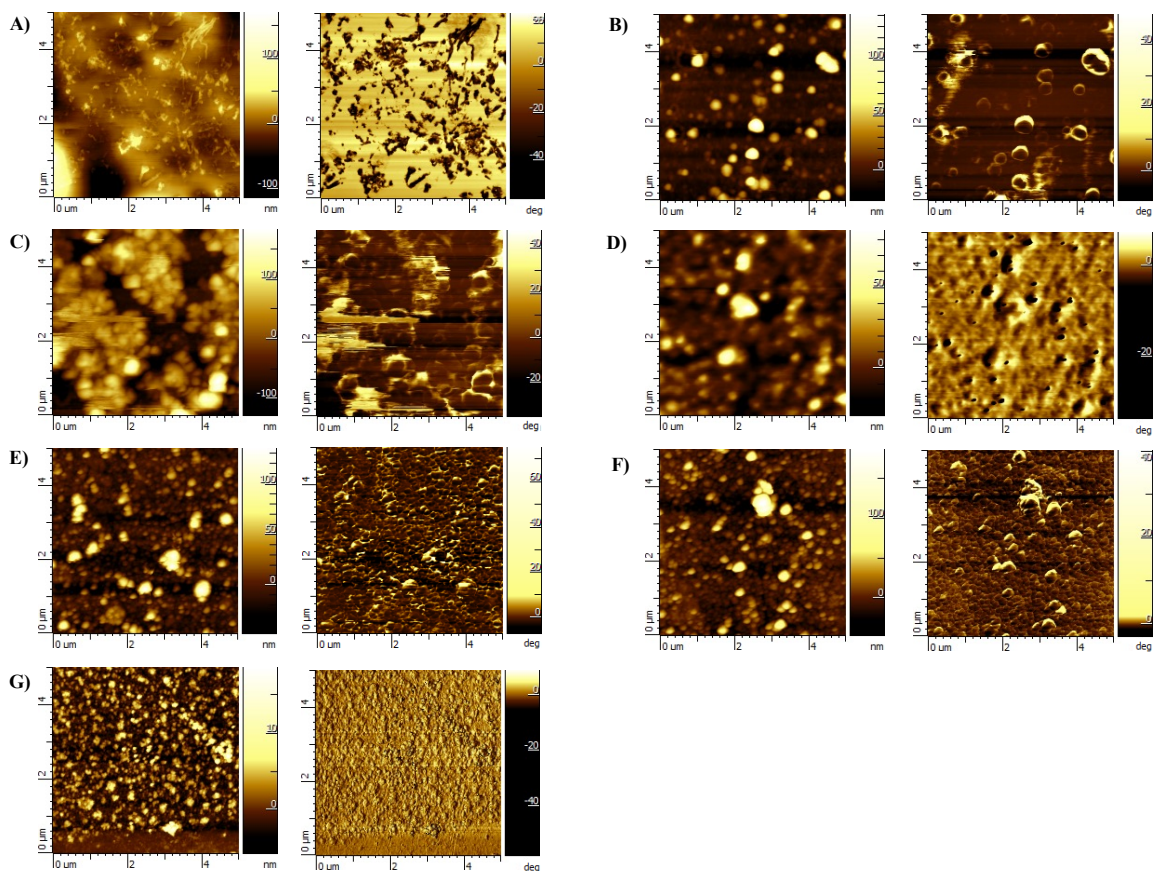


Figure 3 D.9: $5 \times 5 \mu\text{m}$ AFM 2D height images viewed from perpendicular to the film plane (left column) and 3D images (right column) of LO layer-by-layer with **Pc12-100**: LO2 (A), LO3-white (B), LO3-dark (C), LO4 (D), LO5 (E), LO8 (F) and clean glass slide (G).

Appendix 3D

Zisman Plots

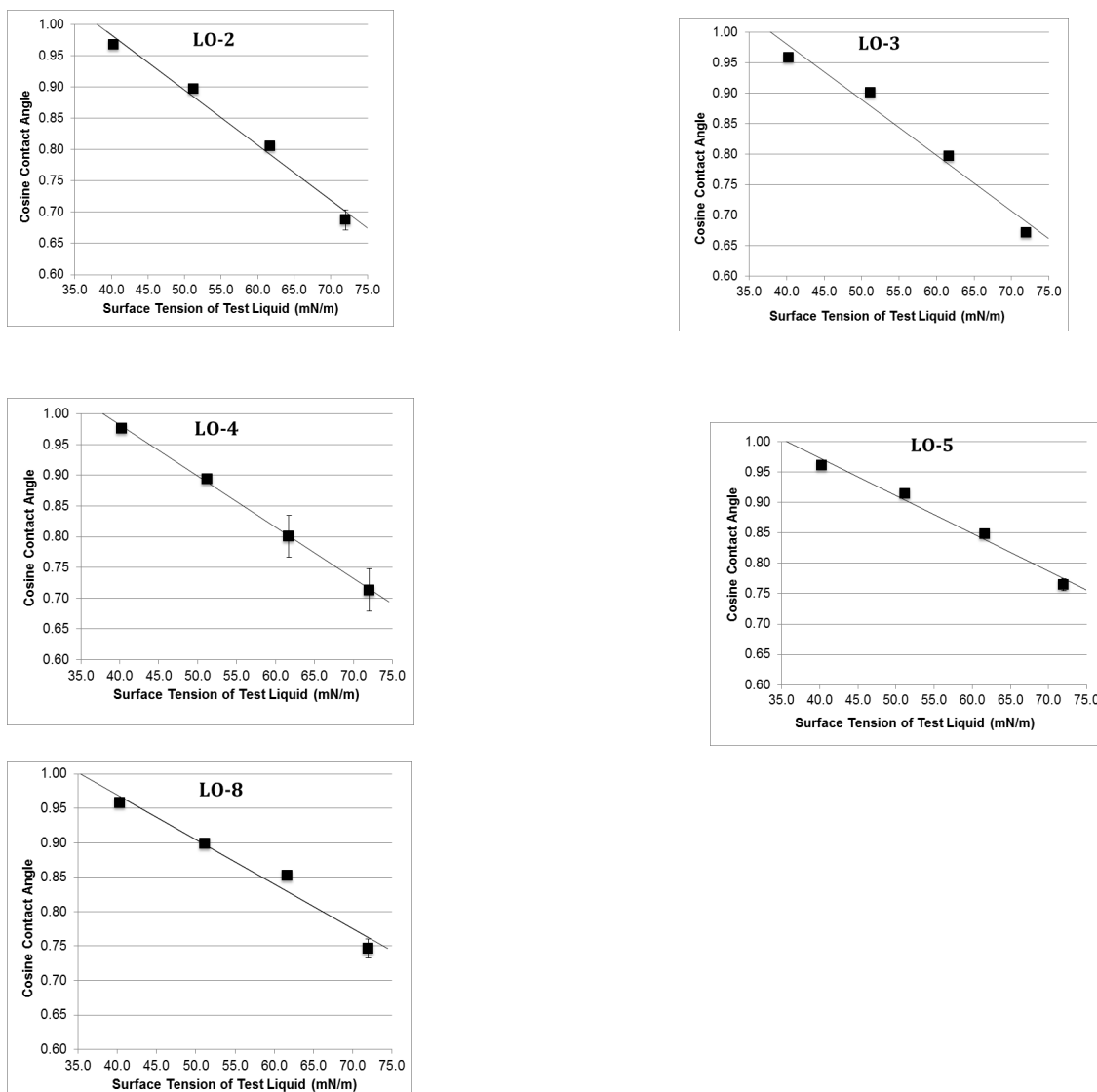


Figure 3 D.1: Zisman Plots from contact angle data for **LO** polymers. Error bars represent the standard deviation of all measurements. In many cases the error bars are smaller than the data marker and are therefore not visible.

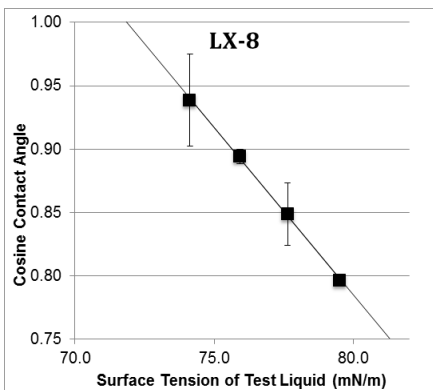
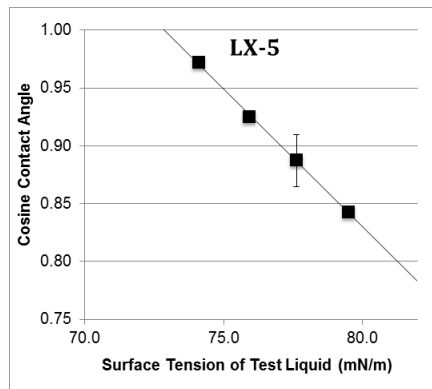
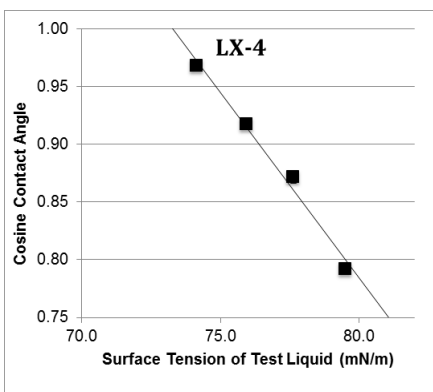
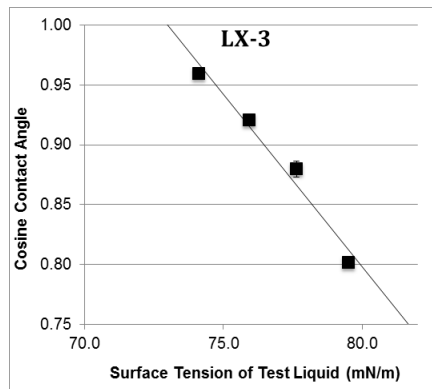
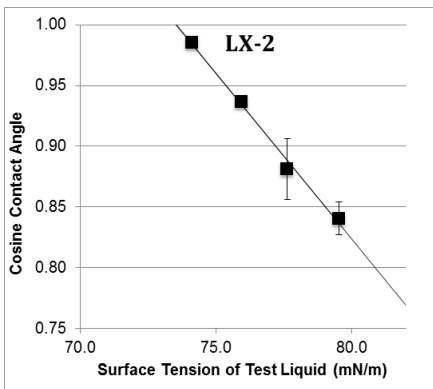


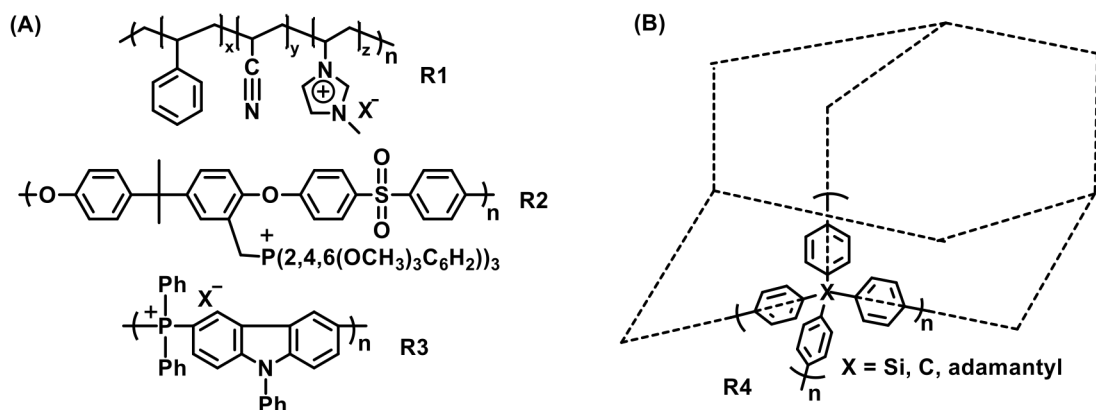
Figure 3 D.2: Zisman Plots from contact angle data for LX polymers. Error bars represent the standard deviation of all measurements. In many cases the error bars are smaller than the data marker and are therefore not visible.

CHAPTER FOUR

A NEW ROUTE TO PHOSPHONIUM POLYMER NETWORK SOLIDS VIA CYCLOTRIMERIZATION**

4.1 Introduction

Organic network solids support an ever-expanding field of research due to their broad applications in gas storage/separation¹⁻⁵ and catalysis.^{6,7} Much effort has been devoted to the development of polymer scaffolds bearing diverse functional units in order to have precise control of physical (pore size, surface area)^{8,9} and chemical properties (polar or ionic).¹⁰ Compared to traditional organic frameworks, ionic hypercrosslinked polymers, specifically those involving ionic liquids as monomers, have attracted growing attention. These materials can possess good thermal and chemical stability, properties that can be tuned upon simple counterion exchange, and which can readily form layer-by-



Scheme 4.1: Examples of polyelectrolytes (A) and a network solid having tetrahedral vertices (B)

** Adapted from X. Yang, Y. Wen, G. Chumanov, R. C. Smith. *J. Polym. Sci., Part A: Polym. Chem.* **2017**, 55, 1620-1625, with permission.

layer self-assembled films with other ionic polymers.¹¹⁻²⁰ For example, Yan, *et al.* reported an alkaline anion exchange membrane **R1** (Scheme 4.1) comprised of copolymerized imidazolium-functionalized ionic liquids with styrene and acrylonitrile. Membranes of **R1** demonstrated good hydroxide ion conductivity and mechanical properties suitable for use in alkaline fuel cells.²¹ Furthermore, cationic polymers with phosphonium units are widely used as organocatalysts, for example, for CO₂ capture and conversion.⁶

Among ionic polymers, phosphonium polyelectrolytes exhibit outstanding chemical stability (i.e., **R2** in Scheme 4.1) compared to their ammonium analogues.²² Tetraarylphosphonium salts of the form [PAr₄]⁺[NTf₂]⁻ are also thermally stable to heating for several days at 425 °C in air, making them promising candidates for ionic units in high-stability polymers.²³ Our group recently reported a new route to tetraarylphosphonium polyelectrolytes having decomposition temperatures of up to 460 °C, with one that is stable at 65 °C in 6 M NaOH(*aq*) for at least 24 h (**R3** in Scheme 4.1).²⁴ All of these properties are necessary for their use in antibacterial coatings^{25,26} and as membranes in alkaline fuel cells and related electrochemical energy conversion technologies.²⁷

Despite their intriguing properties, less work has been reported involving phosphonium salts in organic frameworks compared to the vast number of papers published every year related to organic polymer networks. This is probably because of the less-explored synthetic routes for polymers with tetraarylphosphonium units and the relative difficulty of handling air-sensitive phosphorus precursors. The synthetic routes

for preparing ionic organic frameworks generally employ either bifunctional charge-bearing monomers,^{21,28} or post-polymerization modification of a neutral network solid to introduce ionic moieties.²²

A facile synthetic route with fewer steps and more conveniently available monomers is desired. Among cyclotrimerization routes to porous solids, polymers in which polymerization proceeds via acid-catalyzed formation of 1,3,5-triarylbenzene units from acetophenone derivatives is one of the most-extensively studied methods.²⁹ Kaskel's group, for example, reported that porous monolithic organic frameworks that hold the shape of the reaction vessel can be easily prepared via cyclotrimerization of the monomers in molten *p*-toluenesulfonic acid, which serves as both the acid catalyst and solvent.³⁰ Other studies have examined organic networks having tetrahedral vertices, for example in **R4** (Scheme 4.1B).⁴

Bearing these studies in mind, we envisioned that cyclotrimerization of a diacetyl-functionalized tetraarylphosphonium salt could serve as a tetrahedral vertex upon cyclotrimerization to yield an ionic framework having excellent thermal and alkaline stability. Herein, a simple method for preparing ionic network solids containing tetraarylphosphonium units is described. The surface area, differential affinity for CO₂ and N₂, water uptake and film morphology were also examined.

4.2 Experimental

4.2.1 General considerations

Air-sensitive reactions were performed in an MBraun UNILab glovebox under nitrogen. Chemicals were used without further purification from suppliers.

4.2.2 Synthesis of bis(4-acetylphenyl)-diphenylphosphonium bromide (**M1**)

In a 100 mL pressure vessel, diphenylphosphine (4.000 g, 21.48 mmol), 4'-bromoacetophenone (8.980 g, 45.11 mmol), diisopropylamine (2.174 g, 21.48 mmol) and NiBr₂ (0.282 g, 1.29 mmol) were mixed in 7 mL ethylene glycol with a magnetic stir bar. The tube was sealed with a Teflon cap equipped with a viton O-ring under N₂. The reaction was carried out under N₂ at 180 °C for 15 h. A mixture of 80 mL acetonitrile, 30 mL DI H₂O and 30 drops of HBr was added to the green crude. The mixture has been stirred in 40 °C water bath until no protective group showed in proton NMR. Then the mixture was extracted by dichloromethane and washed with 1 M NaBr(aq) solution twice and deionized (DI) water once. The organic layer was collected and dried over anhydrous Na₂SO₄ overnight. All volatiles were removed under reduced pressure and the crude product was precipitated by addition of 400 mL of diethyl ether. The light yellow powder was collected by vacuum filtration and dried in a vacuum oven overnight. Chromatography was carried out over silica using acetonitrile and methanol (10 : 1, v/v) as the mobile phase to yield the product as a pale yellow powder (7.772 g, 71.87%). ¹H NMR (300 MHz, CDCl₃, δ): 8.38(dd, 4H), 7.92-7.29 (m, 12H), 2.73 (s, 6H); ³¹P NMR (122 Hz, CDCl₃, δ): 23.51; ¹³C NMR (75.4 Hz, CDCl₃, δ): 197.1 (C=O), 142.2, 136.2, 135.4 (d, 10.5 Hz), 134.7 (d, 9.7 Hz), 131.2(d, 13.5 Hz), 130.3 (d, 12.7 Hz), 122.8 (d, 88.5 Hz), 117.1 (d, 88.5 Hz), 27.4 ppm. Anal. calcd for C₂₈H₂₄PO₂Br: C 66.81; H 4.81; found: C 65.56; H 5.00%.

4.2.3 Synthesis of **P1**

The cyclotrimerization procedures followed the method described previously.³⁰ In

a typical reaction, **M1** (0.491 g, 0.975 mmol) and *p*-toluenesulfonic acid monohydrate (PTSA, 0.928 g, 4.88 mmol) were mixed in a glass vial and heated to 120 °C for 24 h under N₂. Soxhlet extraction with ethanol yield red-brown chunks (0.430 g, 93.8%); anal. Calc'd for repeat unit formula C₇₈H₅₇P₃Br₃: C 70.60; H 4.33; found: C 71.05; H 5.07%. The reaction can also be carried out in a stainless steel reaction vessel to yield a reddish-brown film. Films prepared in this way were soaked in ethanol for 3 h to remove excess PTSA prior to drying, IR spectroscopic analysis, TEM and AFM imaging of films.

For TEM analysis of the powder sample, the solid was ground in a ball mill for 25 mins to yield a yellow powder. The IR spectrum of **P1** in powder form was taken to ensure no side reaction happen (IR spectra provided in Appendix 4A).

4.2.4 Characterization

All the NMR spectra were collected on a JOEL ECX-300 MHz spectrometer operating at 300, 121.4 and 75.4 MHz for ¹H, ³¹P and ¹³C, respectively. Thermogravimetric analysis (TGA) was performed on TA Instruments Q60 TGA from 25 °C to 800 °C with a heating rate of 5 °C min⁻¹. Powder X-ray diffraction was measured on an Ultima IV. Fourier transformed infrared spectra were recorded on Shimadzu IRAffinity-1S at 400-4000 cm⁻¹ at room temperature. Nitrogen and CO₂ sorption measurements were collected on a Quantachrome ASIQwinTM at 77 K. The samples were degassed at 80 °C for 7 h before measurements. BET surface areas are determined over a P/P₀ range. Scanning electron microscopy (SEM) was performed on a Hitachi SU-6600 at 20 KV. A Hitachi H9500 transmission electron microscope, operating at a voltage of 300 KV, was employed for direct observation of film of **P1**. Film sample were first mixed

with LR white embedding resin (catalyzed) and dried in 60 °C overnight. The sample was then cut by to yield 80 nm thick slices. Sample slides were dried in air and placed on 200 carbon formvar copper TEM grid for observation. Atomic force microscopy (AFM) images were collected using an AIST-NT SmartSPM in non-contact mode with HQ:NSC14/AL BS cantilevers from Mikro-Masch with spring constant of ca. 5.0 N/m. The **P1** in film was used directly without any treatment. AFM images were processed with AIST-NT SPM Control Software. For base stability measurement, solids were soaked in 6 M NaOH solution at room temperature and 60 °C over a 24 h period, respectively. Then the solids were soaked in DI water for another 24 h to remove excess hydroxide ions. Base stability was evaluated by comparing the IR spectra before and after base treatment. Powder sample was soaked in DI water at room temperature for 24 h and then weighted (W_w) after the water on the surface was removed. The wet solid was dried in a vacuum oven until the weight remains constant (W_d) to confirm the reversibility of the process. The formula to calculate water absorption was: water absorption = $(W_w - W_d) / W_d \times 100\%$.

4.3 Results and Discussion

4.3.1 Design of Synthesis

The proposed synthetic route for **M1** was inspired by the Ni-catalyzed P–C coupling route described by Cristau’s group (Scheme 4.2).³¹ This method involved using an excess (~5 equiv) of tolylbromide as solvent/reactant and heating at 200 °C for at least 24 h with ~70% yield. In order to decrease the amount of wasted aryl halide, shorten the reaction time, and improve the yield, we modified the procedure to include

diisopropylamine as a base to facilitate the requisite deprotonation steps.²⁴ Under these conditions, we found that the reaction went smoothly in ethylene glycol solvent after 15 h at 180 °C under N₂. Upon workup, **M1** was isolated as a highly hygroscopic yellow powder (Scheme 4.3).

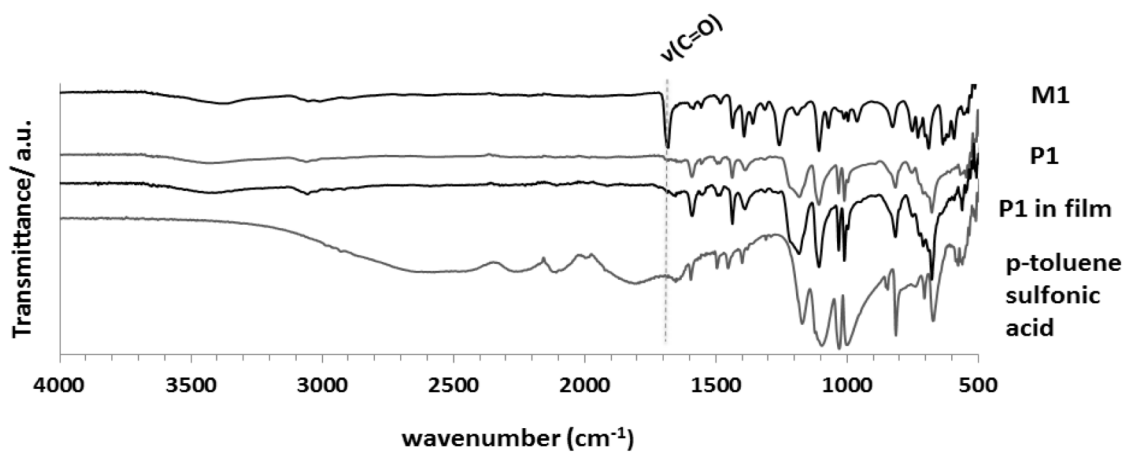


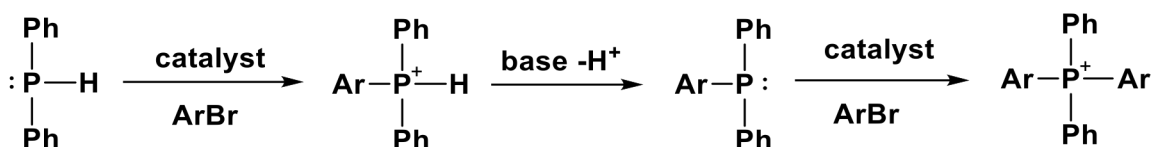
Figure 4.1: IR spectra of **M1**, **P1** (powder), **P1** (film) and *p*-toluene sulfonic acid.

To confirm the stability of a phosphonium species to the reaction conditions, commercial tetraphenylphosphonium bromide was first heated with PTSA under conditions identical to those used for the proposed cyclotrimerization. No degradation of the tetraphenylphosphonium salt was observed under these conditions, as probed by NMR spectra.

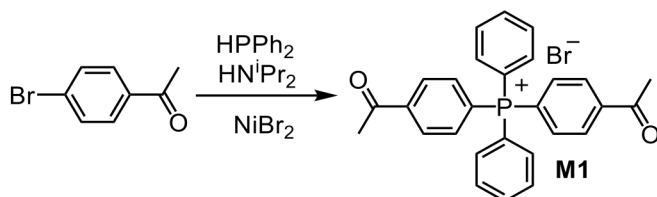
Cyclotrimerization of **M1** was carried out in a glass vial with 5 equiv of *p*-toluene sulfonic acid (PTSA) at 120 °C under N₂. The mixture melted around 100 °C, initially yielding a viscous yellow liquid. After 24 h of heating, the mixture had solidified, resulting in a dark brown monolith that holds the shape of the glass reaction vessel. When

a shallow stainless steel mold was used, the mixture formed a very smooth film (as determined by AFM, vide infra). The cyclotrimerization of **M1** proved to be a facile route to synthesize tetraarylphosphonium material to form smooth films or a variety of shapes based on the reaction vessel employed.

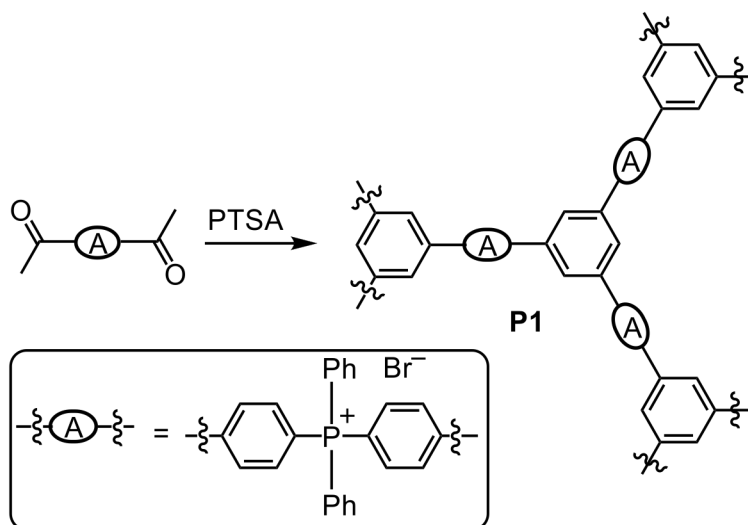
Removal of excess PTSA from as-prepared **P1** was affected either by soaking the



Scheme 4.2: P-C coupling route to $[\text{Ar}_2\text{PPh}_2]^+$ salts from HPPH_2 .



Scheme 4.3: Synthetic route to prepare **M1**.



Scheme 4.4: Synthetic route to prepare **P1**. PTSA = *p*-toluenesulfonic acid.

film in ethanol or by Soxhlet extraction with ethanol. The molecular composition of **P1** (in both powder and film state) was determined by IR spectroscopy (Figure 4.1). Solution NMR analysis was not possible due to the characteristic insolubility of network solids. By comparing the IR spectra of monomer **M1**, *p*-toluenesulfonic acid and **P1** in powder and film (Figure 4.1), it is clear that the carbonyl groups (C=O stretch at 1680 cm^{-1})³² have been completely consumed (within instrument detection limit) with concomitant emergence of the C=C stretch at 1600 cm^{-1} attributable to the 1,3,5- trisubstituted benzene rings in **P1**. The small band at 890 cm^{-1} is from out-of-plane bending vibrations of 1,3,5-trisubstituted benzene rings. The broad absorption in $2300\text{-}3000\text{ cm}^{-1}$ for *p*-toluenesulfonic acid is also absent in **P1** powder and film, confirming its success removal by ethanol treatment. The integrity of phosphorus center attached to phenyl ring was confirmed by the absorbance band at 1436 cm^{-1} .³³ The conversion from **M1** to **P1** was also confirmed by the close agreement between theoretical and experimental composition as determined by elemental microanalysis. The cross-linking degree can be calculated by the integrating the absorption bands of aliphatic and aromatic C-H stretch according to Kaskel group.³⁰ The ratio of aliphatic/aromatic C-H integration for **M1** and **P1** are 0.0422 and 0.0140, respectively. The cross-linking degree for **P1** is 67%, comparable to the value, 49%, reported in Kaskel group. The quantitative conversion of **M1** to **P1** is a significant improvement over the extents of reaction observed in the preparation of many neutral materials prepared by analogous methods. The X-ray powder diffraction analysis indicates that the material so-formed is amorphous (Appendix 4B).

4.3.2 Thermal and Chemical Stability

On the basis of our prior work with linear tetraarylphosphonium polymers,^{24,34} we expected **P1** to have good thermal stability. TGA was thus applied to probe the thermal stability of **P1**. The 5% decomposition temperatures ($T_{d,5\%}$) for **P1** are 379 °C and 370 °C in air and N₂, respectively (Figure 4.2). This value is comparable to the other polymer networks, for example, the diamond-like framework from the tetrahedral-vertex solid **R4** (Scheme 4.1B).⁴ Compared to neutral polymers prepared by same method, **P1** shows better thermal stability which is attributable at least in part to the absence of unreacted acetyl groups. Under N₂, **P1** has a char yield of about 40%, which is higher than most organic polymers but typical of other high-aromatic-content materials. In air the weight loss is essentially complete at ~710 °C, comparable to what was observed for other polymers synthesized via cyclotrimerization.

Tetraarylphosphonium polyelectrolytes are of particular interest compared to

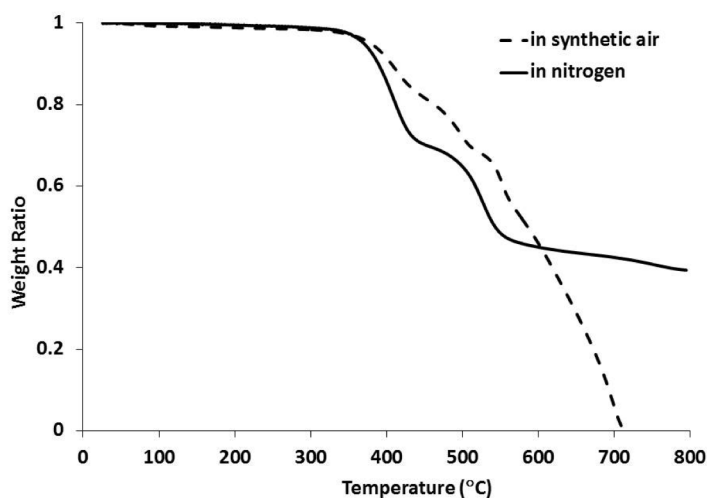


Figure 4.2: TGA curves of **P1** under N₂ (solid line) and synthetic air (dashed line).

alkylphosphonium analogues due to their generally improved alkaline stability.^{22,24} To assess the extent to which **P1** withstands alkaline exposure, films of the material were soaked in 6 M NaOH solution at room temperature or 60 °C for 24 h. The structure of **P1** after base treatment was determined by IR spectra (Figure 4.3). A comparison of the spectra before and after base treatment are almost identical other than the change in peaks at $\sim 1000\text{-}1050\text{ cm}^{-1}$ attributable to the expected exchange of bromide to hydroxide counteranion in **P1**,³³ without loss of the phosphonium network structure. The good chemical stability indicates that the highly cross-linked network in **P1** could prevent the attack from hydroxide ion.

4.3.3 Film Morphology and Physisorption

As-synthesized films of **P1** were examined by atomic force microscopy (AFM), revealing a very smooth surface with root mean squared roughness (R_{rms}) of 3 nm (AFM

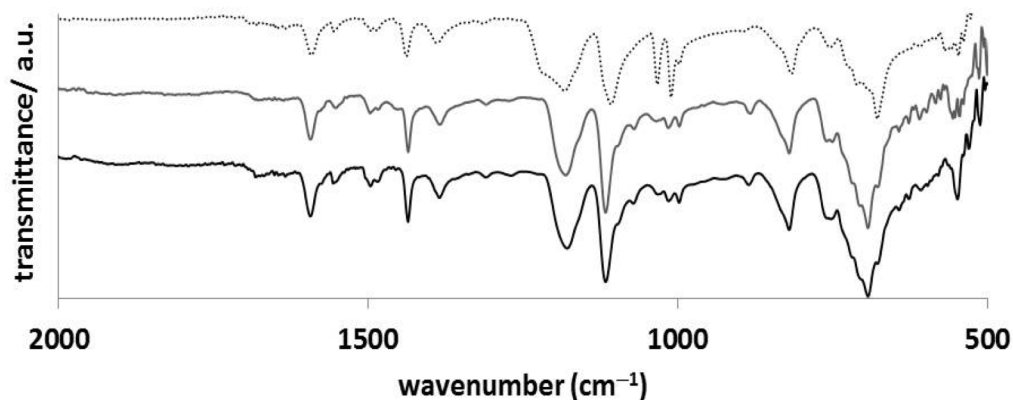


Figure 4.3: IR spectra of **P1** (top, dashed line) and **P1** after soak in 6 M NaOH(aq) for 24h at room temperature (middle, grey line) and 60 °C (bottom, black line).

images are provided in Appendix 4B). The transmission electron microscopy (TEM) and scanning electron microscopy (SEM) images (Appendix 4B) showed that **P1** has a layered structures similar to those of a polymer previously synthesized via cyclotrimerization,³⁰ but revealed no other features of note.

The surface area measurement was carried out by nitrogen physisorption at 77 K (Figure 4.4). The isotherm shape is typical for type-II isotherms according to the IUPAC classification, indicating a non-porous material.³⁵ The specific surface area and total pore volume based on BET are 9.021 m²/g and 0.014 cm³/g, respectively. This value was comparable to some charged polymer made from ionic liquids via cyclotrimerization as well as other organic frameworks.²⁸ Polymers tend to form non-porous solids when flexible chains allow for space-efficient packing.³⁶ Another possible reason for the small specific surface area of **P1** is due to the better solubility of **M1** in *p*-toluene sulfonic acid, which leads to less macrophase separation and formation of a more closely-layered structure during synthesis.³⁶ A similar situation was observed by the Kaskel group when they used different monomers bearing diacetyl group to synthesize polymers. They found that monomers bearing amino groups tend to have nonporous structure because the amino groups were protonated to form ammonium moieties during synthesis, leading to a better solubility in molten *p*-toluenesulfonic acid through ion pair formation.¹⁰ The phosphonium moieties in a growing sample of **P1** similarly improve its solubility in the highly polar PTSA versus neutral organic monomers. This may also explain the improved extent of reaction in forming **P1** compared to that observed for materials prepared from less soluble neutral analogues.

The ionic nature of **P1** could potentially be exploited for selective interaction with polar molecules. To assess this possibility, we examined the ability of **P1** to adsorb CO₂. The sorption isotherms of CO₂ at 273 K indicate a type-II material. During the whole process, the volume increases gradually, which indicates a stable physisorption as

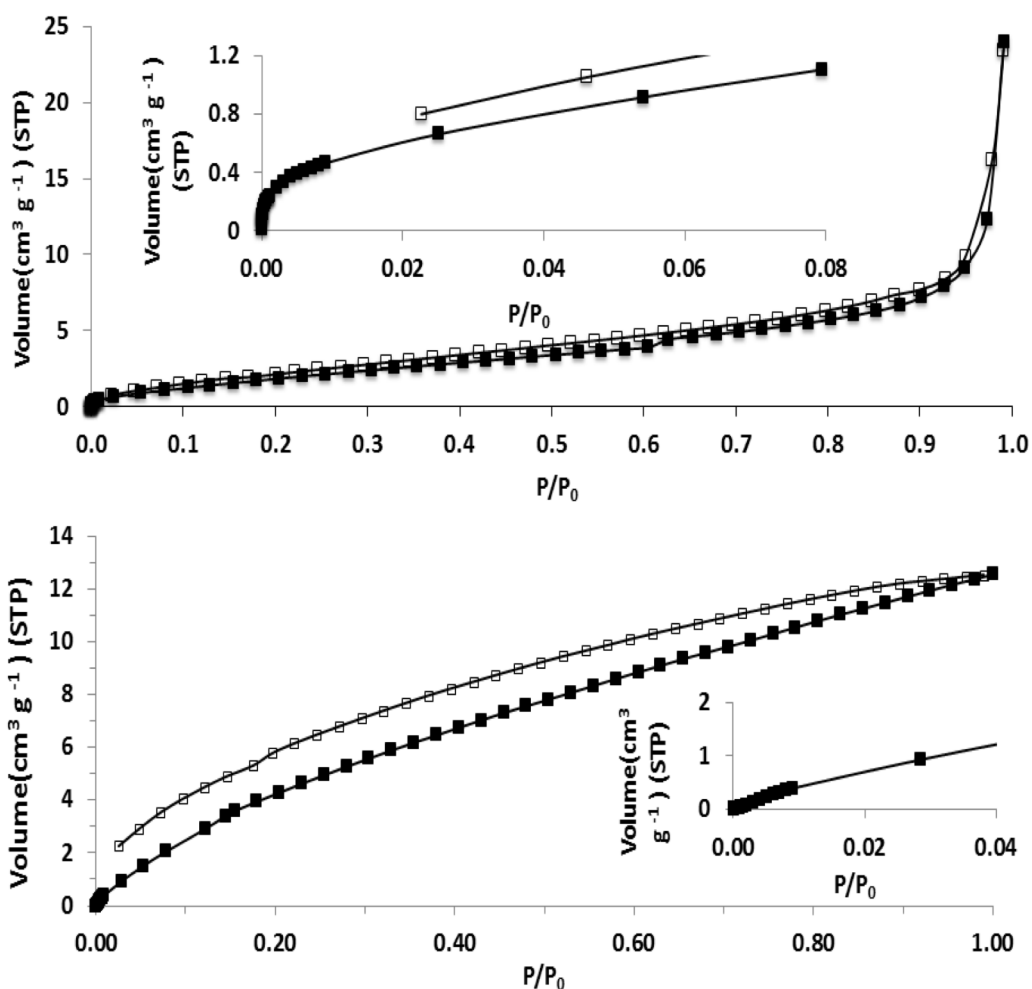


Figure 4.4: Nitrogen sorption isotherms at 77 K (top) and CO₂ sorption isotherms at 273 K (bottom) of **P1**. Adsorption points are presented by filled squares and desorption by empty squares.

pressure increases. The specific surface area measured by BET is 27.913 m²/g, which is larger than the result yield by N₂. This is as expected, because CO₂ is known as a surface sensitive gas and the isotherm shape /surface area measured for CO₂ reveals a stronger interaction between **P1** and CO₂. This observation is also consistent with the widespread use of phosphonium salts as CO₂ capture/catalysis reagents.⁶

Water is another polar molecule that might be expected to be taken up by **P1**. Due to the non-porous structure of **P1** revealed by N₂ sorption, the water uptake is only 10.63%. This number is comparable to the values reported by Kaskel (12±3%), which indicates weak interaction with water.¹⁰

4.4 Conclusions

A versatile route for phosphonium-modified framework synthesis via cyclotrimerization was demonstrated. The polymer shows good alkaline and thermal stability as well as affinity for CO₂. These properties suggest potential applications in gas separation, catalysis and alkaline fuel cells.

4.5 References

1. J. L. C. Rowsell, A. R. Millward, K. S. Park, O. M. Yaghi. *J. Am. Chem. Soc.* **2004**, *126*, 5666-5667.
2. W. G. Lu, J. P. Sculley, D. Q. Yuan, R. Krishna, Z. W. Wei, H. C. Zhou. *Angew. Chem. Int. Ed.* **2012**, *51*, 7480-7484.
3. H. Furukawa, N. Ko, Y. B. Go, N. Aratani, S. B. Choi, E. Choi, A. O. Yazaydin, R. Q. Snurr, M. O'Keeffe, J. Kim, O. M. Yaghi. *Science* **2010**, *329*, 424-428.

4. D. Q. Yuan, W. G. Lu, D. Zhao, H. C. Zhou. *Adv. Mater.* **2011**, *23*, 3723-3725.
5. W. G. Lu, D. Q. Yuan, D. Zhao, C. I. Schilling, O. Plietzsch, T. Muller, S. Brase, J. Guenther, J. Blumel, R. Krishna, Z. Li, H. C. Zhou. *Chem. Mat.* **2010**, *22*, 5964-5972.
6. J. Q. Wang, J. G. W. Yang, G. S. Yi, Y. G. Zhang. *Chem. Commun.* **2015**, *51*, 15708-15711.
7. N. B. McKeown, P. M. Budd. *Chem. Soc. Rev.* **2006**, *35*, 675-683.
8. G. Ferey, C. Mellot-Draznieks, C. Serre, F. Millange, J. Dutour, S. Surble, I. Margiolaki. *Science* **2005**, *309*, 2040-2042.
9. B. F. Zhang, Z. G. Wang. *Chem. Commun.* **2009**, 5027-5029.
10. F. M. Wisser, K. Eckhardt, D. Wisser, W. Bohlmann, J. Grothe, E. Brunner, S. Kaskel. *Macromolecules* **2014**, *47*, 4210-4216.
11. X. Yang, C. A. Conrad, W. Wan, M. S. Bedford, L. Hu, G. Chumanov, R. C. Smith. *J. Mater. Chem. C* **2015**, *3*, 4537-4544.
12. C. A. Conrad, M. S. Bedford, A. A. Buel, Y. Galabura, I. Luzinov, R. C. Smith. *Polym. Int.* **2015**, *64*, 1381-1388.
13. G. Decher. *Science* **1997**, *277*, 1232-1237.
14. P. Schaaf, J. B. Schlenoff. *Langmuir* **2009**, *25*, 14007-14010.
15. J. A. Jaber, J. B. Schlenoff. *Curr. Opin. Colloid Interface Sci.* **2006**, *11*, 324-329.
16. S. L. Kristufek, T. R. Maltais, E. G. Tennyson, N. C. Osti, D. Perahia, A. G. Tennyson, R. C. Smith. *Polym. Chem.* **2013**, *4*, 5387-5394.
17. E. G. Tennyson, S. He, N. C. Osti, D. Perahia, R. C. Smith. *J. Mater. Chem.* **2010**, *20*, 7984-7989.

18. E. G. Tennyson, R. C. Smith. *Inorg. Chem.* **2009**, *48*, 11483-11485.
19. S. T. Hemp, M. Q. Zhang, M. H. Allen, S. J. Cheng, R. B. Moore, T. E. Long. *Macromol. Chem. Phys.* **2013**, *214*, 2099-2107.
20. S. T. Hemp, M. S. Zhang, M. Tamami, T. E. Long. *Polym. Chem.* **2013**, *4*, 3582-3590.
21. B. C. Lin, L. H. Qiu, J. M. Lu, F. Yan. *Chem. Mat.* **2010**, *22*, 6718-6725.
22. S. Gu, R. Cai, T. Luo, Z. Chen, M. Sun, Y. Liu, G. He, Y. Yan. *Angew. Chem. Int. Ed.* **2009**, *48*, 6499-6502.
23. C. G. Cassity, A. Mirjafari, N. Mobarrez, K. J. Strickland, R. A. O'Brien, J. H. Davis, Jr. *Chem. Commun.* **2013**, *49*, 7590-7592.
24. W. Wan, X. Yang, R. C. Smith. *Chem. Commun.* **2017**, *53*, 252-254.
25. T. J. Cuthbert, T. D. Harrison, P. J. Ragogna, E. R. Gillies. *J. Mater. Chem. B* **2016**, *4*, 4872-4883.
26. T. J. Cuthbert, R. Guterman, P. J. Ragogna, E. R. Gillies. *J. Mater. Chem. B* **2015**, *3*, 1474-1478.
27. K. J. T. Noonan, K. M. Hugar, H. A. Kostalik, E. B. Lobkovsky, H. D. Abruna, G. W. Coates. *J. Am. Chem. Soc.* **2012**, *134*, 18161-18164.
28. J. S. Lee, H. M. Luo, G. A. Baker, S. Dai. *Chem. Mat.* **2009**, *21*, 4756-4758.
29. J. R. Sampey. *J. Am. Chem. Soc.* **1940**, *62*, 1953-1953.
30. M. Rose, N. Klein, I. Senkovska, C. Schrage, P. Wollmann, W. Bohlmann, B. Bohringer, S. Fichtner, S. Kaskel. *J. Mater. Chem.* **2011**, *21*, 711-716.
31. H. J. Cristau, A. Chene, H. Christol. *J. Organomet. Chem.* **1980**, *185*, 283-295.

32. T. Islamoglu, M. G. Rabbani, H. M. El-Kaderi. *J. Mater. Chem. A* **2013**, *1*, 10259-10266.
33. L. W. Daasch, D. C. Smith. *Anal. Chem.* **1951**, *23*, 853-868.
34. M. S. Bedford, X. Yang, K. M. Jolly, R. L. Binnicker, S. B. Cramer, C. E. Keen, C. J. Mairena, A. P. Patel, M. T. Rivenbark, Y. Galabura, I. Luzinov, R. C. Smith. *Polym. Chem.* **2015**, *6*, 900-908.
35. K. S. W. Sing, D. H. Everett, R. A. W. Haul, L. Moscou, R. A. Pierotti, J. Rouquerol, T. Siemieniewska. *Pure & Appl. Chem.* **1985**, *57*, 603-619.
36. P. M. Budd, B. S. Ghanem, S. Makhseed, N. B. McKeown, K. J. Msayib, C. E. Tattershall. *Chem. Commun.* **2004**, 230-231.

APPENDICES

Appendix 4A

NMR and IR spectra

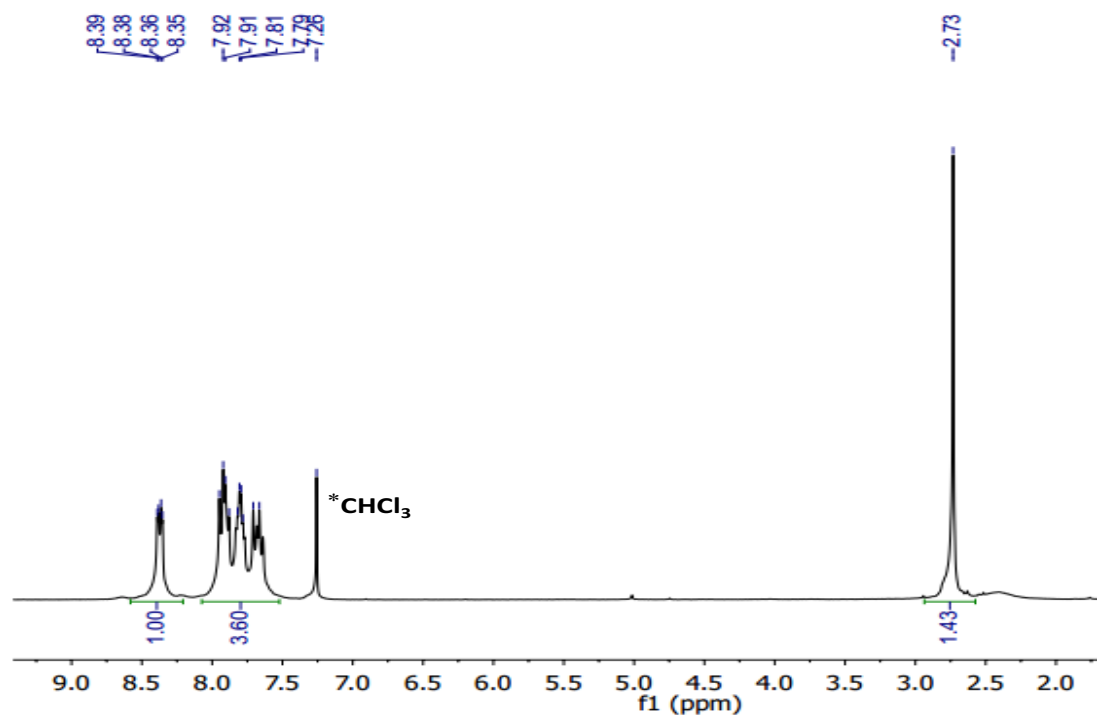


Figure 4 A.1: Proton NMR spectrum of **M1** (CDCl₃, 300 MHz). Each peak marked with an asterisk corresponds to a solvent signal.

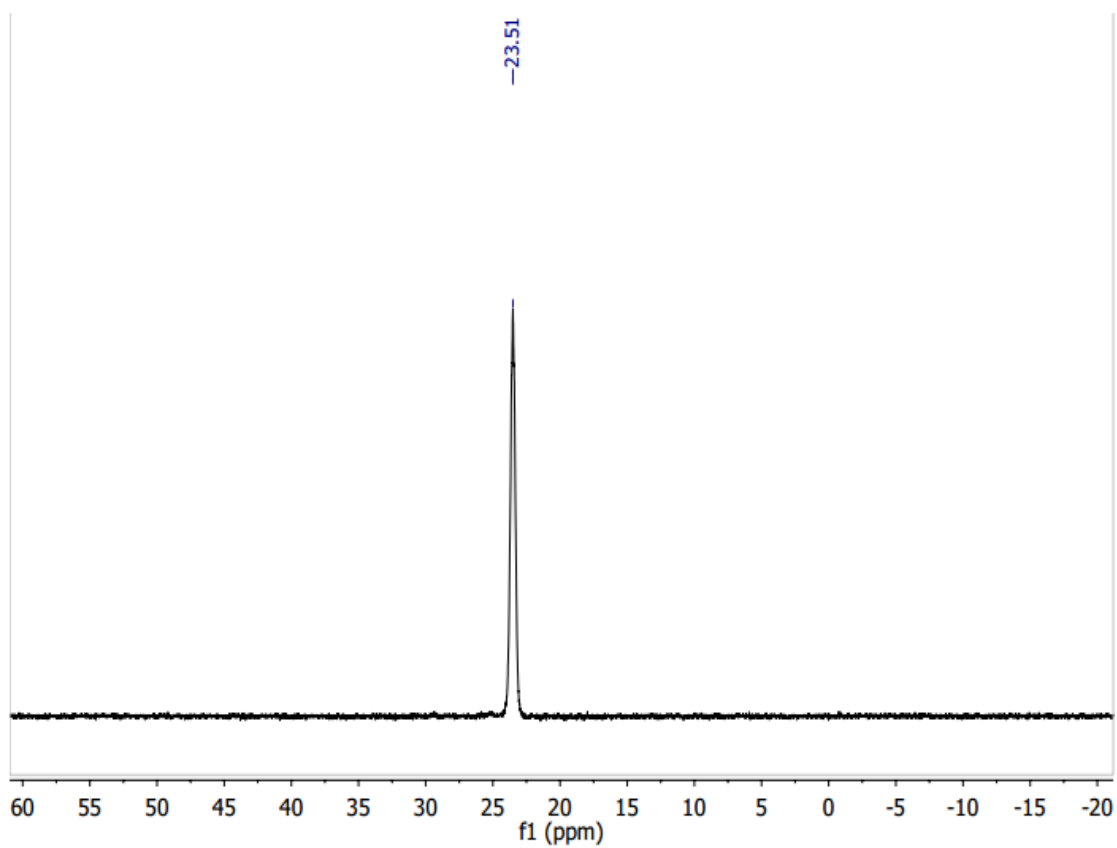


Figure 4 A.2: Phosphorus-31 NMR spectrum of **M1** (CDCl₃, 121 MHz).

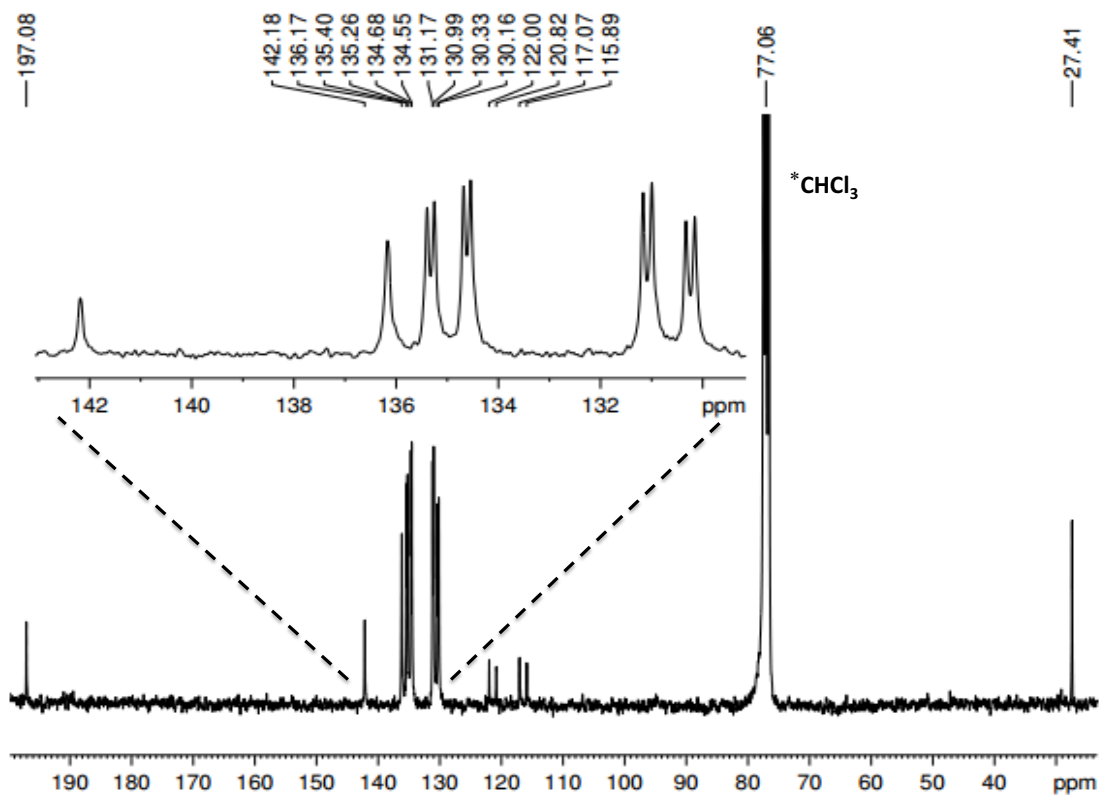


Figure 4 A.3: Carbon-13 NMR spectrum of **M1** (CDCl₃, 75 MHz). Each peak marked with an asterisk corresponds to a solvent signal.

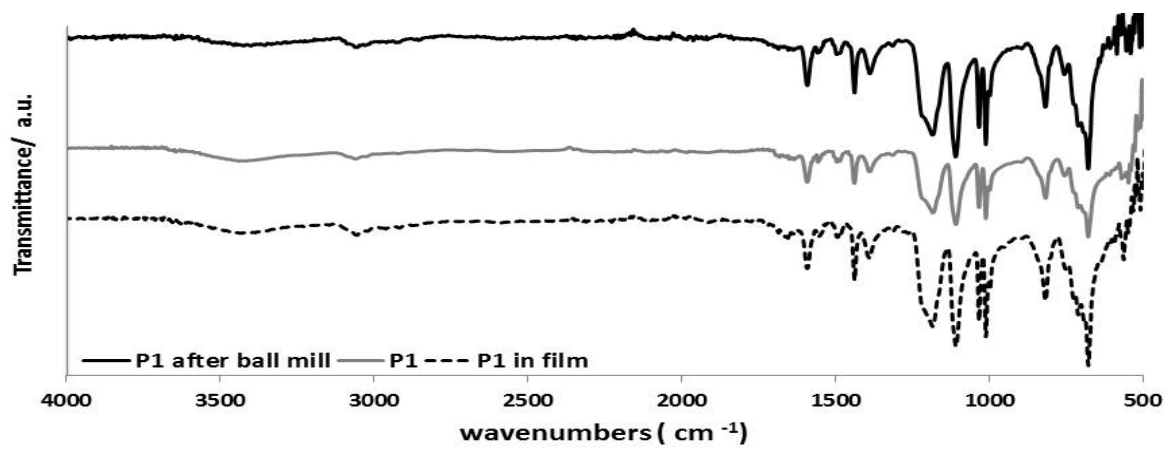


Figure 4 A.4: IR spectra of **P1** in different forms

Appendix 4B

X-ray powder diffraction Trance

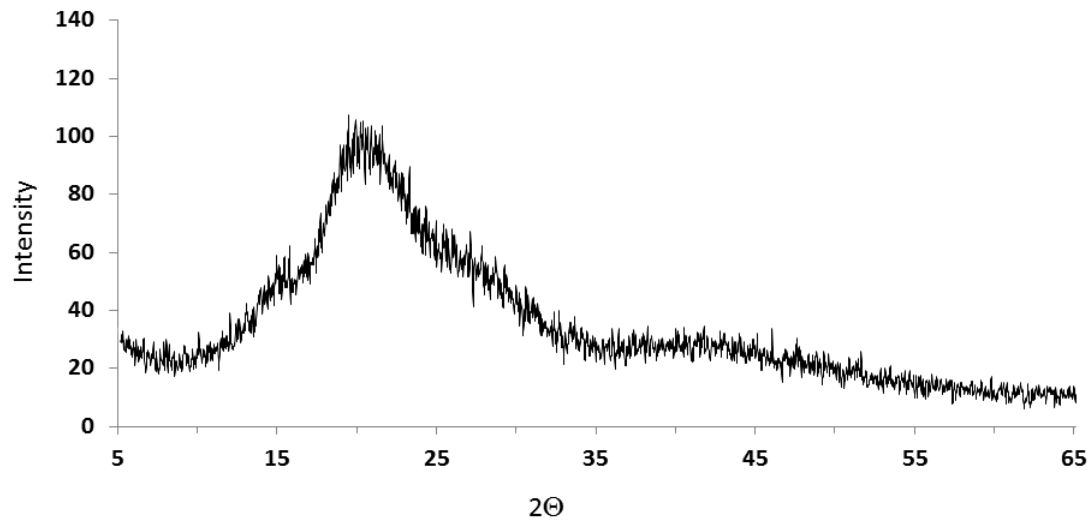


Figure 4 B.1: X-ray powder diffraction of **P1**.

Appendix 4C

AFM, SEM and TEM images

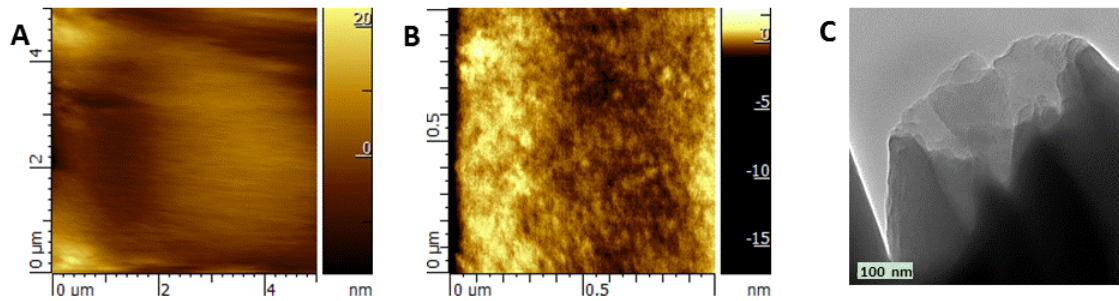


Figure 4 C.1: AFM 2D height $5 \times 5 \mu\text{m}$ (A) and $1 \times 1 \mu\text{m}$ (B) images and TEM image (C) of **P1** in film.

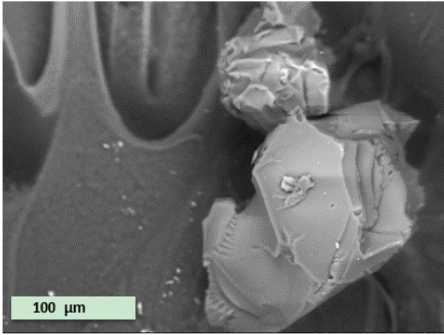





Figure 4 C.2: SEM image (scale bar = 100 μm) of **P1**

Appendix 4D

Reprint Permission

0150017 RightsLink® by Copyright Clearance Center

 **RightsLink®** [Home](#) [Account Info](#) [Help](#) 

 **Title:** A new route to phosphonium polymer network solids via cyclotrimerization
Author: Xiaoyan Yang, Yimei Wen, George Chumanov, Rhett C. Smith
Publication: Journal of Polymer Science Part A: Polymer Chemistry
Publisher: John Wiley and Sons
Date: Mar 7, 2017
© 2017 Wiley Periodicals, Inc.

Logged in as: Xiaoyan Yang
Account #: 3001055175
[Logout](#)

Order Completed
Thank you for your order.

This Agreement between Xiaoyan Yang ("you") and John Wiley and Sons ("John Wiley and Sons") consists of your license details and the terms and conditions provided by John Wiley and Sons and Copyright Clearance Center.

Your confirmation email will contain your order number for future reference.

[Printable details.](#)

License Number	4130041400231
License date	Jun 15, 2017
Licensed Content Publisher	John Wiley and Sons
Licensed Content Publication	Journal of Polymer Science Part A: Polymer Chemistry
Licensed Content Title	A new route to phosphonium polymer network solids via cyclotrimerization
Licensed Content Author	Xiaoyan Yang, Yimei Wen, George Chumanov, Rhett C. Smith
Licensed Content Date	Mar 7, 2017
Licensed Content Pages	6
Type of use	Dissertation/Thesis
Requestor type	Author of this Wiley article
Format	Print and electronic
Portion	Full article
Will you be translating?	No
Title of your thesis / dissertation	Synthesis and Structure-Property Relationships of Phosphonium Polymers
Expected completion date	Aug 2017
Expected size (number of pages)	200
Requestor Location	Xiaoyan Yang 101 regency dr. Apt-59 CENTRAL, SC 29630 United States Attr: Xiaoyan Yang
Publisher Tax ID	EUB0007151
Billing Type	Invoice
Billing address	Xiaoyan Yang 101 regency dr. Apt-59 CENTRAL, SC 29630

<https://100.copyright.com/AppDispatchServlet> 1/2

6/15/2017

Rightslink® by Copyright Clearance Center

United States
Attn: Xiaoyan Yang
0.00 USD

Total

Would you like to purchase the full text of this article? If so, please continue on to the content ordering system located here: [Purchase PDF](#)

If you click on the buttons below or close this window, you will not be able to return to the content ordering system.

[ORDER MORE](#)

[CLOSE WINDOW](#)

Copyright © 2017 [Copyright Clearance Center, Inc.](#) All Rights Reserved. [Privacy statement](#). [Terms and Conditions](#).
Comments? We would like to hear from you. E-mail us at customercare@copyright.com

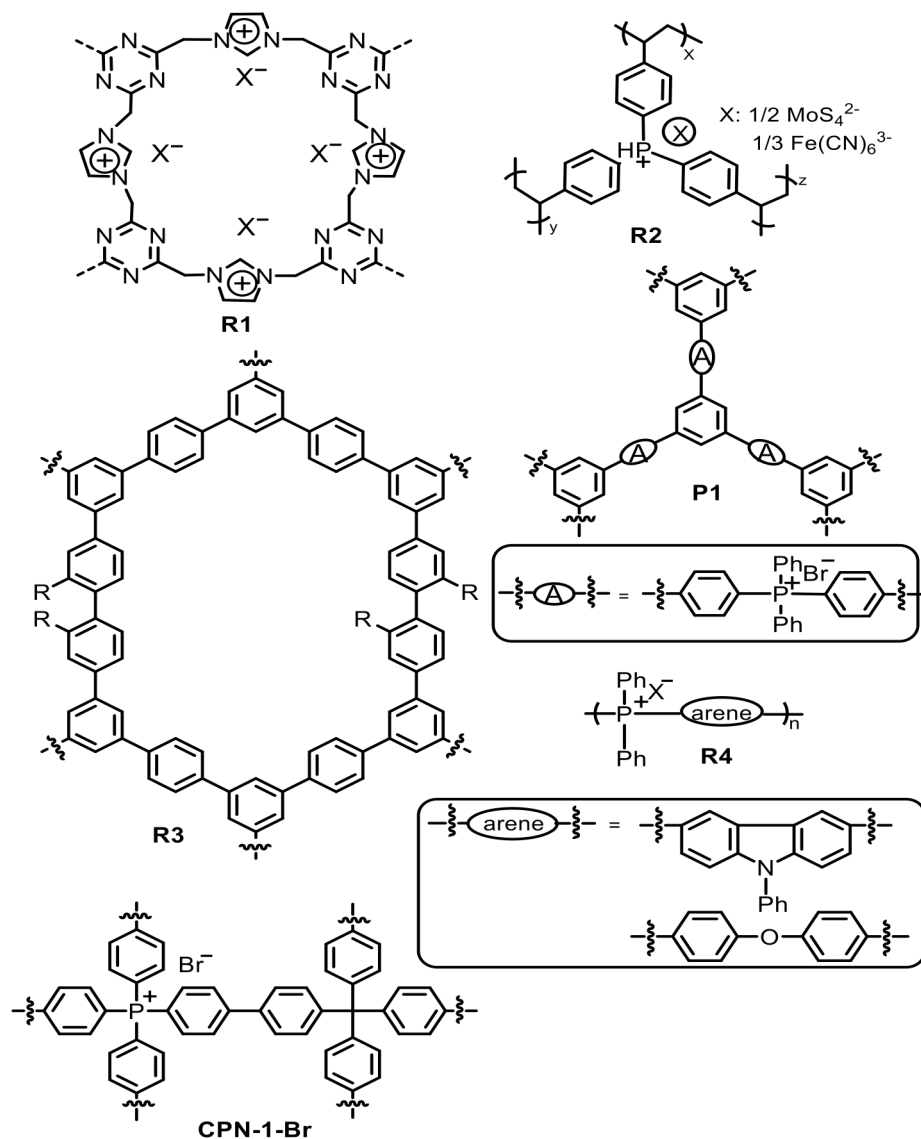
CHAPTER FIVE
STRUCTURE-PROPERTY RELATIONSHIPS OF PHOSPHONIUM POLYMER
FRAMEWORKS: THERMAL STABILITY, CHEMICAL STABILITY AND
SURFACE AREA^{††}

The advent of covalent organic frameworks (COFs) has extended to two- and three-dimensional frameworks having robust properties such as low density and high internal surface area, making them promising for catalysts, gas separation and storage, and drug delivery applications.¹⁻¹⁰ Among COFs, polymer frameworks incorporating ionic groups with intriguing properties such as high gas selectivity and electrochemical activity have received increasing attention.^{7,11} Ionic polymer frameworks with cationic sites such as phosphonium and imidazolium groups have been reported to be promising candidates in ion-exchange membrane and CO₂ capture.¹¹⁻¹³ For example, Thomas's group reported a tetraphenylphosphonium COFs synthesized from Yamamoto coupling (CPN-1-Br) that had BET surface area of 1455 m²/g and CO₂ uptake of 2.49 mmol/g at 273 K and 1 bar.² Compared to their ammonium analogues, phosphonium salts often have dramatically improved thermal and chemical stability.¹⁴⁻¹⁶

Driven by the growing interest, tailoring properties of ionic polymer frameworks with functional groups have been carried out since then. Long and coworkers carried out an extensive structure-property relationship study of phosphonium polymers and their applications in gene delivery.^{14,17} The Smith group has explored chromophore-derivatized phosphonium polymers, layer-by-layer assembly of phosphonium polymers with

^{††} This chapter is being developed for submission to a journal for publication.

conjugated polyelectrolytes, and studied on incorporating tetraarylphosphonium groups into polymer main chains to improve their thermal and alkaline stability.¹⁸⁻²⁵



Scheme 5.1: Example of COFs.

Tetraarylphosphonium salts in the form of $[\text{PAr}_4]^+[\text{NTf}_2]^-$ was demonstrated to be thermally stable in air under 425 °C for 120 h. As expected, polymers incorporating tetraarylphosphonium units in their backbone, like **R4** (Scheme 5.1), for example, can be

thermally stable up to 460 °C as well as exhibiting <3% decomposition in 6 M NaOH at 60 °C for 24 h.

There are two common methods for generating functional ionic polymers. The first method is post-polymerization modification.^{26,27} For example, **R2** in Scheme 5.1 was prepared by post-polymerization modification to afford a material having superior electro-catalytic activity for the hydrogen evolution reaction (HER) under acidic conditions.⁷ The second route is to design specific monomers as building blocks for polymer frameworks.²⁸ Polymerization with functionalized monomers required fewer steps and enables more precise control in incorporation of functional groups desired for endowing specific properties. An ionic example is Dai's report of a cross-linked imidazolium polymer (**R1** in Scheme 5.1) exhibiting high anion-exchange capacity that was synthesized in one step via cyclotrimerization.²⁹

In our previous work, tetraarylphosphonium polymer frameworks like **P1** (Scheme 5.1) have good thermal and chemical stability, making them attractive candidates for ion-exchange membranes and CO₂ capture applications.²⁵ Considering the relatively small specific surface area of **P1** (9 m²/g), it is desired that phosphonium polymer frameworks with higher specific surface areas that may facilitate interaction with CO₂ could be prepared. Kaskel's group reported that the pore size of **R3** (Scheme 5.1) could be precisely tuned by controlling the monomer ratio and conditions for its synthesis from 1,4-diacetylbenzene and 4,4'-diacetylbiphenyl. The specific surface area of such copolymers can be as high as 720 m²/g and the R group influences the surface polarity and thus affinity for particular gas molecules.³⁰ Tilford, *et al.* further

demonstrated that the pore size and gas adsorption properties could be tuned by selecting different alkyl-functionalized monomers.²⁸

Herein, we examine tetraarylphosphonium-derivatized COFs **P1-P4** prepared via copolymerization of **M1** and **M2** (Scheme 5.2). The effect of phosphonium content on the thermal stability, alkaline stability, water uptake, specific surface area and affinity of CO₂ were elucidated.

5.2 Experimental

5.2.1 General considerations

Air-sensitive reactions were performed in an MBraun UNILab glovebox under nitrogen. Chemicals were used without further purification from suppliers.

5.2.2 Synthesis of **P2**

The cyclotrimerization procedures and synthesis of **M1** followed the method described previously.^{25,31} In a typical reaction, **M1** (0.400 g, 0.795 mmol), **M2** (0.129 g, 0.795 mmol) and *p*-toluenesulfonic acid monohydrate (PTSA, 1.512 g, 7.95 mmol) were mixed in a beaker with a watch glass as cover and heated to 120 °C for 24 h under N₂. Soxhlet extraction with ethanol yield 0.472 g (118.9%) black chunks.

5.2.3 Synthesis of **P3**

M1 (0.250 g, 0.497 mmol), **M2** (0.161 g, 0.993 mmol) and *p*-toluenesulfonic acid monohydrate (PTSA, 1.417 g, 7.45 mmol) were mixed in a beaker with a watch glass as cover and heated to 120 °C for 24 h under N₂. Soxhlet extraction with ethanol yield 0.394 g (109.8%) dark brown chunks.

5.2.4 Synthesis of **P4**

M1 (0.300 g, 0.596 mmol), **M2** (0.387 g, 2.384mmol) and *p*-toluenesulfonic acid monohydrate (PTSA, 2.834 g, 14.90 mmol) were mixed in a beaker with a watch glass as cover and heated to 120 °C for 24 h under N₂. Soxhlet extraction with ethanol yield 0.579 g (111.9%) red chunks.

5.2.5 Anion Exchange

Around 50 mg of polymer samples were soaked in 1 M LiNTf₂ (aq) ([NTf₂]⁻, Tf = -SO₂CF₃) for 72 h at room temperature. Then the solids were washed by DI water several times before soaked in DI water for 24 h to remove excess bis(trifluoromethane)-sulfonamide anion ([NTf₂]⁻). IR spectra (See Appendix 5A) and elemental analysis used to assess the extent of anion exchange (Table 5.2). The percent yields for **P2-NTf₂**, **P3-NTf₂** and **P4-NTf₂** are 80.0%, 95.3% and 77.1%, respectively.

5.2.6 Characterization

Fourier transformed infrared spectra were recorded on Shimadzu IRAffinity-1S at 400-4000 cm⁻¹ at room temperature. Nitrogen and CO₂ sorption measurements were collected on a Quantachrome ASIQwinTM at 77 K. The samples were degassed at 80 °C for 10 h before measurements. BET surface areas are determined over a P/P₀ range (0.05-0.30). Thermogravimetric analysis (TGA) was performed on TA Instruments Q60 TGA from 25 °C to 800 °C with a heating rate of 5 °C min⁻¹ under N₂. For base stability measurement, solids were soaked in 6 M NaOH solution at room temperature and 60 °C over a 24 - 120 h period, respectively. Then the solids were soaked in DI water for another 24 h to remove excess hydroxide ions. Base stability was evaluated by comparing the IR spectra before and after base treatment. Polymer samples were soaked in DI water

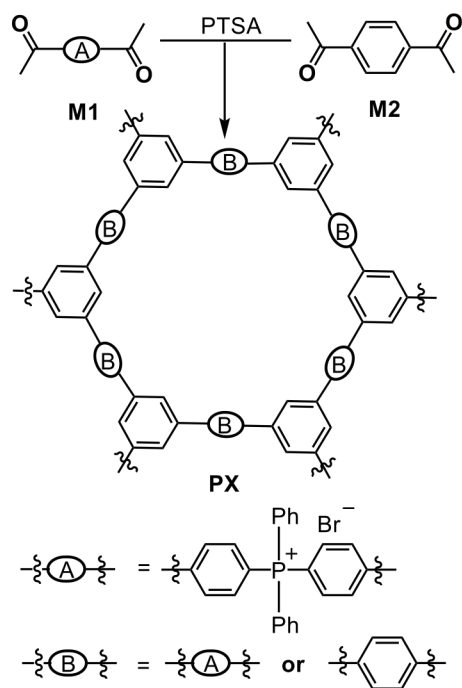
at room temperature for 24 h and then weighed (W_w) after the water on the surface was removed. The wet solid was dried in a vacuum oven until the weight remains constant (W_d) to confirm the reversibility of the process. The formula to calculate water absorption was: $\text{water absorption} = (W_w - W_d) / W_d \times 100\%$.

5.3 Results and discussion

5.3.1 Design of Synthesis

Cyclotrimerization of **M1** and **M2** were carried out in different ratios in an effort to elucidate the influence of phosphonium monomer (**M1**) incorporation on salient properties. Thus, polymers having 100%, 50%, 33% and 20% **M1** feed ratio (**P1-P4**, respectively, Scheme 5.2) were prepared. The reaction went smoothly under N_2 and yielded dark-colored monoliths, a result consistent with observations reported in the course of synthesizing similar, ion-free analogues of **P1-P4**.³⁰ IR spectra and elemental microanalysis (Table 5.2) were undertaken for initial structural characterization. Analysis of IR spectra (Figure 5.1) reveal that in all cases the band attributable to the carbonyl functionality (1690 cm^{-1}) is absent in **P1-P4** within the detection limit, indicating quantitative consumption of carbonyl groups during polymerization. Soxhlet extraction effectively removed any remaining *p*-toluenesulfonic acid, as evidenced by disappearance of the broad band at $2300\text{-}3000\text{ cm}^{-1}$. Elemental microanalysis results of **P1-P4** agree well with the theoretical value that was calculated based on total conversion by cyclotrimerization (Table 5.2). Among the three polymers, experimental microanalysis results for **P2** best approximate the ideal model with 100% cyclotrimerization. This is probably due to the better solubility of **M1** than **M2** in PTSA, which lead to higher

conversion by cyclotrimerization.³⁰ This is further confirmed by the microanalysis of **P1** which is very close to the theoretical values of microanalysis based on total conversion by cyclotrimerization.²⁵ Similar to **P1**, the C=C stretch at 1591 cm⁻¹ attributable to the 1,3,5-trisubstituted benzene rings present in all polymer samples.²⁵ The band at 825 cm⁻¹ in **M2**, attributable to out-of-plane bending of benzene rings, shifted to lower wavenumbers as the amount of *para* substituted benzene rings increase due to **M1**.³⁰ The



Scheme 5.2: Synthetic route of polymer network **PX** (X=1, 2, 3 and 4) from cyclotrimerization of **M1** and **M2** in a molar ratio of 0:1 (**P1**), 1:1 (**P2**), 1:2 (**P3**) and 1:4(**P4**).

intensity of the band at 1116 cm⁻¹, attributable to the stretch of P⁺-Ph, was expected to depend on the amount of phosphonium sites in the polymer framework.^{15,32} Analysis of

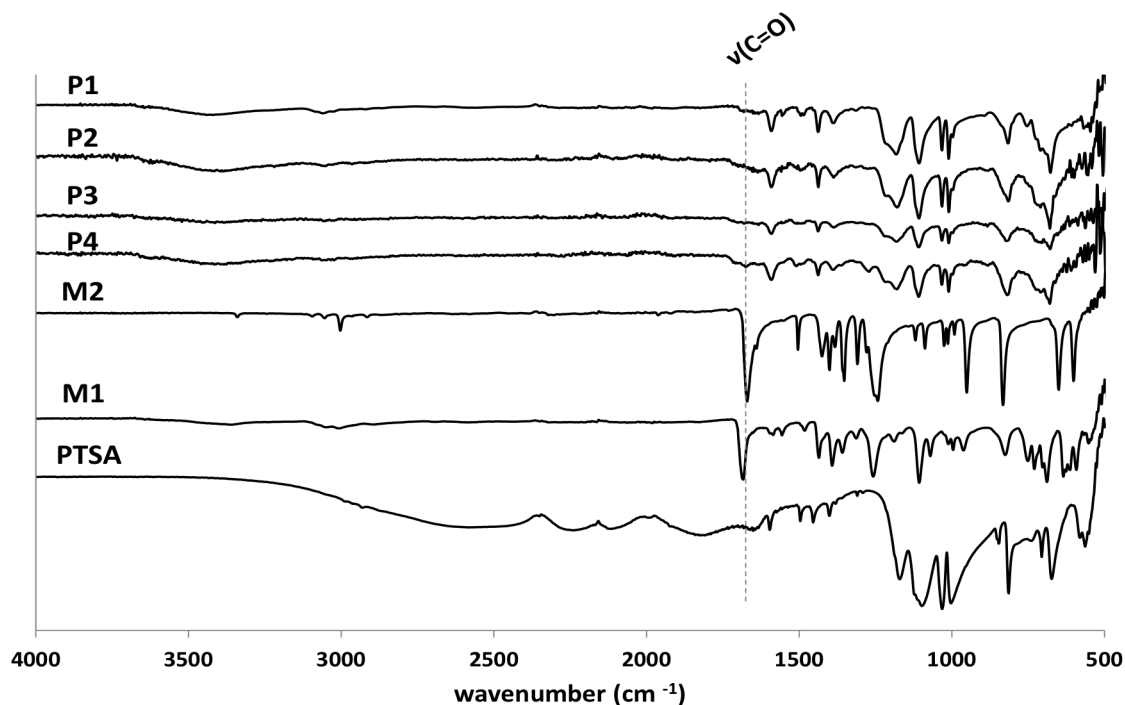


Figure 5.1: IR spectra of Phosphonium-containing COFs (**P1-P4**) and starting materials **M1**, **M2** and *p*-toluene sulfonic acid.

the relative intensities of the bands at 1591 and 1116 cm^{-1} for **P1-P4** is summarized in Table 1. From **P1** to **P4**, the molar percentage of phosphonium decreases from 100% to 20% of the monomers, with concomitant decrease in absorbance at 1116 cm^{-1} . The ratio of absorbance at 1116 and 1591 cm^{-1} correlates linearly with the percentage of phosphonium units in the COFs (Figure 5.2).

5.3.2 Thermal Stability

The thermal stability of **P1-P4** (Figure 5.3 and Table 5.2) was evaluated by TGA under N_2 . One notable trend is that the char yield varies linearly with phosphonium content in the COF, extrapolating to a maximum char yield of $\sim 70\%$ that has been reported for analogous phosphonium-free polyphenylene materials (Figure 5.3B).^{33,34} The

Table 5.1: Absorbance of bands at 1591 and 1116 cm^{-1} for **P1- P4**.

Polymer	Phosphonium Content (%)	Absorbance		1116:1591
		1116 cm^{-1}	1591 cm^{-1}	
P1	100	0.368	0.117	3.146
P2	50	0.148	0.060	2.478
P3	33	0.143	0.064	2.222
P4	20	0.088	0.049	1.803

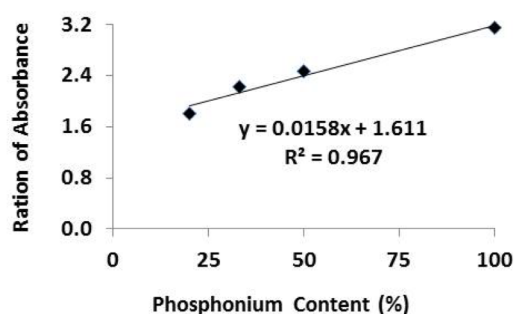


Figure 5.2: Scatter plot of absorbance ratio at 1116:1591 cm^{-1} to the phosphonium content for **P1-P4**.

$T_{d,5\%}$ for **P1-P4** all lie within the range of 350-370 $^{\circ}\text{C}$.²⁵ Our previous work revealed that the first degradation phenomenon in these materials is attributable to loss of HBr ,^{25, 35} and that exchange of bromide counterions for ditriflamide ($[\text{NTf}_2]^-$) can consequently lead to significant improvements in thermal stability.^{32,36} The ditriflamide analogues **P2-NTf₂**, **P3-NTf₂** and **P4-NTf₂** were thus prepared for analysis by TGA. The characteristic bands for the anion C–F stretch and asymmetric SO_2 stretch at 1172 and 1338 cm^{-1} , respectively,^{15,37} coupled with changes in bands at 1000-1050 cm^{-1} corresponding to the anion change in the IR spectra provide a facile way to follow the anion exchange process (data from Appendix 5A are summarized in Table 5.2).²⁵ The elemental microanalysis

results for **P2-NTf₂**, **P3-NTf₂** and **P4-NTf₂** likewise reveal near quantitative anion exchange in all three cases. The $T_{d,5\%}$ for [NTf₂]⁻ exchanged COFs (414-435 °C) are notably higher than was observed for the corresponding bromide parents **P1-P3**. Among the three phosphonium polymer frameworks, the thermal stability of **P2** increased the most (by ~80 °C) after anion exchange. This is expected because it has the greatest percent mass loss attributable to HBr loss among the three COFs that were anion-exchanged.

The char yield of **P2-NTf₂**, **P3-NTf₂** and **P4-NTf₂** increases as the phosphonium content increase which is consistent with what was found in **P2-4**. By comparing the char

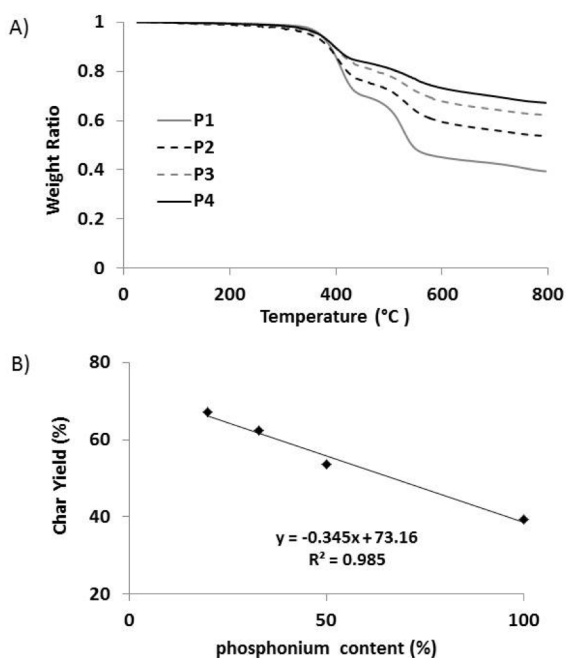


Figure 5.3: A) TGA curves of **P1** (grey solid line), **P2** (black dash line), **P3** (grey dash line) and **P4** (black solid line) for data collected under N₂, B) Relationship between char yield and phosphonium content in COFs

yield and microanalysis results of carbon content in Table 2, it is obvious that more carbon residue was preserved in **P2-NTf₂**, **P3-NTf₂** and **P4-NTf₂** after heated to 800 °C under N₂ compared to **P2-4**.

Table 5.2: Thermal properties and elemental microanalysis (calculated assuming complete conversion and experimental results) of **P1-P4**

Copolymer Network	Phosponium Content (%)	$T_{d,5\%}$ (°C)	Char Yield (%)	Microanalysis (Found)			Microanalysis (Theoretical)		
				C%	H%	N%	C%	H%	N%
P1	100	370	39.4	71.05	5.07	0.00	70.60	4.33	0.00
P2	50	352	53.7	76.90	4.42	0.00	75.36	4.99	0.00
P3	33	366	62.3	80.11	4.48	0.00	76.40	4.88	0.00
P4	20	369	67.2	84.03	4.56	0.00	80.86	5.10	0.00
P2-NTf₂	50	435	54.8	57.38	3.43	1.75	60.37	3.29	1.76
P3-NTf₂	33	417	56.8	63.55	4.11	1.17	65.14	3.50	1.52
P4-NTf₂	20	414	58.4	66.11	4.06	1.18	71.60	3.78	1.19

5.3.3 Chemical Stability and Water Uptake

In order to probe the extent to which repeat unit composition influences chemical stability of the COFs, a film of each was soaked in 6 M NaOH(aq) for 120 h at room temperature or 60 °C. Every 24 h, a sample of each COF film was taken from each film for analysis by IR spectroscopy (Appendix 5A, Figure 5A.3-8). Analysis of the ratio of absorbance at 1116 cm⁻¹ to the absorbance at 1591 cm⁻¹ as a function of time allowed for the quantification of phosponium unit decomposition. The ratio of absorbance was normalized based on the value before soaking in 6 M NaOH (Figure 5.4).

Under room temperature, the amount of decomposition increased as the proportion of the hydrophobic phenylene repeat units increased: ~20% decomposition

was observed for **P2**, whereas ~40% decomposition was observed for **P4** at room temperature. Both the nucleophilicity and basicity of the hydroxide anion are increased in hydrophobic environments compared to in aqueous solution, so it is not surprising that this decomposition trend is observed.

It is of interest to find that **P2-P4** exhibited similar degradation in high temperature in 6 M NaOH(aq) at 60 °C for 120 h (Figure 5.4B). One possible reason for this difference is that less amount of carbonate ions was formed in high temperature

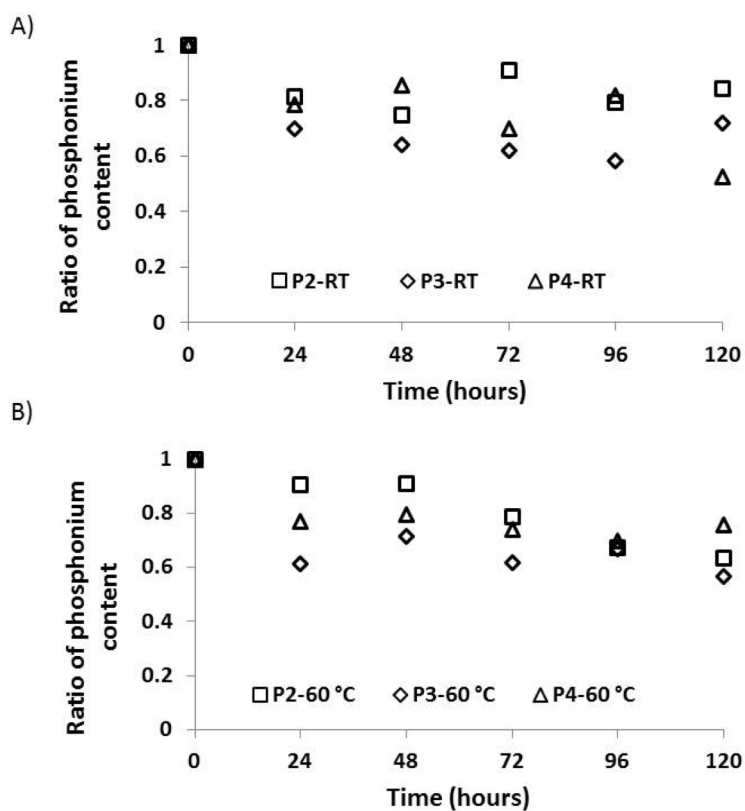


Figure 5.4: Changes in the ratio of absorbance at 1116 cm^{-1} to the absorbance at 1591 cm^{-1} when soaking **P2** (square), **P3** (diamond) and **P4** (triangle) in 6 M NaOH(aq) for 120 hours at room temperature (A) or 60 °C(B).

which could react with phosphonium units to form phosphine oxide.³⁸ In the room temperature, more carbonate ions formed in the solution and react with phosphonium units. The degradation was also dependent on the accessible of carbonate to phosphonium sites by the fact that the degradation increased as the surface area increased from **P2** to **P4**. (Table 5.3 and Figure 5.4A).

All of the COFs absorbed a significant amount of water after soaking in DI water for 24 h at room temperature (Table 5.3 and Figure 5.5). Consistent with BET analysis of porosity (*vide infra*), **P2** absorbed the least amount of water, while **P3** and **P4** absorb the most. The fact that water uptake scales with porosity of the materials rather than with ionic character suggests that the water is pulled into the structure by capillary action and held predominantly by cohesive interactions rather than interaction with the network structure at a molecular level. Furthermore, due to the highly cross-linked nature of COFs, no change in film volume or shape was observed upon water uptake. This is an important feature for membrane applications in which swelling can lead to physical failure of the membrane.

5.3.4 Physisorption

The surface areas of **P1-4** were estimated by BET measurement under N₂ at 77 K (Figure 5.6A). The isotherms of three copolymer frameworks indicated a mixture of Type I and Type II isotherms under the IUPAC definitions.³⁹ The specific surface areas estimated by BET (S_{BET}) are summarized in Table 5.3. The S_{BET} of polymer frameworks can depend not only on the composition, but on microstructure as well. Microstructure can in turn be influenced by relative component solubility and efficiency of the network-

forming reaction under the assembly conditions.⁴⁰ **P1** (100% **M1** content) was non-porous with $S_{\text{BET}} \sim 9 \text{ m}^2/\text{g}$ while reported polyphenylene COFs prepared by cyclotrimerization of **M2** was porous with $S_{\text{BET}} \sim 780 \text{ m}^2/\text{g}$.^{25,30} The S_{BET} of **P2** (3.49 m^2/g) was similar to that of **P1** ($\sim 9 \text{ m}^2/\text{g}$) but notably lower S_{BET} of **P3** and **P4**. One possible hypothesis is that the high phosphonium content in **P2** (50% of junctions) dominated the physisorption property. Phosphonium monomer **M1** has significantly

Table 5.3: Specific surface area and water uptake for **P1-P4**.

Polymer	Phosphonium Content (%)	$S_{\text{BET}} (\text{m}^2/\text{g})$		n_{CO_2} at 273K, 1 bar (mmol/g)	Water uptake (%)
		N_2	CO_2		
P1	100	9.02	27.91	0.49	10.63
P2	50	3.49	50.32	0.86	36.71
P3	33	46.87	87.06	1.37	46.83
P4	20	63.08	85.97	1.36	45.95

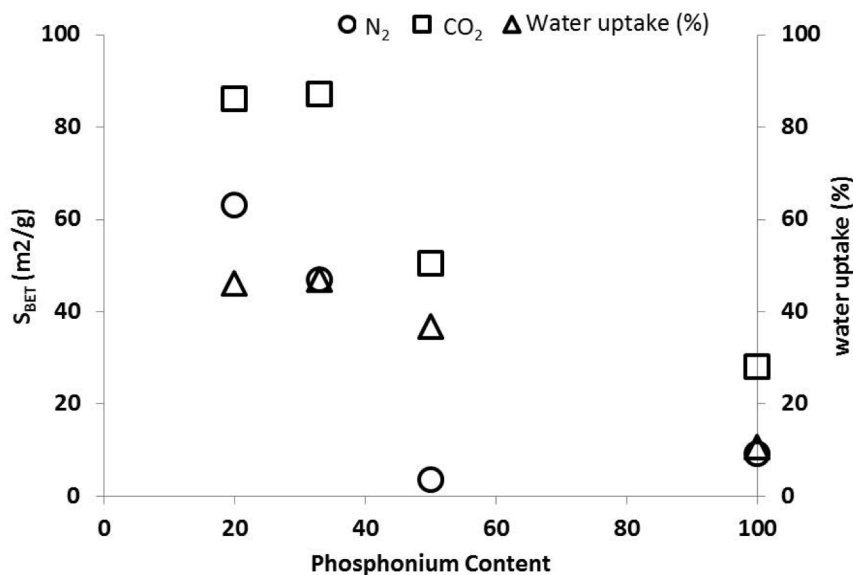


Figure 5.5: Specific surface area and water uptake for **P1-P4**.

better solubility in PTSA compared to **M1** due to its ionic nature leading to more ideal network formation and packing, resulting in lower S_{BET} . Similar effects have been observed on other COFs comprised of monomers having differential solubility.^{25,30} As the phosphonium content decreases from 50% to 33-20%, the porosity of **P3** and **P4** increased accordingly. An analysis of the absorption-desorption data for **P3** and **P4** reveal open isotherms, which are generally attributed to localized polymer swelling during adsorption.^{30,40-42}

Phosphonium units have some affinity for CO_2 , which has been exploited for CO_2 capture and phosphonium-mediated catalysis employing CO_2 as a reagent.^{2,11} These data suggest that COFs such as **P1-P4** might be useful in such applications, so CO_2 their adsorption characteristics are of interest (Figure 5.6B). The S_{BET} for **P1-P4** (Table 5.3) were all higher than for the corresponding values for N_2 adsorption, confirming that there is a molecular affinity of the phosphonium species for CO_2 .²⁵ As it was discussed in the introduction, tetraphenylphosphonium COFs CPN-1-Br had BET surface area of 1455 m^2/g and CO_2 uptake of 2.49 mmol/g at 273 K and 1 bar. Despite of the relatively smaller surface area of **P3**, it exhibited higher CO_2 capture capability which was 1.37 mmol/g at 273 K and 1 bar.

5.4 Conclusions

Four phosphonium-containing COFs have been prepared and their thermal stability, alkaline stability, and gas adsorption properties characterized. The introduction of 1,4-diacetylbenzene in progressively greater ratios of monomer feed led to predictable trends in all of these properties. The relatively high alkaline stability, resistance to

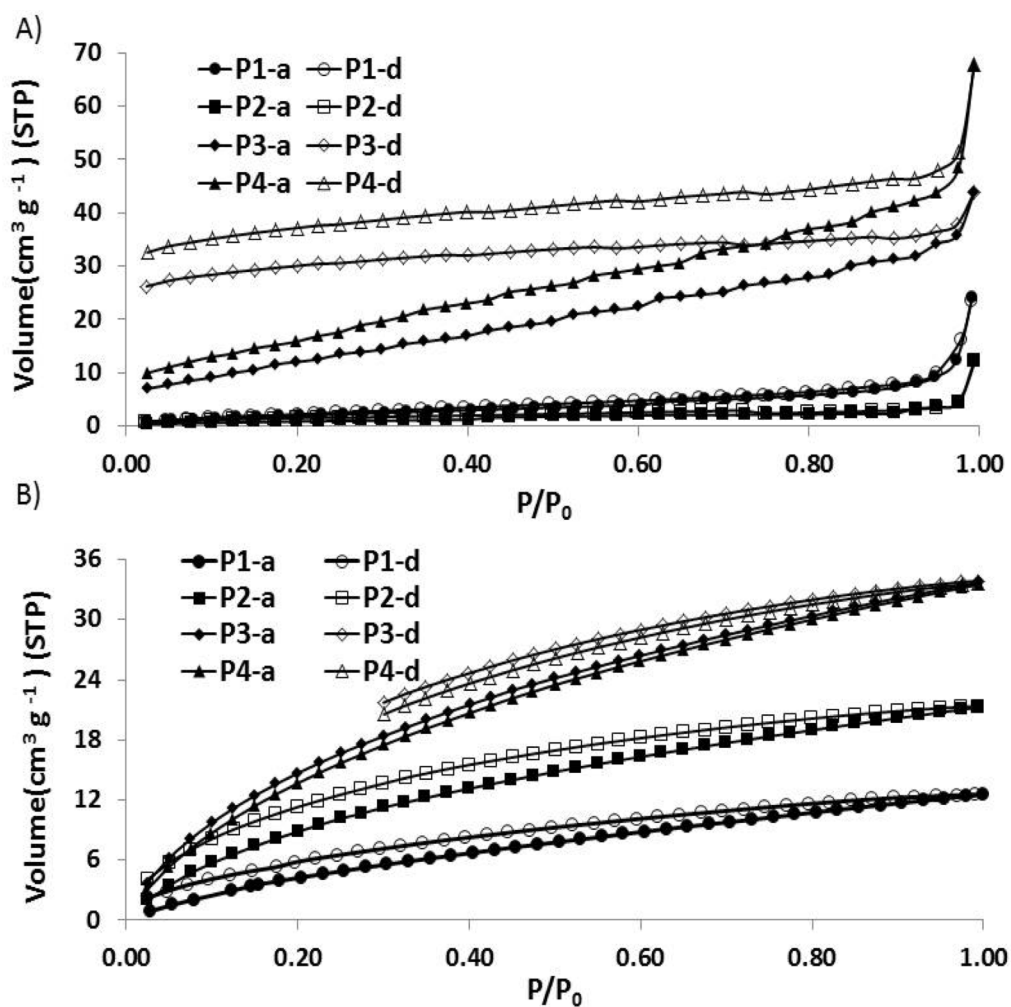


Figure 5.6: Nitrogen sorption isotherms at 77 K (A) and CO₂ sorption isotherms at 273 K (B) of **P1**(circle), **P2**(square), **P3**(diamond) and **P4**(triangle). Adsorption points are presented by filled squares and desorption by blank squares.

swelling upon water uptake, and affinity of phosphonium moieties for CO₂ suggests that optimized variations of these COFs could be useful components of alkaline fuel cells or gas separation systems. Future work related to exploring such application of phosphonium COFs are underway.

5.5 References

1. C. S. Diercks, O. M. Yaghi. *Science* **2017**, 355, 923-930.
2. S. Fischer, A. Schimanowitz, R. Dawson, I. Senkowska, S. Kaskel, A. Thomas. *J. Mater. Chem. A* **2014**, 2, 11825-11829.
3. Z. S. Wu, L. Chen, J. Z. Liu, K. Parvez, H. W. Liang, J. Shu, H. Sachdev, R. Graf, X. L. Feng, K. Mullen. *Adv. Mater.* **2014**, 26, 1450-1455.
4. S. W. Yao, X. Yang, M. Yu, Y. H. Zhang, J. X. Jiang. *J. Mater. Chem. A* **2014**, 2, 8054-8059.
5. A. F. Bushell, M. P. Attfield, C. R. Mason, P. M. Budd, Y. Yampolskii, L. Starannikova, A. Rebrov, F. Bazzarelli, P. Bernardo, J. C. Jansen, M. Lanc, K. Friess, V. Shantarovich, V. Gustov, V. Isaeva. *J. Membrane. Sci.* **2013**, 427, 48-62.
6. Y. L. Zhu, H. Long, W. Zhang. *Chem. Mat.* **2013**, 25, 1630-1635.
7. S. Han, Y. L. Feng, F. Zhang, C. Q. Yang, Z. Q. Yao, W. X. Zhao, F. Qiu, L. Y. Yang, Y. F. Yao, X. D. Zhuang, X. L. Feng. *Adv. Funct. Mater.* **2015**, 25, 3899-3906.
8. W. G. Lu, J. P. Sculley, D. Q. Yuan, R. Krishna, Z. W. Wei, H. C. Zhou. *Angew. Chem. Int. Ed.* **2012**, 51, 7480-7484.
9. D. Q. Yuan, W. G. Lu, D. Zhao, H. C. Zhou. *Adv. Mater.* **2011**, 23, 3723-3725.
10. R. S. Sprick, A. Thomas, U. Scherf. *Polym. Chem.* **2010**, 1, 283-285.
11. J. Q. Wang, J. G. W. Yang, G. S. Yi, Y. G. Zhang. *Chem. Commun.* **2015**, 51, 15708-15711.
12. S. Gu, R. Cai, T. Luo, Z. Chen, M. Sun, Y. Liu, G. He, Y. Yan. *Angew. Chem. Int. Ed.* **2009**, 48, 6499-6502.

13. B. C. Lin, L. H. Qiu, J. M. Lu, F. Yan. *Chem. Mat.* **2010**, *22*, 6718-6725.
14. S. T. Hemp, M. Q. Zhang, M. H. Allen, S. J. Cheng, R. B. Moore, T. E. Long. *Macromol. Chem. Phys.* **2013**, *214*, 2099-2107.
15. J. S. Luo, O. Conrad, I. F. J. Vankelecom. *J. Mater. Chem.* **2012**, *22*, 20574-20579.
16. C. G. Cassity, A. Mirjafari, N. Mobarrez, K. J. Strickland, R. A. O'Brien, J. H. Davis, Jr. *Chem. Commun.* **2013**, *49*, 7590-7592.
17. S. T. Hemp, M. S. Zhang, M. Tamami, T. E. Long. *Polym. Chem.* **2013**, *4*, 3582-3590.
18. M. S. Bedford, X. Yang, K. M. Jolly, R. L. Binnicker, S. B. Cramer, C. E. Keen, C. J. Mairena, A. P. Patel, M. T. Rivenbark, Y. Galabura, I. Luzinov, R. C. Smith. *Polym. Chem.* **2015**, *6*, 900-908.
19. C. A. Conrad, M. S. Bedford, A. A. Buel, Y. Galabura, I. Luzinov, R. C. Smith. *Polym. Int.* **2015**, *64*, 1381-1388.
20. S. L. Kristufek, T. R. Maltais, E. G. Tennyson, N. C. Osti, D. Perahia, A. G. Tennyson, R. C. Smith. *Polym. Chem.* **2013**, *4*, 5387-5394.
21. E. G. Tennyson, S. He, N. C. Osti, D. Perahia, R. C. Smith. *J. Mater. Chem.* **2010**, *20*, 7984-7989.
22. E. G. Tennyson, R. C. Smith. *Inorg. Chem.* **2009**, *48*, 11483-11485.
23. W. Wan, X. Yang, C. S. Rhett. *J. Polym. Sci., Part A: Polym. Chem.* **2017**.
24. X. Yang, C. A. Conrad, W. Wan, M. S. Bedford, L. Hu, G. Chumanov, R. C. Smith. *J. Mater. Chem. C* **2015**, *3*, 4537-4544.
25. X. Yang, Y. Wen, G. Chumanov, R. C. Smith. *J. Polym. Sci., Part A: Polym. Chem.* **2017**, *55*, 1620-1625.

26. A. Nagai, Z. Q. Guo, X. Feng, S. B. Jin, X. Chen, X. S. Ding, D. L. Jiang. *Nat. Commun.* **2011**, *2*, 536-543.
27. S. Y. Ding, J. Gao, Q. Wang, Y. Zhang, W. G. Song, C. Y. Su, W. Wang. *J. Am. Chem. Soc.* **2011**, *133*, 19816-19822.
28. R. W. Tilford, S. J. Mugavero, P. J. Pellechia, J. J. Lavigne. *Adv. Mater.* **2008**, *20*, 2741-2746.
29. J. S. Lee, H. M. Luo, G. A. Baker, S. Dai. *Chem. Mat.* **2009**, *21*, 4756-4758.
30. F. M. Wisser, K. Eckhardt, D. Wisser, W. Bohlmann, J. Grothe, E. Brunner, S. Kaskel. *Macromolecules* **2014**, *47*, 4210-4216.
31. M. Rose, N. Klein, I. Senkovska, C. Schrage, P. Wollmann, W. Bohlmann, B. Bohringer, S. Fichtner, S. Kaskel. *J. Mater. Chem.* **2011**, *21*, 711-716.
32. G. Witschard, C. E. Griffin. *Spectrochimica Acta* **1963**, *19*, 1905-1910.
33. J. A. John, J. M. Tour. *J. Am. Chem. Soc.* **1994**, *116*, 5011-5012.
34. A. J. Chalk, A. R. Gilbert. *J. Polym. Sci., Part A: Polym. Chem.* **1972**, *10*, 2033-2043.
35. F. Barontini, V. Cozzani, L. Petarca. *Ind. Eng. Chem. Res.* **2001**, *40*, 3270-3280.
36. W. Wan, X. Yang, R. C. Smith. *Chem. Commun.* **2017**, *53*, 252-254.
37. K. Hanke, M. Kaufmann, G. Schwaab, M. Havenith, C. T. Wolke, O. Gorlova, M. A. Johnson, B. P. Kar, W. Sander, E. Sanchez-Garcia. *Phys. Chem. Chem. Phys.* **2015**, *17*, 8518-8529.
38. Z. Y. Deng, J. H. Lin, J. C. Xiao. *Nat. Commun.* **2016**, *7*, 1-8.
39. K. S. W. Sing, D. H. Everett, R. A. W. Haul, L. Moscou, R. A. Pierotti, J. Rouquerol, T. Siemieniowska. *Pure & Appl. Chem.* **1985**, *57*, 603-619.

40. A. Derylo-Marczewska, J. Goworek. *Langmuir* **2001**, *17*, 6518-6523.
41. P. M. Budd, B. S. Ghanem, S. Makhseed, N. B. McKeown, K. J. Msayib, C. E. Tattershall. *Chem. Commun.* **2004**, 230-231.
42. S. J. GREGG, K. S. W. SING. Adsorption, Surface Area and Porosity, 2nd edition; Academic Press INC.(London) LTD: London, **1982**.

APPENDICES

Appendix 5A

IR spectra and TGA traces

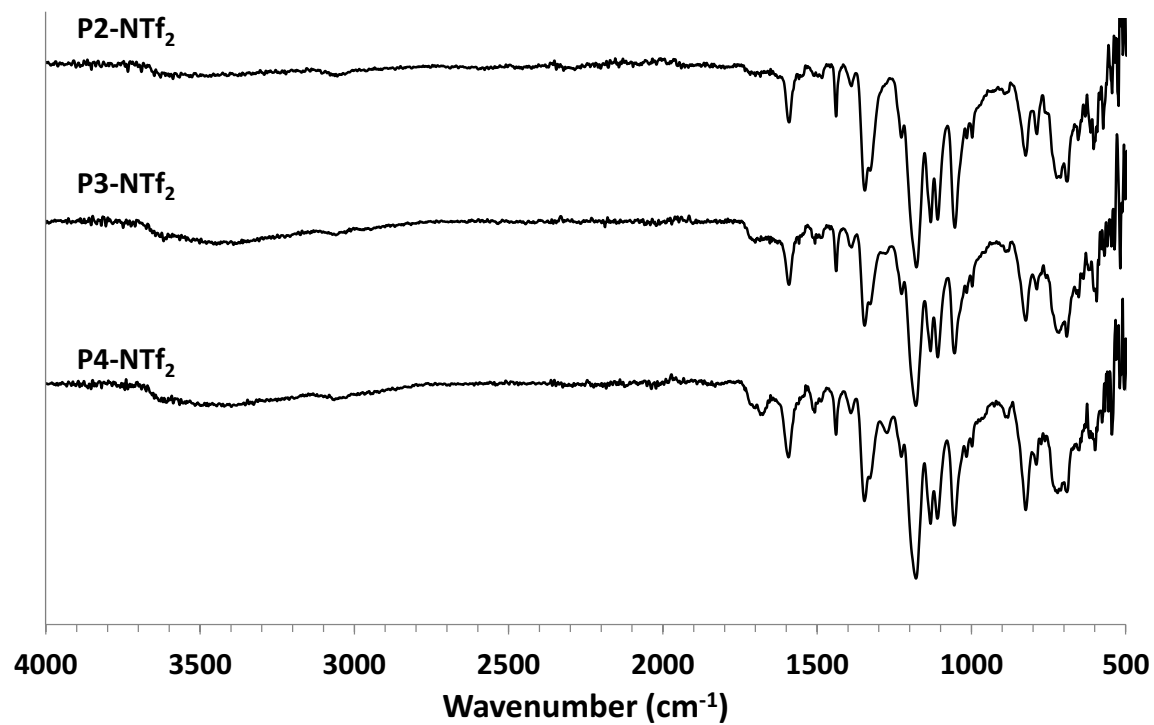


Figure 5 A.1: IR spectra of P2-NTf₂, P3-NTf₂ and P4-NTf₂

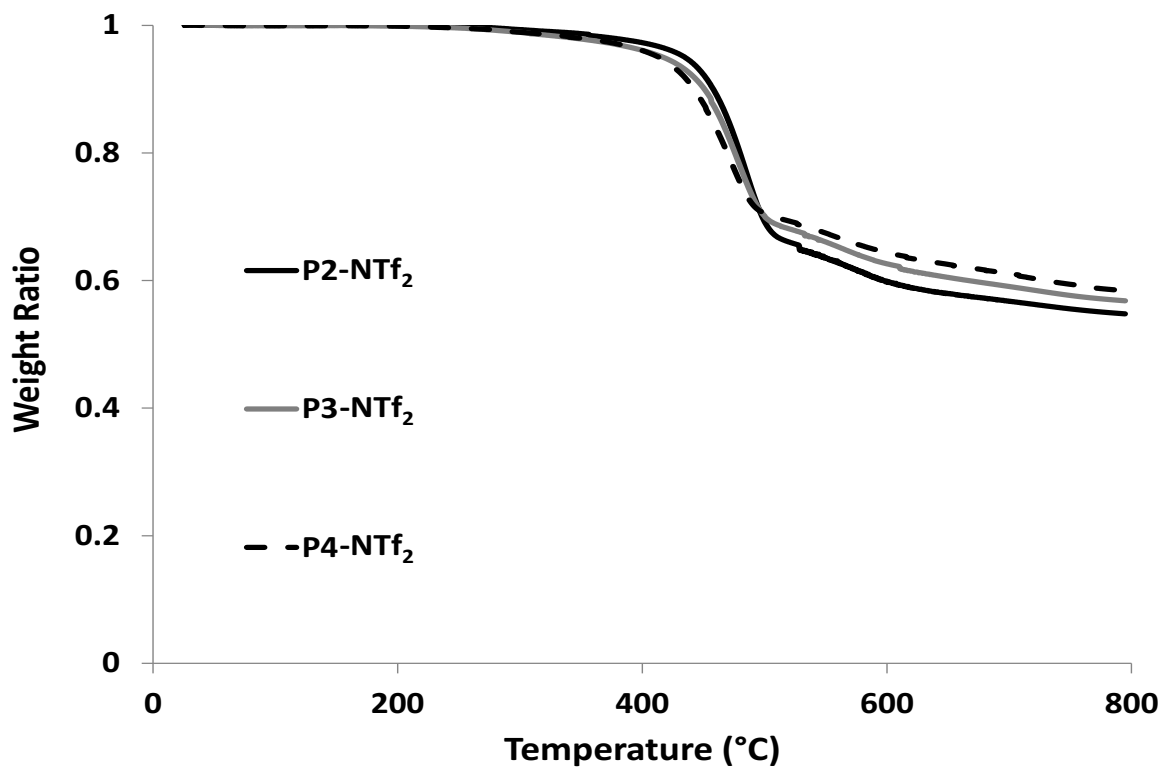


Figure 5 A.2: TGA of P2-NTf₂, P3-NTf₂ and P4-NTf₂

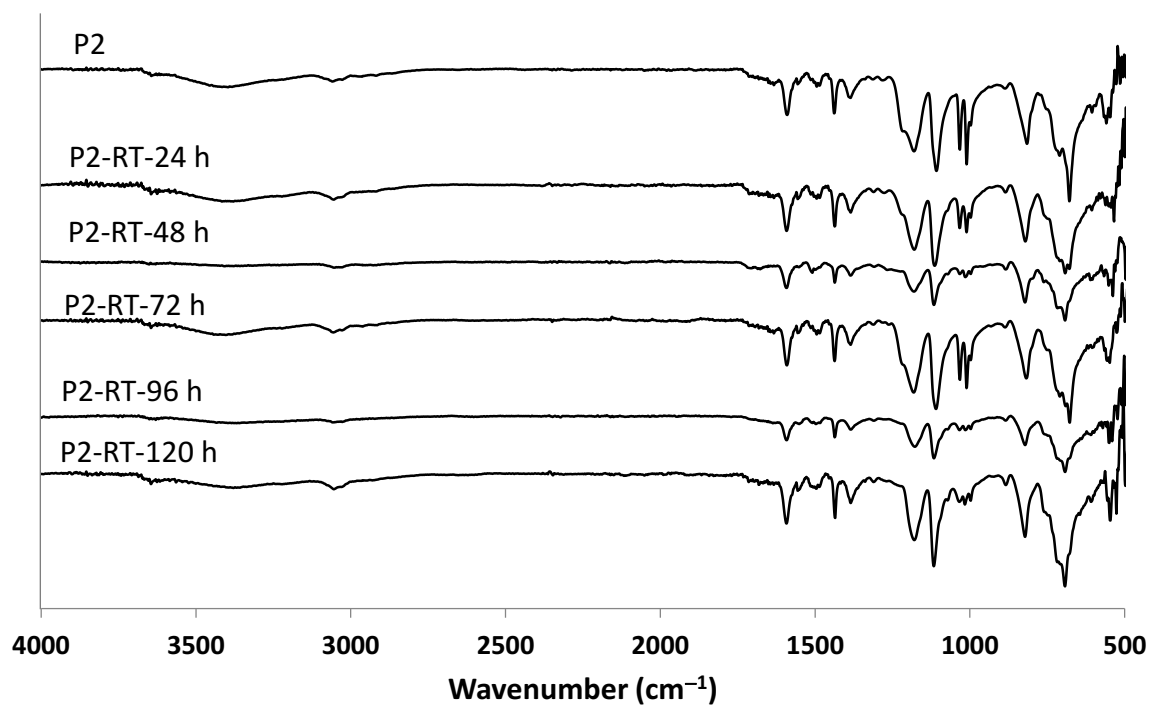


Figure 5 A.3: IR spectra of **P2** soaked in 6 M NaOH at RT for 120 h

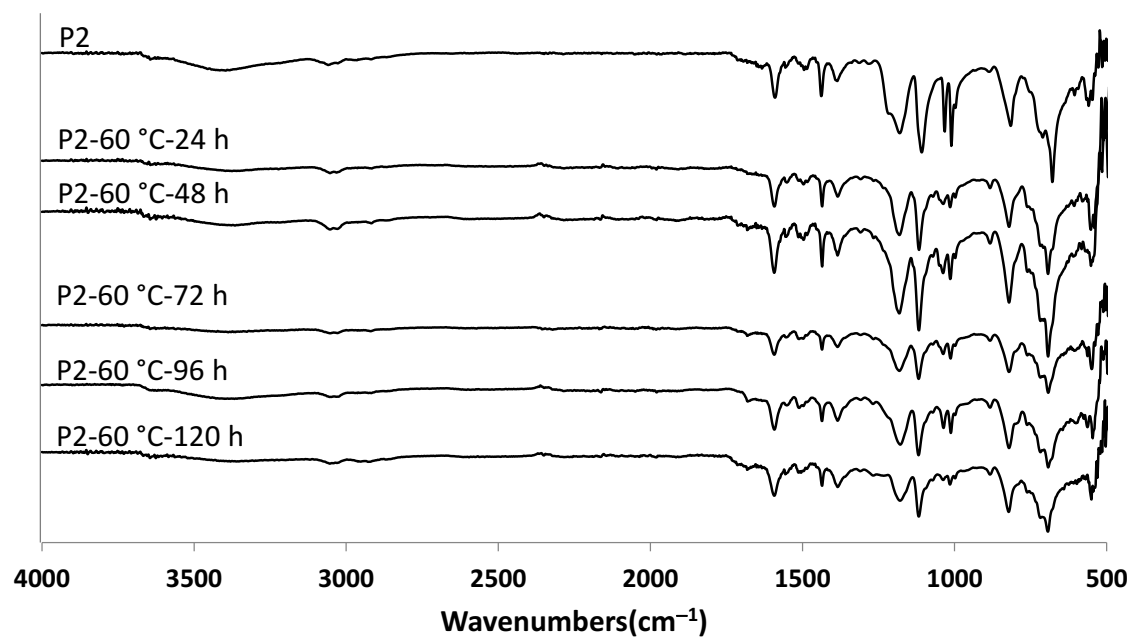


Figure 5 A.4: IR spectra of **P2** soaked in 6 M NaOH at 60 °C for 120 h

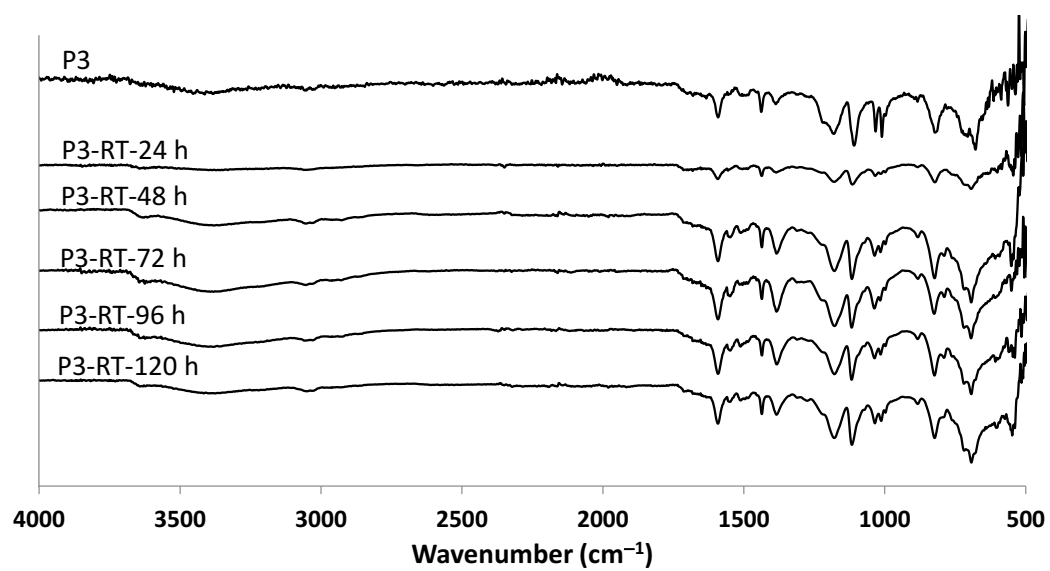


Figure 5 A.5: IR spectra of **P3** soaked in 6 M NaOH at RT for 120 h

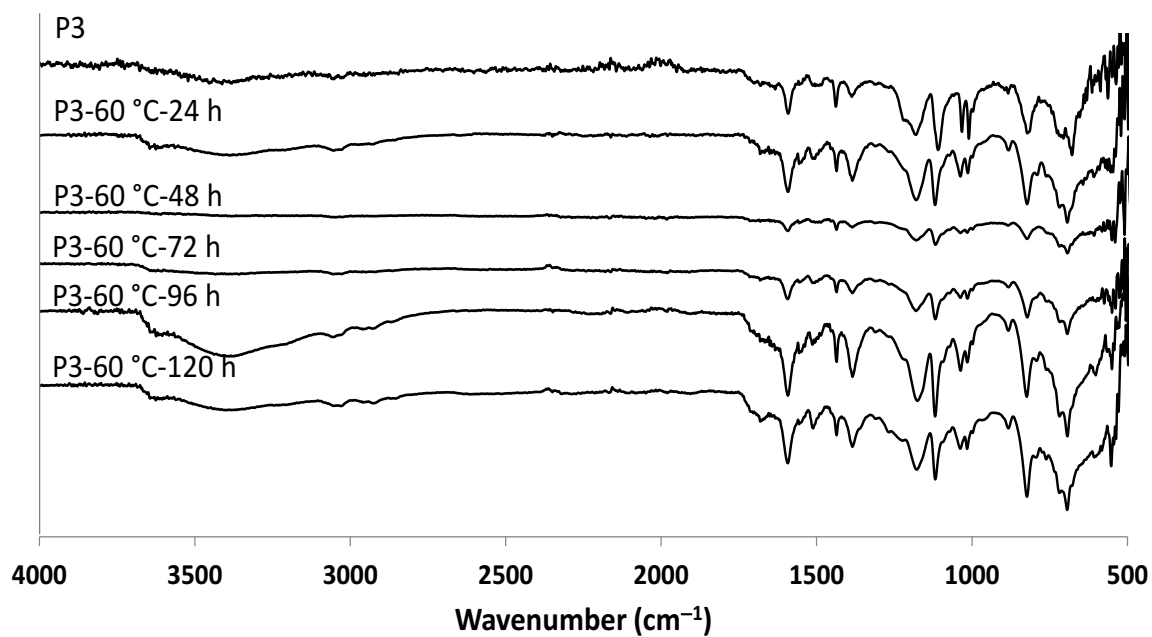


Figure 5 A.6: IR spectra of **P3** soaked in 6 M NaOH at 60 °C for 120 h

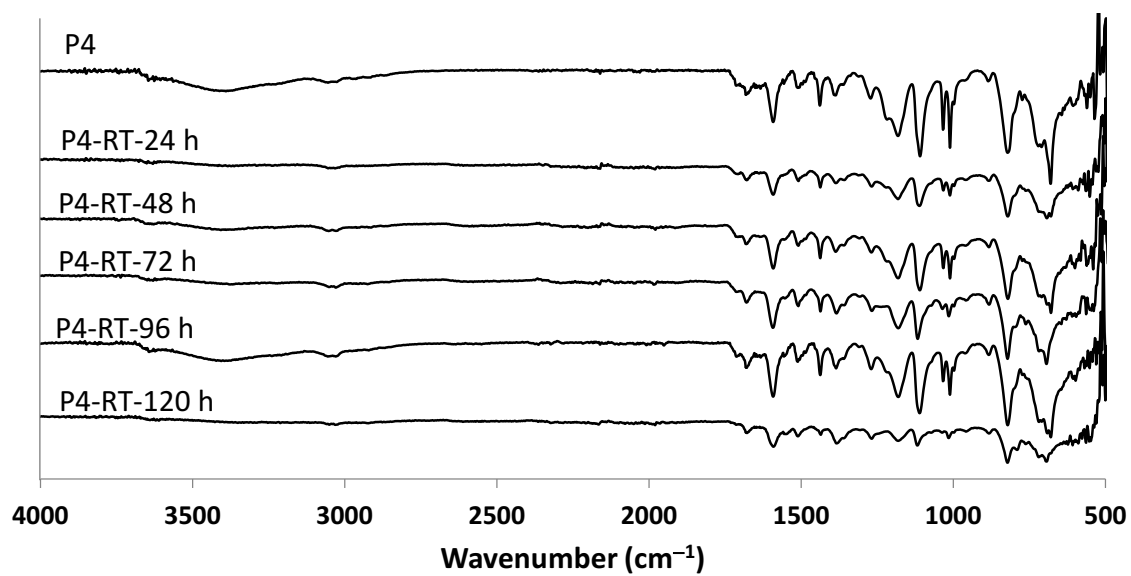


Figure 5 A.7: IR spectra of **P4** soaked in 6 M NaOH at RT for 120 h

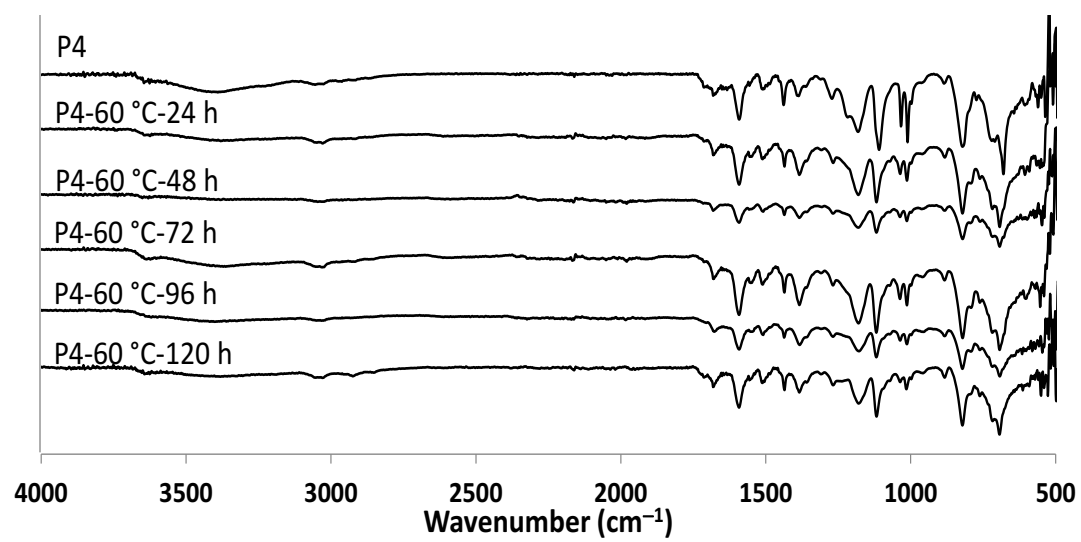


Figure 5 A.8: IR spectra of **P4** soaked in 6 M NaOH at 60 °C for 120 h